STUDY OF ISSUES IN THE DEVELOPMENT OF ELECTRONICALLY OPERATED PROSTHETIC ARM

Thesis

Submitted for the award of

DOCTOR OF PHILOSOPHY

by

Hardeep Singh Ryait
(Regd. No.-90604503)

Under the supervision of

Dr. A.S. Arora,
Professor, EIE,
SLIET, Longowal

Dr. Ravinder Agarwal,
Associate Professor, EIED,
Thapar University, Patiala

Electrical & Instrumentation Engineering Department,
Thapar University, Patiala- 147004
August 2011

Certificate

I hereby certify that the work which is being presented in the thesis entitled, "Study of issues in the development of electronically operated prosthetic arm", for the award of degree of Doctor of Philosophy in Electrical and Instrumentation Engineering Department, Thapar University, Patiala, is an authentic record of my own work carried out under the supervision and guidance of Dr. Ravinder Agarwal, Associate Professor, EIED, Thapar University, Patiala and Dr. Ajatshatru Arora, Professor, EIE, SLIET, Longowal.

The matter presented in this thesis has not been submitted by me for the award of any other degree of this or any other University.

(Hardeep S. Ryait)

This to certify that the above statement made by the candidate is correct and true to the best of our knowledge.

(Dr. Ajatshatru Arora)
Professor
EIE, SLIET
Longowal

(Dr. Ravinder Agarwal)
Associate Professor
EIED, Thapar University
Patiala

i

Acknowledgments

The quest for knowledge is a journey that is long and difficult but equally rewarding. That is why it is a necessity to have strong support from the people around you to make this journey a success. Without the support from many people, I would not have completed my work. It is pleasant aspect that I have now the opportunity to express my gratitude for all of them.

First of all, I would like to express my gratitude to my thesis advisors, Prof. (Dr.) Ajatshatru Arora, Professor (EIE), SLIET, Longowal and Prof. (Dr.) Ravinder Agarwal, Associate Professor (USIC), Thapar University, Patiala, for motivation, patient guidance and every-time support. Success can never be attained without proper guidance. I am truly very fortunate to have the opportunity to work with them. I found their guidance to be extremely valuable. Personally, I feel them as a part of my family. I am also thankful to Prof. (Dr.) S. Ghosh, Head Electrical and Instrumentation Engineering Department for extending administrative support.

Finally, I would like to thank my family for standing by me through all the joys and sorrows that life had to offer. My heartfelt thanks and life-long gratitude go to my Mother and Father for all their love, constant support, encouragement and sacrifices and affection that they have showered upon me. I would like to express my heartily thanks to my wife and daughter for always being supportive. I am also heartily grateful to my friends especially to Dr. Satish Kumar for their valuable cooperation and motivation while I was getting frustrated with the confusions during the work.

I would also like to thank all of them, whose names remain unmentioned but who have never retraced back from helping me whenever the need arose. My acknowledgements would not be complete without expressing my gratitude towards Almighty God. I feel very fortunate to come to know Him during all these years of my life and have continually been blessed by His endless love ever since. He is the true shepherd of my life.

Hardeep S. Ryait

Abstract

The arms and legs are very important parts of the human body. The arm physiology is an extremely complex to study. People's working capability is badly affected when they suffer an amputated arm. Artificial replacements with prosthetic devices to get a satisfactory level of performance for essential functions with the currently available prosthetic technology are very difficult. The natural solution to amputation is biological regeneration of the missing limb. As this is not currently possible it is important to find viable solutions for providing multifunctional prostheses. Realization of a successful prosthesis is the need with complete understanding of the associated practical, clinical and economic factors. Presently, myoelectric arm prostheses are becoming popular because they are operated by a natural contraction of intact muscles. With the requirement of such multifunctional low cost prosthesis, following objectives were defined for present work-

1. Study of various methodologies and algorithms for SEMG signal analysis to control myoelectric arm
2. A comparative study on the analysis of SEMG signal based on different postures/movements of arm.
3. To develop more powerful, flexible, and efficient SEMG signal interpretation with the locations of electrodes on different acupressure points of human arm i.e. from shoulder to wrist.
4. Development of a control methodology to use myoelectric signals from muscles which act in synergy with hand function as the control signals to operate the prosthesis.
5. On the basis of above studies, development of a prototype model for realization of control methodology for elbow movement.

Surface Electromyogram (SEMG) is a complex signal, which is controlled by the nervous system and is dependent on the anatomical and physiological properties of muscles. SEMG detector (electrodes) at the surface of the skin collects signals from different motor units at a time, which may generate interaction of different signals. These SEMG signal gets corrupted by noise while traveling through different tissues. The sources of these noises are environmental (such as 50 Hz power-line) or biological

(such as motion artifact) interference. Due to these complexities, detection of SEMG signals with powerful and advance techniques is becoming a very important requirement in biomedical engineering.

In the present work SEMG acquisition system was designed keeping the economics and application in mind. The amplifier provides the input for the analog interface of the computer using sound card (which is default adapter for softscope). The SEMG acquisition system was developed to measure and record the signals from the subjects. Users have the options to select a variety of voltage scales and time scales to display the output signals with great advantage of portability.

After acquiring SEMG signal, important aspect is to extract the features which are representative of SEMG pattern for different arm functions. The study of different parameters in relation to SEMG variations with force level has been carried out and it has been found that both amplitude-related parameters and selected statistical parameters give good view of force level. A function slope has been tried for as SEMG parameter and it produced good representation of the SEMG. It has also been observed that prolonged use of the prosthetic device may result in lower amplitudes of SEMG signals. Thus, a prosthetic controller based on amplitude should have the capability of adjusting the threshold level in order to get proper degree of controllability.

Acupressure points are places on the skin that are especially sensitive to bioelectrical impulses in the body and conduct those impulses readily. Traditionally, Asian cultures conceived of the points as junctures of special pathways that carried the human energy that the Chinese call *chi* and the Japanese call *ki*. Stimulating these points with pressure, needles, or heat triggers the release of endorphins, which are the neuro-chemicals that relieve pain and relaxes muscles. In tune with objective 3, as an additional study to find electrode locations to have multifunctional prosthesis, acupressure points were considered. The study explored that those electrode sites may be considered where even very weak correlation between the SEMG and (more than one) limb functions exist. This study verifies the SEMG activities on acupressure points if selected sensibly which encourage advancing the work for specific movement measurement. Further, the pressure points are compared with other locations on arm for SEMG observations.

In the next stage of this work, the interpretation of SEMG signals from the locations of human arm i.e. from shoulder to wrist was done to discriminate hand/wrist

movements. The objective of the present study was to develop such a system so as to assess different muscles activities on arm during four basic movements namely opening (op) / closing (cl) / down (d) / up (u) of hand wrist/grip and find out the suitable number of channels for movement classification with best electrode locations. Six locations including two pressure points were considered. Principal component analysis was used to determine the best location with different sets of electrode numbers. After the principal component analysis of data from different locations, it is found that in two channel locations namely "cbet (below elbow thumb side) and cbeb (below elbow little finger side)" and in three channel locations namely "cam (below arm middle palm side)", "camb (on opposite side of cam)" and "cbet (below elbow thumb side)" were best suited to discriminate the four chosen movements. However, the pressure points showed low performance with respect to other locations. Best location were related to the maximum loading percentage to PC1 and appropriate numbers of channel of the acquisition system to monitor movements again depended upon the loading percentage to PC1 but shall vary within *i.e.* different movement shall have different contribution percentage for better discrimination.

Finally, the SEMG analysis on the elbow movement for the four movements [extension, flexion, supination and pronation] is discussed which results in control methodology for single-channel and two-channel prototype elbow. A prototype elbow based on SEMG analysis for the above elbow had been developed using microcontroller based hardware. The design employs SEMG-RMS to DC conversion using AD536 IC which gave satisfactory results. With proper synchronizing of the prototype arm position and the SEMG contraction the specific sequence of movements are achieved successfully. The prototype has been realized differently for two movement control (extension/flexion) and four movement control (extension/flexion/pronation/supination).

This work presents a successful creation of inexpensive SEMG platform. A principal component analysis of data from different locations to discriminate the four chosen movements was usefully used.

Contents

Chapter 3 SEMG signal acquisition system and methodology

Chapter 4 SEMG analysis at acupressure points

Chapter 5 SEMG analysis for hand function differentiation

Chapter 6 Developments of electronic prosthetic elbow

List of figures

List of table

Appendix chapter 6

CHAPTER 1

INTRODUCTION

The greatest of all creations is human body, the marvelous machine—precise and efficient to study. The human body has a dynamic framework of bone and cartilage called skeleton. The human skeleton is flexible in nature that is made to move with the help of joints. Muscles uniformly bonded over the skeleton helps in the execution of movements. The brain computes and sends throughout the body billions of bits of information which controls every action like the flicker of an eyelid or to move any body part. In the human body, nerves carry the information back and forth from the central nervous system. Brain is attached to the central nervous system. Long bone such as in the arm or leg is considered as lever. Joints and articulated surfaces are considered to be frictionless. Tendons and tendon sheets can be considered sliding surfaces or cables. Muscles are the motors of the human machine. Hence, the body is considered to act as a machine via mechanical parts [Online ref. 1]. While describing motion of the human body the related terms could be confusing. The terms are described as anatomical positions. Extension is a movement of the lever head normally forward or downwards while flexion is a movement of the lever head rearwards. Similarly it is easier to think of the movements in terms of a standard coordinate system [Online ref.1].

The human body is an exquisite combination of interacting systems which can be analyzed using multidisciplinary engineering principles i.e. chemical, mechanical and electrical engineering principles through application to the human body [Farrell, 2002]. Biomechanics of the human muscle movements can be determined through the use of sensors and a specialized computer. These sensors detect movement in the muscles and allow the computer to follow the muscle movement completely. Biomechanics of the human muscles is the calculation of forces applied to the muscles, joints and bones while completing a task. This can include the heat, the pressure and the tension of the muscles, joints and tendons. This is done through the monitoring of muscles in concerned site and muscles surrounding this site [Chapman, 2008]. These studies can be termed as a gift to the amputees which is termed as prosthetic devices. Research areas of actuators and mechanisms have shown steadily

growing technological advances in externally activated prostheses. The advances include the use of piezoelectric materials, special metal alloys, polymers and new motor applications. The advances in mechanisms also include mechanical designs based on the anatomy of the human hand and improvements in the way these components are combined. Prosthesis can be simple artificial limb looking like the human limb known as cosmetic prosthesis, which is made up of latex or silicon but is not able to perform any activity. It can be used to hide distorted image of an amputee. Another type is a robotic structure of human hand whose control is from control cables which are operated through shoulder's movement, mouth, chest, other hand etc. called as body powered prosthesis. In this case specified operations can be performed. Body - powered terminal devices (hooks, hands, etc.) come in various configurations which are controlled by the user's pull on the control cable to open the hand or hook and the grip strength is limited by the number of rubber bands on the hook or the spring tension in the hand. Fig. 1.1 shows flow chart of the controlling strategy [Wongsiri et al., 2003]. Another flexible grasping motion control for a hand with two fingers was described [Kuba et al., 1992]. This control of reference grasping force was decided in advance for the operation. The way to extend the grasping control by including the operator to the control loop was explained. This study was carried out to know how to interface human and an artificial hand based on human being property.

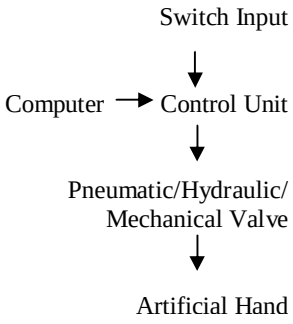

Fig. 1.1 Flowchart of control strategy [Wongsiri et al., 2003]

In almost all cases the harness and cable system can be both the best and worst aspect of a body - powered system. Negative aspects developed as the same pressure may create discomfort and contribute to long-term nerve compression and overuse

problems. Important consideration of body - powered designs are being of less expensive.

There has been lot of efforts worldwide to improve the activities in the functional range of the prosthetic hand. Prosthetic arm can be classified depending upon controlling techniques. The two most common prosthetic systems are body - powered and myoelectric designs [Tomovic and Boni, 1962; Micera et al., 2010]. Fig. 1.2 shows the symbolic representation of prosthesis (a) internally powered and controlled (b) externally powered prosthesis and (c) prosthesis externally powered and both externally and internally controlled. Here P and C stand for power and control elements respectively.

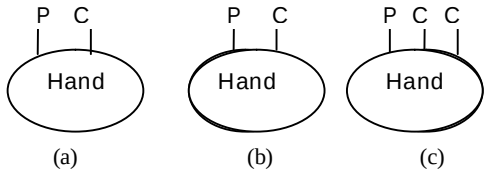

Fig. 1.2 Symbolic representation of prosthesis [Tomovic & Boni, 1962]

Myoelectric control is the most common type of externally-powered systems. A myoelectrically-controlled prosthesis uses electrical impulses, generated by contraction of the amputee's own remaining muscles, to operate a motor in a mechanical hand, hook or elbow. Most myoelectric systems provide proportional control of the speed and grip strength of the hand or other electric terminal devices (electric hook or work device) based on the strength of the muscle contraction of the wearer.

Another type is the hybrid prostheses which combine body-powered and electrically-powered components. For example, a terminal device may be myoelectrically controlled while the elbow unit is body - powered. Many combinations of systems are used to optimize individual functional performance. A hybrid method for adapting a three fingered dexterous and compliant artificial hand so as to describe preconfiguration before grasping some specified rigid object was showed. This category could also be specially designed for one specific task or activity such as devices for tools, cooking, fishing, skiing, baseball, hockey, archery and billiards, as well as for musical instruments. Amputees could frequently choose to utilize more than one type of prosthesis as part of their daily life. For example, a person may wear

a myoelectric system for most activities, or utilize a body-powered system for heavy-duty or wet tasks [Finat et al., 1998].

The main factors of the rejection of conventional prosthetic hands were:

- Heavy weight: although commercial prosthetic hands have about the same mass as human hands they appear to be unpleasantly heavy because the mass is transmitted by a lever arm to the short stump of the amputated arm.
- Low functionality: Conventional prosthetic hands can only perform a single pincer-like grip movement. Therefore, the gripping abilities are restricted, for example to pick up a pinball with the artificial hand. The fingers have only one degree of freedom and can not adapt to the shape of an object. The consequence is reduced force, which is necessary to hold an object stable.
- Robot-like movement: The movements to appear to be unnatural.

To overcome these disadvantages a lot of efforts have been done worldwide. In the present scenario, research activities are improving the functional range of an electrically driven prosthetic arm. In the body movement, the complex and nonlinear information processing is done from the brain to the body limbs. Motor command firstly is sent from the nervous system to each muscle via motor neurons. It activates the muscles and causes the muscle tensions. Secondly, the muscle tensions act on the related joint and cause the joint torque. Finally, the joint torque realizes the motion corresponding to the joint dynamics.

In the case of amputee, a part of this information processing flow is cut off. It is inconvenient for them to live a daily life. For the expansion and the improvement of amputee's activity in daily living, several kinds of Surface Electromyographic (SEMG) controlled prosthetic hands have been developed. The use of SEMG signals to control the prosthetic hand provides the amputees with a control feeling similar to moving their normal hand.

An SEMG signal also called as a group motor action potential is an electrical impulse that produces contraction of muscle fibers in the body. The term is most often used in reference to skeletal muscles that control movements. Myoelectric signals are detected by placing three electrodes on the skin. Two electrodes are positioned to acquire the voltage between them when a myoelectric signal occurs. The third electrode is placed in a neutral area and its output is used to cancel the noise that can

otherwise interfere with the signals from the other two electrodes. The output voltage is processed using a device called as differential amplifier. The output of this amplifier has much higher voltage than the myoelectric signals themselves. This higher voltage, which produces significant current, can be used to control electromechanical or electronic devices. This signal is normally a function of time and is describable in terms of its amplitude, frequency and phase.

Acquiring SEMG signal for analysis can be done by using bio-potential acquisition systems such as DELSYS BAGNOLI-2, EMG sensor system using PCMCIA data acquisition card (NI DAQ PCI-6010) [Xiang, 2007], BIOPAC data acquisition etc.

The technology of SEMG recording is relatively new. There are still limitations in detection and characterization of existing nonlinearities in the SEMG signal, estimation of the phase, acquiring exact information due to derivation from normality. In traditional systems reconstruction algorithms has various limitations and considerable computational complexity and many shows a high variance. Recent advances in technologies of signal processing and mathematical models have made it practical to develop advanced SEMG detection and analysis techniques. Various mathematical techniques and artificial intelligence have received extensive attraction.

In the present research work, the main emphasis has been given to study different issues of electronically operated prosthetic arm, analysis of SEMG signal to discriminate motions of arm/wrist acquired from different electrode locations on arm. The proposed work has been split into three parts; the receiving/processing SEMG signal from the muscle of interest and interpreting the SEMG signal; statistically using principal component analysis for observing the best locations for different numbers of acquisition channels and the designing of prototype elbow.

1.1 Need of arm prosthetics

In the United States 41,000 persons were registered who had an amputation of a hand or a complete arm [Schulz et al., 2001]. A survey has shown that the number of amputees in India in 1981 was approximately half a million. It was estimated that the number of amputees with no prosthesis increased annually by 17,000. Resources for medical care are limited in poorer countries and the need for prosthetics in this third world is clearly immense [Meanley et al., 1995]. With the same frequency of occurrence (1 in 6100) there would be 1,000,000 such persons worldwide [Schulz et

al., 2000]. The prevalence rate in 1996 was 4.9 per 1,000 persons. 50,000 new amputations happen every year in USA based on information from National Center for Health Statistics [Online ref. 2]. Ratio of upper limb to lower limb amputation is 1:4. Most common is partial hand amputation with loss of one or more fingers; the next common is loss of one arm. 30% have upper limb loss, wrist and hand amputations are estimated to make up 10% of upper limb population, trans-radial amputations make up 60% of total wrist and hand amputations which mean 70% of all persons with upper limb amputations have amputations distal to the elbow [Online ref. 3].

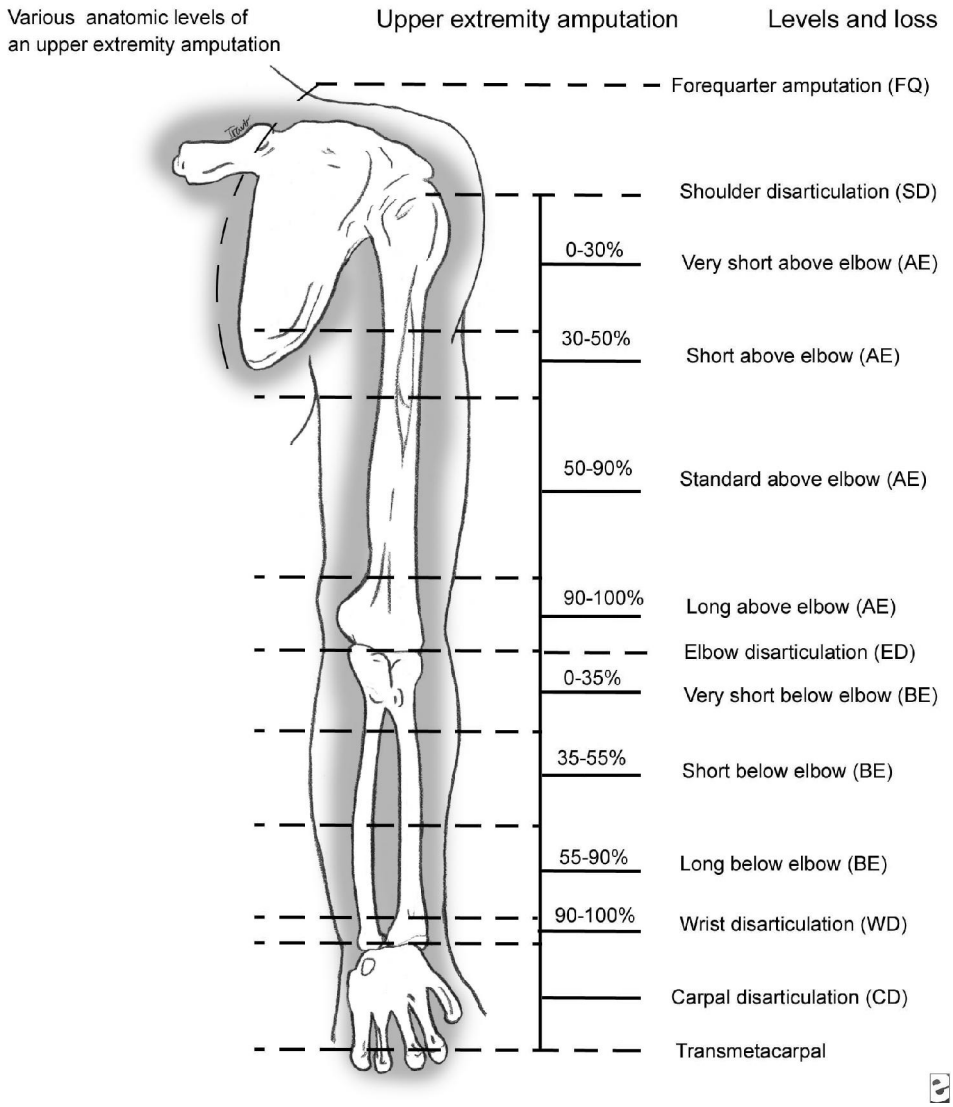

Fig. 1.3 Amputation levels [Kelly, 2010(Online ref. 18)]

The most common being partial hand amputation with the loss of one or more fingers; next most common being loss of one. Statistical data indicates the existence of some 350,000 persons with amputations in the USA, of whom 30% have upper-limb; of this 30% wrist and hand amputations are estimated to make up 10% of the upper-limb population. This means that 70% of all persons with upper-limb amputations have amputations distal to the elbow [Weir et al., 2000]. 60% of arm amputations are between ages 21 and 64 years and 10% are under 21 years of age. The Fig. 1.3 depicts the levels of an upper extremity amputation. Trauma is the most common reason for amputation in patients aged 15-45 years, with tumors being a distant second. Upper extremity amputations tend to be rare in patients who are older than 60 years, but they may be required secondary to tumor or medical disease [Meier, 2005].

These statistics gives us the need of prosthetic devices but above all the need of knowledge of implementing and using these devices is essential. Fig 1.3 emphasizes the need of prosthetic devices for “long above elbow” and “wrist disarticulation” where loss shown is the most. SEMG based technology can be the one of the solutions.

1.2 Introduction to acupressure points on human arm

Acupressure has been practiced as a healing art for at least 5,000 years. It is said to be the most popular method for treating pain and illness in the world. This is a proven, natural and cost effective self-care system of home treatment. Acupressure philosophy is based on the same principles as acupuncture. By using pressure instead of needles, acupressure works to stimulate specific reflex points located along the lines of energy which run through the body, called meridians. There are many meridian lines, each of which corresponds to an individual organ of the body. When the vital energies are able to flow through the meridians in a balanced and even way the result is good health. When pain or illness is experienced then it is an indication that there is a block or leak in the energy flow within the body [Online ref. 5; Online ref. 6; Online ref. 7].

1.3 Arm Movement for performing routine work

Mimicking all the functions of hand in prosthesis is near impossible with present day technology whereas the study of different functions of hand along with the movements required to perform those functions may lead to a practical solution. The

functional jobs of human hand can be divided into two major categories, i.e. based on day to day work and skilled work as indicated in Table 1.1.

Acupoint 08 Bend the arm, hand to shoulder, and place finger on the end of the crease of the arm; open the arm and stimulate the point	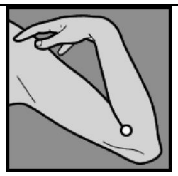
Acupoint 03 Two thumb widths above the outside of the wrist, lined up with the middle finger	
Acupoint 02 Two thumb widths from the largest crease on the inside wrist; the point is between the tendons in the middle of the wrist	
Acupoint 12 On the largest crease of the inner wrist, on a line with the thumb	

Fig. 1.4 Acupressure points on arm [Online ref. 7]

Table 1.1
Common functions of human arm

Category	Function	Movement required
Day-to-Day work	Picking up items	Elbow extension & Grasp
	Placing items	Elbow extension & Release
	Lift object	Elbow flexion & Power grasp
	Pouring liquid from a bottle in a glass	Grasp, wrist movement & arm pronation
	Shaking hand	Grasp with wrist movement
	Combing	Grasp with wrist movement
	Eating	Grasping & Elbow flexion
	Throwing	Grasp with wrist movement
	Calling indication	Wrist movement
Skilled work	Typing, Writing and Drawing	Precision grasp and precision wrist movement
	Playing stick games	Grasp with wrist movement

It is quite evident form Table 1.1 that 90% of day-to-day functions are extension, flexion, grasp and release movement. Other works normally requires one out of four movements like wrist flexion, wrist extension, pronation or supination [Arora, 2002].

1.4 Literature review

1.4.1 Abroad

The development of prostheses has roughly paralleled the progress of amputation. The surviving amputee must have wish for the prosthesis. An Italian vase of the fourth century B.C. shows a lower-limb amputee supporting himself with a wooden pylon. An artificial leg dating to about 300 B.C. was unearthed at Capua, Italy, in 1858. It was made of bronze and iron, with a wooden core, apparently for a below-knee amputee. The prosthesis was destroyed during an air raid on London in 1941. Marcus Sergius, who lost his right hand in the Second Punic War (218 202 B.C.), was fitted with an iron hand, which he apparently used effectively [Vanderwerker, 1976]. There has been lot of efforts worldwide to improve the activities in the functional range of the prosthetic hand. This section gives the brief idea about the classification of prosthetic hand and major developments in each category. Prosthetic arm can be classified depending upon controlling techniques. The two most common prosthetic systems are body - powered and myoelectric designs [Tomovic and Boni, 1962; Micera et al., 2010]. The new generation of hands could provide the user with much more functionality and capabilities. Body - powered terminal devices (hooks, hands, etc.) come in various configurations which are controlled by the user's pull on the control cable to open the hand or hook and the grip strength is limited by the number of rubber bands on the hook or the spring tension in the hand [Wongsiri et al., 2003]. The design of pneumatic controlled arm-movement controlled by a foot switch was developed This test was performed on an amputee wearing the artificial arm and simple tasks such as picking up objects and drinking water were performed [Wongsiri et al., 2003]. A very lightweight artificial hand driven by a new type of powerful small size flexible fluidic actuator was presented. These actuators were completely integrated in the fingers which made possible the design of a very compact and lightweight hand that could either be used as a prosthetic hand or as a humanoid robot hand [Schulz et al., 2001]. A joint controller for an anthropomorphic robot hand driven by flexible fluidic actuators was developed for position and force control for

robotic systems. These flexible and compact actuators were integrated directly into the finger joints, where they were driven either pneumatically or hydraulically [Beck et al., 2003].

Most of the theoretical studies relating the surface electromyogram to muscular force suggested that the amplitude of the electromyograph should increase proportionately with the square root of the tension. However, direct experiments showed a linear relationship between them [Ray and Guha, 1983; Bergamasco and Scattareggia, 1995]. A prosthesis control system was described based on microprocessor hardware whereby control of an artificial limb for above-elbow amputees in several degrees of freedom. This design employed time series identification techniques for parameter discrimination. System involved one set of electrodes for discriminating and controlling five limb functions. This system feeds to a motor control and actuation unit identical to that of the toe-controlled system of which was used by a bilateral above-elbow amputee [Graupe et al., 1982]. In another work, the flexible grasping motion control for a hand with two fingers was described. This control of reference grasping force was decided in advance for the operation. This way to extend the grasping control by including the operator to the control loop was explained. This study was carried out to interface human and an artificial hand based on human being property [Kuba et al., 1992]. For grasping, three fingers and for re-grasping, four fingers are needed, also the hand should be as large as a human hand. Such a hand was mounted on a PUMA 560 robot. Each finger possessed three degrees of freedom [Pfeiffer, 1996]. It is possible to continuously decode finger position from surface EMG signals collected from a generalized electrode placement in a healthy subject. A new three-fingered poly-articulated myoelectric prosthesis equipped with position, force, and slip sensors which allowed maintaining a stable grasping of the object without affecting the user attention was developed. Force sensors at the level of the fingertips as well as palm sensors were integrated in the structure [Graupe, el at., 1994].

A new type myoelectrically controlled prosthetic hand which simulated the dynamic properties of the muscle and stretch reflex was developed. This prosthetic hand consisted of the processing units of surface EMG signals, the digital servo system or DC motor giving the one-degree of freedom mechanical hand. Usefulness of the developed prosthetic hand was showed by myoelectric control experiments with both the healthy subject and the amputated subject [Okuno et al., 1996]. A method and a

process for developing a soft artificial hand similar to a real human hand for the soft actuator which was a pneumatic artificial muscle were used. Actuator was called the "Mckibben artificial muscle". The Mckibben artificial muscle was a pneumatic actuator having spring-like characteristics, physical flexibility and light weight mostly suitable for robotic applications such as the control of an artificial hand [Lee and Shimoyama, 1996]. Amputees could frequently choose to utilize more than one type of prosthesis as part of their daily life. For example, a person may wear a myoelectric system for most activities, or utilize a body-powered system for heavy-duty or wet tasks [Finat et al., 1998]. The development of a sensor for detecting human muscle contraction, which captured myoelectric signals, in order to control a myoelectric prosthesis of superior limb was realized. This analysis of the signal was carried out through software running in a microcontroller to decide opening or closing of the artificial hand. New functions (for example, if the hand is open, close, and semi-close, etc.) could also be added with a simple alteration in the microcontroller program without any hardware alterations [Fermo et al., 2000]. New state functions (for example, if the hand is open, close, and semi-close, etc.) could be easily added to the prosthesis with a simple alteration in the microcontroller program, without any hardware alteration. It proposes a strategy for controlling the artificial hand based on the myoelectric signal and using a motor that derives the prosthesis mechanisms. This way the patient had a more accurate and easier control of the movement of the prosthetic device thus leading to a faster adaptation. Through a control strategy method to analyze the myoelectric signal can be defined. Thus, several kinds of actuating of the artificial hand can be obtained by a simple binary signal or through the analysis of the myoelectric signal. A new approach for controlling the prosthetic hand-torque control of each joint was studied. This joint torque was estimated from EMG signals using artificial neural network. The learning system was based on feedback error learning scheme [Morita et al., 2001]. Electrical prosthetic hands were developed for patients, which would fit according to their body shape [Saito et al., 2005]. A model for predicting force production about the elbow using recorded SEMG was developed. In this model the parameters were derived from the SEMG data. An estimated parameter used in this model was the relative cross sectional area of each muscle. This model consists of three basic blocks: the signal processing block, the moment / angle relation and the moment / angular velocity relation. In the signal processing block, the RMS value of the recorded SEMG was calculated since the

RMS value represents an estimate of the SEMG power and little calculation was required. The recorded SEMG was also appropriately scaled using the muscle serial cross sectional area [Bouchard et al., 1999]. Conventional prostheses have a simple electronic controller, guided solely by the visual feedback to the operator. A Southampton hand controller developed was based using a microprocessor where information about the forces, points of contact, the shape of the object and whether the object was slipping was used to create a secure grasp. There were touches and slip sensors in each of the fingertips and the controller was in the electronics package on the side of the hand. In the Southampton Hand control scheme, the hand starts PARKed, with the processor in a power down-state. Contraction of command muscles on the forearm caused the hand to move into the POSITION state from where the controller progresses round in a clockwise direction as dictated by user input via the arm muscles or contact with the target object [Kyberd, 2000]. The first prototype of a five-fingered prosthetic hand and the first attempt to control this mechanism was introduced. The mechanism had twenty degrees of freedom and is actuated by only three motors. The neural network (feed forward with back propagation training) was used to recognize the type of grasp [Zajdlik, 2006]. It was hoped that these results will serve as a foundation from which to encourage further investigation into more intuitive method for SEMG.

The elbow joint is one of the most important joints as it forms an integral part of almost all arm movements in day to day activities [Bouchard, 1999]. Many prototypes are being developed by researchers to improve degree of freedom and simplicity as-if natural arm [Saridis et al., 1982; Kuribayashi et al., 1992; Patterson and Katz, 1992; Merletti and Lo Conte, 1995; Doringer and Hogan, 1995; Jarc et al., 2006; Casolo et al., 2008]. A prototype of a self-contained above-elbow prosthesis which had electric-powered wrist and elbow joints controlled by an Intel 8751 microcomputer was developed. This technique was used to control the positioning of above elbow prosthesis using the motion of the intact shoulder [Gibbons et al., 1987]. Myoelectric signal (MES) data from remnant muscles in residual upper limbs and analogous intact muscles of thirty-two upper-limb deficient subjects were obtained. Spectral parameters (mean frequency, median frequency, and equivalent statistical bandwidth) of the MES were calculated and examined for significant differences between the remnant muscle data and intact muscle data. Other factors were examined for possible significant effect on the spectral content of the MES. Although no pattern of spectral

difference between the MES of residual versus intact limb muscles was found, spectral differences were apparent by visual inspection in most cases [O'Neill et al., 1994].

Practical technique for the design and evaluation of elbow prostheses was developed for use in a laboratory environment and issues were well explained [Abul-Haj et al., 1987]. Myoelectric control system designs were developed for upper arm prostheses based on the signal characteristics of intact muscles of non-amputees [Patricia et al., 1994; Zardoshti-Kermani et al., 1995; Al-Assaf et al., 2006]. Myoelectric prosthesis is much appreciated for their easiness in controlling the movements and for the absence of wires and braces [Ryait et al., 2009; Joshi et al., 2009]. Differences in pattern of SEMGs must be detected for various arm functions (i.e. elbow bending, elbow extension, wrist pronation, wrist supination, grasp, etc.) taken at one or several stump muscles. Similarly, parallel to the research of prosthesis interfaces, improved functional artificial hands were investigated to provide adaptive grasps using low number of actuators [Ishikawa et al., 2000; Light et al., 2001; Schulz et al., 2001; Schulz et al., 2005]. Innovative exoskeletons for the elbow require a strong collaboration between robotics and neuroscience. The robotic system was coupled to the human user and the exoskeleton design based on the human model in terms of biomechanics, control and learning strategies [Kiguchi et al., 2001; Cattin et al., 2003; Pau et al., 2010]. New approaches for classification of electromyography of the flexion and extension signals were introduced by the researchers. Multivariate autoregressive model was applied to a two-channel set of SEMG signals from the biceps and triceps muscles during flexion and extension positions of the elbow. The coefficients were used to define the strength of the direction of the signals flow between the channels. The classification was demonstrated was limited for two dimensional features. A multichannel setup enables more accurate estimation of the movement [Latif et al., 2008]. In an investigation, the use of the orthogonal method for elbow induced wrist force estimation was done while arm motion was restricted to elbow extension and flexion in horizontal plane and under three operating conditions: isometric, isotonic and light load. These results were evaluated with different nonlinear basis functions. The EMG electrodes were attached to the bicep brachii proximal to the elbow, tricep brachii long head and brachioradialis muscles [Kitamura et al., 2006; Mobasser et al., 2007]. An actuated artificial elbow prosthesis (robotic

elbow prosthesis) for human forearm motion assist that integrated a human and a robot into one system and performed as a joint assertive device for the elderly or physically disabled persons was developed. An example of implantable joint actuator with angular position sensor as an actuated artificial joint was proposed. This elbow prosthesis was supposed to be implanted inside of the human arm by elbow arthroplasty and to acts as an inner skeleton power assist robot [Kundu, and Kiguchi, 2007].

Acquiring SEMG signal for analysis can be done by using bio-potential acquisition systems such as DELSYS BAGNOLI-2, EMG sensor system using PCMCIA data acquisition card (NI DAQ PCI-6010) [Xiang, 2007]. Voluntary muscle activity can be successfully detected by a laboratory set-up using appropriate filter algorithms [Schauer et al., 2004]. Methodological problems related to FFT based techniques for the estimation of spectral parameters of the surface myoelectric signal remained challenges in this field [Merlettit et al., 1989; Reaz, 2006]. Techniques for determining the median frequency of an SEMG signal on line and in real time were the attractive developments [Stulen and De Luca, 1981; Micera et al., 2010]. The modern spectrum analysis uses various biomedical signal processing techniques and power spectrum estimates of SEMGs [Lindstrom et al., 1977; Ogino el.at, 1983; Micera et al., 2010]. Performance of various SEMG signal analysis along with hardware implementations encouraged SEMG applications related to prosthetic hand and human computer interactions [Shahid et al., 2005]. Many studies represent the electromyogram of a single motor unit by considering it as a time function determined by a convolution integral where a point process input passes through a filter whose impulse response was the shape of a single motor unit action potential [Agarwal et al., 1975; Micera et al., 2010]. Different patterns of time-frequency distribution of the myoelectric signals were observed in different biomechanical phases of the movement [Bonato et al., 1996]. Mathematical models include time-frequency approaches, Fourier transform, Wigner-Ville Distribution, statistical measures and higher-order statistics. AI approaches towards signal recognition include Artificial Neural Networks, dynamic recurrent neural networks, and fuzzy logic system. Genetic Algorithm has also been applied in evolvable hardware chip for the mapping of SEMG inputs to desired hand actions [Reaz, 2006; Micera et al., 2010].

The prosthesis should not only duplicate the human hand in shape, functionality, sensorization, perception and sense of body-belonging but it should also be controlled as the natural one in the most intuitive and undemanding way.

Myoelectric prosthesis control is difficult to achieve because of the challenging problems in optimal selection of features, extracted from a myoelectric signal. Dimensionality reduction strategies can be categorized into feature selection and feature projection methods according to desired movements. Dimensionality reduction means to retain myoelectric information, that is important for discrimination and to discard irrelevant data. "Guilin Hills Selection Method" showed a statistical cluster analysis technique with the goal to control electrically powered upper limb prostheses with a minimum number of sensors and a low-power processor [Buchenrieder, 2007]. This method distinguished four hand-positions from myoelectric signals with two sensors. This method also suggested feature combinations that lead to less robust classifications but required fewer sensors. In another work, Principal Components Analysis (PCA) based algorithm was used to drive a 16 DoFs under-actuated prosthetic hand prototype (called CyberHand) with a two dimensional control input, in order to perform the three prehensile forms mostly used in activities of daily living. Principal Components set was derived directly from the artificial hand by collecting its sensory data while performing 50 different grasps and subsequently used for control [Matrone et al., 2010]. A 15 channels of surface myoelectric signal was used to collect data but confirmed that only three channels are needed to provide excellent pattern recognition-based myoelectric control systems (97% classification accuracy on average), provided the channels are chosen carefully. It was noted that there was a slight drop in classification accuracy when increasing channels. One explanation given for classification accuracy degradation was when adding channels there was some loss of useful data during the PCA (for the 15 channel input case). A second explanation given was that adding additional channels to the data increases the complexity of the feature set. PCA assumes that the variance in the data corresponds to good feature clustering. It was observed that PCA is suitable for data with a low number of channels [Hargrove et al., 2007]. If adding additional channels to the data changes the feature cluster to a complex shape then performance of the PCA will be degraded.

This encourages the present investigation for the use of PCA for establishing number of channels w.r.t. limb/arm movements for an elbow prosthetic. Functionality,

controllability and cosmetics are the key issues to be addressed in order to accomplish a successful functional substitution of the human hand by means of prosthesis.

1.4.2 India

Most of the theoretical studies relating the SEMG to muscular force suggested that the amplitude of the SEMG should increase proportionately with the square root of the tension. It has linear relationship. Variations in action potential magnitudes and firing frequency have not been taken into account. Mathematical correlations were incorporated in a model, the linearity between the SEMG and the muscular force was greatly improved [Ray and Guha, 1983]. A comprehensive technique to identify single motor unit (SMU) potentials and to decompose from electromyographic signals into their constituent SMU potentials was developed. This technique was based on one-channel SEMG recordings and was implemented for many clinical SEMG tests [Fang et al., 1999]. Electromyography signals in the operation of devices external to the human body. It finds numerous applications requiring good precision, quick response, design flexibility and ease in control. A variety of myoelectric controller algorithms exist but there is immense scope for optimization. An intelligent system was proposed which was capable of optimizing the system speed and the number of actions that can be selected. Such an optimization involves rigorous mathematical analysis. The intelligent system monitors the actions performed [Venkataramanan et al., 2004]. A control strategy for below-elbow prosthesis was presented. The neural network has been used for the classification. Further, the criteria for the modification of the stored pattern have been made bi-directional and the matching criteria have been designed for bit-by-bit matching [Arora, 2007].

1.5 Objectives of the present work

The following are the objectives of the present work:

1. Study of various methodologies and algorithms for SEMG signal analysis to control myoelectric arm
2. A comparative study on the analysis of SEMG signal based on different postures/movements of arm.

3. To develop more powerful, flexible, and efficient SEMG signal interpretation with the locations of electrodes on different acupressure points of human arm i.e. from shoulder to wrist.

4. Development of a control methodology to use myoelectric signals from muscles which act in synergy with hand function as the control signals to operate the prosthesis.

5. On the basis of above studies, development of a prototype model for realization of control methodology for elbow movement.

1.6 Organisation of the thesis

The thesis consists of seven chapters. Chapter 1 deals with brief description of background of SEMG, the need for prosthetic devices and objectives of the present investigation. Chapter 2 elaborates the physiological description of generation and detection of SEMG signals, followed by an overview of human arm anatomy. Chapter 3 provides details of implementation of single/multi-channel SEMG acquisition system. This chapter further discusses the PC based acquisition process using Matlab along with programming concepts and functions/parameters. Various SEMG parameters were considered for characterization of the signal. These SEMG parameters, had been experimented with variable force exerted by the muscles of above-elbow and below elbow, are discussed. Chapter 4 includes the description of selective acupressure points and SEMG signal activities at these points. In Chapter 5 the analysis has been done on the SEMG signals from six locations on arm for four movements of hand taken from three male subjects. To understand the optimum requirement of number of channels for such interpretations principal component analysis was used. Chapter 6 discusses SEMG analysis on the elbow movement for the four operations [extension, flexion, supination and pronation] which results in control methodology for single-channel and two-channel prototype elbow. A prototype elbow based on SEMG analysis for the above elbow has been discussed using microcontroller based hardware. A study with an amputee is also included. Chapter 7 gives conclusion and future recommendation of the present research work.

CHAPTER 2

PHYSIOLOGY OF SURFACE ELECTROMYOGRAPHIC SIGNAL (SEMG)

This chapter elaborates the historical development of the SEMG, ionic pump which mobilizes the muscles, details of anatomy of human arm and elbow *w.r.t.* specific movements and in the end different mathematical modeling of SEMG are accumulated to draw SEMG properties for proper organization of the work.

Dutch anatomist and biologist, Jan Swammerdam (1637-1680) discovered that stroking the innervating nerve of the frog's muscles gastrocnemius generated a contraction. Alessandro Volta (1745-1827) developed a device which produced electricity, which could be used to stimulate muscles. Luigi Galvani (1791) credited as the father of neurophysiology for his similar work with frogs' legs and showed that electrical stimulation of muscular tissue produces contraction and force. Carlo Matteucci in 1838 showed that bioelectricity is connected with muscular contraction and again in 1842 demonstrated the existence of the action potential accompanying a frog's muscle. Emil Du Bois-Reymond (1818-1896) in 1848 detected electrical activity in voluntary muscle contractions of man. He had placed subject's fingers in saline solution with removed skin to reduce transfer resistance and detected signal through electrodes connected to galvanometer when subjects contracted muscles. Herbert Jasper (1906-1999) in 1942 constructed the first electromyograph at McGill University (Montreal Neurological Institute). He also created a unipolar needle electrode and used his instruments to perform groundbreaking work with epilepsy and neurology. SEMG technologies are due to the efforts by many such researches and still needed to be explored.

2.1 Human bio-signals

The simple example of biomedical signal is body temperature. Its importance and valued in the assessment of fever of an ill patient, is an example of a biomedical signal application. There are many more bio-medical signals in the human body which can give us the significance for monitoring the health conditions. Many signals are present in normal human beings which brain generates to control body

movements. Interpretation, decomposition and application of biological signals and other forms of bioelectrical manifestations of physiopathological events needed to be decoded. Bioelectrical signal means a collective electrical signal acquired from any organ that represents a physical variable of interest. Extracting the information contained in these signals is a tempting task that many engineers and physiologists undertake with pleasure and determination a challenge that is difficult to resist. Some of those kinds of signals are: the electrocardiogram (ECG), the electromyogram (EMG) and the electroencephalogram (EEG).

EMG is the study of muscle electrical signals. EMG is sometimes referred to as myoelectric activity. Muscle tissue conducts electrical potentials similar to the way nerves do known as muscle action potential. Surface EMG (SEMG) is a method of recording the information present in these muscle action potentials from the skin surface. This signal is normally a function of time and is describable in terms of its amplitude, frequency and phase. The SEMG signal measures electrical currents generated in muscles during its contraction representing neuromuscular activities. The nervous system always controls the muscle activity (contraction/relaxation). SEMG signal is a complicated signal, which is controlled by the nervous system and is dependent on the anatomical and physiological properties of muscles as shown in Fig. 2.1[*Kyberd, 2000*]. Fig.2.1 shows the time and frequency variations in SEMG. SEMG signal acquires noise while traveling through different tissues. Moreover, the SEMG detector, particularly if it is at the surface of the skin, collects signals from different motor units at a time which may generate interaction of different signals. The action potential is the electrical signal that accompanies the mechanical contraction of a single cell when stimulated by an electrical current (neural or external) as shown in Fig. 2.2 [*Farnsworth, 2004*]. It is caused by the flow of sodium (Na^+), potassium (K^+), chloride (Cl^-), and other ions across the cell membrane. The action potential is the basic component of all bioelectrical signals. Nerve and muscle cells are encased in a semi-permeable membrane that permits selected substances to pass through while others are kept out. Body fluids surrounding cells are conductive solutions containing charged atoms known as ions. In their resting state, membranes of excitable cells readily permit the entry of K^+ and Cl^- ions, but effectively block the entry of Na^+ ions (as the permeability for K^+ is 50-100 times that for Na^+). The inability of Na^+ to penetrate a cell membrane results in the following:

- Na^+ concentration inside the cell is less than that outside. So, the outside of the cell is more positive than the inside of the cell.
- To balance the charge, additional K^+ ions enter the cell, causing higher K^+ concentration inside the cell than outside.
- Charge balance cannot be reached due to differences in membrane permeability for the various ions.

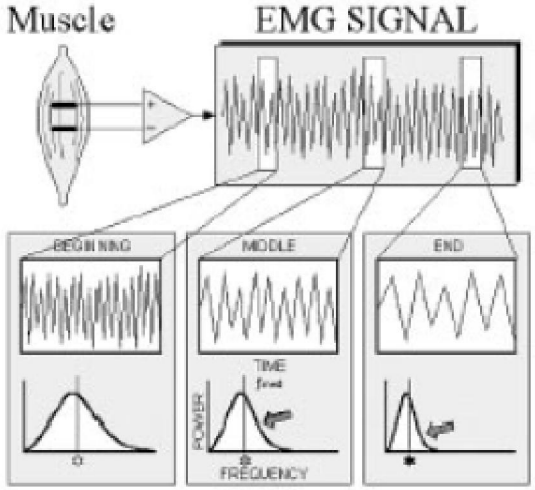

Fig. 2.1 Spectral modification which occurs in the EMG signal during sustained contractions [*Kyberd, 2000*]

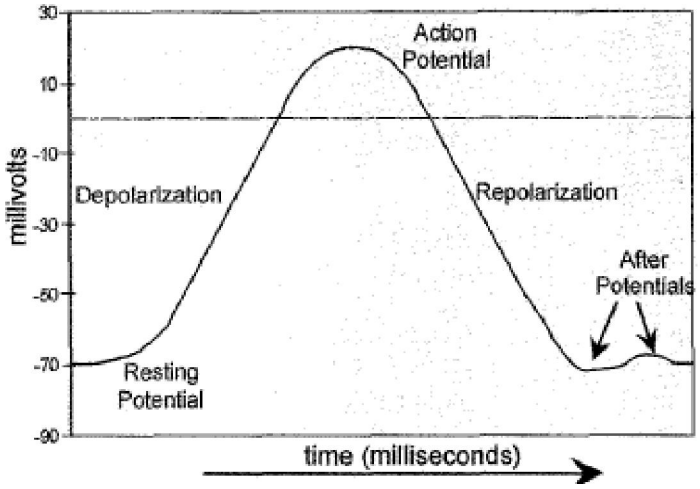

Fig. 2.2 Typical waveform of an action potential [*Farnsworth, 2004*]

A state of equilibrium is established with a potential difference, with the inside of the cell being negative with respect to the outside. A cell in its resting state is said to be

polarized. Most cells maintain a resting potential of the order of – 60 to -100 mV until some disturbance or stimulus upsets the equilibrium.

When a cell is excited by ionic currents or an external stimulus, the membrane changes its characteristics and begins to allow Na^+ ions to enter the cell. This movement of Na^+ ions constitutes an ionic current, which further reduces the membrane barrier to Na^+ ions. This leads to an avalanche effect: Na^+ ions rush into the cell. K^+ ions try to leave the cell as they were in higher concentration inside the cell in the preceding resting state, but cannot move as fast as the Na^+ ions. The net result is that the inside of the cell becomes positive with respect to the outside due to an imbalance of K^+ ions. A new state of equilibrium is reached after the rush of Na^+ ions stops. This change represents the beginning of the action potential, with a peak value of about +20 mV for most cells.

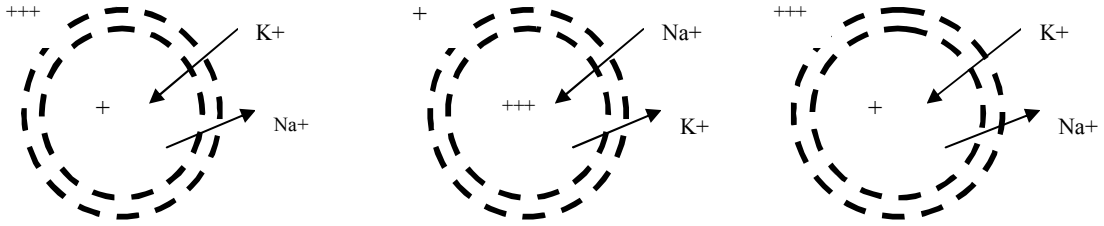

Fig. 2.3 (a) Resting state **(b) Depolarization** **(c) Repolarization**

An excited cell displaying an action potential is said to be depolarized, the process is called depolarization. After a certain period of being in the depolarized state the cell becomes polarized again and returns to its resting potential via a process known as repolarization. Membrane depolarization, while increasing the permeability for Na^+ ions, also increases the permeability of the membrane for K^+ ions via a specific class of ion channels known as voltage-dependent K^+ channels. The key to the mechanism for repolarization lies in the time-dependence and voltage-dependence of the membrane permeability changes for K^+ ions compared with that for Na^+ ions. The permeability changes for K^+ during depolarization occur considerably more slowly than those for Na^+ ions, hence the initial depolarization is caused by an inrush of Na^+ ions. However, the membrane permeability changes for Na^+ spontaneously decrease near the peak of the depolarization, whereas those for K^+ ions are beginning to increase. During repolarization, the predominant membrane permeability is for K^+ ions, because K^+ concentration is much higher inside the cell than outside, there is a

net efflux of K^+ from the cell, which makes the inside more negative thereby effecting repolarization back to the resting potential. The voltage-dependent K^+ permeability change is due to a distinctly different class of ion channels than those that are responsible for setting the resting potential.

A mechanism known as the Na^+ - K^+ pump extrudes Na^+ ions in exchange for transporting K^+ ions back into the cell. This transport mechanism carries very little current in comparison with ion channels, and makes a minor contribution to the repolarization process. Na^+ - K^+ pump is essential for resetting the Na^+ and K^+ balance of the cell, but the process occurs on a longer time scale than the duration of an action potential. Nerve and muscle cells repolarize rapidly, with action potential duration of about 1ms. Fig. 2.3 demonstrates the cell mechanism of Na^+ -K^+ pump during action potential [*Bruce, 1999*]

The action potential is always the same for a given cell, regardless of the method of excitation or the intensity of the stimulus beyond a threshold: this is known as the all-or-none or all-or-nothing phenomenon. After an action potential, there is a period during which a cell cannot respond to any new stimulus, known as the absolute refractory period (about 1ms in nerve cells).

2.1.1 Propagation of an action potential

Once initiated by a stimulus, the action potential propagates along the whole length of a fiber without decrease in amplitude by progressive depolarization of the membrane as shown in Fig. 2.4 [*Alberts et al., 1998]*. Current flows from a depolarized region through the intra-cellular fluid to adjacent inactive regions, thereby depolarizing them. Current also flows through the extra-cellular fluids, through the depolarized membrane, and back into the intra-cellular space, completing the local circuit. The energy to maintain conduction is supplied by the fiber itself. Axons often have an insulating sheath that lets nerve impulses travel faster. This sheath is made of a fatty substance called myelin, which consists of glial cell membranes wrapped around the axon as shown in Fig. 2.5. The myelin of the neurons in the brain is composed of oligodendrocytes, while that of the neurons in the peripheral nervous system is composed of Schwann cells. The myelin sheath does not cover the entire axon; it leaves small sections uncovered. These small exposed sections are called nodes of Ranvier. They are spaced from 0.2 to 2 millimeters apart. The reason that the myelin

sheath speeds up neural conduction is that the action potentials literally jump from one node of Ranvier to the next. In fact, these nodes are the only places where the ion exchanges that generate the action potential can take place. This process is called saltatory conduction (from the Latin saltare, meaning "to jump"), as opposed to the much slower, continuous propagation that occurs in non-myelinated axons. In this way the information in the form of chemical ions flows in the human body.

In many ways the action potential is not the movement of voltage or ions but the flow of these ion channels opening and closing moving down the axon. This movement of the ion channels explains why the action potential is slow relative to the normal flow of electricity. The normal flow electricity is the flow of electrons in an electrical field and electricity travels at the speed of light while these ion channels movement is considerably more slowly. These are mechanical movements and cannot move nearly at the speed of light. The nerve cell in the spinal cord gets excited which causes an electrical signal, or action potential, to move down the axon of the nerve cell (*i.e.* the axon that travels down the arm from the spinal cord). Once the action potential reaches the axon terminal, neurotransmitters are released and travel through the synaptic cleft (the space between the axon terminal of the nerve cell in the spinal cord and the receptors on the muscle cell) to neurotransmitter receptors on the muscle cell. The neurotransmitters and neurotransmitter receptors bind, which causes the muscle cell to get very excited. Once the muscle cell is excited then the muscle contracts (or moves) as shown in the Fig. 2.6 [*Beals et al., 1999*].

The nervous system depends on neurons working together to transmit signals. Neurons are special cells that have plasma membranes capable of generating and conducting electric impulses. Each neuron is composed of dendrites that collect information from other neurons, a cell body where nerve impulses are initiated, an axon along which impulses are conducted, and axon terminals that synapse with a target cell such as another neuron or muscle tissue.

The electric potential of neurons is responsible for signal transmission. The inside of a neuron generally has an excess of negative charges. When a neuron is unstimulated, the difference in electric charge across the plasma membrane is the resting potential. A neuron is sensitive to physical or chemical changes that cause changes in the resting potential. A sudden and rapid reversal in charge across the membrane is called an action potential. When a neuron is stimulated, the action potential moves along the axon to the axon terminals to the target cell. The post-synaptic membrane of the target

cell integrates the information it receives. In order for the target cell to be stimulated, the stimulus must be greater than the target cell's action potential. Neurotransmitters that affect the membrane bring about an excitatory postsynaptic potential (EPSP). When several EPSP's arrive at the cell body simultaneously, the potential is summed over the number of synaptic knobs, and an action potential may be reached as shown in Fig. 2.7[*Stencel, 1992*].

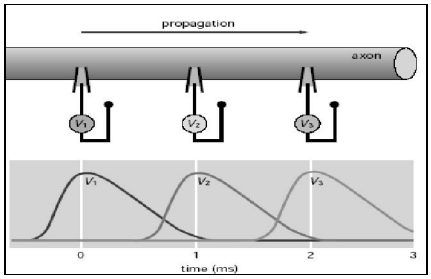

Fig. 2.4 Propagation of an action potential in an axon [*Alberts et.al, 1998]*

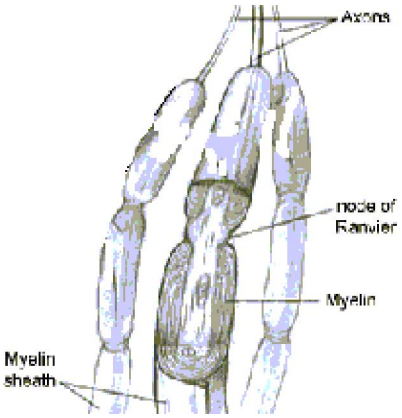

Fig. 2.5 Axon myelination

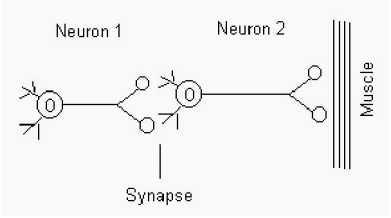

Fig. 2.6 Neurotransmitters and neurotransmitter receptors bind [*Beals et.al, 1999*]

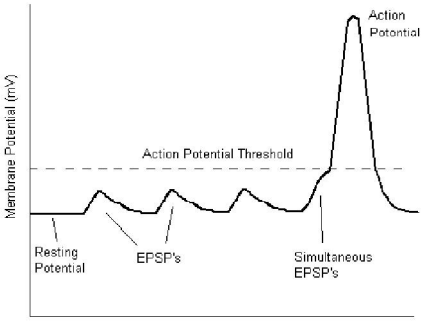

Fig. 2.7 Action Potential with EPSP [*Stencel, 1992*]

2.2 Anatomy of human arm

The human arm is multitalented – its hand can perform powerful grasping tasks as well as delicate ones. The large forceful muscles for the former have their proximal attachments in the arm and forearm in order to achieve the desired angle of pull. They attach to appropriate parts of the hand and wrist by means of long tendons, but their muscle bellies and origins are far from the hand, hence the designation "extrinsic". They run down the forearm and cross the wrist and hand. Some control only the bending or straightening of the wrist. Others influence the movement of the fingers or thumb. Many of these muscles help position and hold the wrist and hand while the thumb and fingers perform fine motor skills. Intrinsic muscles are small and are entirely confined to the region distal to the long bones of the forearm. The intrinsic muscles guide the fine motions of the fingers by getting the fingers positioned and holding them steady during hand activities. The flexors are on the underside of the forearm and the extensors are on the top. The forearm has the convenient dividing line of its two long bones (radius and ulna) and the strong interosseous membrane that connects them. The muscles on the volar side are said to lie in the anterior compartment, and generally flex or pronate the hand. They can be envisioned as being in 3 groups- superficial, middle, and deep [*Online ref.8; Online ref.9; Boyd et al., 1956; Arora, 2002, Netter, 2006; Online ref. 19*].

Extrinsic muscles, anterior compartment (flexor-pronator group) as showed in Fig. 2.8(a) Superficial, (b) Middle and (c) Deep. Muscles on the dorsal side of the interosseous membrane are said to lie in the posterior compartment, and generally extend or supinate the hand. They can be further subdivided according to their actions (acting on the wrist joint, fingers, or thumb).

Posterior compartment (extensor-supinator group) as shown in Fig. 2.9(a) Wrist-level hand motion, (b) Finger motion and (c) Thumb motion. Table 2.1-2.6 explains the functional anatomy of the arm which will help to acquire SEMG for particular movement/posture from a selected electrode site [Online ref.8; *Boyd et al., 1956; Arora, 2002; Netter, 2006; Online ref. 19*].

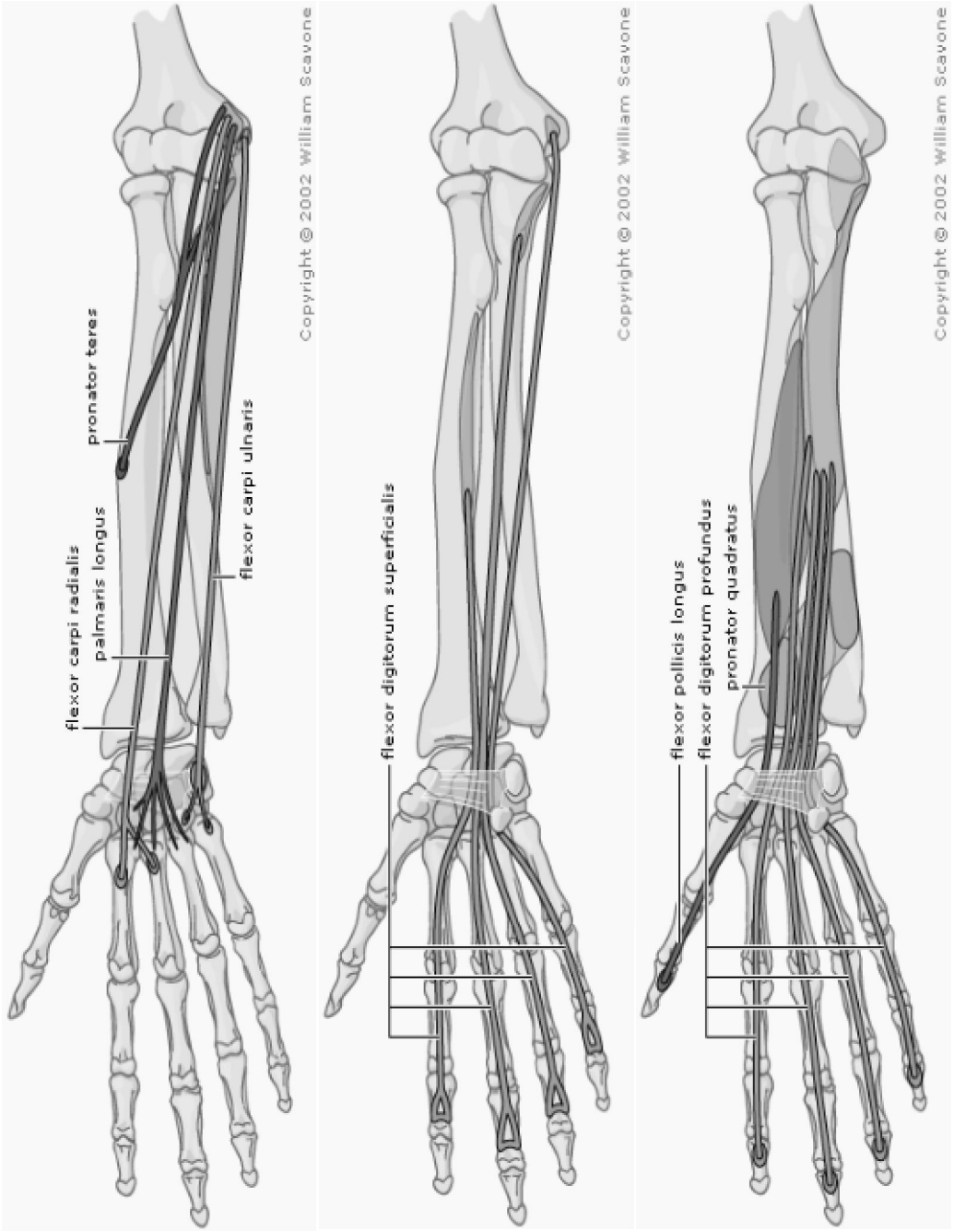

Fig. 2.8 (a) Superficial muscles of the anterior compartment
(b) Middle muscle of the anterior compartment
(c) Deep muscles of the anterior compartment [*Online10*]
Illustrations on this page by William Scavone, MA, CMI
Kestrel Illustration Studio, LLC [http://www.kestrelstudio.com]

Table 2.1
Functionality description of superficial muscles group

Important muscles	Action
Pronator Teres Origin: Humeral head: medial epicondyle, medial supracondylar ridge and medial intermuscular septum Ulnar head: medial border of coronoid process	Pronates forearm and flexes elbow
Flexor Carpi Radialis Origin: Common flexor origin of medial epicondyle of humerus	Flexes and abducts wrist
Palmaris Longus Origin: Common flexor origin of medial epicondyle of humerus	Flexes wrist and tenses palmar aponeurosis
Flexor Carpi Ulnaris Origin: Humeral head: common flexor origin of medial epicondyle. Ulnar head: aponeurosis from medial olecranon and upper three quarters subcutaneous border of ulna	Flexes and adducts wrist. Fixes pisiform during action of hypothenar muscles

Table 2.2
Functionality description of middle muscles group

Important muscles	Action
Flexor Digitorum Superficialis Origin: Humeral head: common flexor origin of medial epicondyle humerus, medial ligament of elbow. Ulnar head: medial border of coronoid process and fibrous arch. Radial head: whole length of anterior oblique line	Flexes proximal interphalangeal joints and secondarily metacarpophalangeal joints and wrist

Table 2.3
Functionality description of deep muscles group

Important muscles	Action
Flexor Pollicis Longus Origin: Anterior surface of radius below anterior oblique line and adjacent interosseous membrane	Flexes distal phalanx of thumb
Flexor Digitorum Profundus Origin: Medial olecranon, upper three quarters of anterior and medial surface of ulna as far round as subcutaneous border and narrow strip of interosseous membrane	Flexes distal interphalangeal joints, then secondarily flexes proximal interphalangeal and metacarpophalangeal joints and wrist
Pronator Quadratus Origin: Lower quarter of anteromedial shaft of ulna	Pronates forearm and maintains ulna and radius opposed

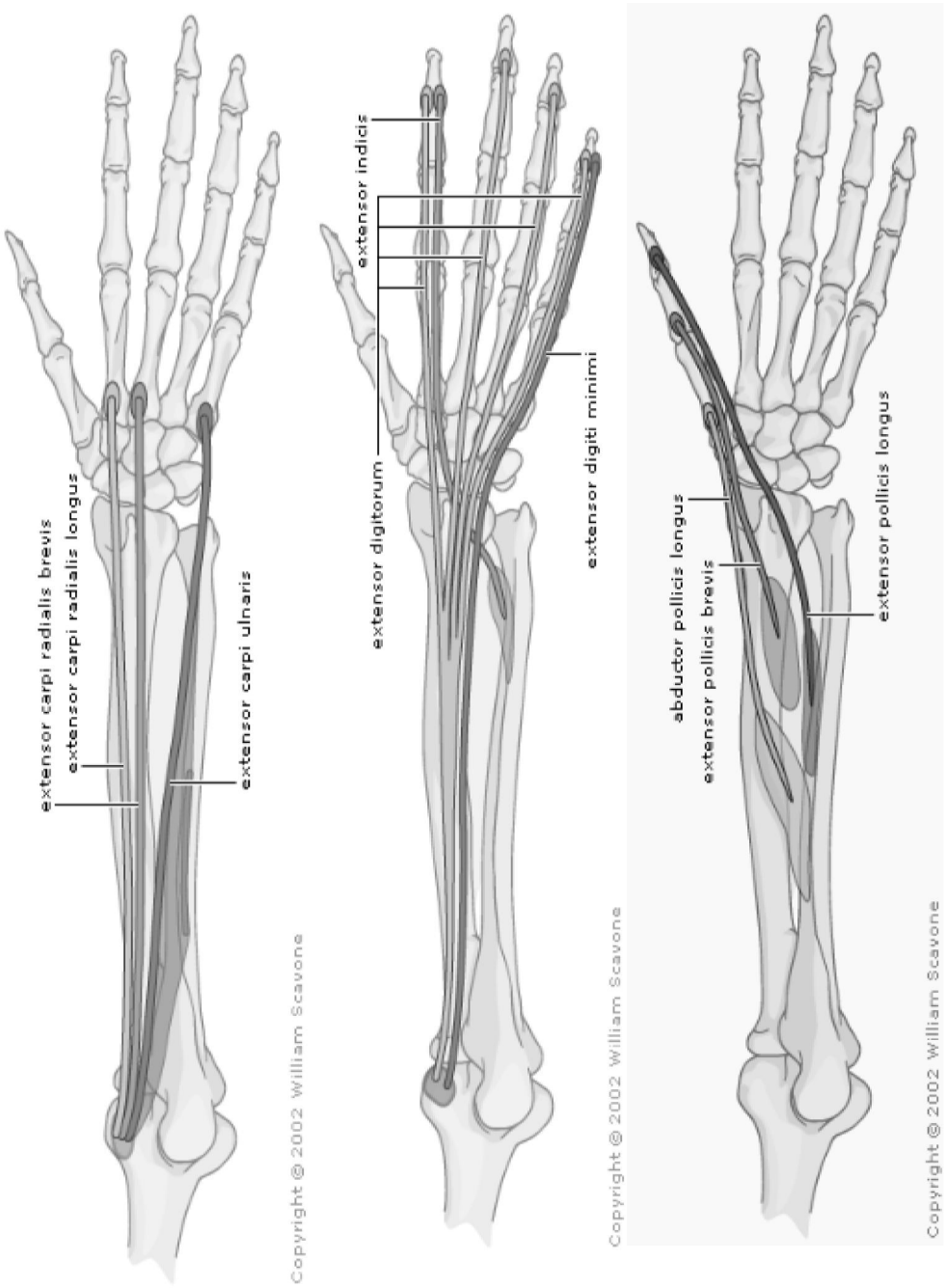

Fig. 2.9 (a) Muscles of the posterior compartment that act on the hand at the wrist joint
(b) Muscles of the posterior compartment that act on the fingers
(c) Muscles of the posterior compartment that act on the thumb [*Online10*]
Illustrations on this page by William Scavone, MA, CMI
Kestrel Illustration Studio, LLC [http://www.kestrelstudio.com]

Table 2.4
Functionality description of wrist/hand motion muscles group

Important muscles	Action
Extensor Carpi Radialis Longus Origin: Lower third of lateral supracondylar ridge of humerus and lateral intermuscular septum	Extends and abducts hand at wrist
Extensor Carpi Radialis Brevis Origin: Common extensor origin on anterior aspect of lateral epicondyle of humerus	Extends and abducts hand at wrist
Extensor Carpi Ulnaris Origin: Common extensor origin on anterior aspect of lateral epicondyle of humerus	Extends and adducts hand at wrist

Table 2.5
Functionality description of fingers motion muscles group

Important muscles	Action
Extensor Digitorum Origin: Common extensor origin on anterior aspect of lateral epicondyle of humerus	Extends all joints of fingers
Extensor Indicis Origin: Lower posterior shaft of ulna (below extensor pollicis longus) and adjacent interosseous membrane	Extends all joints of index finger
Extensor Digiti Minimi Origin: Common extensor origin on anterior aspect of lateral epicondyle of humerus	Extends all joints of little finger

Table 2.6
Functionality description of thumb motion muscles group

Important muscles	Action
Abductor Pollicis Longus Origin: Upper posterior surface of ulna and middle of posterior surface of radius and interosseous membrane	Abducts and extends thumb at carpometacarpal joint
Extensor Pollicis Brevis Origin: Lower third of posterior shaft of radius and adjacent interosseous membrane	Extends metacarpophalangeal joint of thumb
Extensor Pollicis Longus Origin: Middle third of posterior ulna (below abductor pollicis longus) and adjacent interosseous membrane	Extends interphalangeal and metacarpophalangeal joints of thumb

2.2.1 Muscles group for elbow movement

The elbow joint is a complex of three joints that share the same synovial sheath. These are the humeroradial, humeroulnar and superior radioulnar joints. The humeroradial and humeroulnar joints allow flexion and extension at the elbow whilst the superior radioulnar, humeroradial and the more distal inferior radioulnar joints allow the specialized actions of supination and pronation. This action is a rolling of the radius around the ulna that produces an apparent rotation of the wrist around a longitudinal axis. The elbow flexors and extensors can be seen in Fig. 2.10 [*Online ref.11*].

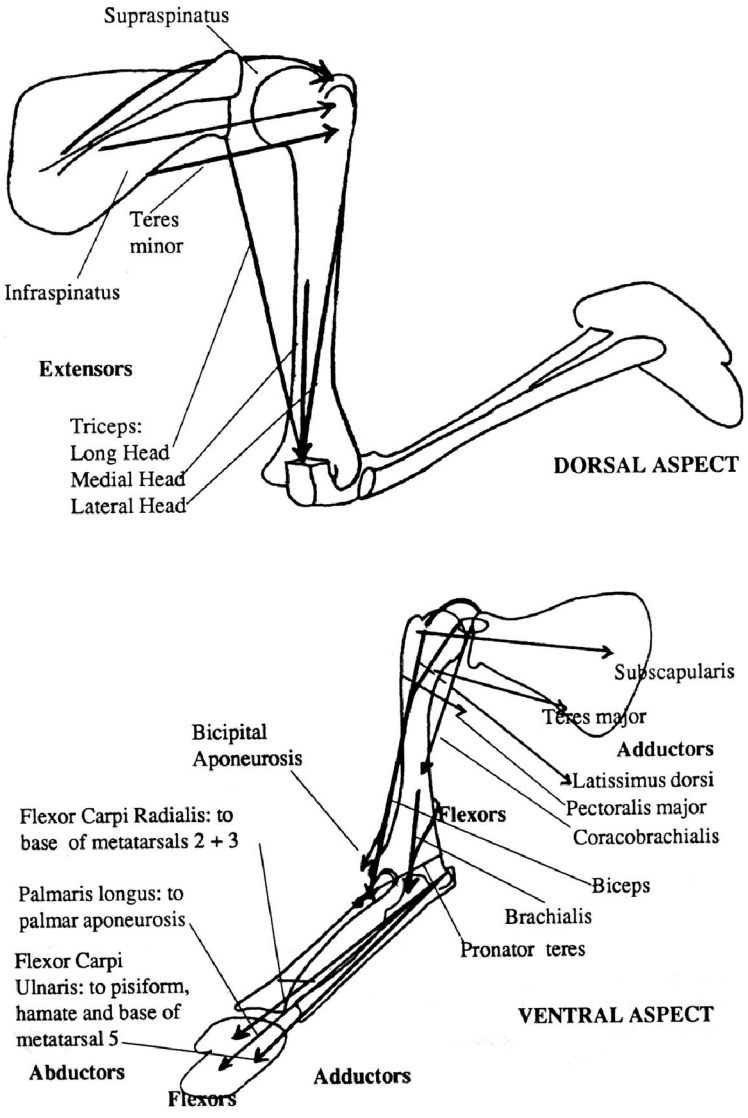

Fig.2.10 Dorsal aspect and Ventral aspect of the arm [*Sellers: Online ref.11***]**

Triceps is the main extensor; brachialis and biceps brachii are the main flexors. Biceps brachii is also a major supinator and this action stops it being an effective flexor of the prorated forearm. The study needed to be carried out in the muscles segments; firstly, muscles act to flex at the elbow, secondly muscles act to extend at the elbow, thirdly muscles that act to pronate and finally muscles act to supinate. Using the anatomy of active muscles helped in finding the location for the placement of electrodes.

Anatomy of arm is divided into the following four groups of muscles as contributing in assisting a particular movement.

2.2.1.1 Muscles that act to flex at the elbow

These groups of muscles include biceps brachii (prime mover), brachialis and brachioradialis. The Brachialis (Fig. 2.11a) is attached to the humerus and ulna. This muscle is only able to move the elbow joint and is always active in any movement of this joint. It lies underneath biceps brachii and is not very obvious externally. When extending the forearm, it stabilizes the movement by slowly relaxing. Biceps brachii (Fig. 2.11b) muscle acts across two joints — the elbow and the shoulder and produces a more complex range of movement than brachialis. Biceps brachii has no attachment to the humerus at all. It attaches to the scapula by two separate tendons so called 'biceps'. Due to these complicated attachments biceps brachii is able to produce a variety of movements. Brachioradialis (Fig. 2.11c) is a muscle of the forearm that acts to flex the forearm at the elbow [*Online ref.8; Online ref.12; Online ref.13, Online ref.19*].

2.2.1.2 Muscles that act to extend at the elbow

The groups of muscles include triceps brachii (prime mover) and anconeus. The Triceps brachii muscle (Fig. 2.11d) is the large muscle on the back of the human upper limb. It is the muscle principally responsible for extension of the elbow joint (*i.e.* straightening of the arm). It is called a three headed muscle because there are three bundles of muscle, each of different origin, joining together at the elbow. The anconeus (Fig. 2.11e) is a small triangular muscle, which lies on the elbow joint and appears to be a continuation of the triceps brachii. It assists in extending the forearm.

2.2.1.3 Muscles that act to pronate the arm

The groups of muscles include pronator teres, pronator quadrates and brachioradialis. The pronator teres is a short muscle connecting the ends of the humerus (upper arm bone) and ulna to the radius (forearm bones). Its function is to rotate the arm toward the inside when the hand is turned so that palm is facing downward [*Online ref.8*].

2.2.1.4 Muscles that act to supinate at the elbow

The groups of muscles include supinator, biceps brachii and brachioradialis. The supinator (Fig. 2.11e) muscle assists Biceps brachii in supinating the hand, which is turning it over so that the palm faces up. To isolate the supinator muscle, supinate the hand whilst extending the elbow as this takes out the biceps muscle [*Online ref.8; Online ref.12; Online ref. 13; Online ref. 19*].

2.3 The Human elbow joint

The elbow joint consists of three bones: the distal humerus, the proximal ulna, and the proximal radius; and three distinct articulations: the humeroulnar, humeroradial, and superior radioulnar joints as seen in Fig. 2.12. While the humeroulnar and humeroradial articulations are distinct from one another, together they form the elbow articulation. The humeroradial articulation exists primarily to assist the superior radioulnar joint. The humeroulnar joint is the main source for bending at the elbow and can be modeled as a hinge joint. In fact, prosthetic elbows are designed as a simple hinge joint. The superior radioulnar joint is mechanically described as a pivot joint with a single axis of motion. The elbow joint complex can be kinematically modeled as two revolute joints: one allowing for flexion/extension (bending) at the elbow and the other for pronation/supination (twisting) of the forearm. The flexion-extension axis is pitched 10-15 from parallel due to the shape of the articulation between the ulna and humerus, known as the “carrying angle”. This angle differs between males and females, where it averages 11 for adult men and 14 for adult women. It also differs between adults and children, where it averages 6 for children [*Goehler, 2007*].

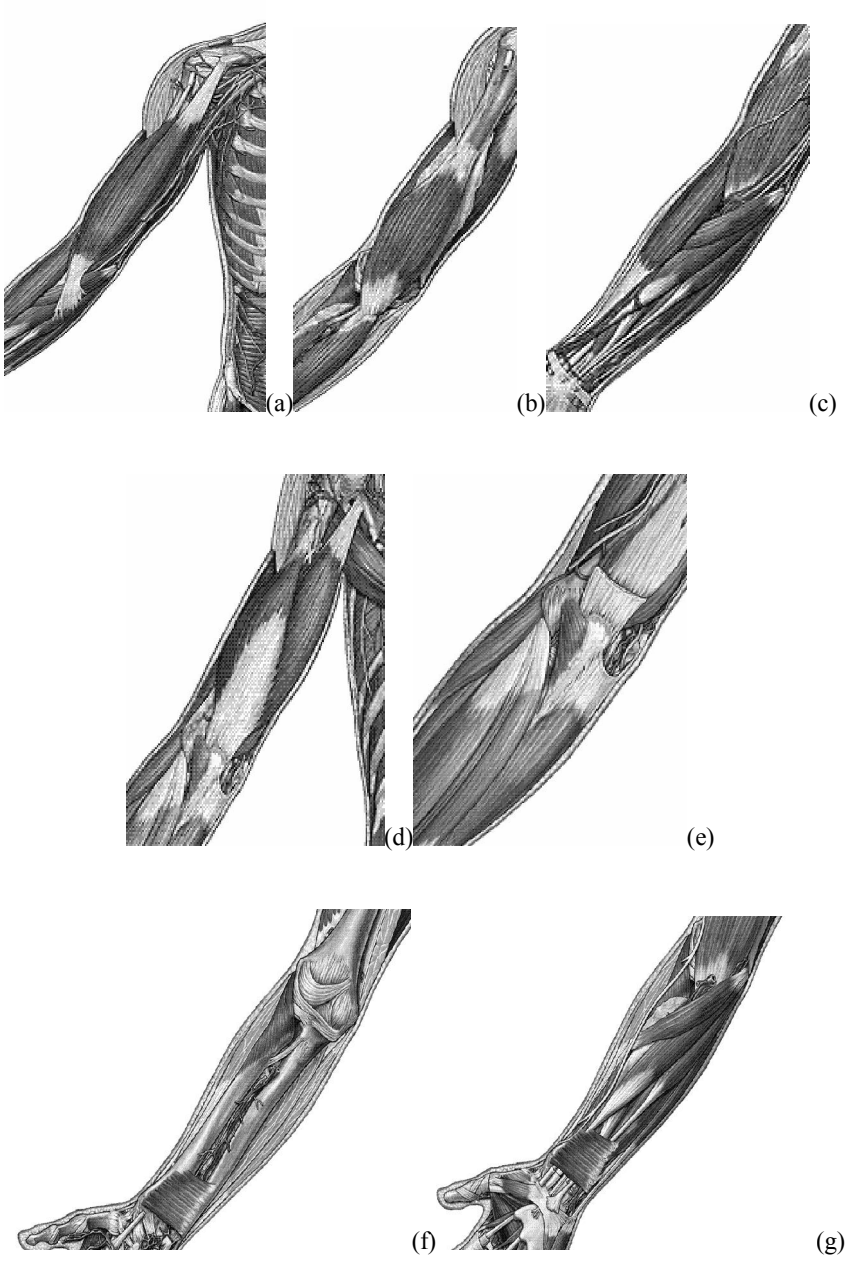

Fig. 2.11 (a) Biceps brachii (b) Brachialis (c) Brachioradialis (d) Triceps brachii (e) Anconeus (f) Supinator (g) Pronator teres & Pronator quadratus
Illustrations by Mary Jo Adams, KNR 181 Anatomy Labs, Horton [*Online ref.14; Online ref.19*]

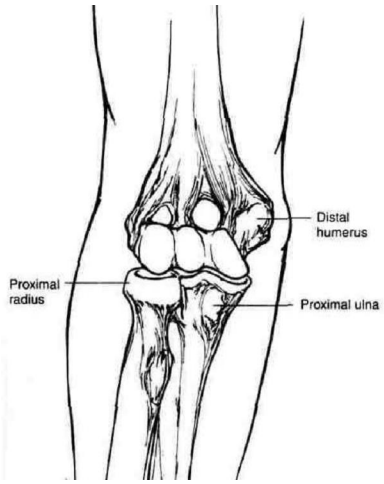

Fig. 2.12 Human elbow joint [*Goehler, 2007*]

2.4 Selection of SEMG locations on arm based on active muscles groups

Anatomical study of muscle groups for both above elbow and below elbow for the movements like flexion/extension/supination/pronation/wrist-up/down helped to demark six locations on below elbow and two on above elbow portion. These selected locations were used for further analysis as per the thesis objectives later in the chapters.

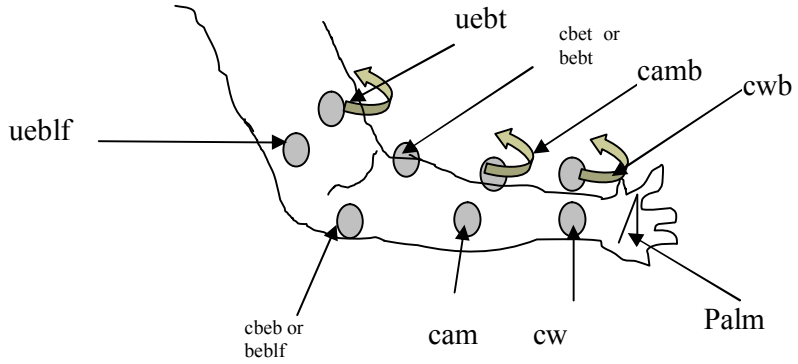

Fig. 2.13 Selective locations for SEMG analysis

For below elbow analysis, locations were prefixed with letter "c" for easy identification. Descriptions of the syntax used [below elbow]➔ cw = on wrist palm side; cwb = on opposite side of the wrist; cam = below arm middle palm side; camb = on opposite side of cam; cbet = below elbow thumb side; cbeb = below elbow little finger side.

Syntax for elbow movements analysis ➔uebt = above elbow thumb side; ueblf = above elbow little finger side; bebt = below elbow thumb side; beblf = below elbow little finger side.

2.5 Mathematical models of SEMG

Recent advances in technologies of signal processing and mathematical models have made it practical to develop advanced SEMG detection and analysis techniques. In 2006 various mathematical techniques and artificial intelligence have received extensive attraction [*Huang et al., 2000*]. Mathematical models include wavelet transform, time-frequency approaches, Fourier transform, Wigner-Ville Distribution, statistical measures and higher-order statistics.

The study of SEMG is becoming more popular for its unique capabilities as described by human-robot interaction and control of prosthetic arms. Human factor studies include the voluntary and non-voluntary (reflex) excitation. It is mentioned that in many applications, such as analysis of sports activities, ergonomic design analysis, or teleoperation of robotic devices, the use of force sensors for the measurement of generated limb forces is impractical or inconvenient. The use of inexpensive and easily portable active electromyogram electrodes and position sensors would be advantageous in these applications compared to the use of force sensors, which are often very expensive and require bulky frames [*Mobasser et al., 2007*]. A human-robot interaction prototype of implantable two DOF inner skeleton robots (*i.e.*, robotic elbow prosthesis) to assist the elbow flexion-extension motion and forearm supination-pronation motion had also designed and developed [*Kundu et al., 1992*]. The robotic prosthesis was controlled based on the activation patterns of the muscles electromyogram signals by applying a fuzzy-neuro control method. The EMG controlled elbow prosthesis can be expected to be an artificial joint for the next generation. To use myoelectric or electromyogram signals as command and/or control signals, it is necessary to process the signal in order to extract the information [*Arora, 2002*].

A number of methods for processing SEMG signals have been used for the purpose of control of limb prosthesis segments of the SEMG signal to preserve information. For the study of developments of prosthesis hand the main sections are SEMG signal properties, mathematical model for explaining the SEMG signal and the design approach for artificial hand. In the present study different types of the statements on SEMG properties and models based on different mathematical facts along with their end equations is recorded. Also, the study on types of controlling methods for artificial hand is described as one form being body - powered terminal devices and other being myoelectric controls type. Mathematical modeling of the

electromyographic signal (EMG) signal is a tool to explore proper methods of muscle activity. It gives the understanding how different physiological and physical factors alter the signal detected at the skin surface.

2.5.1 EMG Model as low pass filter

EMG of a single motor unit can be defined as function of time by a convolution integral [*Agarwal et al., 1975*] as given below:

$e(t) = \int_0^t h(t-\tau)\,p(\tau)\,d\tau$, where p ($\tau$) is series of unit impulses or Dirac delta functions which passes through a filter whose impulse response is h (t) as in Fig. 2.14. The time function h (t) describes the shape of a single motor unit action potential. The Fourier Transform (FT) of equation is E (jω) = H (jω) P (jω), where H (jω) is the FT of the impulse response and P (jω) is the FT of the random pulse train.

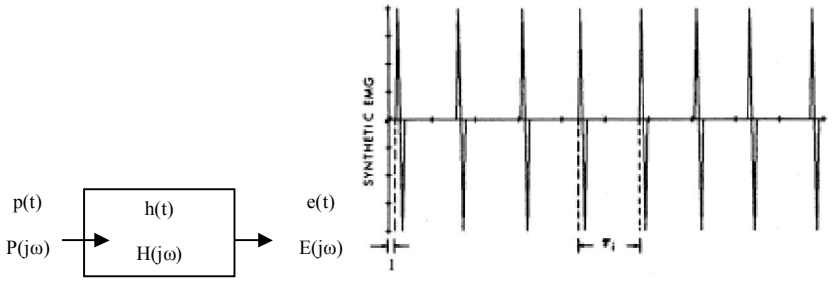

Fig. 2.14 EMG for a single motor unit model as low pass filter [*Agarwal et al., 1975*]

The FT for a train of such pulses from a single unit of this shape is given by:

$$H(j\omega) = \left(\frac{4bj}{c\omega^2}\right) e^{-j\omega c}\left[2\sin\frac{\omega c}{2} - \sin(\omega c)\right]$$

2.5.2 Non-stationary model for the EMG

In this model [*Shwedyk et al., 1977*], neural pulse train inputs were considered which passed through linear, time invariant systems that represented the motor unit action potential (MUAP). Fig. 2.15 shows the EMG signal generation model. The outputs were then summed to produce the EMG. It was assumed that in the production of muscle force, the controlled parameter was the number of active motor units, n (t). The model then showed that the EMG can be represented as an amplitude modulation process of the form EMG = [K n (t)] $^{1/2}$ w (t) with the stochastic process, w (t), having the spectral and probability characteristics of the EMG during a constant contraction.

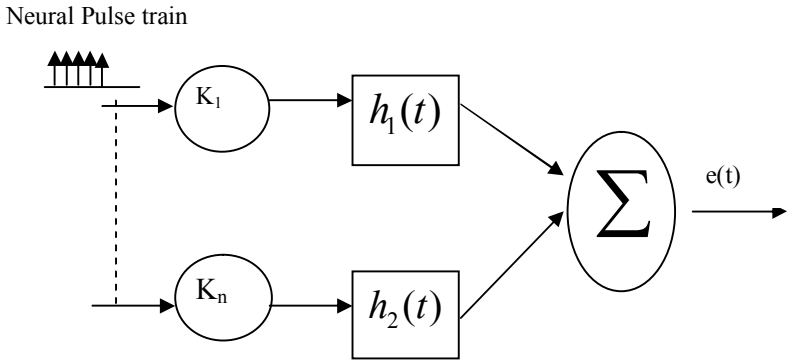

Fig. 2.15 Model for EMG signal generation [*Shwedyk et al., 1977*]

2.5.3 Pseudo-periodic model for myoelectric signal

This model represented that SMES as an infinite train of bursts of activity [*Helal et al., 1989*]. Assuming linearity between MUAP's and the detection site, each burst results from the summation of N MUAP's filtered through low-pass functions:

$$SMES(t) = \sum_{n=-\infty}^{+\infty} \sum_{n=1}^{N} \int_{-\infty}^{+\infty} h_u(t).AMUAP(t - \tau - nT - \xi_n^u) d\tau$$

where, T is the activation period of the muscle, h_u (t) are filter functions between MU'S and the detection site, AMUAP(t) is the average MUAP assumed identical for the N MU'S, ξ_n^u are random delays of MUAP's in each burst, n is the burst index, u is the MU index. SMES (t) is a process of infinite energy. Final result shows that the filter function between $\varphi_{AMUAP}(f)$ and $\varphi_{SMES}(f)$ consists of two characteristic parts, denoted as $W(f)$ and $B(f)$,

2.5.4 Auto-regression model

Auto-regression (AR) modeling has become a common technique for parameterizing linear systems / signals [*Knox et al., 1993*]. The model is based on the linear difference equation for the discrete time signal, $x(n) = \sum_{k=1}^{p} a_k x(n-k) + u(n)$, where the input u (n) is assumed to be white noise. The coefficients, a_k are estimated by a least squares minimization of the estimation error. Auto-regressive coefficients confirmed to be possible features for a pattern recognition scheme for upper limb EMG. Although the EMG signal is not fully stationary, it was taken as-if this signal is sufficiently stationary per each limb function considered to yield AR parameters

whose range of variation with time is adequately small to facilitate discrimination between limb functions [*Graupe et al., 1994*].

2.5.5 Integral pulse frequency and amplitude modulation, IPFAM model

A basic IPFAM model of EMG signals during locomotion was developed [*Zhang et al., 1995*]. The IPFAM model has three main elements: the PFM, the PAM, and the linear system. The PFM describes the variations in the EMG caused by changes in the nerve firing rates, the PAM describes the association of the EMG amplitude with variations in muscular force, and the linear system, p(t), represents the compound motor unit action potential (CMUAP) including the effects of propagation dispersion and tissue filtering. In the IPFAM model, the potential rises until a pre-determined threshold is reached, which causes an action potential or event to occur. With the frequency modulating signal $1+ m_l\cos(2\pi f_p t + \theta)$ and the amplitude modulating signal $A_o+ A_s\cos(2\pi f_s t + \gamma)$, where A_o, is the DC-level, m_l is the modulation depth, A_s is the amplitude, f_p is the PFM modulating frequency, and f_s , is the PAM modulating frequency, the expression of the IPFAM can be derived as: $E(f) = \frac{A_o}{T_o} A(f) + \frac{A_o}{2T_o}\{B(f) + C(f)\}$, where A (f), B (f) and C (f) are the three mentioned functions.

2.5.6 SEMG to force model

Fig. 2.16 shows the block diagram of EMG to force model [*Anctil et al., 1998*]. This model consists of three basic blocks namely the signal processing block, the moment / angle relation and the moment / angular velocity relation. In the signal processing block, the RMS value of the recorded SEMG was calculated. The moment / angle block contains the force / length properties of the individual muscles. These properties were derived from static contractions of the muscles at different angles and loads. The last block consists of two sub blocks: the moment to force conversion and the force /angular velocity relation which describes the force / velocity properties of the muscles. Data were collected under static and dynamic both conditions. In the static case, the subject holds the applied load with a constant elbow angle and the angle was varied from 40 to 130 degrees in intervals of 10 degrees. These measurements were used to determine the moment / angle properties of the muscles. In case of dynamic,

the subject moved the elbow at approximately constant velocity from 40˚ to 130˚ (flexion) and from 130˚ to 40˚ (extension) for different loads.

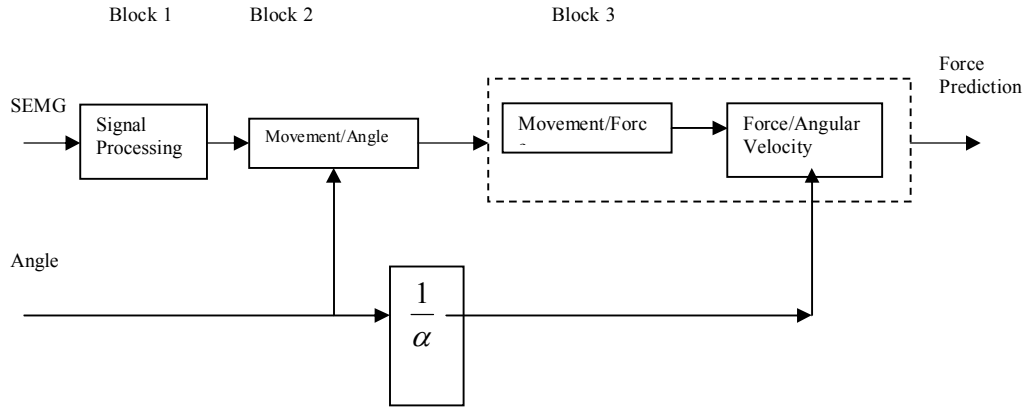

Fig. 2.16 EMG to force model block diagram [*Anctil et al., 1998*]

2.5.7 Dipole model

An efficient new method for modeling surface electrode potentials in which action potential is represented in terms of two oppositely directed dipoles propagating down the fiber [*Anctil and Slawnych, 1998*]. In a dipole model, the current is assumed to be concentrated at two different points along the fiber. Potential φ recorded by a point electrode in response to a source current I located at a distance R using the definition of a partial differential, φ_2 (t) can be expressed as follows:

$$\phi_2(t) = -\delta(\frac{\partial \phi_1}{\partial x}) = \frac{Iz\delta}{4\pi\sigma\sqrt[3]{x^2+y^2+z^2}}, \text{ where } \phi_1(t) = \frac{I}{4\pi\sigma R}$$

σ is the conductivity of the medium. The potential recorded by a surface electrode in terms of a spatial integration of the potential function with respect to the electrode surface A:

$$\phi_{SE}(t) = \frac{1}{A}\int_{-X_e/2}^{X_e/2}\int_{-Z_e/2}^{Z_e/2}\phi_2(t)dz_e dx_e = \frac{I\delta}{4\pi\sigma A}\left(\ln\left(x+\sqrt{x^2+y^2+z^2}\right)\right)\Bigg|_{-Z_e/2}^{Z_e/2}\Bigg|_{-X_e/2}^{X_e/2}$$

Fig. 2.17 shows the comparison of the potentials derived from a single muscle fiber using the discrete point and analytical methods. The potential calculated using the analytical method is illustrated by the heavy lines, and the corresponding discrete point potentials are illustrated by the thinner lines. The number of points used to derive each discrete point potential is indicated to the left of the potentials in a schematic depiction of the surface electrode **[***Anctil and Slawnych, 1998*]. According to this research the relationship between the numbers of points used to define the electrode and the amplitude and inter-peak distance errors. The error values drop to

approximately 5% with an electrode represented by 20 points, and it is less than 1% when the number of points is equal to 100.

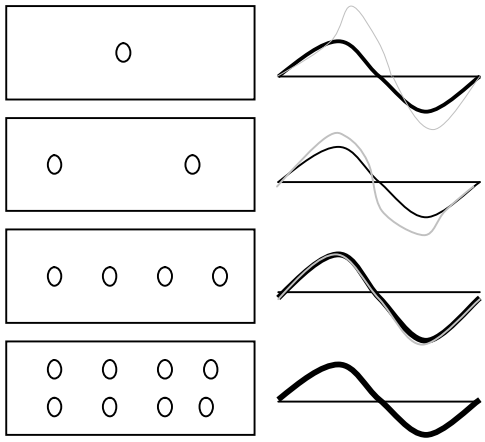

.

Fig. 2.17 Comparison of the potentials derived from a single muscle fiber

[*Anctil and Slawnych, 1998*]

2.6 SEMG Properties

A myoelectric signal or electromyography (EMG), also called a motor action potential, is an electrical impulse that produces contraction of muscle fibers in the body. Myoelectric signals are detected by placing three electrodes on the skin. Normally the EMG is acquired in differential mode. Two electrodes are positioned so there is a voltage between them when a myoelectric signal occurs. The third electrode is placed in a neutral area, and its output is used to cancel the noise that can otherwise interfere with the signals from the other two electrodes. Myoelectric signals have frequencies ranging from a few hertz to about 300 Hz and voltages ranging from approximately 10 μV to 1 mV. A Typical SEMG pattern is shown in Fig.2.18.

Fig. 2.18 Typical SEMG pattern

SEMG is the current state-of-the art technique to control externally-powered prostheses. Electromyogram is an electric manifestation of muscle contractions. SEMG signal collected from surface of the skin a non-invasive bioelectric signal which can be used in different rehabilitation applications and artificial extremities control [*Weir et al., 2003; Khezri, et al., 2007*]. SEMG signal are composed of MUAP generated by the activated motor units. The motor unit is the smallest functional entity of the muscle that can be voluntary activated. It consists of a group of muscle fibers all innervated from the same motor nerve. With increasing muscle force SEMG becomes interferential due to the increase in the number of activated MUAPs recruited at increasing firing rates, making it difficult for the neurophysiologist to distinguish individual MUAP waveforms [*Chauvet et al., 2001*]. The electromyographic signal from upper limb musculature can be used to identify motion commands for the control of an externally powered prosthesis hand [*Hudgins et al., 1993*]. The SEMG decomposition described a new technology for obtaining new parameters of the EMG signal which provide insight into the control of motor units during muscle contractions. Whereas the SEMG signal detected from the muscle is almost exclusively used to relate the amplitude and timing of the muscle excitation to other characteristics of muscle contractions. The new parameters provide information appertaining to the firing rate of motor units, the relationship of firing rates among the concurrently active motor units and the force produced by the muscle among other parameters [*Agarabi et al., 2004*]. SEMG signals are also used as a control signal for prosthetic devices such as prosthetic hands, arms and lower limbs [*Gopura and Kiguchi, 2008*]. In clinical setting, the level of threshold is set empirically so as to prevent cross-talk from another SEMG site interfering with the signal of the site being set-up [*Weir et al., 2003*]. Alternatively, an algorithm can be used to automatically detect onset using a threshold based on the statistics of the measured signal [*Micera et al., 2010*]. SEMG signals acquired from muscles require advanced methods for detection, decomposition, processing, and classification. The various methodologies and algorithms for SEMG signal analysis to provide efficient and effective ways of understanding the signal and its nature was described. The some of the hardware implementations using SEMG focusing on applications related to prosthetic hand control, grasp recognition and human computer interaction were also discussed. This knowledge will help researchers to develop more powerful, flexible, and efficient applications [*Reaz et al., 2006; Micera et al., 2010*].

SEMG property is very important for understanding human body movements. Several investigators have given their opinions relating to SEMG properties as shown in Table 2.7. This study will help us to understand the technical characteristics of SEMG which will help further in developing the acquisition system and prosthetic devices.

Table 2.7

Description of SEMG signal- properties

Author	Description of SEMG Signal Properties
Graupe,1975	EMG signal is a time series model and could be considered stationary over sufficiently short time interval.
De Luca, 1979	The EMG signal stochastic with typical amplitude of 0-6mV. The usable frequency range of 0-600Hz.
Huang *et al.,* 2000	Surface EMG signals are nonlinear and stochastic. They are contributed by the summation of triggered motor units with respect to the measuring electrode location
Kiguchi *et al.,* 2004	The EMG signal (0.01–10 mV, 10–2,000 Hz) is one of the most important biological signals which directly reflect human muscle activities since it is generated when the muscles contract. The EMG is a measure of an integration of electrical potentials from many muscle fibers.
Reaz *et al.,* 2006	The amplitude range of EMG signal is 0-10 mV (+ 5 to -5) prior to amplification. EMG signals acquire noise while traveling through different tissue.
Micera *et al.,* 2010	The amplitude of SEMG without amplification ranges from -5 mV to 5 mV or 0 to 1.5 mV (rms). SEMG bandwidth ranged from 0 Hz to 500 Hz.

Chapter's Summary:

The elaboration in this chapter helps in understanding bio-potential, SEMG properties and muscle anatomy. This will help in developing acquisition system and prosthetic devices.

CHAPTER 3

SEMG SIGNAL ACQUISITION SYSTEM AND METHODOLOGY

This chapter describes the implementation of a cost-effective SEMG amplifier and the SEMG recording methodology using MATLAB is presented. The SEMG amplifier is so planned to be the essential part of the control system of the multifunctional robotic arm.

SEMG exhibits complex behavior with nonlinear dynamic properties. This behavior takes the form of SEMG patterns with different complexities. Still there is a need of behavior analysis in a simplified way to assess the activity of muscles of hand - grip. It is an exceedingly complicated signal which is affected by various factors such as the anatomical and physiological properties of muscles, the control scheme of the peripheral nervous system, as well as the characteristics of the instrumentation for detection and processing [De Luca, 1979; O'Neill, Morin and Scott, 1994; De Luca, 1996; Cram et al., 1998]. Microcontroller bioinstrumentation prototype system as part of the development of an active prosthesis structure that allows the acquisition and the processing of electromyographic signals and other data related to the articulate movement. The information obtained is processed in order to obtain appropriate myoelectric parameters for prosthesis control [Delis et al., 2008; Mangieri et al., 2008].

Many ways for such integrated designs were proposed out of which the less complicated, efficient, mobile and cost-effective was selected for the present investigation. The aim was to develop a system which could be an efficient data acquisition system whereas the same circuit could be used in prosthetic device for SEMG detection. Moreover the set-up should portable so that it could be used at location where subjects desire. Such an experimental set-up was realized to interface with soft-scope of MATLAB using PC-sound card for acquisition via softscope. The development of the setup was to explore an easy technique to store raw SEMG signals, collect SEMG by the specially designed surface bipolar electrodes and to describe the extracted parameters of SEMG signal with the help of the MATLAB/ MS-EXCEL. The emphasis was given on approach of analyze for various parameters like RMS-value, slope of the SEMG wave-shape, standard deviation, variance, etc. for the relationship between electrode location and various arm movements.

3.1 Design of single channel experimental set-up

The basic building blocks of the SEMG signal detection are depicted in Fig. 3.1. The system was used to build a single-channel SEMG experimental set-up consisting of bipolar electrodes, differential amplifier, non-inverting amplifier, filter circuit and isolating interface module. Each is discussed independently below:

3.1.1 Surface electrodes

There are two types of electrodes for obtaining EMG signals, inserted (invasive) electrodes and surface electrodes. The ease of use and lack of pain associated with surface electrodes makes their implementation for this project preferable. Surface electrodes come in many varieties, with most characterized by the number of contacts. Some different types of surface electrodes are monopolar, bipolar, tripolar and multipolar (all of whose geometry is described by there name).

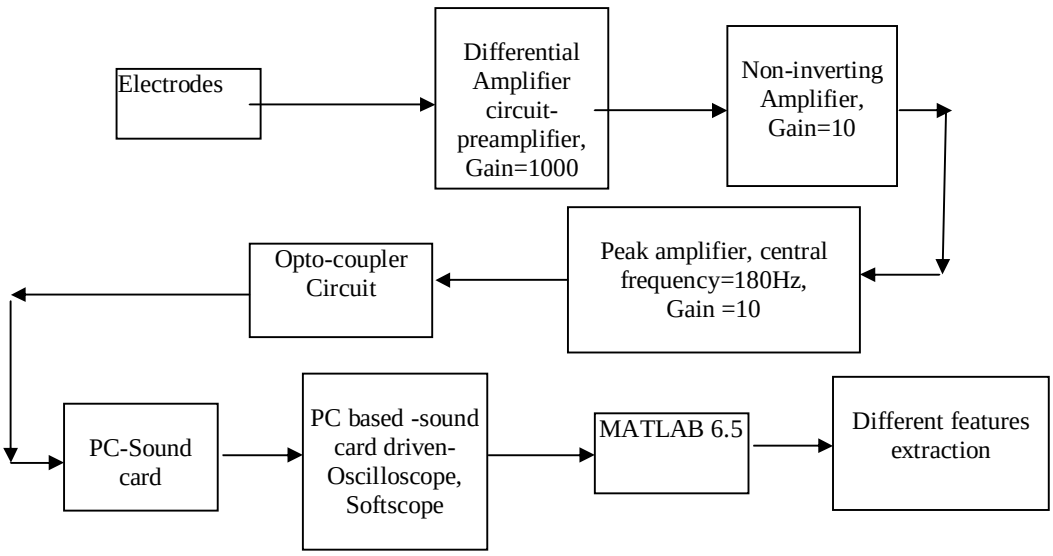

Fig. 3.1 Block diagram of single channel acquisition system

For the purpose of the present investigation a bipolar electrode configuration was used along with a reference electrode in order to implement the differential amplifier. SEMG amplifier was designed to use a skin surface electrode, which was a bipolar electrode. Three Ag-AgCl type electrodes were arranged at the vertices of the equilateral triangle having dimension of one inch, which were placed at distance in order to avoid short circuiting among the electrodes. Electrodes were soldered to a

snap-on and sewed on a piece of plastic as shown in Fig. 3.2. Electrodes were placed firmly to the skin to avoid unstable skin contact by using strap wrapped around the forearm as shown in the Fig. 3.3.

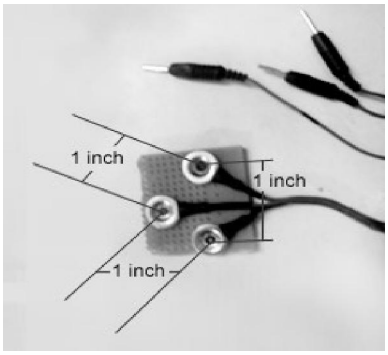

Fig. 3.2 Electrode used

Fig. 3.3 Strap wrapped around the arm with electrodes

The signal was picked up by the electrodes and transmitted to amplifier. Any bipolar electrode readily available in the market can also be used with small alteration in the gain of non-inverting amplifier. The purpose of the non-inverting amplifier was to provide fine tuning of required gain.

With the bipolar electrode the optimal position of the electrodes is parallel to the muscle fibers in order to maximize the probability of proper signal acquisition. Fig. 3.4 shows an example of electrode placements and the resulting potentials. As per figure, the desired position for electrodes is on the belly of the muscle and not on the outer edge of the muscle where other muscles could interfere with the muscle under examination. The spectrum plot describes the location of the electrodes [De Luca, 1997]. For the multifunctional analysis which is the prim objective of the present investigation the placement becomes the vital issue.

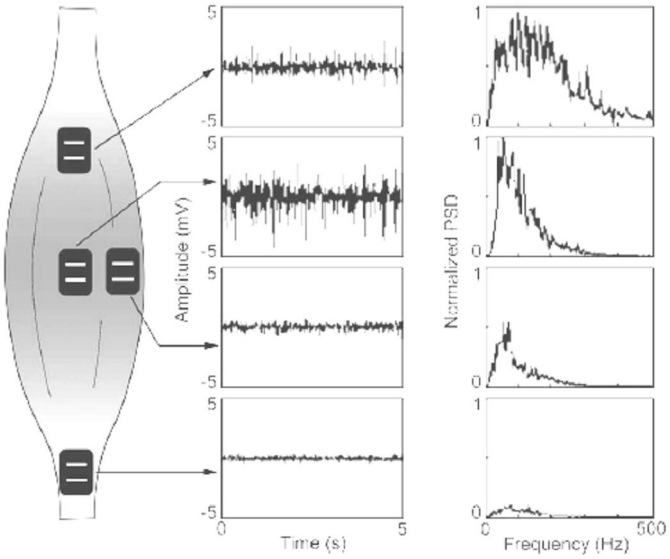

Fig. 3.4 Electrode placement and their related FFTs [De Luca, 1997]

3.1.2 Amplifier section

Amplifiers suitable for biomedical applications must usually have a high common-mode rejection and a high differential input resistance. Although several integrated-circuit operational amplifiers possess these qualities, it has been difficult to obtain satisfactory performance with respect to the SEMG properties in practical circuits. Advent of modern electronics and the process of differential amplification have enabled the measurement of SEMG signals of low noise and high signal fidelity. With differential amplification, it is possible to measure the full effective bandwidth of the EMG signal. There are several important properties to consider in a pre-amplifier:

- High common mode rejection ratio
- Very high input impedance
- Short distance to the signal source
- Strong DC signal suppression

In the present research work, SEMG signals were acquired in deferential mode operational amplifier using LM324 having a gain of 1000 by placing bipolar electrode on the skin. The SEMG signal was again amplified by a non inverting amplifier with a gain of 10. Both amplifiers were prepared using single chip LM324 [datasheet]. Three Opamps of LM324 were used to make the electronics circuit compact. LM324 was selected for its general purpose applications, low-cost, CMRR about 65-80 and importantly single power supply driven. Fig.3.5 shows pre amplifier and amplifier

circuit used in the study. The circuit was selected as it operates on single power supply. The same circuit will be beneficial for prosthetic device.

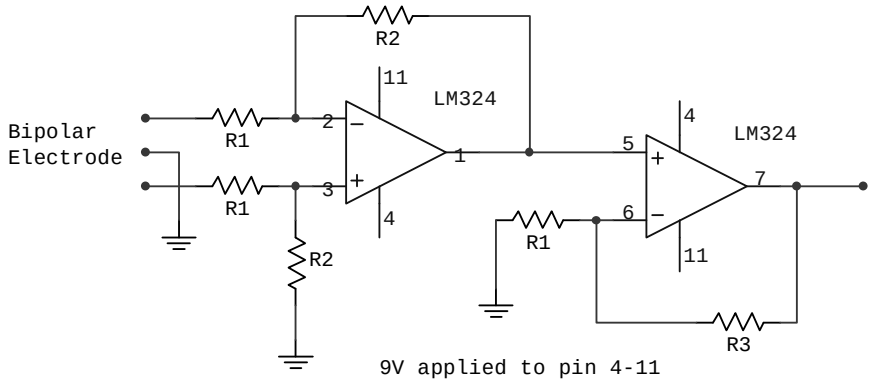

Fig. 3.5 Pre amplifier and amplifier circuit

3.1.3 Peak filter section

SEMG signals are specified between 20 to 300 Hz [Reaz et al., 2006; Arora, 2007; Ryait et al., 2009]. It emphasized the need of a band pass filter. To eliminate the interference of 50 Hz and hum by the nearby AC source, a narrow peak filter with central frequency of 180 Hz [Texas Instruments, 2001] was used. The peak filter used is advantageous as it gives additional gain of 10 at central frequency. Fig. 3.6 shows the circuit diagram of the peak filter and Fig. 3.7 shows its frequency response. This filter circuit passes all the frequencies and increases the amplitude of frequencies near central frequency having narrow band width. It results in neither elimination nor attenuation of the frequency spectrum within this bandwidth as by other conventional filters. The values of the components were calculated by the following design equations [Texas Instruments, 2001].

Design Equations:

- Pick C2 = C3
- Calculate R1 = $\dfrac{1}{2*\pi*C2*\text{Frequency}}$
- Calculate R2 = R1+ 19*R1
- Calculate R3 = R1/19
- Calculate C1 = C4 = 100 to 1000 times C2

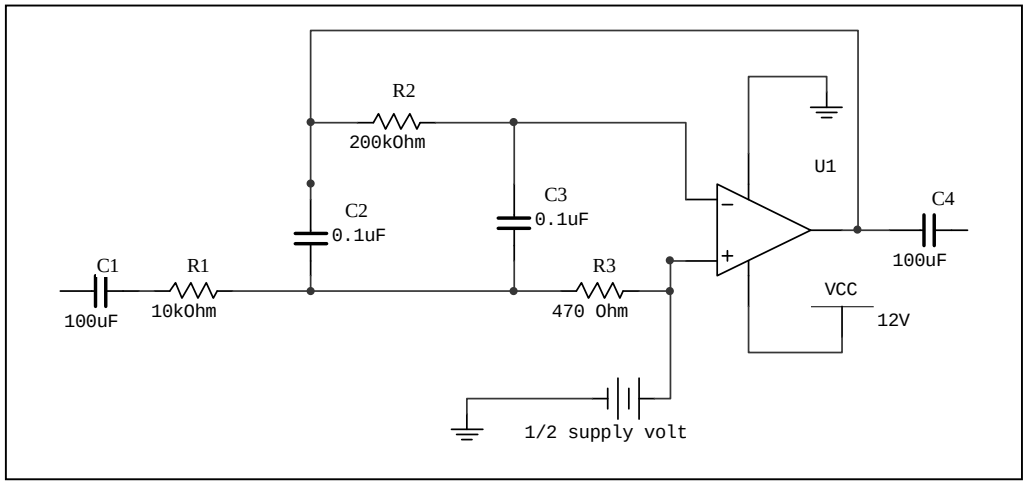

Fig. 3.6 Peak filter amplifier

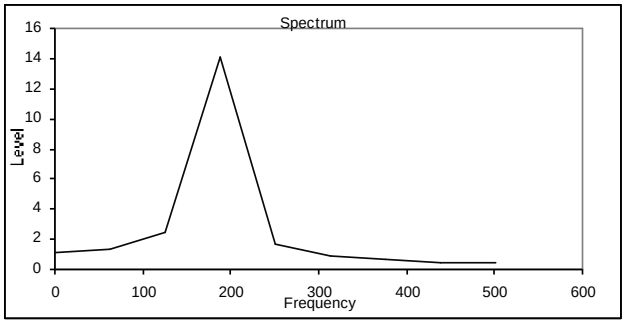

Fig. 3.7 Spectrum of the peak filter at 180Hz (Multisim plot)

SEMG signal has been classified in the range of 10 to 300 Hz by most of the researches and is widely accepted. 50 Hz interference is always distorting SEMG. When prosthetic device is developed with wide band-pass filter, the chances to interference increases and harmonics (i.e. 150 Hz, 200 Hz, etc) plays the vital role in the malfunction of the prosthetic. Usually notch filters and comb-notch filters are used to remove the interference. In the present investigation the circuit as shown in Fig. 3.6 was selected with central frequency 180 Hz. This was selected to be precise in the range >100 Hz and < 200 Hz having narrow bandwidth to reduce AC interference. This adds a benefit of additional gain in the pass-band. This amplifies the desired SEMG only. Bandwidth and gain factor do not depend on R3. Therefore, R3 can be used to modify the mid frequency with out affecting bandwidth or gain. The aim was to develop RMS based control-methodology for elbow prosthesis; therefore this very circuit was selected.

3.1.4 Interfacing section

For capturing and analysis using MATLAB an interface circuit was used where signal was passed to opto-coupler as isolating circuit. This isolating circuit feeds the mic-in socket of the sound card of computer (when operated by AC supply only). The sound card output was acquired by MATLAB softscope. The SEMG measurements were synchronized with MATLAB-softscope, sampled at 8 kHz. Computer having in-built sound card was used for data acquisition. Interfacing was developed to connect SEMG signal amplifier circuit and the sound card. MATLAB softscope was initialized for acquiring the data by using winsound as its adaptor. This interface was developed with MCT2e opto-coupler with transistor biasing. The transistor used was of another MCT2e. It helps in faithful amplification and isolation of the amplifier signal. It provides positive DC offset to the input signal. The output of the circuit was interfaced to computer from the mic- IN/OUT probe. The anti aliasing, low pass filter of 1500 Hz cut-off frequency was placed just before input of sound card. This filter was used to eliminate the effect of overlapping of frequencies to get proper FFT.

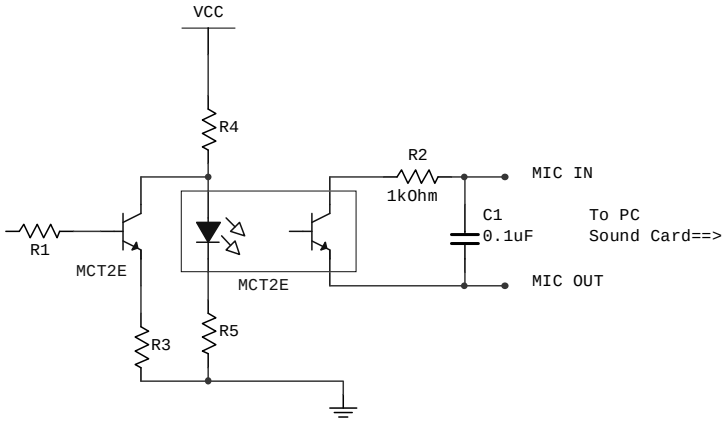

Fig. 3.8 Interfacing circuit

Fig. 3.8 shows the interfacing using MCT2e optocoupler receives amplified signal from the peak filter at resistor “R1”. R1 was connected to the base of a transistor of another MCT2e optocoupler which passes the positive half to resistor “R4”, the collector resistor working as open collector configuration. The second optocoupler was working as a load. The diode of this optocoupler swings as the current in the output circuit. It remains forward biased for all the time due to V_{cc} (9 volts). The variation of diode current passes optically to the transistor. This transistor gets V_{cc}

from the mic-in port of computer. The transistor was made to work as headphone-mic. The variations of its collector current were passes to ADC of sound card of the computer in the same way as by headphone-mic as shown in Fig. 3.9[www.mathswork.com]. This very circuit is used when AC rectified supply was used.

A typical data acquisition session consists of four steps:

1. Initialization: Creating a device object.
2. Configuration: Adding channels and controlling acquisition behavior with properties.
3. Execution: Starting the device object and acquiring or sending data.
4. Termination: Deleting the device object.

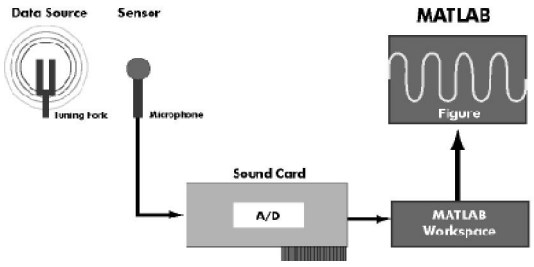

Fig. 3.9 Aquisition system [www.mathswork.com]

Most soundcards are wired to the positive DC bias voltage to the ring but a small number of non-standard soundcards have the bias voltage wired to the tip. A few cards have a jumper which enables or disables the power to the microphone jack. If the jumper is put on, the bias voltage (+ 5 V through a few kilo ohm resistors) is wired to the tip. Newer main boards with stereo microphone support will provide the bias voltage for both the tip and ring. Stereo cards with just two audio channels have only the green (output), blue (input) and pink (microphone) jacks.

3.1.5 Acquiring data with a sound card

A sound card (also known as an audio card) is a computer expansion card that facilitates the input and output of audio signals to and from a computer under control of computer programs. Typical uses of sound cards include providing the audio component for multimedia applications such as music composition, editing video or audio, presentation, education, and entertainment (games). Many computers have sound capabilities built in, while others require additional expansion cards to provide

for audio capability. Connectors on the sound cards are colour coded as shown in Table 3.1 as per the PC System Design Guide. They have symbols with arrows, holes and sound waves that are associated with each jack position; the meaning of each is given below:

Table 3.1
Sound card color code

Color	Connector
Lime Green	Line-Out, Front Speakers, Headphones
Pink	Microphone
Light Blue	Stereo Line In
Orange	Subwoofer and Center out
Black	Rear Surround Speakers for 5.1 and 7.1 systems
Gray	Middle Surround Speakers for 7.1 systems
Gold	Midi / Game port (Joystick)

Most sound card microphone inputs require a minimum signal level of at least 10 millivolts, but some older 8-bit cards need as much as 100 millivolts. The typical impedance of the PC soundcard microphone input is in order of 1 to 20 kohms (can vary from card to card). Sound Blaster soundcards (SB16, SB32, AWE32, AWE64 or Live) from Creative Labs have a 3.5mm (1/8 inch) pink stereo jack for the microphone input as shown in Fig. 3.10, with the following pin out:

1. Signal input (tip)
2. +5V bias (ring)
3. Ground (sleeve)

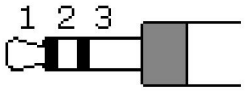

Fig. 3.10 Microphone jack

3.1.6 Softscope

SoftScope is a graphical user interface for selecting and configuring data acquisition sources in MATLAB and then acquiring, viewing, and analyzing data using a familiar, oscilloscope-like interface. SoftScope quickly verify hardware operation and perform live data analysis using a library of built-in measurement functions. SoftScope was extended with the analysis functions and export data from SoftScope to the MATLAB workspace.

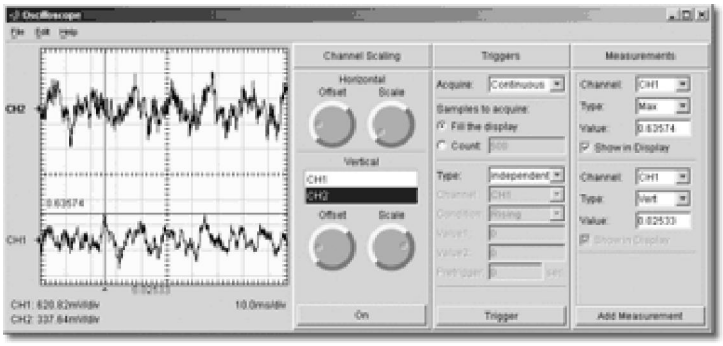

Fig. 3.11 Snapshot of Oscilloscope screen

3.2 Design of two channel Experimental Set-up

In the single channel approach the mic-in socket was used to design the interfacing circuit whereas in two channel system the stereo Line-in socket was used. The difference between the two is shown in the Fig. 3.12. R and L stands for right channel and left channel respectively.

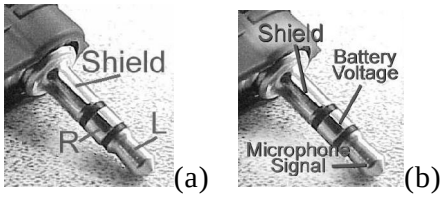

Fig. 3.12 (a) Stereo Line-in (b) Mic-in socket

Two channel acquisition was done using stereo control was developed using coupling capacitors as isolators/interfacing components. Here interfacing circuit was not used as output of the amplifier was kept restricted to 3 volts (as recommended by sound card orts). Rest all other sections are the same as explained earlier. Fig. 3.13 shows the block diagram for the two channel recording system used in the investigation. Channel is symbolized to the two inputs of line in socket. Simultaneously two signals can be acquired from the channels. This helps in the study of SEMG signals from two different locations. Using sound card and win-adaptor gives additional befit to acquire the signal at sampling rate of 8000Hz to 44100Hz.

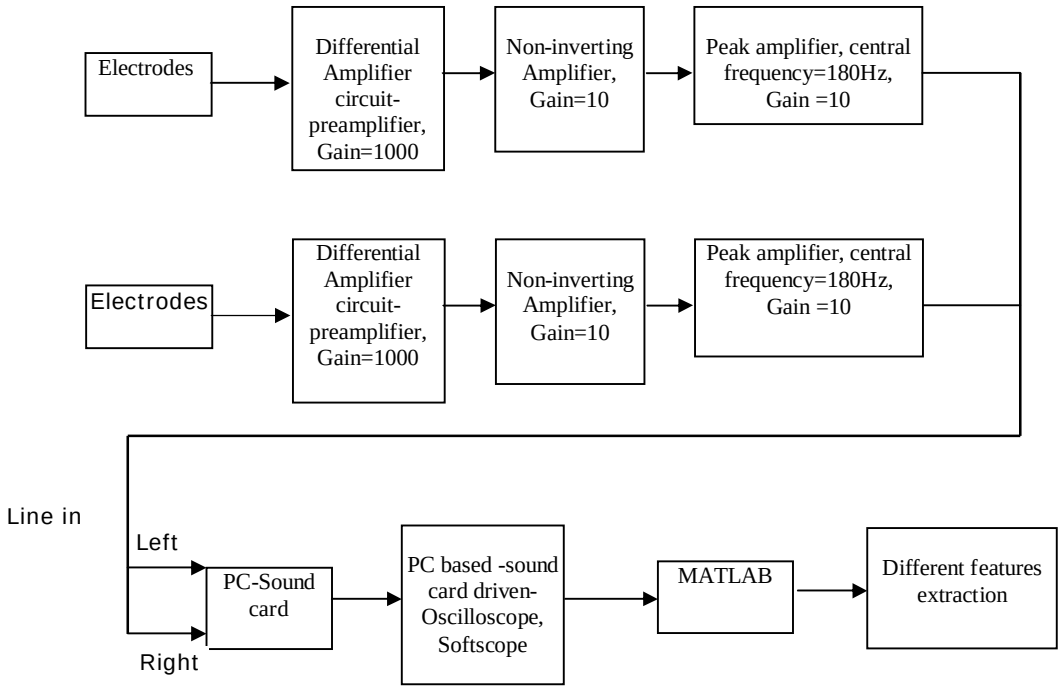

Fig. 3.13 Block diagram of two channel acquisition system

3.3 Methodology Used

The softscope initialized for the hardware setting to use winsound. The trigger of softscope was kept at continuous mode. After triggering the waveform appears on the softscope it was stored in the workspace manually. Two forms of dataset were recorded: In the first way 960 data samples were recorded in continuous mode for the time window of 120 msec of softscope at sample rate of 8000 Hz in the work space. The samples were stored in the workspace with a specific name. In the second approach 5000 samples were recorded in continuous mode at sample rate of 8000 Hz. The time window becomes 0.625 sec. MATLAB program was made to filter 70 Hz to 240 Hz as band pass filter- FIR filter. Then Y = fft(X, n) returns the n-point DFT. Each DFT is of 4096 point. The whole process of the recording and analysis is given in the flowchart shown in Fig. 3.14. The softscope initialize the hardware setting to use winsound as its adaptor. The sound card driver was kept to Line-in for the recording. The trigger of softscope was kept at continuous mode. After triggering the waveform appears on the softscope which was stored in the workspace manually by selecting export function.

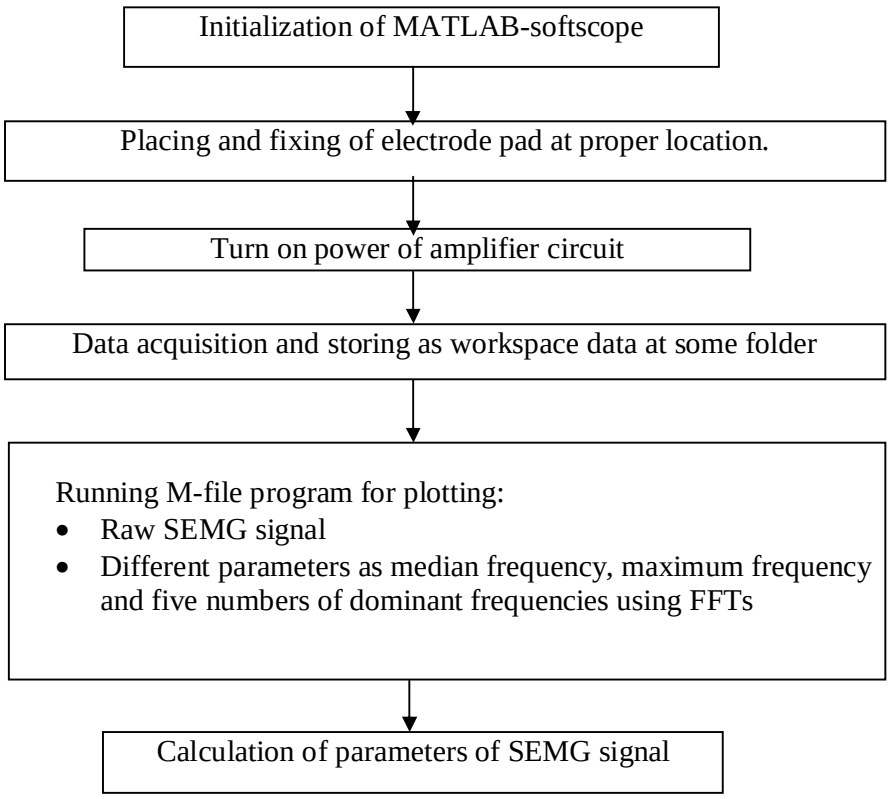

Fig. 3.14 Flow chart for feature extractions

3.4 Parameters evaluated for analysis

For the prosthetic devices the controllers based on the available technologies are complex and bulky. Seven parameters were evaluated for the interpretation of SEMG signal.

1. SEMG signal is an alternating signal of some frequency so RMS value was calculated in MATLAB using the data from workspace using the formula as:

$$V_{rms} = \sqrt{[V_{mean}]^2}$$

The unit of measurement is volts.

2. Energy and power of a signal are also very useful to characterise signals. Total energy of a discrete time signal x[n] over $[n_1]$, $[n_2]$ was calculated by formula:

$$Es = \sum_{n_1}^{n_2} |x[n]|^2$$

The unit of measurement is volts-square.

3. Another interesting feature was proportionality relations between SEMG signal's frequency and amplitude. To deduce these features collectively, a term "Slope" was developed. Slope of a signal is the ratio of amplitude and time interval of the peak pulse in the signal. The time interval is the duration from the time when signal reaches the peak to the time where signal reaches to the next peak. Fig. 3.15 shows evaluation of parameter "Slope". SEMG is a complex signal with large portion of noise; hence the parameter Slope individually gives the relation of amplitude rise to the variation in the frequency. Change in frequency parameter was less as compared to amplitude. The parameter "Slope" is an easy way to extract SEMG signal information taking both amplitude and frequency variations into consideration simultaneously. The unit of measurement is volts/sec.

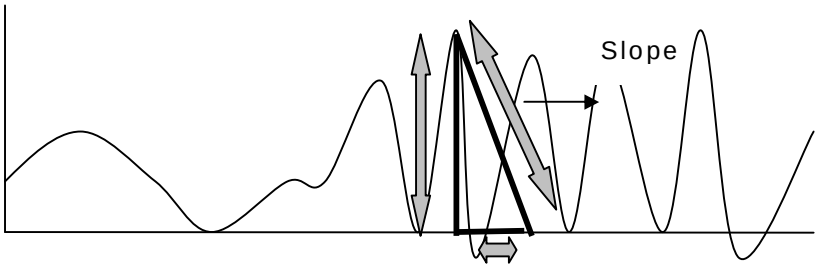

Fig. 3.15 Evaluation of parameter "Slope"

4. Another parameter median frequency (mf) as described by De Luca [Stulen et al., 1981] was calculated. It is mean of frequencies having magnitude more than half of the peak amplitude. The unit of measurement is Hz.
5. Next parameter is the most prominent frequency (peak freq). The unit of measurement is Hz.
6. Another parameter is average frequency (Av freq) which is mean value of five dominant frequencies of the FFT spectrum. The unit of measurement is Hz.
7. Lastly, the amplitude (peak freq ampl) of peak freq was deduced by FFT. For explanation of behaviour of each selected parameters middle section of the arm muscle (i.e. below elbow and above the wrist) was selected. The unit of measurement is volts.

A program was developed to plot the waveforms of raw filtered SEMG signal, FFT plots and to calculate different parameter above mentioned parameters.

3.5 Observations for establishing working of acquisition system and chosen parameter for SEMG signals

Many parameters were discussed above for the analysis with the aim to develop RMS based prototype elbow, the amplitude based parameters needed to be studied. This section establishes the observations about the parameters for SEMG analysis to be done in consecutive chapters. Importantly to observe are V_{rms} and slope. These parameters were tested for SEMG, force exertion measurements and under muscle-fatigue to observe both the increase and decrease as per the set convention of SEMG behaviour.

3.5.1 SEMG variations for hand gripping

To understand the SEMG signal's behavior the measurements were carried out. Three cases were studied; firstly NO SEMG, secondly LOWSEMG and thirdly HIGHSEMG.

3.5.1.1 Acquisition Details

Arm was kept at rest. Initially the data was acquired without moving the hand, called NO SEMG case. Secondly keeping arm as it is, but closing of the hand grip i.e. closed with moderate force called LOWSEMG case. Thirdly, closed with full tight clinched gripped called as HIGHSEMG case was studied. Six parameters were evaluated for the interpretation of SEMG signal as explained in the section above.

1. RMS value (V_{rms})
2. Energy of signal (Es)
3. Slope
4. Median frequency (mf)
5. Peak frequency (Peak freq)
6. Peak frequency amplitude (Peak freq ampl)

The study was carried out to relate grip force of hand with the above mentioned parameters to observe the behavior of V_{rms} and slope which were later used for statistical analysis and prototype development. Middle section of the arm muscle (i.e. below elbow and above the wrist, palm side) was used for the signal measurement as shown in the Fig. 3.16.

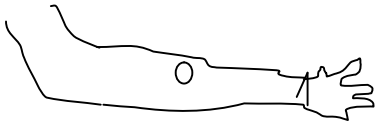

Arm è Elbow ….to…… wrist

Fig. 3.16 Location for SEMG analysis

3.5.1.2 Results and discussions

Fig. 3.18- 3.19 shows the captured SEMG waveform and the FFTs of the three cases (NO SEMG, LOW SEMG and HIGH SEMG) respectively. FFT plots confirm the action of narrowband filter and the rise in the amplitude with the force. Table 3.2 shows all the six calculated parameters for comparison. Fig. 3.17 and Table 3.2, V_{rms} gives an indicative rise in the three cases and depict the proportionality with the force of contraction of the muscles. With the slope function, the force level can be defined with an ease. It is amply clear that all the amplitude related parameters give relationship of SEMG activity and force level. Frequency based parameters like mf and peak freq remained in the selected band confirming SEMG acquisition. This gives the effectiveness of the Peak filter used in acquisition system and confirms the frequency from the SEMG frequency band.

Table 3.2
Parameters for comparison

	NO SEMG	LOW SEMG	HIGH SEMG
V_{rms} (V)	0.0226	0.0706	0.2908
Es (V^2)	0.2343	2.395	40.6822
Slope (V/sec)	45.0413	111.0816	566.0864
mf (Hz)	148.4375	175.7813	198.2422
Peak freq(Hz)	149.4141	205.0781	214.8438
Peak freq ampl(V)	3.061	10.8305	58.7226

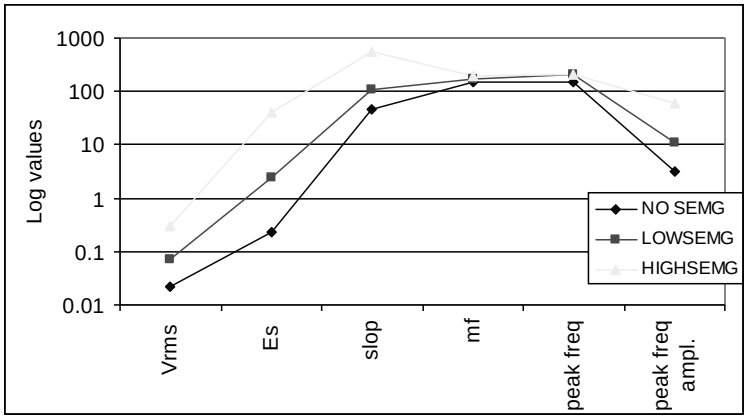

Fig. 3.17 Plots for comparison of chosen parameters

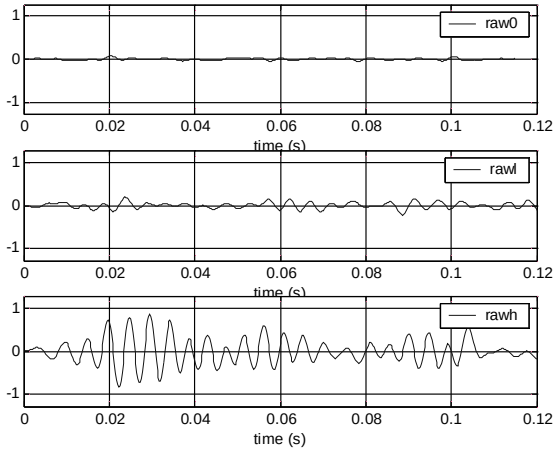

Fig. 3.18 Plots for NO SEMG, LOWSEMG and HIGHSEMG from the location

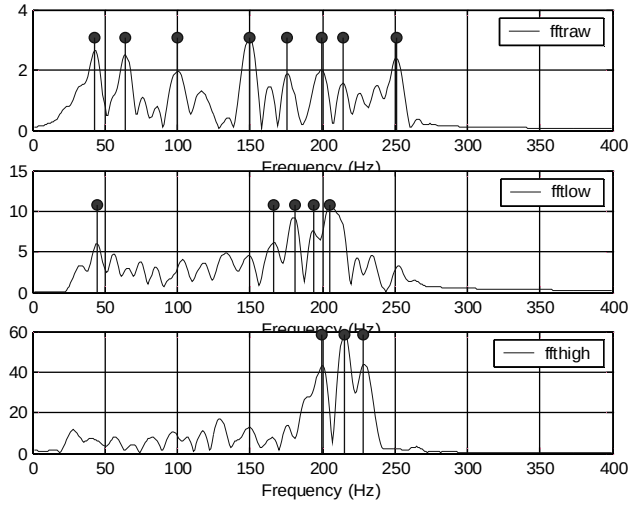

Fig. 3.19 Plots for ffts of NO SEMG, LOWSEMG and HIGHSEMG from the selected location

3.5.1.3 Statistical approach

The electrical activity of a muscles measured by SEMG exhibits complex behavior with nonlinear dynamic properties. This behavior takes the form of SEMG patterns with different complexities. Considering this fact, the statistical theory may be a better approach than traditional linear methods in characterizing the intrinsic nature of SEMG. The study of the characterization can contribute to the understanding of the SEMG dynamics and underlying muscles processes and search for its physiological significance. SEMG patterns at the locations for the different three cases of grip were considered for the statistical analysis. In the present study, SEMG analysis for various parameters like standard deviation, average absolute deviation, variance etc. were

calculated. The data samples were recorded and processed by program and then exported to MS-EXCEL where the in-built statistical functions were used for comparison. Few of the selected functions were:

1. The standard deviation was measure to see dispersion from the average value (the mean). The equation used for standard deviation is given below:

$$\sqrt{\frac{n\sum x^2-(\sum x)^2}{n^2}}$$

2. Average of the absolute deviations is a measure of the variability in a data set which calculates the average of the absolute deviations of data points from their mean. The equation used for average deviation is:

$$\frac{1}{n}\sum\left|x-\bar{x}\right|.$$

3. Sum of squares of deviations calculates the sum of squares of deviations of data points from their sample mean. The equation used for the sum of squared deviations is:

$$\sum\left(x-\bar{x}\right)^2$$

4. Variance calculates variation based on the entire population. The equation is:

$$\frac{n\sum x^2-\left(\sum x\right)^2}{n^2}$$

Table 3.3 shows the statistical observation of above parameters. This comparison helps in understanding the statistical parameters in the analysis of SEMG as shown in Fig. 3.20. Later in chapter 5 and 6, the principal component analysis will be based on covariance. SEMG relation with the force exerted by muscles has been represented by statistical parameters mentioned above.

However, sum of squares of deviations of data points from their sample mean shows remarkable change. Parameter variance was also showing discriminating result.

Table 3.3
Statistical parameters vs SEMG

Statistical Parameters	NO SEMG	LOW SEMG	HIGH SEMG
Standard Deviation	0.022	0.110	0.192
Average Deviation	0.018	0.085	0.155
Sum of Squares of Deviations of Data Points from their Sample Mean.	0.234	5.619	17.00
Variance	0.0005	0.0122	0.037

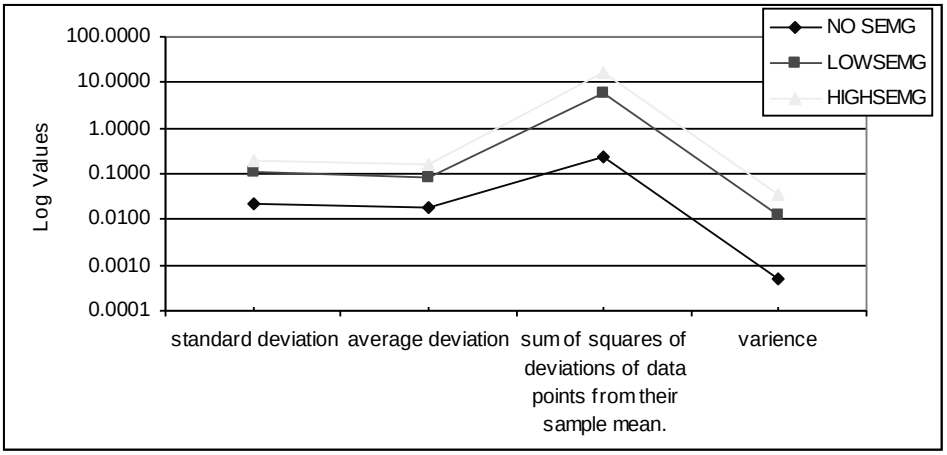

Fig.3.20 Plots comparing amplitudes of dominant frequencies

3.5.2 Below elbow Force – SEMG relationship using gripping equipment

Same analysis was carried out again to further establish the relation using grip force measuring exercising instrument as shown in Fig. 3.21. This study helped in understanding relationship of the chosen parameters with the force exerted by the grip. A grip-force measuring exercising instrument was used as shown in Fig. 3.21 and location of acquisition as shown in Fig. 3.22 (mid of arm, palm side)

Fig. 3.21 Exercising Gripper with measuring gauge

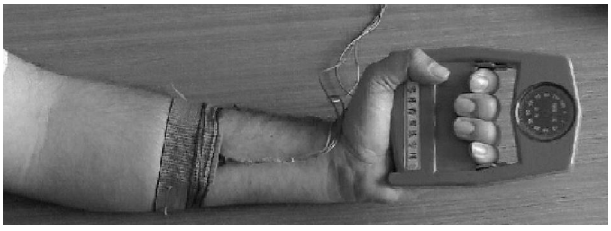

Fig. 3.22 Exercising gripper with electrode on the selected location

3.5.2.1 Acquisition Details: An instrument was used to exercise the gripping of hand. As the grip was tighten the gauge shows the deflection for the force exerted during gripping, known as gripping force. This study helps in getting descriptive relationship of the SEMG vs. parameters at pressure points with the force exerted through the grip. The force measuring instrument can measure up to 140 kg of grip force. A person has different maximum voluntary contraction and hence the maximum force. It was observed that the maximum level was 38 kg approximately with comfortable exertion. Hence at different gripping force say 3 kg, 6 kg, 9 kg etc., the SEMG was recorded from the location using single channel acquisition system. The parameters selected for the study were V_{rms}, Slope, Median Freq, Variance, Standard deviation and Av Freq [As explained in section 3.4].

Table 3.4
Parameters for comparison

Force [kg]	V_{rms}	Slope	Median Freq	Av Freq	Sum of squares of deviations of data points from their sample mean	Variance	Standard deviation
0	0.0632	639.99	148.44	155.92	4.1838	0.0043	0.0659
3	0.0989	1110.5	170.9	178.06	9.4510	0.0103	0.1017
6	0.1251	1129.9	159.18	162.27	17.3406	0.0180	0.1343
9	0.1417	1429.3	157.23	145.02	21.7080	0.0225	0.1502
13	0.1749	1962.1	159.18	169.43	33.0264	0.0343	0.1853
20	0.2455	3239.1	170.9	167.32	68.0239	0.0707	0.2660
28	0.3683	3281.2	166.02	165.69	145.4499	0.1513	0.3890
38	0.3532	3763.6	175.78	166.83	145.8791	0.1517	0.3896

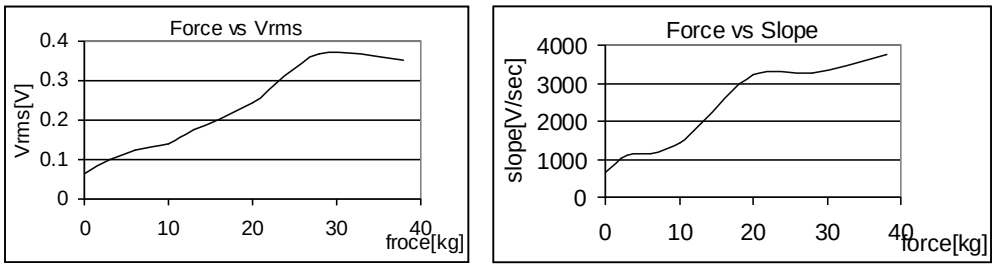

Fig. 3.23 Plot between force vs V_{rms} and force vs slope

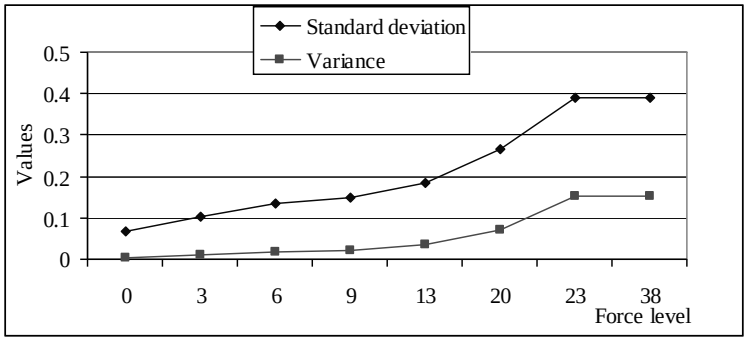

Fig. 3.24 Plot of force vs standard deviation and variance

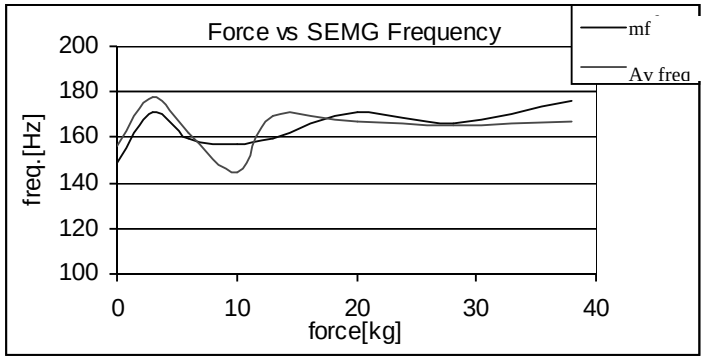

Fig. 3.25 Plot of force vs median frequency and average frequency

3.5.2.2 Results and discussions

At different gripping force, the SEMG was recorded from the location say 3 kg, 6 kg, 9 kg etc.. Variation was kept from 0- 38 kgs. Fig. 3.23 –3.25 is shows parametric comparisons as per Table 3.4. Fig. 3.23 shows the variation of force and V_{rms} which remains linear from 0 to approximately 85% of the maximum force exerting capacity of the person, similarly the slope values change are remarkably observed. After that SEMG generated by the body remains constant or start to decrease due to fatigue. Fig. 3.24 refers to statistical parameters "variations and standard deviation" which further justifies the observation made by Fig. 3.23. Lastly, Fig. 3.25 refers that SEMG Av freq to verify the frequency values from the selected SEMG band only.

3.5.3 Above elbow Force – SEMG relationship using gripping equipment

One of the objectives is to study the elbow movement. So SEMG variation for above elbow muscles for bending of elbow was studied using apparatus bullworker exercising machine as shown in the Fig. 3.26. One end of the bullworker was kept fixed and on the other end force is applied by the arm as shown. As the arm bends the bullworker was pressed and the indicator for the force/pressure applied moves. On releasing the force the indicator remains at the level of maximum exerted force.

3.5.3.1 Acquisition details

Three male subject of age group 30-35 years were selected. Location selected was middle of the above elbow arm, palm side (on biceps). Recording was done by using single channel system with parameters chosen were: V_{rms}, Es, pk amp, Slope, mf, Av freq and peak freq [As explained in section 3.4]. To study the force exerted by the

above elbow muscles, bullworker exercising equipment was used. This equipment has been scaled in kg to measure the force exerted at its both ends. One of the ends was kept fixed and the other end was press as shown in Fig. 3.26. Four force levels were selected for the study marked as cw80, cw100, cw110 and cw130. cw80 indicates the force exerted by the above elbow muscles is of 80kg and is so for the others. This study gives the observation of above elbow SEMG with force exerted which encouraged the analysis for finding suitable locations along with suitable no.s of electrodes for elbow movements. The same is discussed in chapter 6.

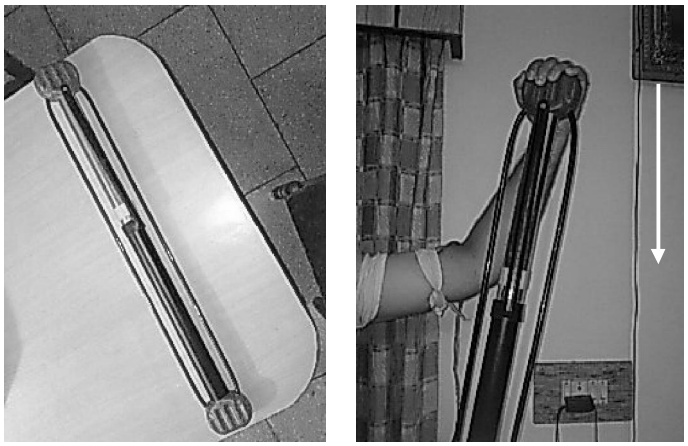

Fig. 3.26 Bullworker exercising equipment

Table 3.5
SEMG variations and force on Bullworker

	cw80	cw100	cw110	cw130
V_{rms}	0.0722	0.122	0.1369	0.1834
Es	2.5222	7.1996	8.7935	16.3072
pk amp	12.3011	22.1937	31.5855	34.4348
slope	642.9719	1164.8	1411.1	2342.6
mf	163.0859	150.3906	168.9453	165.0391
Av freq	147.8271	134.0332	136.8408	180.7861
pk freq	169.9219	174.8047	178.7109	163.0859

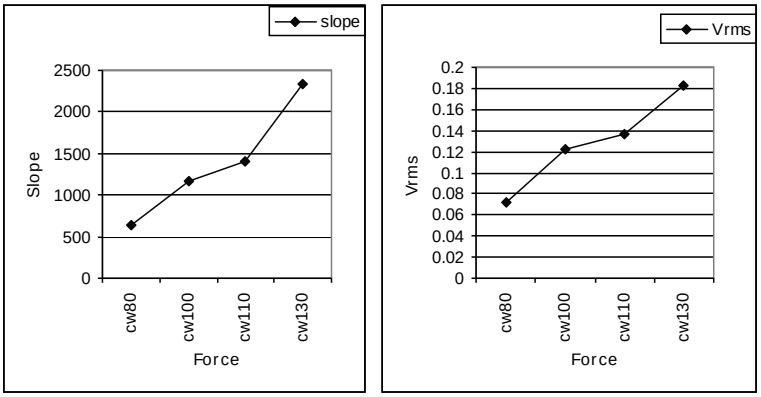

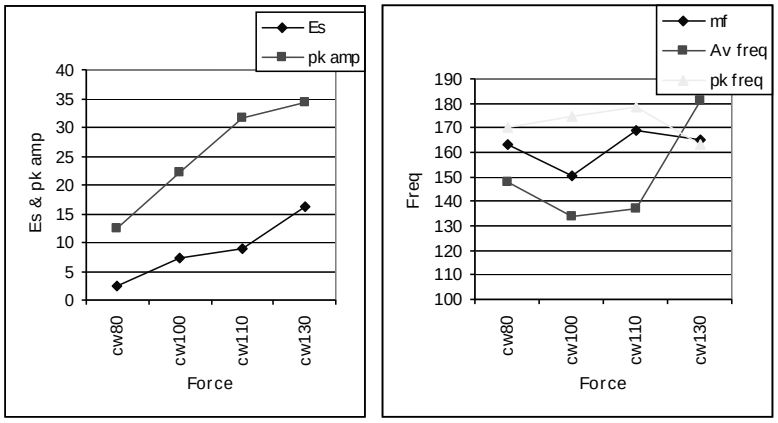

Fig. 3.27 Plot for the SEMG parameters measured by exercising equipment

3.5.3.2 Results and discussions

Four selected force levels were taken for the analysis and shown in Table 3.5. Each parameter had different range, so different plots were opted to plot for comparison. Again a linear increment was registered for slope, V_{rms}, Es and pk amp but mf, Av freq and pk freq showed a little rise in frequency.

Therefore in any muscle, when the contraction level increases, amplitude dependent SEMG parameters also increase. The fact remains the same for every where i.e. either below elbow muscles or above elbow muscle.

3.5.4 Fatigue of arm muscles for prolonged contraction

SEMG plays vital role in the fatigue test if a muscle is put on contraction for a longer duration the ability to sustain contraction reduces with some pain. The SEMG signal features are analyzed in bicep bracii muscle during fatiguing isometric flexions and recovery periods across a range of force levels was investigated [Lowery et al., 2003, Farina et al., 2004; Hong-Chun et al., 2005; Dingwell et al., 2010, Gaur et al., 2010]. Averaged instantaneous frequency is as an alternative method for the frequency analysis of surface electromyography in the study of muscle fatigue during sustained, isometric muscle contractions [Georgakis et al., 2003]. The effect of the dynamic fatigue differs from that of isometric fatigue and Fourier transform is suitable to study the evolutions of the mean frequency of the SEMG for dynamic fatiguing exercises at moderate speed and low force level [Caohua et al., 2007]. It is possible to observe variations of the time-frequency distribution, probably related to the fatigue processes that take place inside the muscle tissue during dynamic contractions [Bonato et al., 1996]. Different patterns of the time-frequency

distribution of the myoelectric signal in different biomechanical phases of the movement were analyzed. Surface electromyography signals at different levels of maximum voluntary contractions to analyze spectral shifts in mean, median frequencies, root mean square and rectified root mean square to assess muscle fatigue patterns is often computed [Zaman et al., 2007]. Already, numbers of studies mention the good performance of wavelets in transient SEMG processing for fatigue detection, reaction time detection or pattern recognition [Karlsson et al., 2001; Knaflitz et al., 1999].

3.5.4.1 Acquisition Details

In this present analysis prolonged contraction was examined in the case of HIGHSEMG (as mentioned in section 3.5.1.1). The aim was to check whether the amplitude decrease with the time during prolong contraction of a muscle happens to all the frequency components in the SEMG waveform. Measuring instrument was pressed at a force level 28 kg (dial reading) and SEMG was acquired with the gap of duration of about 30 sec keeping the same force applied in gripping. On the other hand another investigation was done to observe the amplitudes of first five dominant frequencies present in the filtered SEMG signal. A comparison was done by extracting the amplitudes of five dominant frequencies in the FFT during prolonged contraction.

Table 3.6
SEMG for prolong contraction

	cin	cin1	cin2	cin3	cin4	cin5
V_{rms}	0.21	0.10	0.08	0.07	0.07	0.03
Es	20.86	4.80	3.20	2.16	2.09	0.52
Slope	402.72	165.55	146.34	152.35	133.13	43.70
mf	191.41	183.59	167.97	164.06	171.88	152.34
Peak freq	191.41	183.59	167.97	164.06	171.88	152.34
Peak freq ampl	42.53	18.89	15.10	8.94	11.02	4.93

Table 3.7
FFT amplitude of dominant frequencies of SEMG for prolong contraction

FFT peaks	cin		cin1		cin2		cin3		cin4		cin5	
	Ampl	Freq.	Ampl	Freq.	Ampl	Freq.	Ampl	Freq.	Ampl	Freq.	Ampl	Freq.
I Peak	42.52	207.0	18.88	203.1	15.09	199.2	8.9	152.3	11.02	183.6	4.93	46.9
II Peak	38.77	191.4	17.98	179.7	9.64	175.8	8.13	195.3	8.41	195.3	3.99	179.7
III Peak	15.60	167.9	11.42	218.8	7.28	156.3	7.89	171.9	8.24	207.0	3.96	148.4
IV Peak	14.78	179.6	6.62	62.5	6.54	46.9	7.17	179.7	7.27	144.5	3.41	58.6
V Peak	11.46	156.2	5.93	230.5	5.86	144.5	6.29	62.5	6.42	214.8	3.00	210.9

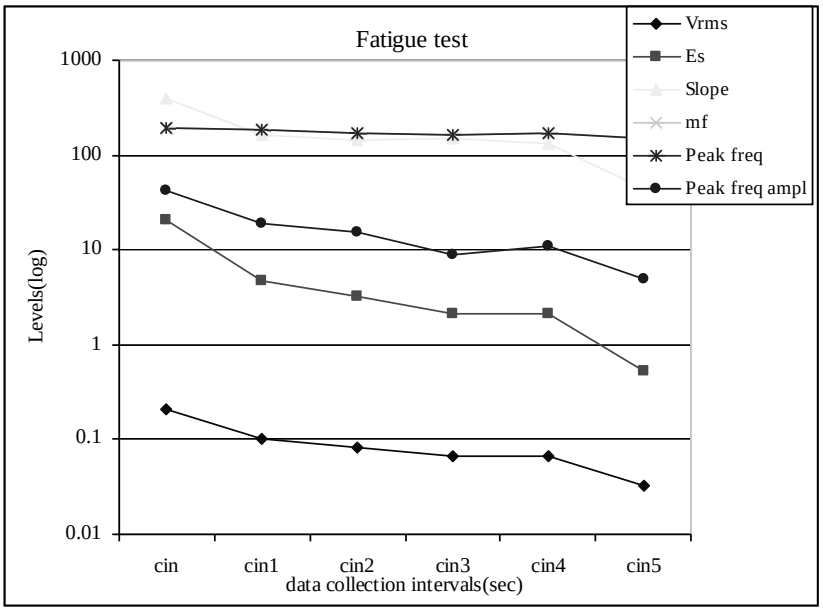

Fig. 3.28 Plots showing effect of prolonged contraction

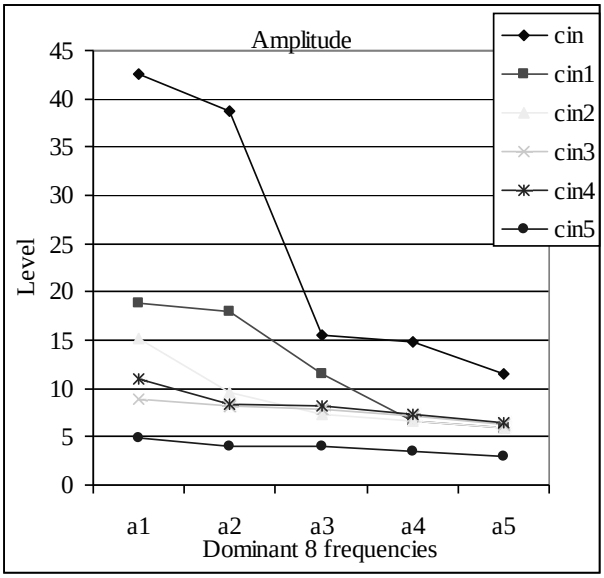

Fig. 3.29 Plots comparing amplitudes of dominant frequencies

3.5.4.2 Results and discussions

Table 3.6 shows the SEMG variation with time where “cin” stands for instant of start of prolonged closing operation of hand grip. “cin1” stands for the values after 30 sec of interval and so on. Fig. 3.28 shows the variation of each calculated parameters of Table 3.6. Muscles have the property that they can produce a very high force initially

but after some time of contraction the ability to induce force reduces along with some pain.

Parameters depending upon the amplitude of SEMG signal such as V_{rms}, Es and pk amp show a decrease in the values with time and parameter slope is also showing the similar characteristics.

Table 3.7 describes the calculated peaks of five dominant frequencies present in the FFT spectrum. Fig. 3.29 shows the variation of the FFT-peak's amplitudes with the duration of time which is again decreasing for all the frequencies components.

It was observed that for the design of proper prosthetic devices an important fact may be kept under preview that prolong use of the device may get poor SEMG signals. The controller should have the capability of adjusting the threshold level after some duration to get proper degree of controllability. The acquisition must be taken within time limit for proper SEMG analysis.

Chapter's Summary:

The SEMG acquisition system has been designed to acquire SEMG signals from muscle on the forearm. The amplifier provides the input for the analog interface of the computer using sound card. The SEMG acquisition system was developed to measure and record the signals from the subjects. Users have the options to select a variety of voltage scales and time scales to display the output signals. The study of different parameters in relation to SEMG variations with force level has been carried out and it has been found that both amplitude related parameters and selected statistical parameters give view of force level. Proposed function slope gives good representation of the SEMG. The design of proper prosthetic devices an important fact may be kept under preview that prolong use of the device may get poor SEMG signals. The controller should have the capability of adjusting the threshold level after some duration in order to get proper degree of controllability.

CHAPTER 4
SEMG ANALYSIS AT ACUPRESSURE POINTS

In this chapter SEMG at acupressure points on arm was studied. For pain relief or reflexive actions acupressure technique are very well accepted. In search of best electrode locations/site acupressure points must also be considered.

Acupressure points (also called potent points) are places on the skin that are especially sensitive to bioelectrical impulses in the body and conduct those impulses readily. Traditionally, Asian cultures conceived of the points as junctures of special pathways that carried the human energy that the Chinese call chi and the Japanese call ki [Online ref. 5; Online ref. 6]. Stimulating these points with pressure, needles, or heat triggers the release of endorphins, which are the neuro-chemicals that relieve pain. As a result, pain is blocked and the flow of blood and oxygen to the affected area is increased. This causes the muscles to relax and promotes healing. Tension tends to concentrate around acupressure points. When a muscle is chronically tense or in spasm, the muscle fibers contract due to the secretion of lactic acid caused by fatigue, trauma, stress, chemical imbalances, or poor circulation. For instance, when under a great deal of stress there may be a stage of having difficulty in breathing. Certain acupressure points relieve chest tension and enable the subject to breathe deeply. When a point is pressed, the muscle tension yields to the finger pressure, enabling the fibers to elongate and relax, blood to flow freely, and toxins to be released and eliminated. Increased circulation also brings more oxygen and other nutrients to affected areas. This increases the body's resistance to illness and promotes a longer, healthier, more vital life.

Acupressure points have high electrical conductivity compared to the skin around them [Cao, 2001]. Western scientists have also mapped out and proven the existence of this system of body points by using sensitive electrical devices. An acupressure point treatment apparatus including an acupressure pointer including a pellet on a figure strap, a finger grounder including plate on a finger strap and a galvanic skin response (GSR) monitor electrically connected to the acupressure pointer and the finger grounder. This invention by Prof. Cao is a novel device for acupressure point therapy. More specifically, the apparatus is invented not only for treatment but for

locating acupressure points on skin [Cao, 2001]. Technically, acupuncture and acupressure points are located with a point locator which includes a low-current galvanometer, commonly known as GSR monitor. A pressure point is located in the region where the electrical resistance of the skin is relatively lower than that of its surrounding. The grounding pole is held in subjects hand to establish ground contact, while the search pole (like pen tip) is pressed at different locations to detect the point. When the tip of the search probe contacts the skin in that region, the low resistance causes a surge of electric current through the GSR monitor. The current surge signifies a pressure point. Proper skin preparation and electrode positioning are essential elements in acquiring quality SEMG measurements. The acupressure points being the lower skin impedance point will defiantly produce the better results for SEMG analysis. Moreover, electrode pressure on the pressure points will assist the SEMG analysis as the blood and bioelectrical energy circulate properly.

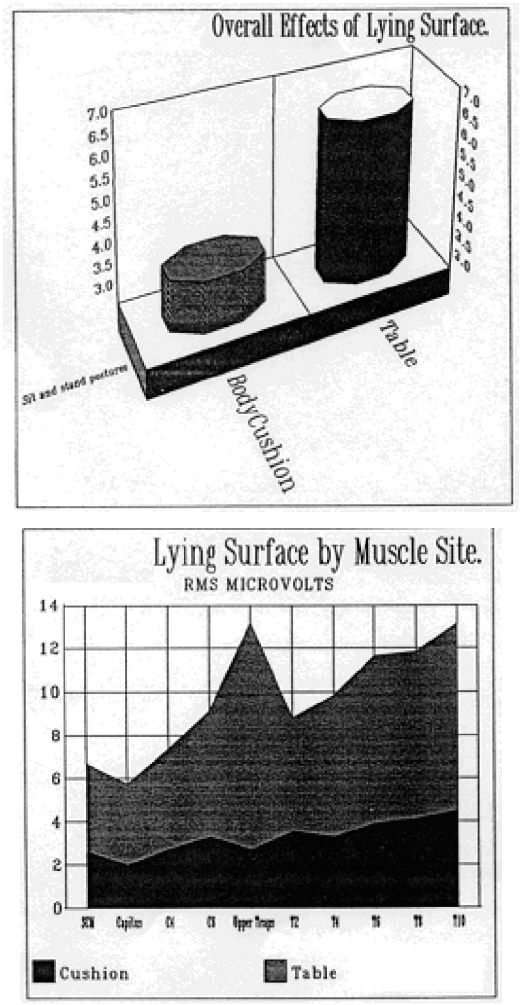

Fig. 4.1 Prof. Cram's result for massage technique comparison [Cram, 1994]

An SEMG analysis was done by a research group [Cram, 1994] where conventional massage system is compared with a combination of Swedish massage and acupressure techniques. The conventional message used body support system having cushion table and acupressure technique used standard massage table. SEMG recordings were taken from upper back and neck regions in three different postures just prior to and immediately following each massage. Fig. 4.1 is showing one of the conclusions of the research that massage with acupressure techniques showed higher values of SEMG-RMS values measured post-massage in all the ten muscles sites. At these points, SEMG signal needed to be compared to have some relational explanation for interpretation of movements/postures. The selections of these conventional acupressure points were made after matching and choosing from the locations as selected in section 3.4 on the basis of active muscle group. These selected acupressure points were shown in Table 4.1.

4.1 SEMG variations for forced gripping at acupressure points

The one major objective of the present investigation is to the study of muscle activities at different selected pressure points during different function of hand. Many research outcomes are available concluding the nature of response of force exerted by a muscle vs. SEMG-RMS parameter to be almost linear [Villasenor-Herrera, 2008]. Four pressure points were selected for the SEMG study on arm as shown in Table 4.1. Here variations between grip force vs. SEMG's V_{rms} (V_{rms}) and SEMG's Average frequency (Av freq) were studied.

4.1.1 Acquisition Details: In both the cases of upper or below prosthetic arm elbow movement and precise gripping are essential. Many research outcomes are available concluding the nature of response of force vs. SEMG to be almost linear (Villasenor-Herrera, 2008). Hence, grip force vs. SEMG-V_{rms} and SEMG-Average frequency were studied. Single channel recording was done from all the three subjects at selected acupressure points with grip-force measuring exercising instrument used in section 3.5.2 and shown in Fig. 4.2. For the SEMG study at the four selected acupressure points on arm as shown in Table 4.1. This study will help in getting descriptive relationship of the SEMG vs. V_{rms} parameter with the force exerted by the grip on pressure points. At different gripping force say 3 kg, 6 kg, 9 kg etc (as per the indication on the display of the instrument) the SEMG was recorded from the location

in the workspace of MATLAB using softscope. The force measuring instrument can measure up to 140 kg of grip force. Each person has different force exerting levels. Subjects had maximum level of 38 kg with comfortable exertion. For the analysis, variation was kept from 0- 38 kgs in steps as shown in Table 4.2-4.3.

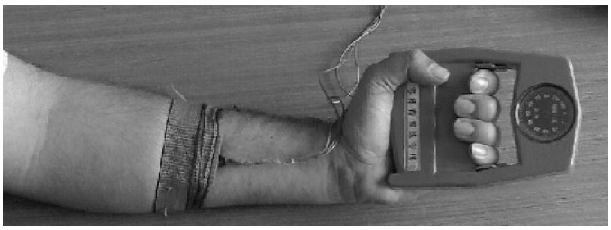

Fig. 4.2 Exercising gripper with electrode on the selected location

Table 4.1
Selective pressure points on human arm [Online ref.5; Online ref.7]

Description	Figure	Location syntax
Name: Great Mount Location: On the middle of the palm-side of the wrist		cw (Consider wrist)
Name: Outer Frontier Gate Location: On the lower arm, on the top side, two thumb widths below the crease of the wrist. In the middle, in the depression between the bones and tendons.		cwb (Consider wrist back)
Name: Crooked Pond Location: On the side of the elbow, on the outer side of the arm. The point is located at the end of the crease at the elbow. This is halfway up the side of the arm.		ce (Consider elbow)
Name: Heavenly Palace Location: On the upper arm, one hand width under the armpit. The point is located in the depression between the muscles from the shoulder and the biceps		cb (Consider biceps)

4.1.2 Results and discussions

For analysis purpose, variation is kept from 0- 38 kgs in steps as shown in Table A4.1-A4.4 (appendix), and selected parameters; Vrms, variance, standard deviation and Av freq were evaluated as explained in section 3. The subsequent plots are shown from Fig. 4.3 (a, b, c)-4.4. it was observed from the study of the three parameters i.e. $V_{rms,}$ variance and standard deviation that variation of force exerted by muscle and V_{rms} remains linear from 0 to approximately 85% of the maximum force exerting capacity of the person, after that SEMG generated remains constant or start to decrease due to fatigue as shown in Fig.4.3 (a, b, c) [Hong-Chun el at.,2005; Caohua el at., 2007; Zaman el at., 2007]. Fig. 4.4 confirms that SEMG's Av freq remains between the selected ranges as per the band pass filter.

This analysis verifies that SEMG activities are there on pressure points if selected sensibly which encourage advancing the work for specific movement measurement. To map the locations for the proper multifunctional prosthetic, selected acupressure points may also be considered. Further, the pressure points are needed to be compared with other locations on arm for SEMG analysis which is further carried out in chapter 5. Another interpretation about SEMG strength with the exerted force is that SEMG strength is found to be more on above elbow compared to below elbow. This gives the assurance that above elbow prosthesis can also be developed with precise controls of grip.

Three plots along with the calculation of the chosen parameters: firstly raw SEMG secondly filtered and lastly FFT of the filtered SEMG (of single subject) are shown in Fig. A4.1-A4.4 (appendix) for 07 selected force levels. They are represented as location syntax with force level i.e. for location "cb (consider biceps)" they are "cb3", "cb6", "cb9", "cb13", "cb20", "cb28" and "cb38".

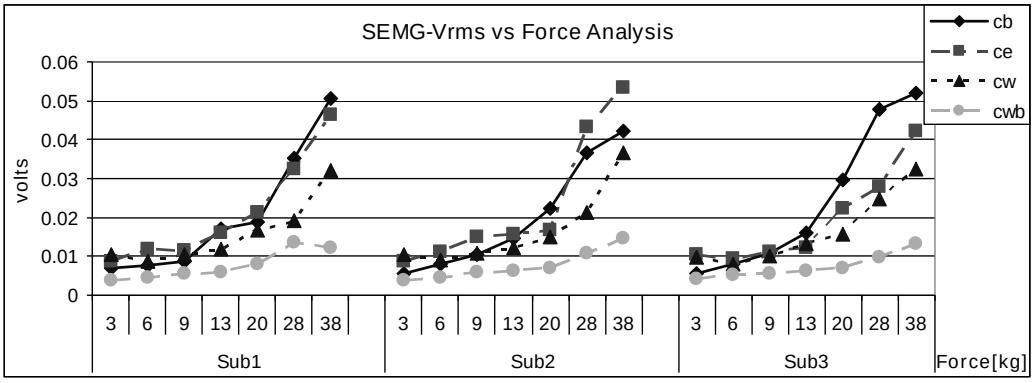

Fig.4.3a Force vs. V_{rms} at selected four pressure points

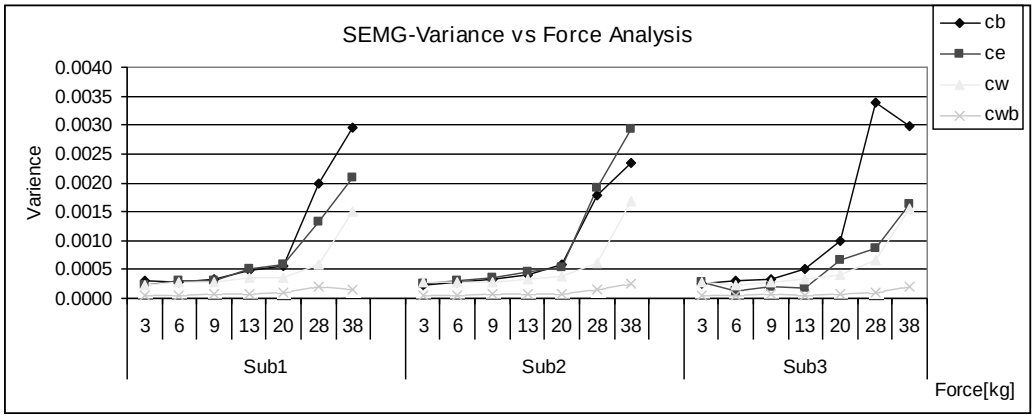

Fig.4.3b Force vs. Variance at selected four pressure points

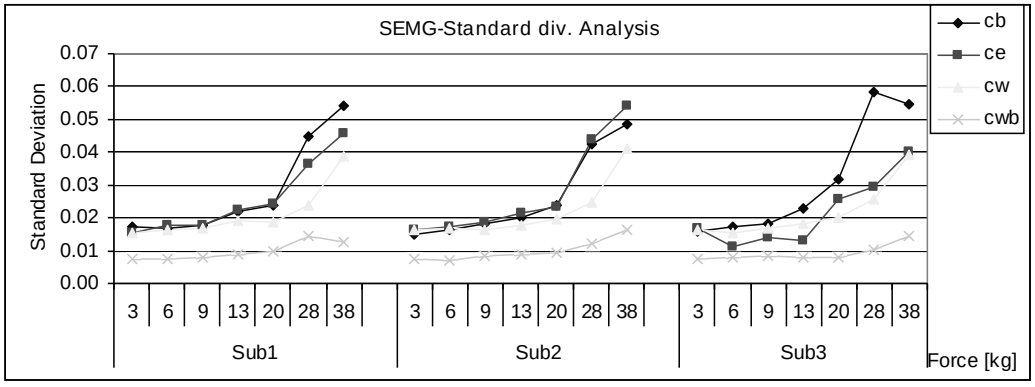

Fig.4.3c Force vs. Standard deviation at selected four pressure points

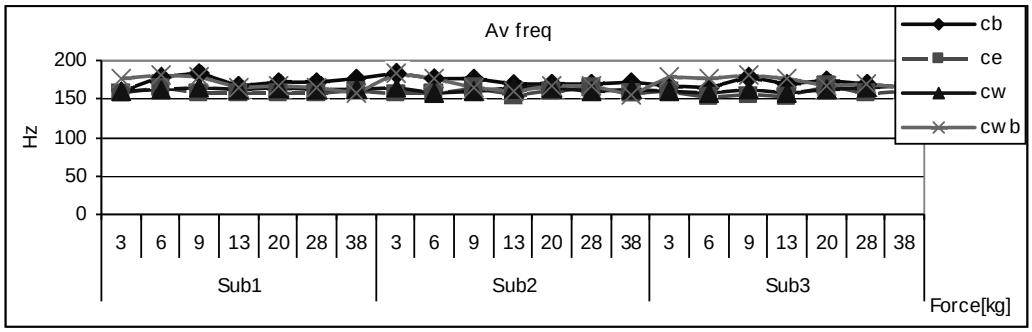

Fig.4.4 Force vs. Av freq at selected four pressure points

4.2 SEMG activities for hand movement discrimination at selected pressure points

SEMG signals are acquired from a superficial muscle by using differential amplifier. Proper location of electrode placement on the skin matters in getting good quality of signal for a specific movement. Many research groups are trying to set electrode sites on human body as SEMG points. These set of points are also being characterized for a specific movement of the respective body part. The SEMG activities must needed to be observed from acupressure points. In this section, SEMG activities were observed from the different location of arm to map the hand movements. In the consecutive chapters, pressure point SEMGs will be studied with other locations.

4.2.1 Acquisition details

In order to demonstrate the classification performance, the scatter plots of SEMG features between two muscles for four movements of wrist were used to confirm the variation. The two muscle groups were selected as shown in Table 4.2. Three subjects of age group 30-35 years were selected for acquiring SEMG. Parameter used for the analysis was V_{rms} as described in section 3.4. The four hand movements were grip-closing (cl), grip-opening (op), wrist-down (d) and wrist-up (u).

Table 4.2
Selected pressure points on human arm

Description	Figure	Location syntax
P-7 Name: Great Mount Location: On the middle of the palm-side of the wrist		cw (consider wrist)
TB-5 Name: Outer Frontier Gate Location: On the lower arm, on the top side, two thumb widths below the crease of the wrist. In the middle, in the depression between the bones and tendons.		cwb (consider wirst back)

4.2.2 Results and discussions

Table 4.3 shows the values of V_{rms} calculated from the respective SEMG signals acquired from the two chosen locations. These two locations are the acupressure points. In the section 4.1, this was concluded that the SEMG at acupressure points behave linear w.r.t the force excreted by the respective muscle under observation. Variance and covariance are often displayed together in a variance-covariance matrix. The variances appear along the diagonal and covariance appears in the off-diagonal elements, as shown Table A4.5a, b, c (appendix). Covariance is a measure of the extent to which corresponding elements from two sets of ordered data move in the same direction.

The objective of this analysis was to advance the finding of SEMG at pressure points can be useful for hand function discriminations. Fig. 4.5 shows scatter plot of the three subjects. The data points of each movement are grouped pattern recognition. It was also classified by using variance-covariance matrix for movement discrimination.

Table 4.3
SEMG-V_{rms} variation at acupressure points "cw" and "cwb"

Movement	subject1		subject2		subject3	
	cw	cwb	cw	cwb	cw	cwb
closing	0.1	0.07	0.08	0.09	0.05	0.22
closing	0.13	0.14	0.11	0.12	0.1	0.18
closing	0.1	0.08	0.12	0.14	0.05	0.17
closing	0.09	0.07	0.13	0.13	0.06	0.19
closing	0.12	0.08	0.12	0.09	0.11	0.23
opening	0.11	0.16	0.22	0.22	0.2	0.48
opening	0.14	0.17	0.24	0.15	0.11	0.42
opening	0.17	0.18	0.14	0.14	0.17	0.54
opening	0.16	0.26	0.19	0.23	0.16	0.56
opening	0.25	0.16	0.2	0.22	0.2	0.52
down	0.09	0.06	0.07	0.05	0.11	0.13
down	0.12	0.1	0.11	0.07	0.18	0.14
down	0.09	0.08	0.05	0.07	0.16	0.2
down	0.08	0.07	0.07	0.06	0.2	0.2
down	0.06	0.08	0.08	0.06	0.18	0.15
up	0.12	0.15	0.1	0.08	0.09	0.35
up	0.16	0.17	0.09	0.09	0.08	0.33
up	0.1	0.16	0.09	0.13	0.06	0.25
up	0.15	0.16	0.09	0.13	0.06	0.43
up	0.16	0.13	0.06	0.11	0.08	0.52

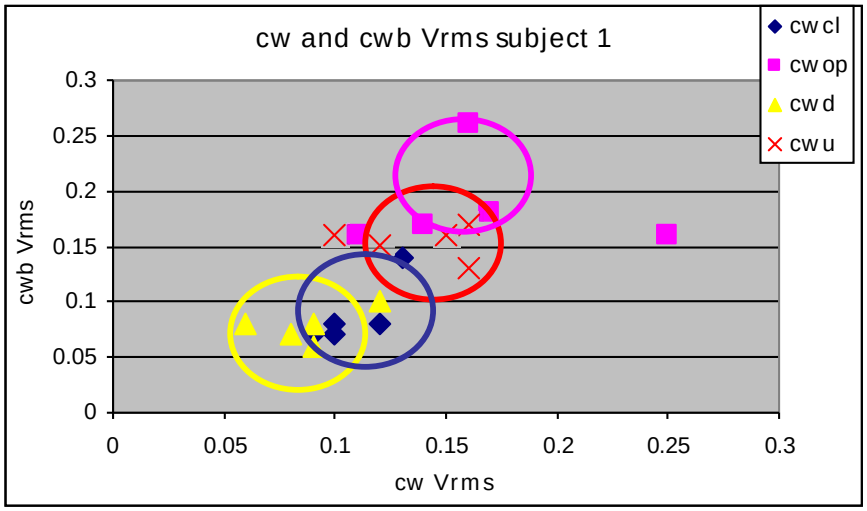

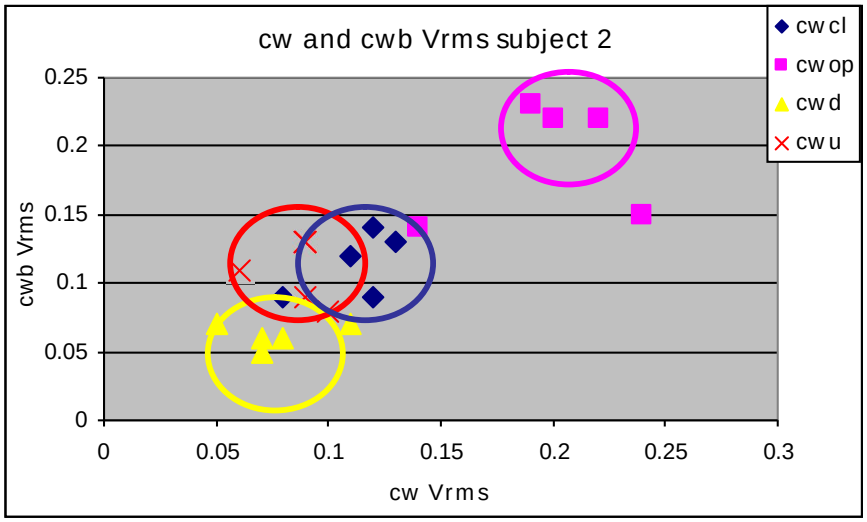

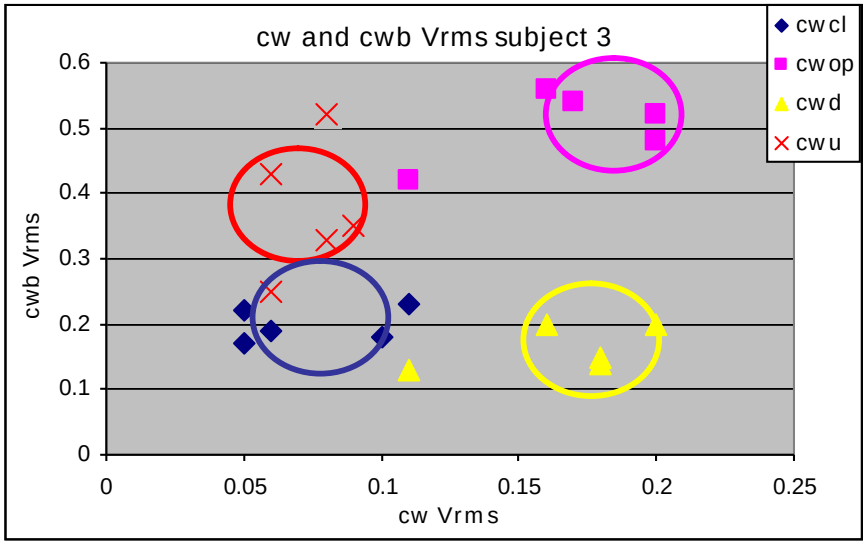

Fig. 4.5 Scatter plots for electrode locations “cw” and “cwb”

In this analysis, V_{rms} was used to indicate the quality of separation using the observation from scatter plot. The scatter plot is between V_{rms} values of "cw (consider wrist)" and "cwb (consider wrist back)" locations. It represents a two channel acquisition system i.e. electrode pairs are at "cw" and "cwb". Fig. 4.5 shows that opening of grip is the best among the chosen movements. However, distance of separation between closing and opening describes that the threshold type of control for the prosthetics can be formulated.

The same observation was studied by using Variance- covariance matrix. This can interpret the variance and covariance statistics in matrix to understand how the variables (i.e. movements) vary and covary. Diagonal elements are the variance and off-diagonal elements are the covariance as shown in Table A4.5 (a, b, c) (appendix) (in italics and bold) for all the three subjects respectively.

The variance describes the best movement under two channel approach considering "cw & cwb" whereas covariance describes the inter-variance difference between the movements. Subject-wise both the variance and covariance were plotted in Fig. 4.6(a, b, c) and Fig. 4.7(a, b, c) respectively.

Considering Variance from Figs. 4.6(a, b & c) it is observed that out of the four chosen operations, the opening of the grip shows the high level of the SEMG activity at "cw and cwb". Similarly Figs. 4.7(a, b & c) (which considers the covariance between the grip closing & opening, wrist up & down and grip opening & wrist up) show that covariance is more for the grip opening & wrist up (op-u) and shows that both the datas are moving in positive direction. Hence, op-u movements will be easily distinguishable for two channel approach at "cw & cwb".

Further, their effectiveness with other anatomically chosen SEMG locations are studies in chapter 5 section 5.3 using PCA.

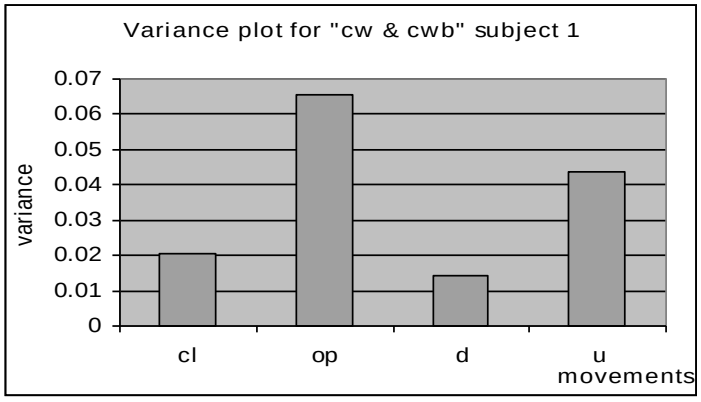

Fig. 4.6a Variance for determining best movement at “cw & cwb”; subject 1

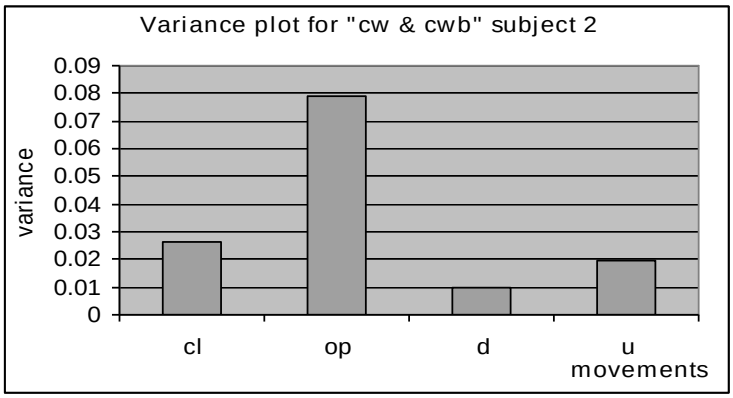

Fig. 4.6b Variance for determining best movement at “cw & cwb”; subject 2

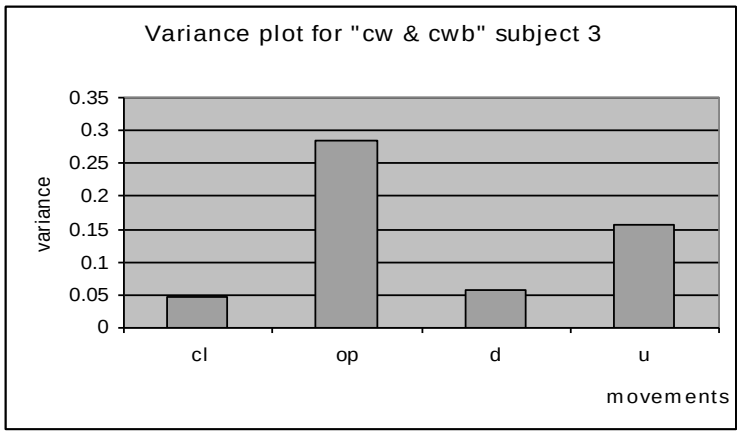

Fig. 4.6c Variance for determining best movement at “cw & cwb”; subject 3

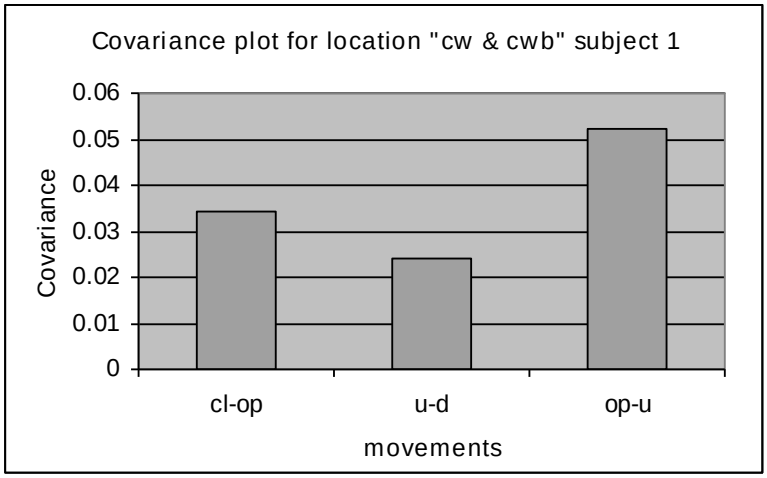

Fig. 4.7a Covariance between movements at “cw & cwb”; subject 1

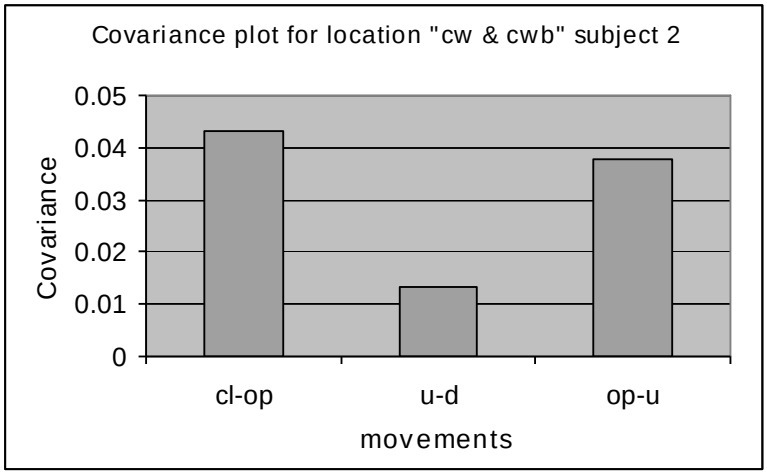

Fig. 4.7b Covariance between movements at “cw & cwb”; subject 2

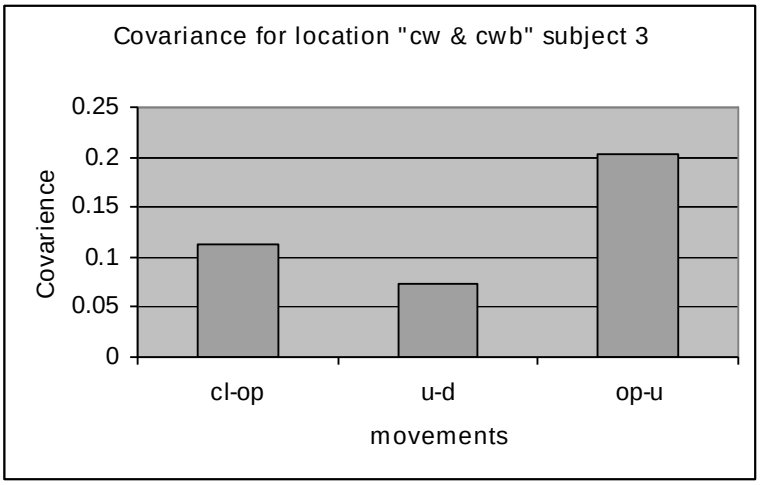

Fig. 4.7c Covariance between movements at “cw & cwb”; subject 3

4.3 SEMG analysis at acupressure points for grip closing and opening

Acupressure points SEMG signal varies with exerted muscle force and hand movement discrimination is also possible if SEMG is analyzed collectively at two or more pressure points. In this section a discriminating analysis is done on three acupressure points of below elbow arm to identify the four movements. It helps in locating acupressure point will be suitable for a specific movement.

4.3.1 Acquisition details

Parameters used for the analysis were: V_{rms}, Es, slope, mf, Av freq, pk freq, and pk amp (as described in 3.4). Three subjects of age group 30-35 years were selected for acquiring SEMG. Single channel recording was used. The two hand movements were selected for the analysis grip-closing (cl), grip-opening (op) as these two movements are mostly performed in day to day activities. Three acupressure points "cw(consider wrist)", "cwb(consider wrist back)", and "ce(consider elbow)" were selected for the analysis as shown in Table 4.1.

4.3.2 Results and discussions

SEMG was acquired as per the methodology as mentioned in chapter 3 section 3.3. All the chosen parameters were calculated and represented in Table 4.4(a,b,c) subject-wise. Two movements were analyzed at three acupressure points making six cases for the study. "cwcl" means closing movement performed and location was "cw", Similarly, "ceop" means opening movement performed with electrode site of "ce (consider elbow)". Fig. 4.8 (a, b, c) shows the plot of each selected parameters with respect to the respective selected acupressure location from the three subjects. In all the three subjects the closing was prominent in SEMG from location "ce (consider elbow)", but grip-opening was prominent in the SEMG from location "cwb (consider wrist back)". Again at location "cwb (consider wrist back)" SEMG threshold could distinguish grip opening/closing as later one generated low amplitude SEMGs. Parameters depending upon the amplitude of the SEMG i.e. V_{rms}, Es, slope and pk amp were behaving all most the same. Frequency dependent parameters showed that the frequency of the SEMG remains constant in the selected range at every location i.e. near 180 Hz.

Table 4.4a
SEMG parameters of subject 1

	Grip-closing				Grip- opening		
	cwcl	cwbcl	cecl		cwop	cwbop	ceop
V_{rms}	0.25	0.24	0.32		0.15	0.32	0.12
Es	31.19	27.11	50.07		10.44	49.12	6.94
slope	3478.00	2159.30	3165.40		1418.10	3576.50	1033.70
mf	182.62	189.45	173.83		181.64	172.85	173.83
Av freq	166.50	192.87	172.97		183.23	158.20	151.12
pk freq	189.45	199.22	192.38		178.71	174.80	190.43
pk amp	55.53	53.03	60.33		33.87	73.77	19.73

Table 4.4b
SEMG parameters of subject 2

	Grip-closing				Grip- opening		
	cwcl	cwbcl	cecl		cwop	cwbop	ceop
V_{rms}	0.19	0.28	0.32		0.14	0.32	0.12
Es	18.00	37.58	50.07		9.54	49.12	6.94
slope	1625.50	2715.10	3165.40		1359.80	3576.50	1033.70
mf	177.73	175.78	173.83		174.80	172.85	173.83
Av freq	166.99	152.83	161.00		162.84	173.46	161.00
pk freq	175.78	196.29	192.38		173.83	174.80	190.43
pk amp	34.89	52.69	60.33		27.00	73.77	19.73

Table 4.4c
SEMG parameters of subject 3

	Grip-closing				Grip- opening		
	cwcl	cwbcl	cecl		cwop	cwbop	ceop
V_{rms}	0.25	0.23	0.29		0.13	0.31	0.12
Es	30.46	25.89	42.90		9.12	48.11	6.52
slope	585.15	412.65	487.68		264.07	558.4	159.5
mf	175.78	185.55	159.18		172.85	170.9	166.99
Av freq	166.75	166.14	173.34		158.33	158.2	151.12
pk freq	190.43	199.22	178.71		173.83	174.8	190.43
pk amp	54.505	52.76	55.967		26.139	73.529	19.649

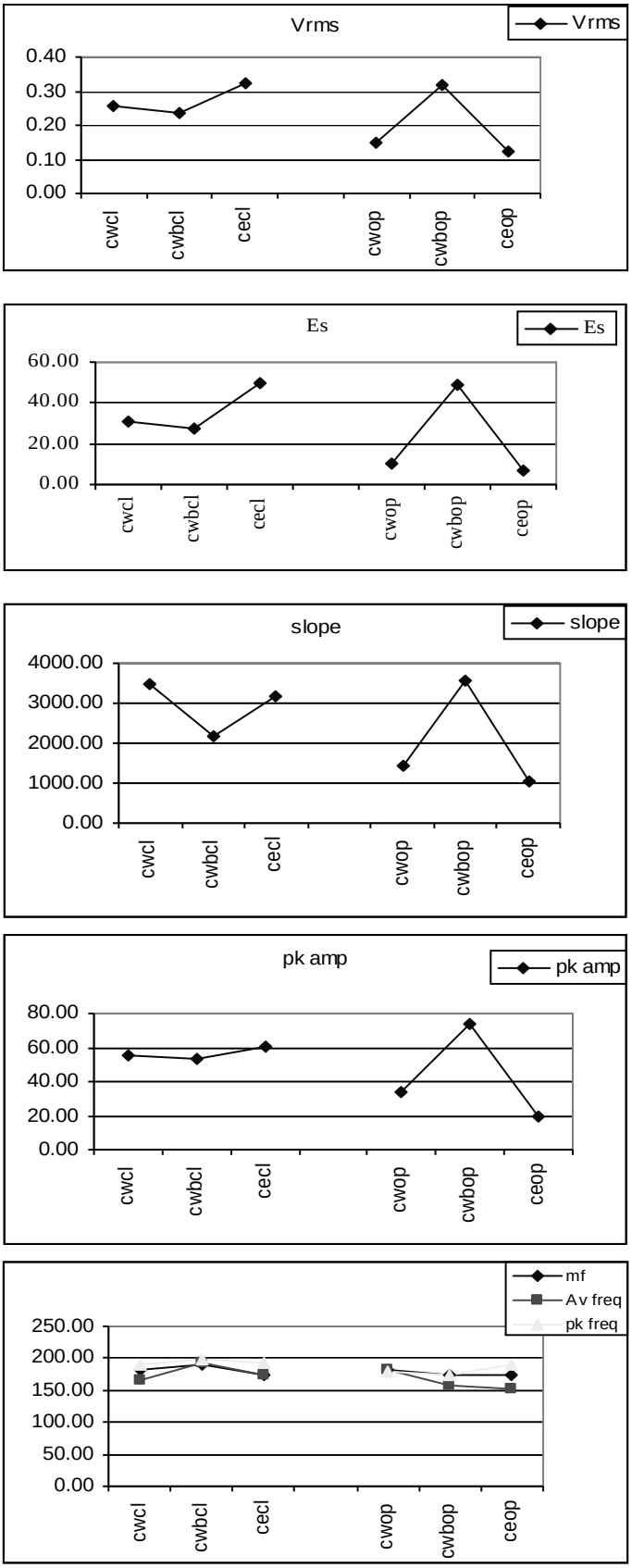

Fig. 4.8a Parameters at acupressure points for grip closing/opening of subject 1

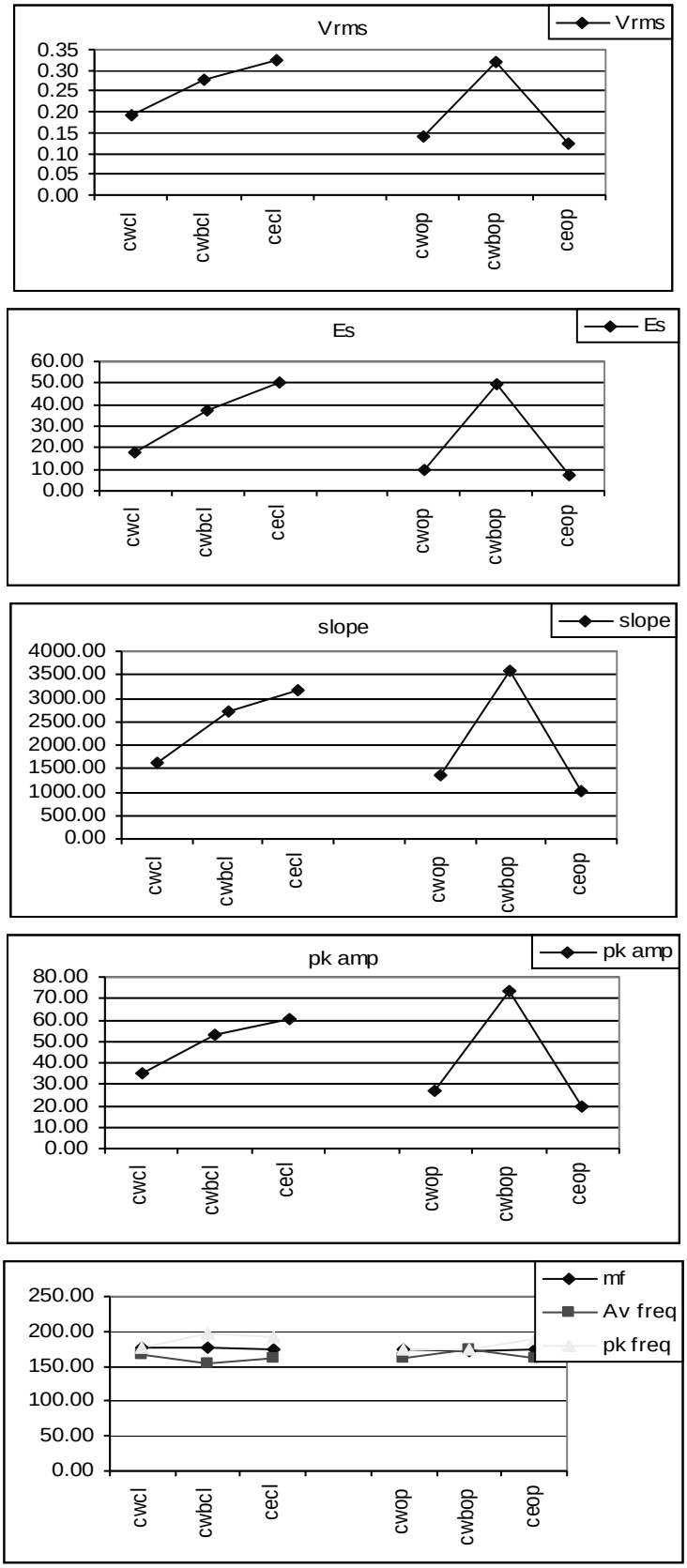

Fig. 4.8b Parameters at acupressure points for grip closing/opening of subject 2

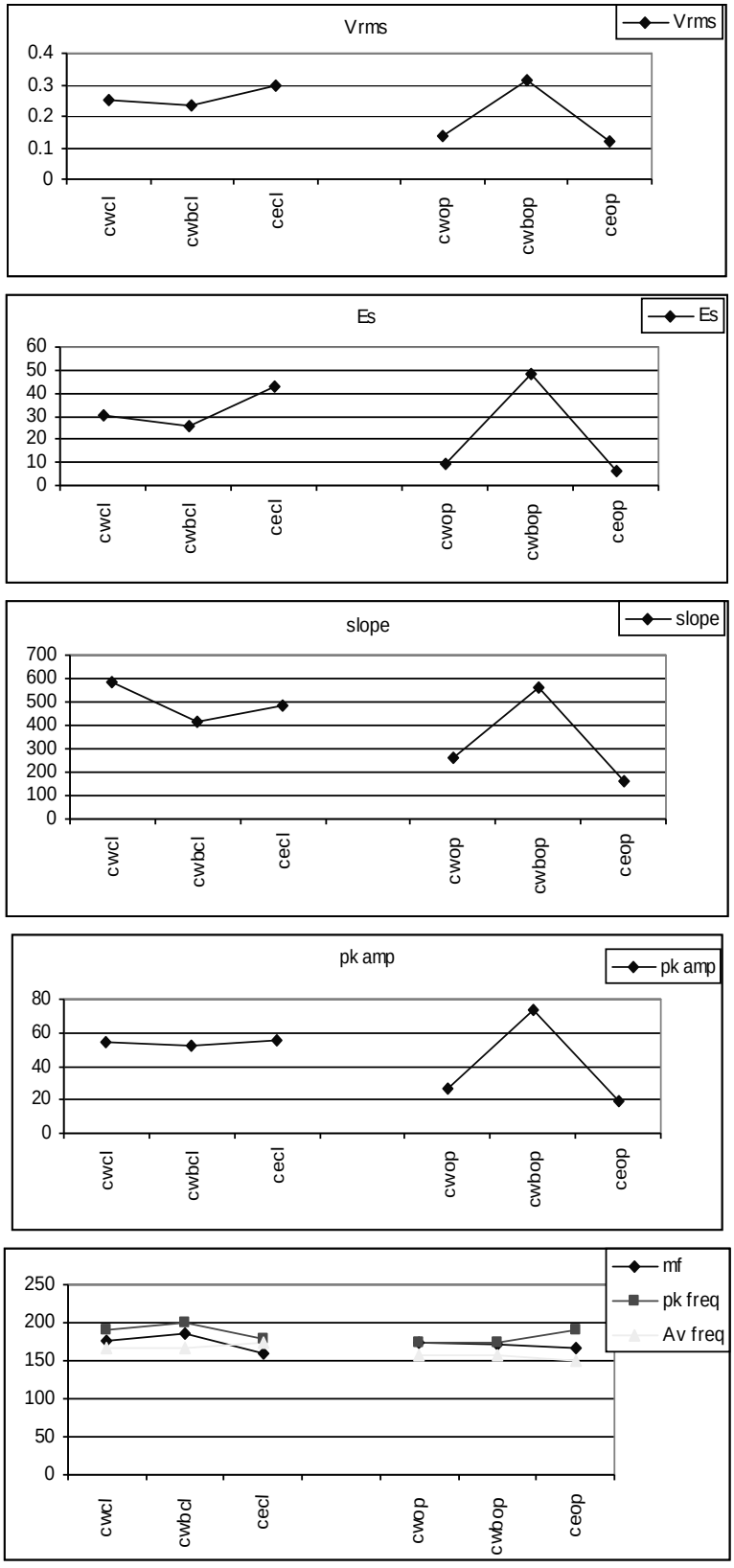

Fig. 4.8c Parameters at acupressure points fro grip closing/opening of subject 3

After studying the Fig. 4.6-4.8, it was observed that V_{rms} and Es almost have same patterns. However, slight differences were observed in slope values as compared to V_{rms} and Es. The slope values dipped more at lower values so it can be concluded that it will be better to use Slope for further investigations. However, the final decision to use Slope or V_{rms} may be taken on the basis of computational complexity and available hardware for implementation. These all observations indicate the SEMG activities on pressure points. Another interesting observation is regarding the closing of grip and level of SEMG at the selected locations. SEMG level is found to be increasing from wrist to above elbow region. Thus, for above elbow prosthetic arm the artificial gripper can be easily realized.

Chapter's Summary:

Researchers have identifying sites on skin as the best SEMG acquiring locations (as European SENIAM research) but acupressure were not considered. The present studies indicate that the acupressure points can also be good SEMG locations to discriminate hand movements. Further it is also concluded that slope can be used as parameter for hand function discrimination.

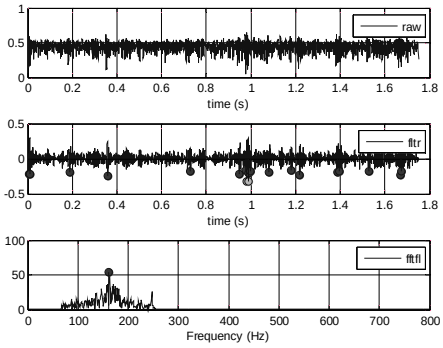

cb3

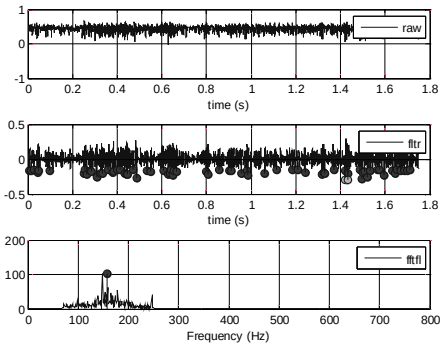

cb6

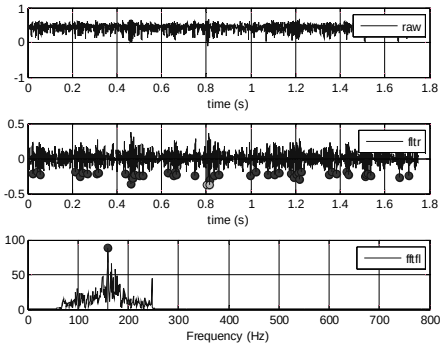

cb9

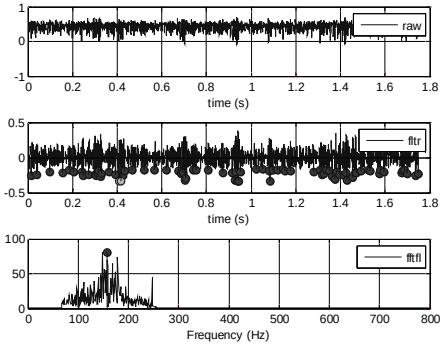

cb13

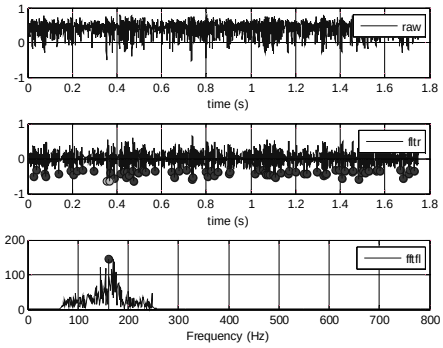

cb20

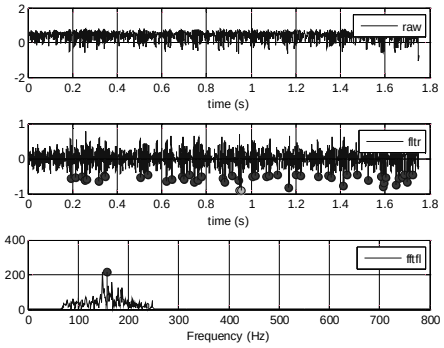

cb28

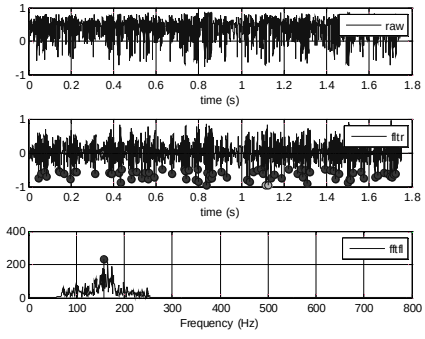

cb38

Fig. A4.1 Plots for electrode location “cb” for 07 selected force levels

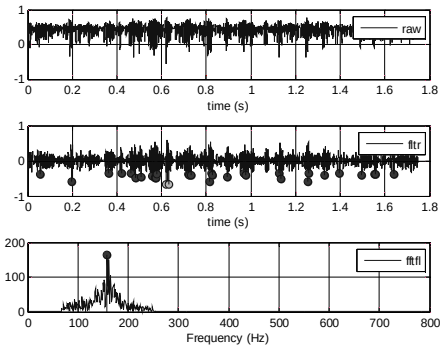

ce3

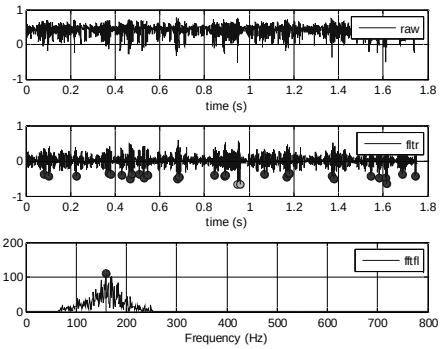

ce6

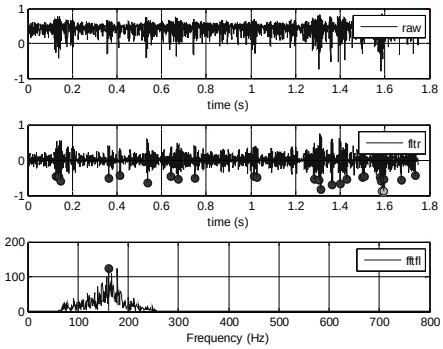

ce9

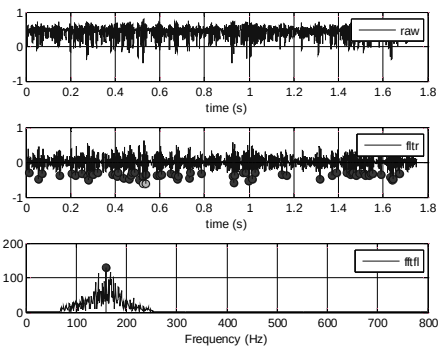

ce13

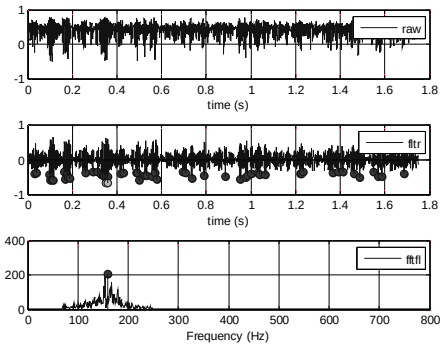

ce20

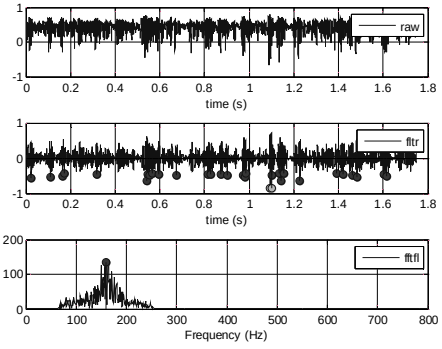

ce28

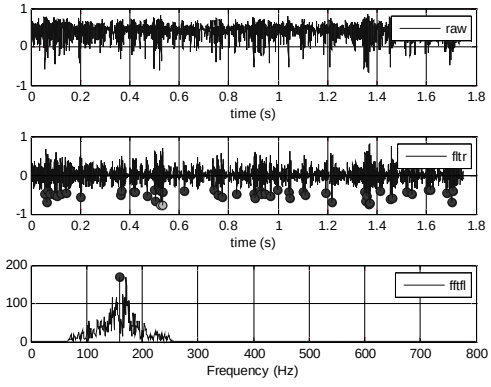

ce38

Fig. A4.2 Plots for electrode location “ce” for 07 selected force levels

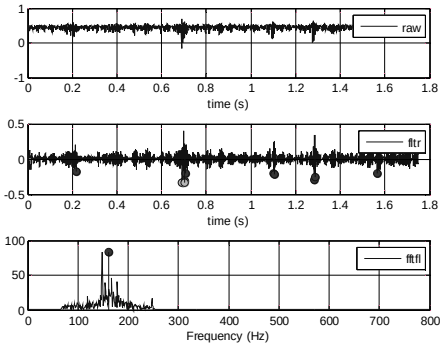

cw3

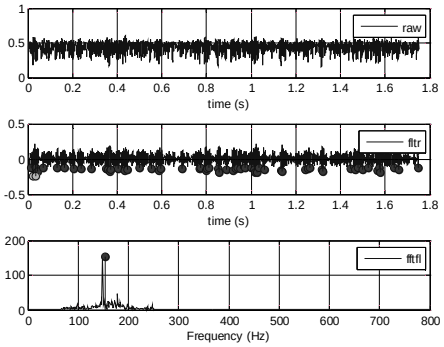

cw6

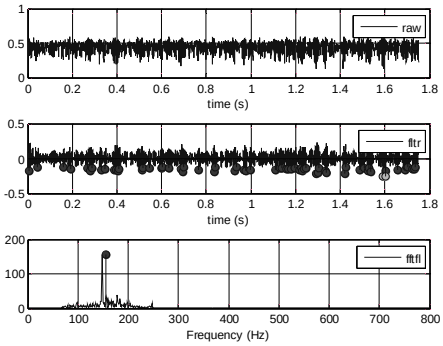

cw9

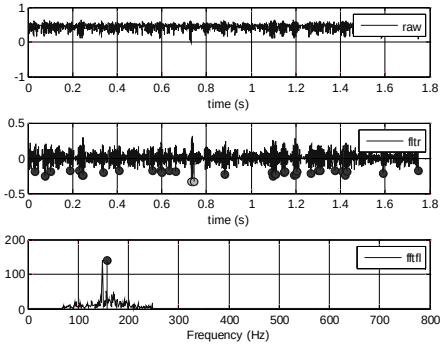

cw13

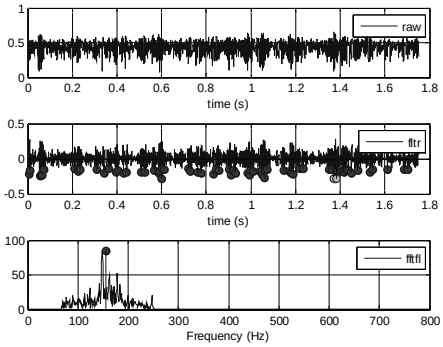

cw20

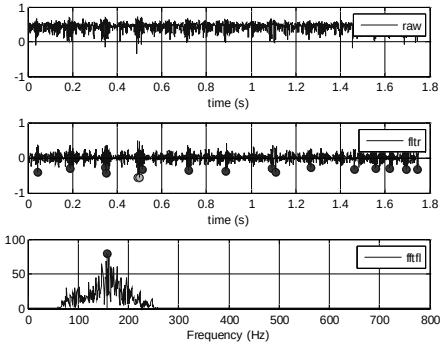

cw28

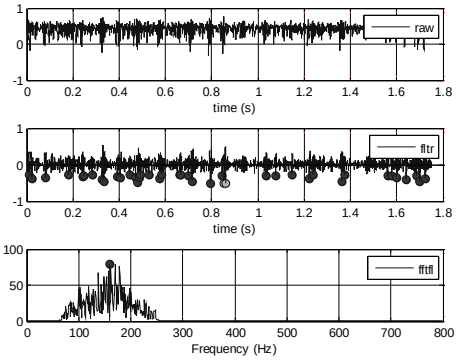

cw38

Fig. A4.3 Plots for electrode location “cw” for 07 selected force levels

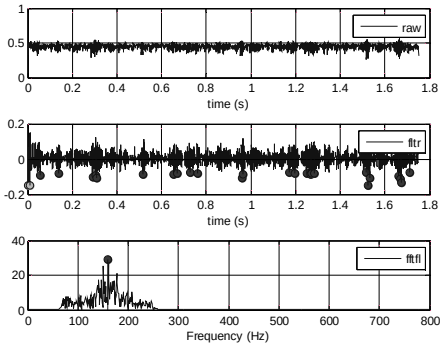

cwb3

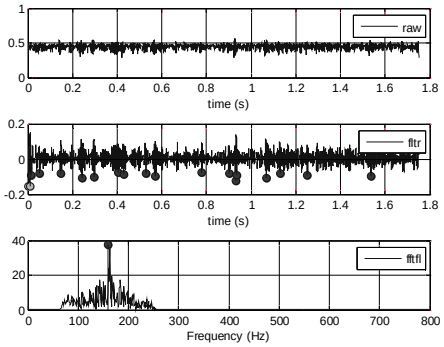

cwb6

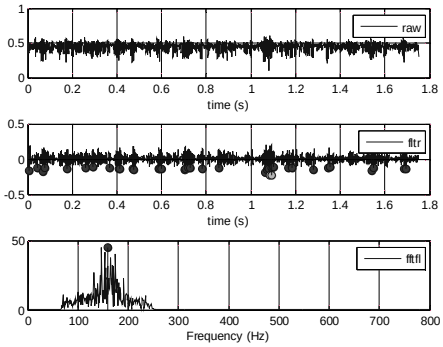

cwb9

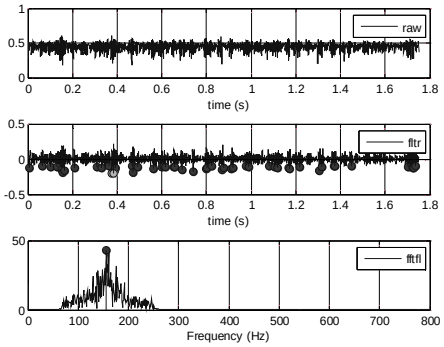

cwb13

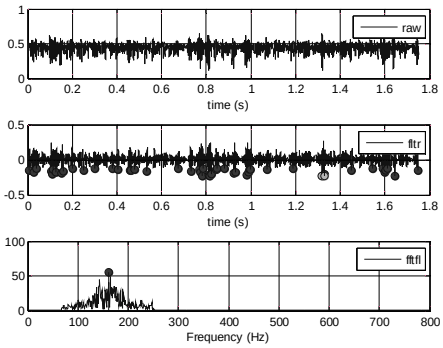

cwb20

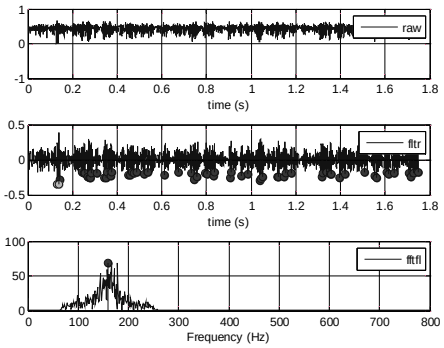

cwb28

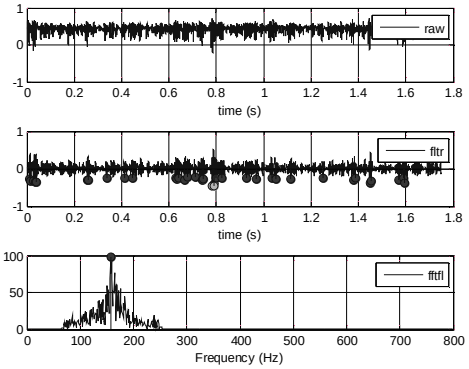

cwb38

Fig. A4.4 Plots for electrode location “cwb” for 07 selected force levels

Table A4.1

SEMG-V_{rms} vs. Grip-force

		V_{rms}			
	Force[kg]	cb	ce	cw	cwb
Sub1	3	0.0069	0.0086	0.0104	0.0037
	6	0.0077	0.0118	0.0087	0.0044
	9	0.0088	0.0114	0.0104	0.0057
	13	0.0172	0.0161	0.0118	0.006
	20	0.019	0.0212	0.0167	0.0079
	28	0.0354	0.0324	0.0191	0.0136
	38	0.0507	0.0463	0.0321	0.0122
Sub2	3	0.0057	0.0086	0.0105	0.004
	6	0.008	0.0112	0.0089	0.0044
	9	0.0103	0.0149	0.0109	0.0058
	13	0.0147	0.0158	0.0121	0.0064
	20	0.0223	0.0169	0.0151	0.0071
	28	0.0366	0.0433	0.0212	0.0109
	38	0.0422	0.0533	0.0367	0.0148
Sub3	3	0.0056	0.0103	0.0097	0.0041
	6	0.0081	0.0095	0.008	0.0053
	9	0.0108	0.0112	0.0101	0.0057
	13	0.0162	0.0121	0.0133	0.0063
	20	0.0296	0.0222	0.0157	0.0069
	28	0.0479	0.0278	0.0247	0.0096
	38	0.0519	0.0421	0.0326	0.0133

Table A4.2

SEMG-Av freq vs. Grip-force

		Av freq			
	Force[kg]	cb	ce	cw	cwb
Sub1	3	161.1328	158.5286	158.8542	176.5951
	6	177.8971	163.8997	162.5977	181.4779
	9	184.4076	157.7148	164.5508	179.1992
	13	167.4805	157.7148	161.7839	163.8997
	20	172.8516	158.2031	163.5742	166.0156
	28	172.0378	158.0404	163.2487	164.388
	38	175.944	158.8542	161.4583	158.3659
Sub2	3	184.5703	157.7148	164.2253	183.431
	6	176.5951	157.5521	156.901	177.5716
	9	175.6185	165.2018	159.668	164.0625
	13	170.4102	156.0872	163.8997	161.1328
	20	168.7826	160.319	165.3646	167.4805
	28	169.4336	164.7135	161.1328	167.3177
	38	171.224	156.901	161.2956	156.0872
Sub3	3	167.3177	161.1328	160.1563	179.1992
	6	165.5273	153.3203	157.8776	177.4089
	9	179.6875	154.6224	163.0859	180.013
	13	168.457	152.5065	158.0404	176.9206
	20	173.9909	166.5039	162.5977	167.3177
	28	169.9219	158.5286	163.737	168.457
	38	165.2018	161.1328	167.9688	164.0625

Table A4.3
SEMG-Variance vs. Grip-force

	Variance				
	Force [kg]	cb	ce	cw	cwb
Sub1	3	0.000293	0.000231	0.000241	0.000053
	6	0.000282	0.000312	0.000272	0.000057
	9	0.000320	0.000315	0.000285	0.000066
	13	0.000477	0.000504	0.000368	0.000076
	20	0.000557	0.000580	0.000357	0.000092
	28	0.001993	0.001313	0.000574	0.000209
	38	0.002955	0.002098	0.001491	0.000157
Sub2	3	0.000220	0.000262	0.000269	0.000053
	6	0.000270	0.000296	0.000276	0.000048
	9	0.000333	0.000353	0.000271	0.000073
	13	0.000409	0.000455	0.000320	0.000083
	20	0.000577	0.000535	0.000377	0.000088
	28	0.001786	0.001916	0.000620	0.000144
	38	0.002349	0.002941	0.001686	0.000265
Sub3	3	0.000251	0.000278	0.000272	0.000053
	6	0.000295	0.000123	0.000239	0.000062
	9	0.000325	0.000196	0.000274	0.000070
	13	0.000513	0.000177	0.000328	0.000060
	20	0.001003	0.000664	0.000398	0.000066
	28	0.003396	0.000867	0.000662	0.000107
	38	0.002990	0.001625	0.001549	0.000206

Table A4.4
SEMG-Standard deviation vs. Grip-force

		Standard deviation			
	Force [kg]	cb	ce	cw	cwb
Sub1	3	0.017129	0.015201	0.015514	0.007285
	6	0.016797	0.017658	0.016497	0.007521
	9	0.017876	0.017741	0.016886	0.008108
	13	0.021834	0.022445	0.019178	0.008730
	20	0.023609	0.024091	0.018894	0.009579
	28	0.044639	0.036230	0.023959	0.014448
	38	0.054363	0.045804	0.038609	0.012516
Sub2	3	0.014818	0.016188	0.016402	0.007296
	6	0.016444	0.017213	0.016617	0.006955
	9	0.018262	0.018792	0.016451	0.008539
	13	0.020236	0.021342	0.017897	0.009090
	20	0.024024	0.023131	0.019428	0.009392
	28	0.042255	0.043776	0.024902	0.012009
	38	0.048462	0.054231	0.041056	0.016264
Sub3	3	0.015854	0.016662	0.016485	0.007248
	6	0.017170	0.011101	0.015467	0.007879
	9	0.018025	0.013983	0.016568	0.008343
	13	0.022640	0.013291	0.018112	0.007732
	20	0.031677	0.025760	0.019951	0.008148
	28	0.058274	0.029442	0.025733	0.010355
	38	0.054684	0.040308	0.039362	0.014364

Table A4.5a
Variance - covariance matrix subject 1

	closing	opening	down	up
closing	0.02032	0.03420	0.01678	0.02884
opening	0.03420	0.06576	0.02836	0.05214
down	0.01678	0.02836	0.01438	0.02420
up	0.02884	0.05214	0.02420	0.04352

Table A4.5b
Variance - covariance matrix subject 2

	closing	opening	down	up
closing	0.02626	0.04332	0.01566	0.02212
opening	0.04332	0.0787	0.02728	0.03774
down	0.01566	0.02728	0.01006	0.01326
up	0.02212	0.03774	0.01326	0.01966

Table A4.5c
Variance - covariance matrix subject 3

	closing	opening	down	up
closing	0.04588	0.11202	0.04472	0.08162
opening	0.11202	0.2858	0.11124	0.20308
down	0.04472	0.11124	0.0563	0.07320
up	0.08162	0.20308	0.07320	0.15546

CHAPTER 5
SEMG ANALYSIS FOR HAND FUNCTION DIFFERENTIATION

This chapter elaborates the experimentation and result obtained. Study was done for below elbow SEMG analysis supported by principal component analysis for hand function differentiation.

Surface electromyogram signal (SEMG) may be affected by various peripheral factors such as spacing; type and size of electrodes that have an influence on the signal [Knaflitz et al., 1991]. Frequency and amplitude of the signal changes depending upon the muscle's location within the body and the stress it undergoes. The signal is random, very small in amplitude and mixed with noise of different frequencies. The electrodes aligned along the muscle length close to each other results in an increase of higher frequency contents [Stashuk et al., 1999]. The prosthesis requires the signal to be picked up from the muscle. It is necessary to learn the muscle control so that myoelectric prosthesis can be used effectively. The decomposition of SEMG consists of a series of algorithms that are successively and iteratively applied to resolve a composite micro SEMG signal into its constituent motor unit action potential. SEMG contains the activity of four or more motor units where the individual action potentials become indistinguishable to the naked eye. The incidence of superposition among two or more motor units' action potentials becomes numerous and the shapes of the motor unit action potentials may approach in similarity [Reaz et al., 2006]. The timing information provides a complete description of the inter pulse interval, firing rate and synchronization characteristics. The morphology of the shapes of the MU action potentials provides information concerning the anatomy and health of the muscle fibers [Knaflitz et al., 1991; Gerber et al., 1988]. Measurement of SEMG depends on a number of factors like amplitude of the SEMG signal, time and frequency domain properties. SEMG signal had been studied for muscle activity by a laboratory set-up and filter algorithm for the frequency spectra [Schauer et al., 2004]. Methodological problems related to DFT based techniques have been studied for the estimation of spectral parameters of the surface myoelectric signal [Merlettit et al., 1989]. Modern spectrum analysis has been recently applied to various biomedical signal processing. Power spectrum estimates of SEMG were obtained by maximum entropy method and compared with the estimates by fast Fourier transform [Ogino et al., 1983]. PC-based

methodologies for SEMG signal analysis provide efficient and effective ways of understanding the signal and its nature. A statistical study showed performance of various SEMG signal analysis along with hardware implementations using SEMG focusing on applications related to prosthetic hand - control, grasp recognition and human computer interaction [Shahid et al., 2005; Reaz et al., 2006; Hargrove et al., 2007]. The SEMG signal readings from upper arm muscles involved in elbow joint movement and sensed elbow angular position / velocity inputs. A single degree of freedom robotic experimental tested has been constructed, which allows for data collection, training and validation [Arora, 2007].

In this chapter firstly the interpretation of SEMG signals from the locations of human arm i.e. from shoulder to wrist was done to discriminate hand/wrist movements. Secondly, Principal component analysis was used to determine the best location with different sets of electrode numbers.

5.1 Interpretations of Wrist/Grip movements from SEMG signals at different locations on arm

Mimicking all the functions of hand in prosthesis is near impossible with present day technology whereas the study of different functions of hand along with the movements required to perform those functions may lead to a practical solution. The functional jobs of human hand can be divided into two major categories, i.e. based on day to day work and skilled work as indicated in Table 1.1, section 1.3. It is quite evident that 90% of day-to-day functions are grasping and release movement. The other works normally requires one out of four movements like wrist flexion, wrist extension, pronation or supination [Arora, 2002]. Two major approaches are being used by the researchers. The first, based on the works of Lawrence, Lyman et al., Jacobsen et al., used multiple electrode sites, at each of which the SEMG function/parameter is strongly correlated with a single limb function. In the second approach based on study of Graupe et al., used one or up to three electrode sites for multifunctional SEMG applications. It aims at recognizing via electrode sites where even very weak correlation between the measured signal and (more than one) limb functions may exist [Graupe, 1994]. Myoelectric prosthesis is very much appreciated for their easiness in controlling the movements and for the absence of wires and braces [Ryait, 2009; Joshi, 2009]. Differences in pattern of SEMGs must be detected for various limb functions (i.e. arm bending, arm extension, wrist pronation, wrist

supination, grasp, etc) taken at one or several stump muscles. Here, SEMG signals were measured with four channel sensor in wrist and were recorded as four channel's time series data, on which computer simulations were carried out for the wrist motions recognition [Yazama et al., 2004]. Another discrimination system used two surface electrodes to acquire the electromyography signal from the flexor digitorum superficialis muscle and the extensor pollicis brevis muscle. Here, eight types of hand movements, such as three-jaw chuck, lateral hand, hook grasp, power grasp, cylindrical grasp, centralized grip, flattened hand and wrist flexion were used as key movements in the discrimination system. The discrimination system achieved a success rate of 85% for off-line test and of 71% for on-line test [Huang et al., 1999].
The objective of the present study was to develop such a system so as to assess different muscles activities on arm during four basic movements namely opening (op) / closing (cl) / down (d) / up (u) of hand wrist/grip and find out the best electrode locations with suitable number of channels.

5.1.1 Acquisition Details

The single channel setup was used to acquire and store raw SEMG signals to describe movements from the SEMG signals extracted from different location on arm. Datasets were stored in workspace of MATLAB for the calculation of the selected parameters. For comparison analysis, four hand positions/movements/postures were selected as shown in Fig. 5.1. To decide the interpretation of the four chosen movements like opening (op)/closing (cl)/down (d)/up (u), two acupressure points (on wrist) were also selected for the additional analysis with other points on arm. Fig. 5.2 shows the selective six points on human arm for the analysis. Five trials were taken for each movement at each location from the three subjects. The subjects were male of age group of 30-35 years. The left arm was selected of each subject. The signals were stored from the six locations in the workspace. The following parameters were considered for the analysis as described in Section 3.4.

1. Slope
2. V_{rms}
3. Av freq

5.1.2 Results and Discussions

To further extend the study of relational interpretations of selected movements on the chosen locations on arm, two analytical approaches were applied for observations:

- Firstly, one movement was selected and its effect on SEMG signal at all the six locations were studied,
- Secondly, at a selected location effect of the chosen movements were studied.

Both the approaches have the same perspective to arrive at a conclusion. Each location was assigned a short syntax as indicated in Table 5.1.

	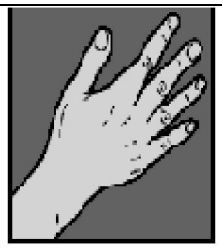		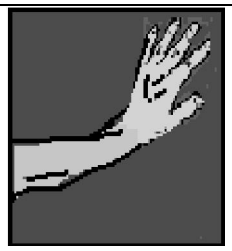
Closing	Opening	Down	Up

Fig. 5.1 Movements for analysis

Table A5.1-A5.4 [appendix] describes the slope values and V_{rms} values derived from the MATLAB program for comparison from six locations on arm for a movement from the three subjects. For the discrimination parameter slope was selected for further analysis. Fig. 5.3 shows overall average slope value (Av; white line) of five trials of each of the three subjects i.e. Av is the overall average of 15 trials. Each trial represents calculated slope value for a movement at different locations. The overall average (Av) gives the broader view of variation of SEMG signal for a movement; say for opening of hand grip highest level of SEMG signal was at location “camb”. On the basis of these observations, Table 5.3 was formulated which narrates maximum or minimum level of SEMG signal occurring at a specific movement. Hence, from Table 5.3 it can be suggested that which movement can be better acquired from which SEMG location using single channel system. Further, to relate slope and $V_{rms,}$ Table 5.2 is shown. The table describes Slope vs V_{rms} parameters for each movement independently at six selected locations on arm using clustering approach (MS-Excel). Both slope and V_{rms} are the parameter whose values depend

upon the amplitude of SEMG and are approximately proportional to each other. Parameter slope was chosen for the further analysis.

Table 5.1
Syntax used for database

Location Syntax	Location	Movement
cwcl	Wrist palm side	Closing
cwop	Wrist palm side	Opening
cwd	Wrist palm side	Down
cwu	Wrist palm side	Up
cwbcl	Wrist opposite -palm side	Closing
cwbop	Wrist opposite -palm side	Opening
cwbd	Wrist opposite -palm side	Down
cwbu	Wrist opposite -palm side	Up
camcl	Mid arm palm side	Closing
camop	Mid arm palm side	Opening
camd	Mid arm palm side	Down
camu	Mid arm palm side	Up
cambcl	Mid arm opposite -palm side	Closing
cambop	Mid arm opposite -palm side	Opening
cambd	Mid arm opposite -palm side	Down
cambu	Mid arm opposite -palm side	Up
cbetcl	Below elbow thumb side	Closing
cbetop	Below elbow thumb side	Opening
cbetd	Below elbow thumb side	Down
cbetu	Below elbow thumb side	Up
cbebcl	Below elbow little finger side	Closing
cbebop	Below elbow little finger side	Opening
cbebd	Below elbow little finger side	Down
cbebu	Below elbow little finger side	Up

Description	Figure	Location syntax
Two thumb widths from the largest crease on the inside wrist; Acupressure point	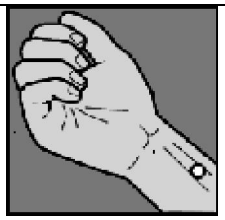	cw (consider wrist palm side)
Two thumb widths above the outside of the wrist; Acupressure point	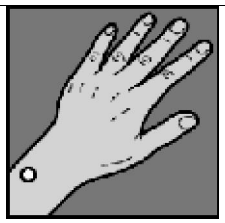	cwb (consider wrist opp. palm side)
This point is located on the crease of the inside of the below elbow on the thumb side.	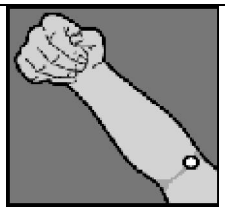	cbebt (consider below elbow thumb side)
This point is located on the crease of the inside of the below elbow on the little finger side.	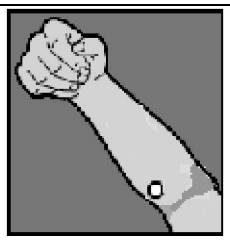	cbeblf (consider below elbow little finger side)
This point is located on the middle of arm on the centre line of the inside of the arm.	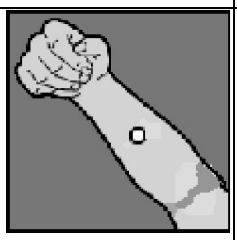	cam (consider mid arm palm side)
This point is located on the middle of arm on the centre line of the backside of the arm.	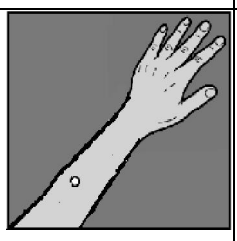	camb (consider mid arm opp. palm side)

Fig. 5.2 Selective points on human arm; two are pressure points [Online ref.7]

Table 5.2a
Clustering plots showing SEMG for comparison from six locations on arm, for an movement

Subject 1	Subject 2	Subject 3
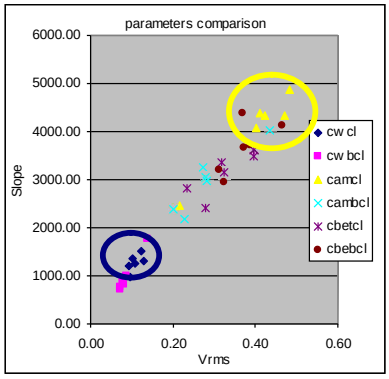	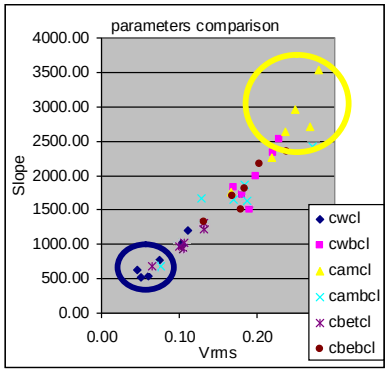	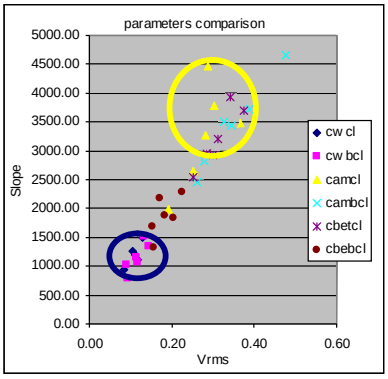
Closing	Closing	Closing
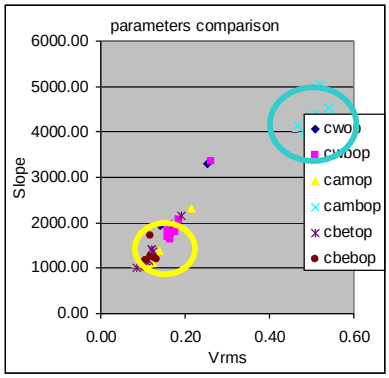	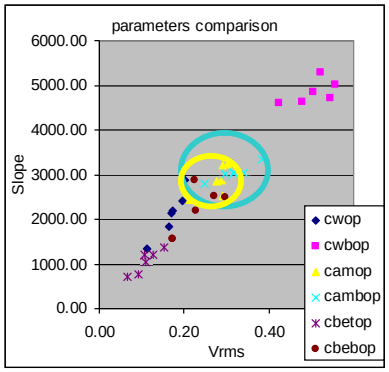	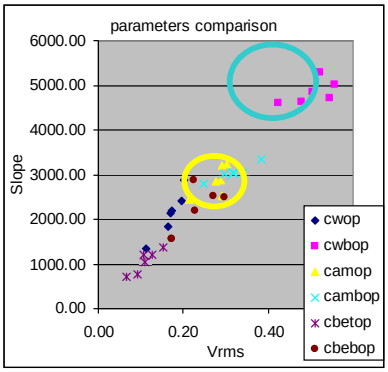
Opening	Opening	Opening
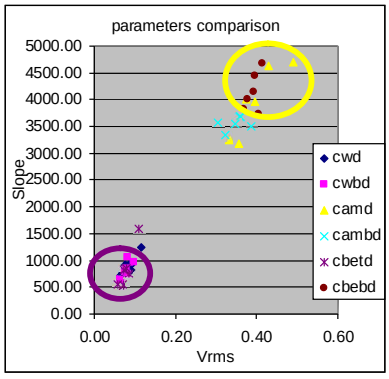	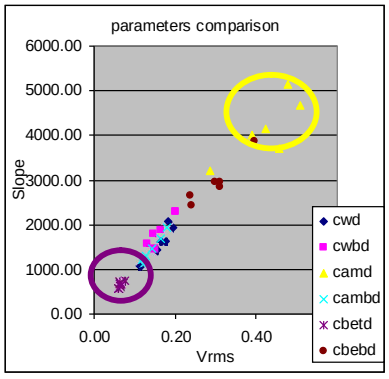	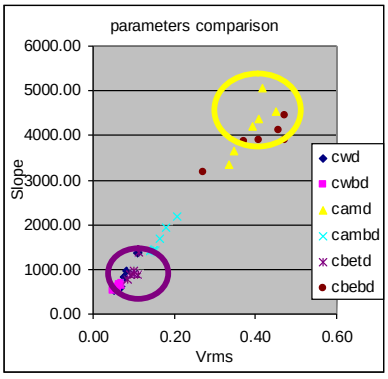
Down	Down	Down
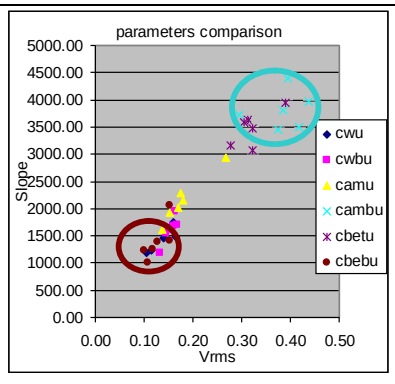	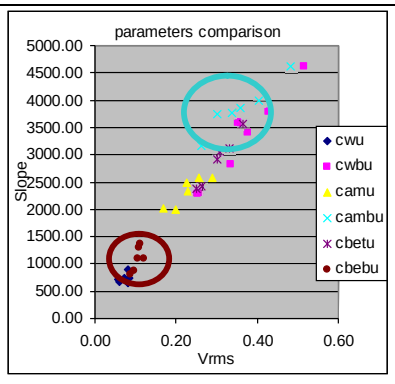	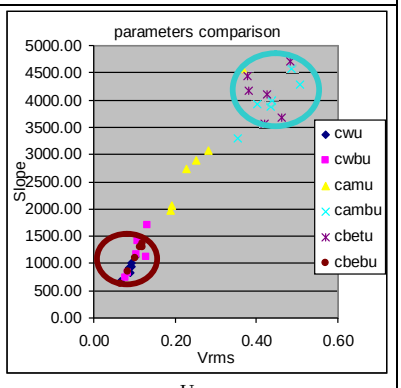
Up	Up	Up

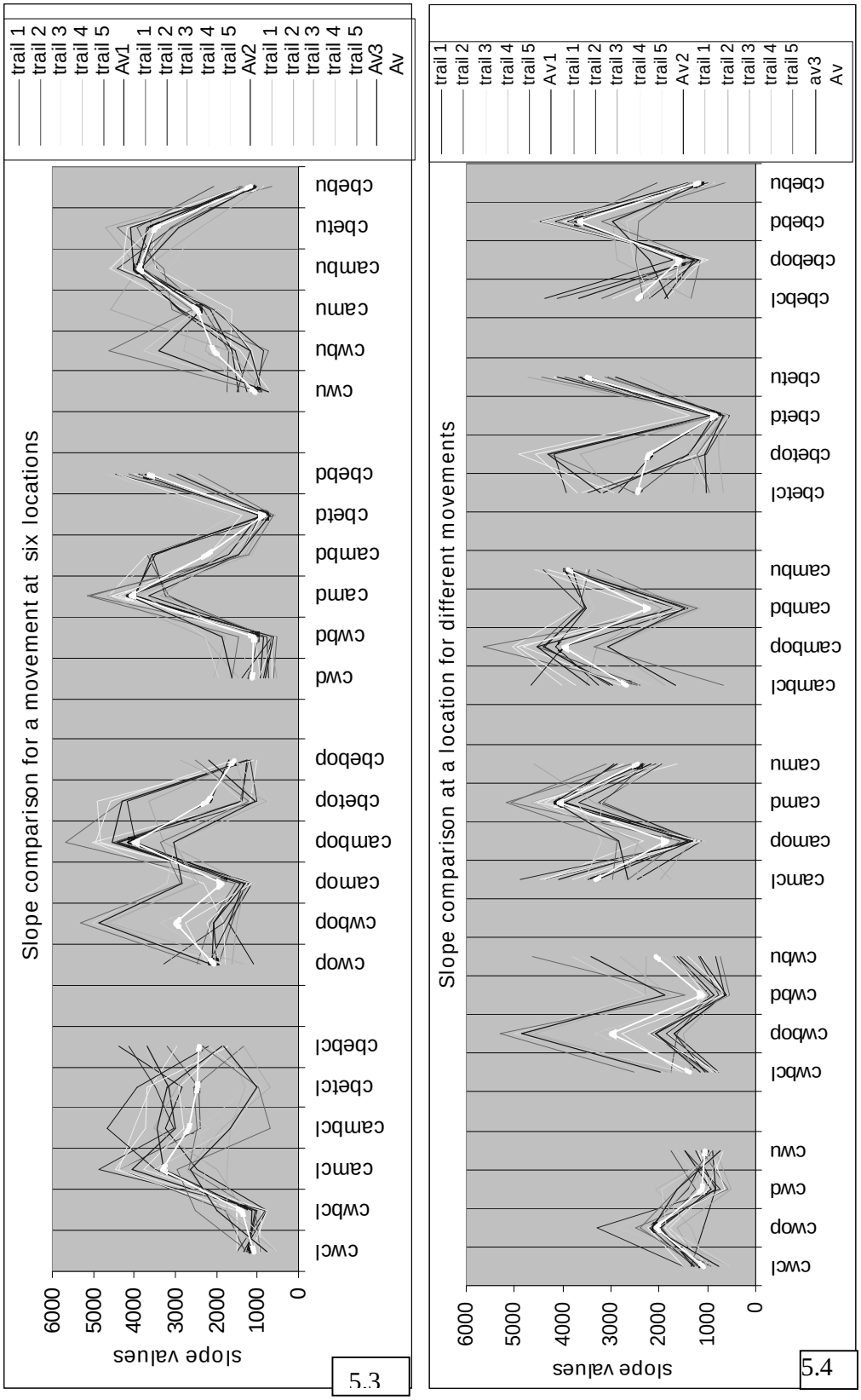

Fig. 5.3 Parameter Slope comparison for a movement at all six locations
Fig. 5.4 Parameter Slope comparison at a location for different movements

Table 5.3
Prominent SEMG locations on arm for different movements

Description	Closing	Opening	Down	Up
Max. dominant location	cam	camb	cam	camb
Min. dominant location	cw	cam	cbet	cw, cbeb

Another aspect of the analysis was to show SEMG at a location for different movements. This is another way to look into the matter and to understand the behavior of SEMG. Table A5.1-A5.4 [appendix] was rearranged as Table A5.5-A5.10 [appendix]. Fig. 5.4 shows calculated slope values of all the five trials of the three subjects along with their overall average (Av; white line) for comparison at six locations on arm individually for a single movement. Av of all the 15 trials gives variation of SEMG signal at a particular location for a movement; say at "cwb" highest level of SEMG signal (slope) was for opening of grip. Table 5.5 was formulated which narrates maximum or minimum slope value of SEMG signal occurring for a specific movement. The multilevel discrimination was evolved for interpretation of the movement with the location. Here arbitrarily level are demarked as: 0 – 1000 = Low, 1000- 2500 = Medium and 2500 – 6000 = High. In RMS based control methodology for the prosthetic devices level/threshold selection is necessary for the classification of movements from a location e.g. at location "cam" as in Table 5.5, closing and down movement gets easily discriminated from opening and up movement. But for discriminating closing and down movements at cam there is a need to consider other locations values. Again Table 5.2b is reorganized in the same manner as Table 5.2 to see the relation of Slope vs V_{rms}.

Table 5.5
Prominent SEMG locations on arm for different movements at a location

Movement	SEMG signal (slope)					
	cw	cwb	cam	camb	cbet	cbeb
Closing	Low	Medium	High	Medium	Medium	Medium
Opening	High	High	Low	High	Medium	Medium
Down	Medium	Low	High	Medium	Low	High
Up	Low	Medium	Medium	High	High	Low

Table 5.2b
Clusters showing prominent movement at a location

Subject 1	Subject 2	Subject 3
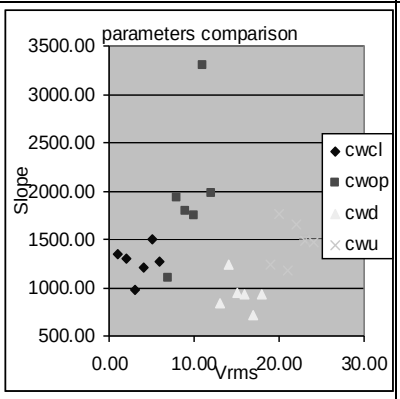	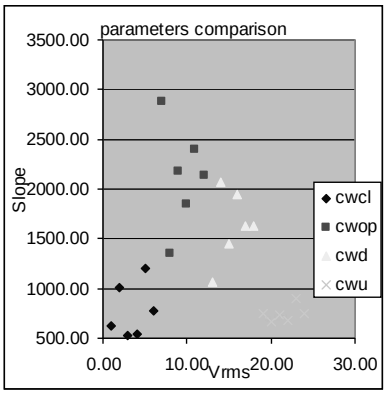	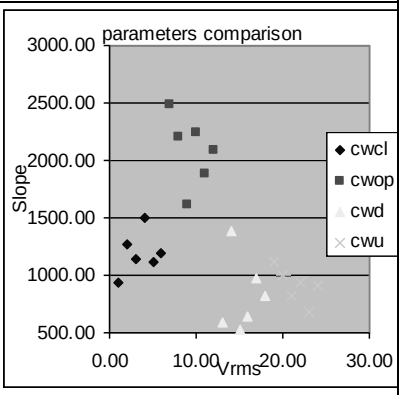
cw	cw	cw
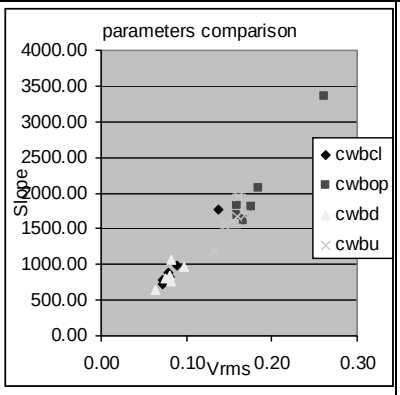	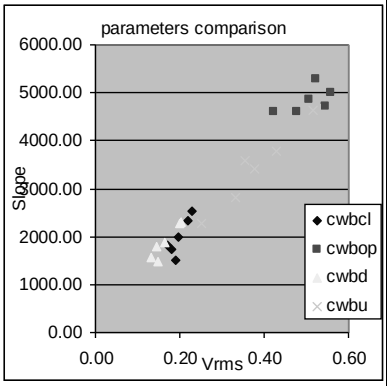	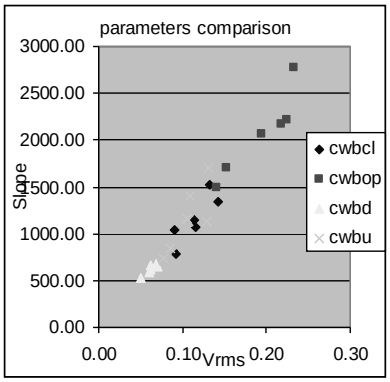
cwb	cwb	cwb
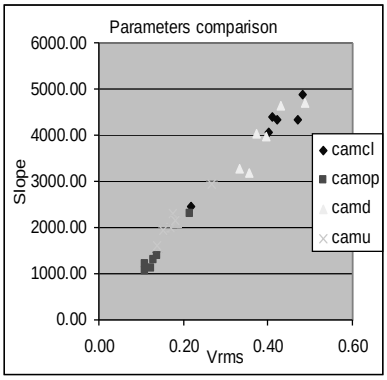	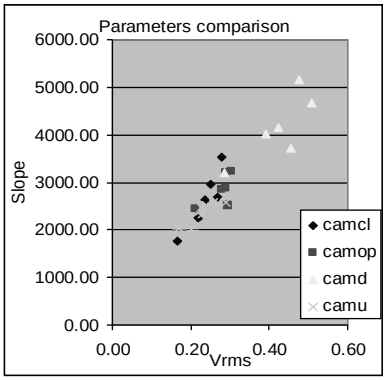	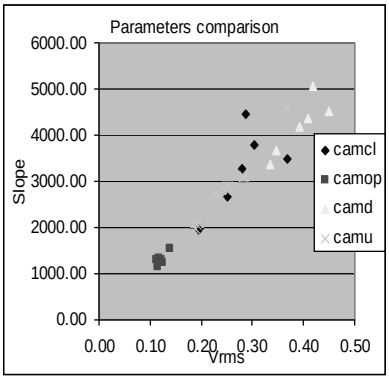
cam	cam	cam

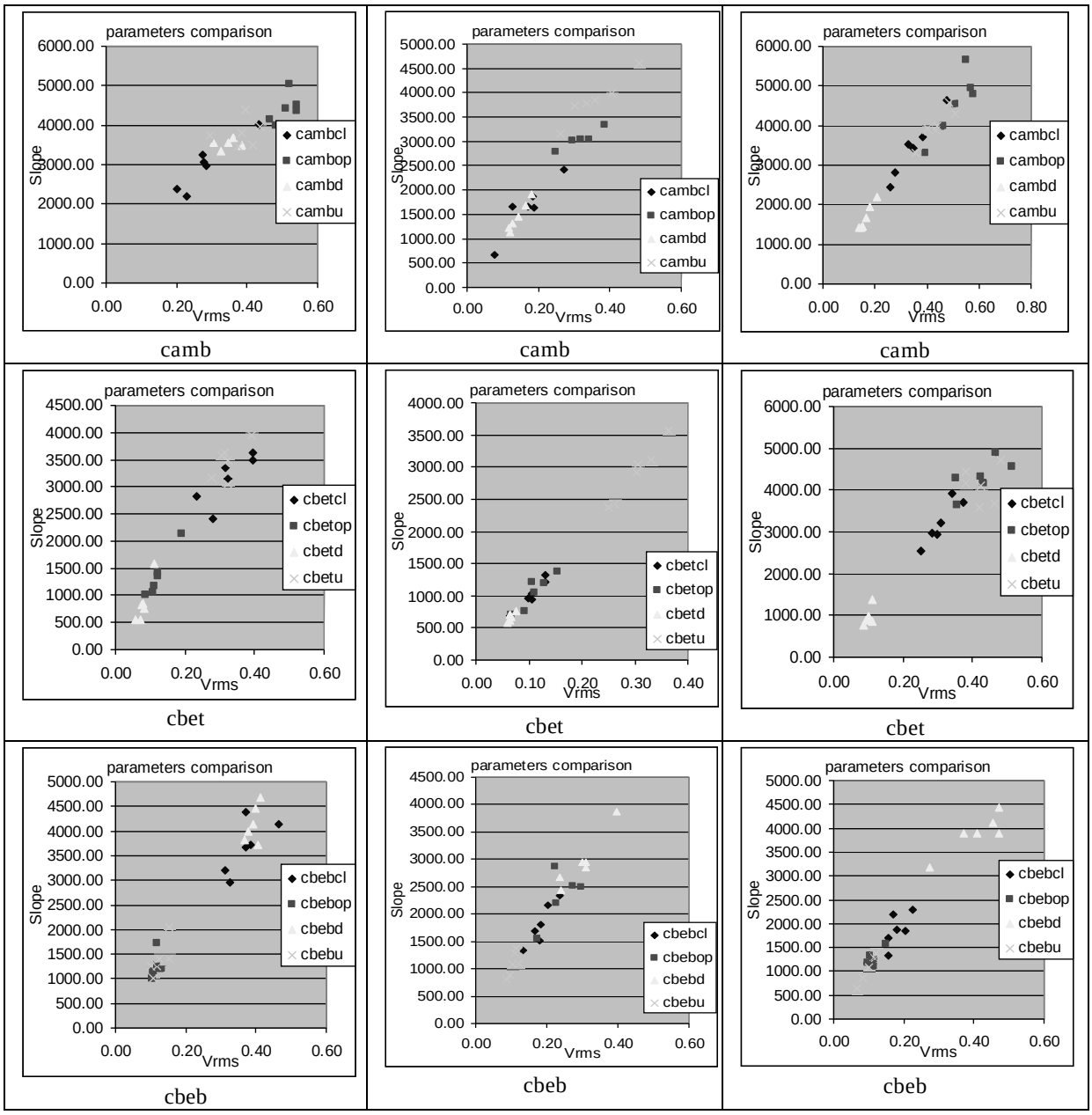

Further, to study the variation in frequencies in SEMG signal occurring at specific movement, average of five dominant frequencies (Av freq) was calculated. This very frequency analysis was done to just to keep a watch on the each trial of SEMG signal captured that trials were from the selected frequency band only and this was due to the narrowband filter used in acquisition circuit. During acquition there are many chances of acquiring distortion which may be due to environmental factors or electrode dislocation. Table A5.11-A5.14 [appendix] shows the calculated Av freq of each trial for a chosen movement. Fig. 5.5 shows the plot of each trial along with Av

freq with their overall average (Av; white line) for comparison from six points of arm and for a single movement. Av of all the trials gives the broader view of variation of SEMG signal's frequency for a movement at a particular location. The investigation did not project any fact for SEMG frequency variation but do confirm the SEMG activity. The reason is because of the presence of narrowband filter during acquisition.

5.2 Statistical Approach using principal component analysis

Principal component analysis (PCA) involves a mathematical procedure that transforms a number of possibly correlated variables into a smaller number of uncorrelated variables called principal components. The first principal component accounts for as much of the variability in the data as possible, and each succeeding component accounts for as much of the remaining variability as possible. Depending on the field of application, it is also named the discrete Karhunen–Loève transform, the Hotelling transform or proper orthogonal decomposition. Large data tables usually contain a large amount of information, which is partly hidden because the data are too complex to be easily interpreted [Micera et al., 2010]. PCA is a projection method that helps in visualizing all the information contained in a data table. PCA helps to find out in what respect one sample is different from another, which variables contribute most to this difference and whether those variables contribute in the same way (i.e. are correlated) or independently from each other. It also enables to detect sample patterns like any particular grouping. Finally, it quantifies the amount of useful information - as opposed to noise or meaningless variation - contained in the data [Staudenmann et al., 2006].

PCA is an analytical technique where complex data set containing few variables are transformed to a smaller set of new variables, which maximize the variance of the original data set. The software called StatistiXL was used. StatistiXL runs as an add-in to Windows™ versions of Microsoft's sophisticated Excel™ spreadsheet program [Online ref. 15]. Data stored in existing Excel™ spreadsheets can instantly be subjected to a wide range of statistical tests.

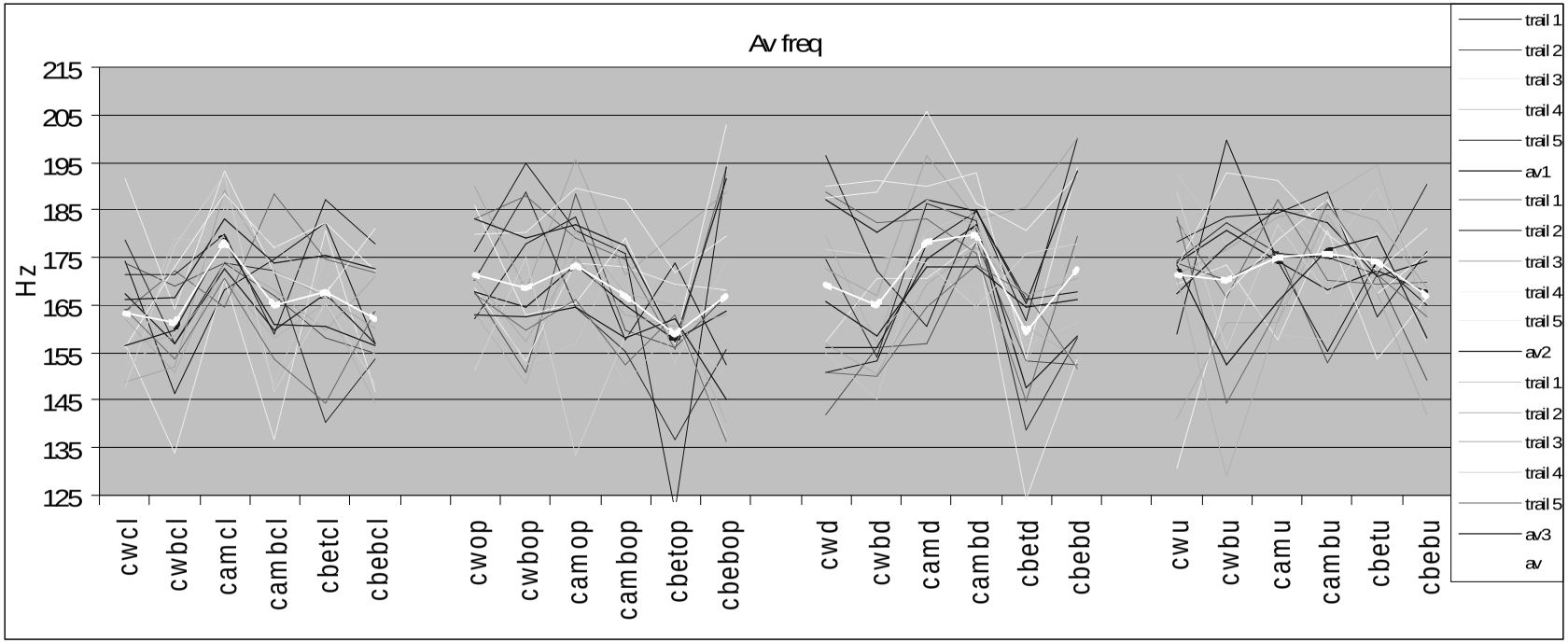

Fig. 5.5 Average frequency comparisons from 6 points of arm, for a movement

In this analysis, principal components (PC) were calculated in terms of percentage of variance. Principal Component Analysis is a technique that attempts to reduce complex data sets consisting of many different variables to a smaller set of new variables that still manage to describe much of the variation in the original data. These new variables, called principal components, are chosen to be independent (i.e. the new variables are not correlated whereas the original, untransformed variables may have been correlated) and to maximize the variance found in the original data set. The more significant PCs are selected based on their eigenvalues, and hopefully far fewer PC variables (e.g. one or two) are required than there were original variables. Principal components are the transformed variables from principal component analysis that maximize the data variance in a series of uncorrelated and orthogonal axes. Component scores are values calculated for each case and each principal component. These are usually plotted for combinations of principal components (e.g. factor scores for component two against factor scores for component one to graphically present the transformed data. The first principal component consists of a principal component coefficient (ai) for each variable (p) such that there is maximal variance in the calculated score for each case (n); the factor score for each case is calculated as a1.Y1 + a2.Y2 + … + ai.Yi + … ap. Yp where Yi is the centered value for the ith (Yi - mean Y for the ith variable). The second principal component consists of the next set of principal component coefficients such that there is a maximal remaining variance in the calculated score for each case, and there is no correlation of the second principal component with the first. Further, sets of principal components (third, fourth, etc.) can be calculated until no statistical significance can be attributed to that component (e.g. by c2 test) or all principal components are computed. Principal component analysis can use either the covariance matrix or the correlation matrix for the data set. All principal components can be extracted or a subset of these based on limits such as the number to extract, the percent of variance to explain or the value of an eigenvalue. The eigenvalues are the solutions (roots) of the S matrix (or R) matrix; they are the values of l for which the determinant of matrix [S -λI] or [R -λI] = 0, where I is the identity matrix. Conceptually, an eigenvalue is the variance of multivariate data along an axis which maximizes the variance. Screenplots can be produced to help in the visual determination of the appropriate number of Principal Components to extract. Results are presented in tabular and graphical form. Descriptive statistics and the correlation or covariance matrix are displayed, if these options are selected. The

eigenvalues are then tabulated along with the percent of variance and cumulative percent of total variance evident in the original dataset that each of the extracted principal components explains. The component loadings are then listed followed by the principal component (PC) score coefficients (eigenvectors). These PC scores are usually graphed for combinations of principal components (e.g. scores for component two against scores for component one, component 3 against component 1, etc) to graphically examine the transformed data. The case-wise PC scores for each extracted component are listed. Graphical output includes bivariate scatter-plots of the various pair-wise combinations of extracted Principal Components. Contributions of original variables to both first and second components (PC1 and PC2 respectively) are shown in the subsequent PCA plots. Within each component, variables have specific loadings and scores coefficients. Loadings represent the correlations between original variable and the principal component and indicate the relative contributions of each variable in each component. Scores represent the distribution and structure for a given component [Online ref. 15 & 16].

These components in the present work means: Component 1 (PC1) – highly varying and Component 2 (PC2) –not varying. The most challenging part of PCA is interpreting the components; (1) higher the component loadings, more important that variable is to the component. (2) combinations of positive and negative loadings are interpreted as bi-polar (3) specific sign is not of importance. Six locations on arm for detection of a wrist movement enforce the use of six sets of bipolar electrodes. This increases circuit complexity. To reduce the number of electrode to perform the four movements, the results were analyzed statistically for finding the best combination for two, three or four channels SEMG systems.

5.2.1 Two channels control strategy:

Two channel control strategy was analyzed for three different combinations of electrode positions i.e. “cw and cwb”, “cam and camb” and “cbet and cbeb”. This is analogous to the two bipolar systems working as simultaneous two channels e.g. one bipolar at location “cw” and other at location “cwb”. The same dataset generated from the single channel acquition system was tabulated in such a fashion that it appears similar to two channel acquition system. Table 5.5, Table 5.6 and Table 5.7 shows the slope values (for each subject independently) arranged collectively for each chosen

movement; say during opening of grip, SEMG values of location “cw” and “cwb” were put under the column heading “cwopen”. Hence “cwopen” will be a group of ten values calculated from the five trials of “cw” and “cwb” each. This is to test the internal variation for a movement. Hence there are twelve such categories to be monitored (4 movements and 3 two channel analogy) which are shown in first row of each table. PCA was applied to the data sets of all the three subjects and the PCA outcomes are shown in Table A5.15 [appendix]. Further, Table 5.8-5.9 presents the descriptive parameters in the reduced form extracted with principal component plots of the three subjects as shown in Fig. 5.6. Two components were selected because they cover at about 80-85% of the total variations. From Fig.5.6 and Table 5.8 it was easily decided that PC1 which was showing above 70% of total variation whereas PC2 remained below 10% in all the subjects. Hence, PC1 was selected for classification. Table 5.8 shows eigenvalues and percentage variance of components. Table 5.9a and 5.9b shows component loadings and component score coefficients respectively. From Fig. 5.6 and Table 5.9a, best locations were observed and recorded in Table 5.10. Table 5.10 indicates “cbet and cbeb” to be the best.

Loadings represent the correlations between original variable and the principal component which indicates the relative contributions of each variable in each component. Therefore, considering Table 5.9a, for four chosen movements in all the three subjects, two channels on wrist location i.e. “cw” and “cwb” contributed mostly less than 50% to PC1. Two channels on mid arm location i.e. “cam” and “camb” contribute mostly above 50% to PC1 and similarly location near below elbow i.e. “cbeb” and “cbet” the contributions were mostly near 80% to PC1. Combinations for 2-channel strategy were compared using Fig. 5.6 in all the three subjects that “cw and cwb” contribute very less to PC1 so it will be least beneficial location. “cbet and cbeb” shows highest contribution to PC1 i.e. loading contribution for all the four movements were good to discriminate between down and up movements. Similarly “cam” and “camb” found to be the better locations for up movement.

The preference of locations for 2-channel strategy should be first given to “cbet (below elbow thumb side) and cbeb (below elbow little finger side)” and then to “cam (mid arm palm side) and camb (mid arm opp. palm side)” because of the percentage variations in PC1 and Table 5.10. The degree of functionality for the selected four movements will be more for 2-channel strategy with locations “cbet and cbeb” for a prosthetic or exoskeleton arm devices.

Table 5.5
Slope value for chosen movements from the combination for two channels
[Subject 1]

	cwclose	cwopen	cwdown	cwup		camclose	camopen	camdown	camup		cbeclose	cbeopen	cbedown	cbeup
From "cw"	1348.8	1099.7	834.6	1241.4	From "cam"	2467.6	1121.1	4018.3	2926.9	From "cbet"	2825.1	2145.1	822.5	3631.1
	1300.5	1931.2	1233.3	1758.8		4327.5	1300.2	3174.5	2292.6		2420.9	1414.1	757.6	3948.6
	970.31	1793.5	944.5	1178.4		4382.8	2317.7	4632.3	1619.1		3620.8	1181.3	555.4	3583.4
	1201.8	1745	932.3	1656		4321.5	1065	4698.1	2007.7		3363.1	1062.9	1590.1	3167.2
	1502.7	3296.1	721.1	1482.8		4870	1197.5	3259.7	1935.1		3489.3	1013.7	552.4	3064.5
From "cwb"	779.9	1691.6	633.7	1548.4	From "camb"	3259.4	4157.6	3501.4	3970.5	From "cbeb"	4375	1719.7	3731	1415.5
	1768.8	1627.2	970.6	1696.3		2393.7	4517.8	3677.3	3451.4		3205.1	1218.8	3825.2	2053.3
	880.9	1807	1060	1675.5		4024.6	5033.6	3677.3	3506.2		2957.1	998.3	4000.2	1244.1
	724.5	3352.3	810.5	1959.5		2182.7	3982.8	3340.6	3728.7		3709.7	1208.1	4668.2	1260.7
	820.1	1835.8	758.5	1192.1		3047.1	4373.5	3563.3	4398.8		4126	1169.6	4457.3	999.2

Table 5.6
Slope value for chosen movements from the combination for two channels
[Subject 2]

	cwclose	cwopen	cwdown	cwup		camclose	camopen	camdown	camup		cbeclose	cbeopen	cbedown	cbeup
From "cw"	934.4	2484.6	589.8	1116	From "cam"	2657.1	1549.4	5069	3082.6	From "cbet"	2534.1	4286.1	763.8	4439.1
	1265.2	2204.7	1389.7	998.3		3476.2	1329.6	3657.6	2063.8		3930.1	4171.3	922.8	3673.1
	1140	1619	525.2	824.1		1977.7	1301	3350	4581.1		2957.1	3631.9	871.5	4709.6
	1499.1	2248.8	639.4	931.2		4467	1143.3	4522.4	1965.7		3693.5	4571.9	884.1	4166.7
	1116.8	1890.9	973.8	677.8		3784.8	1257.3	4374.9	2741.6		2932.4	4899.4	1379.9	3567.1
From"cwb"	1036.1	2163.9	531.7	738.5	From "camb"	2452.8	5659.6	1440.1	3302.6	From "cbeb"	1334.8	1147	3179.7	628.6
	1065.6	1698.9	644.4	837.8		4651.5	3988.6	1411.5	3925.4		2190	1170.2	3898.5	1307.2
	1339.6	1488.8	678.1	1709.6		3513	3300	1943.1	3883.2		2288.8	1332.9	4120.2	1292.9
	1519.9	2767.5	656.1	1124.9		3725.8	4945.4	1424.7	4292.8		1693.1	1580.3	3881.2	1377.8
	790.5	2221.6	582.2	1409.2		2814.8	4805	2193.1	4568.1		1845.9	1097.1	4438	858.9

Table 5.7
Slope value for chosen movements from the combination for two channels
[Subject 3]

	cwclose	cwopen	cwdown	cwup		camclose	camopen	camdown	camup		cbeclose	cbeopen	cbedown	cbeup
From "cw"	622.2	2881.7	1068.7	743.6	From "cam"	2255.7	3241	3196.2	1995.6	From "cbet"	1218.9	710.5	578.3	2421.9
	1007.4	1348.9	2072.1	660.4		1760.1	2522.6	4015.5	2587.2		1317.5	1203.9	706.2	3041.6
	527.2	2182.5	1443.8	727.1		2700.9	2440.8	4671.5	2023.5		682.35	768.9	758.5	2379.1
	543.0	1848.6	1946.9	675.3		3537.1	3194.1	3710.7	2480.7		945.2	1382.5	701.4	3564.2
	1198.4	2402.9	1631.8	904.1		2959.3	2872.8	5156.3	2580.8		964.6	1200.2	623.4	3118.8
From"cwb"	2338	4619.7	1563.4	3579.9	From "camb"	2412.6	2785.6	1922.9	3153.9	From "cbeb"	1510.3	1560.4	3862.4	805.0
	1729.1	4605.1	1786.4	2817.2		1665.8	3041.9	1137.3	3736.5		1695.9	1560.4	2859	1295.3
	1824.6	4721.8	2292.6	2281		1868.4	3049.6	1307.7	3771.1		1331.7	2872.9	2954.6	878.9
	1503.3	5010.1	2283.6	3783.2		1637.1	3019.4	1681.6	4611.5		2169.5	2508.9	2667.1	1099.2
	2532	5296	1467.2	4629.5		674.3	3349.5	1220.1	3985		2340.9	2505.2	2427.1	1369

Table 5.8
Eigenvalues and variance of components for two channels

	Component	Eigenvalue	% of Variance	Cumulative %
Subject 1	PC 1	8088480.29	76.31	76.31
	PC 2	932532.63	8.80	85.11
Subject 2	PC 1	13253346.22	82.92	82.92
	PC2	1199761.04	7.51	90.42
Subject 3	PC 1	10568425.45	83.58	83.58
	PC 2	615462.53	4.87	88.45

Table 5.9a
PCA Component Loadings for two channels

		Subject 1		Subject 2		Subject 3	
	Variable	PC 1	PC 2	PC 1	PC 2	PC 1	PC 2
Combination 1	cwclose	-0.47	-0.23	-0.15	-0.47	0.89	0.00
	cwopen	0.07	0.67	-0.01	-0.03	0.98	0.05
	cwdown	-0.29	-0.03	-0.41	-0.47	0.25	-0.12
	cwup	0.26	0.21	0.36	0.00	0.95	-0.12
Combination 2	camclose	-0.62	0.69	0.00	-0.92	-0.72	0.50
	camopen	0.95	0.09	0.97	0.04	0.42	-0.29
	camdown	-0.35	-0.17	-0.95	0.03	-0.94	-0.02
	camup	0.92	-0.25	0.65	0.59	0.89	-0.24
Combination 3	cbeclose	0.50	0.25	-0.86	-0.31	0.85	-0.46
	cbeopen	-0.14	-0.82	-0.98	-0.05	0.81	-0.23
	cbedown	0.99	0.01	0.96	-0.12	0.92	0.35
	cbeup	-0.97	-0.18	-0.97	0.18	-0.92	-0.27

Table 5.9b
PCA Component Score Coefficients (Eigenvectors) for two channels

		Subject 1		Subject 2		Subject3	
	Variable	PC 1	PC 2	PC 1	PC 2	PC 1	PC 2
Combination 1	cwclose	-0.06	-0.08	-0.01	-0.10	0.20	0.00
	cwopen	0.02	0.50	0.00	-0.01	0.45	0.09
	cwdown	-0.02	-0.01	-0.03	-0.11	0.03	-0.06
	cwup	0.02	0.06	0.03	0.00	0.45	-0.23
Combination 2	camclose	-0.21	0.69	0.00	-0.73	-0.18	0.52
	camopen	0.55	0.15	0.48	0.07	0.04	-0.11
	camdown	-0.07	-0.09	-0.37	0.04	-0.44	-0.03
	camup	0.31	-0.25	0.17	0.52	0.25	-0.28
Combination 3	cbeclose	0.10	0.15	-0.20	-0.24	0.14	-0.31
	cbeopen	-0.02	-0.31	-0.44	-0.08	0.19	-0.22
	cbedown	0.62	0.02	0.42	-0.18	0.36	0.56
	cbeup	-0.39	-0.22	-0.44	0.27	-0.29	-0.35

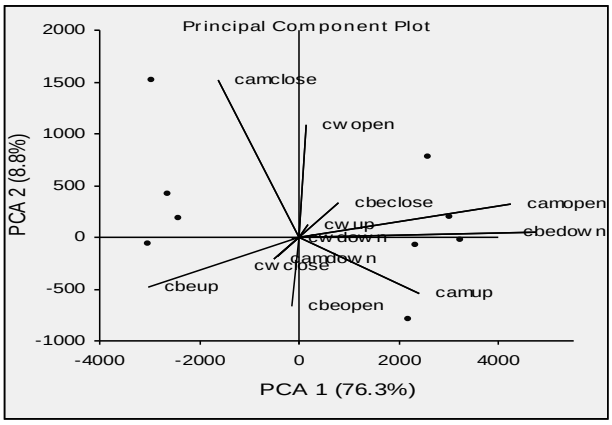

(a)

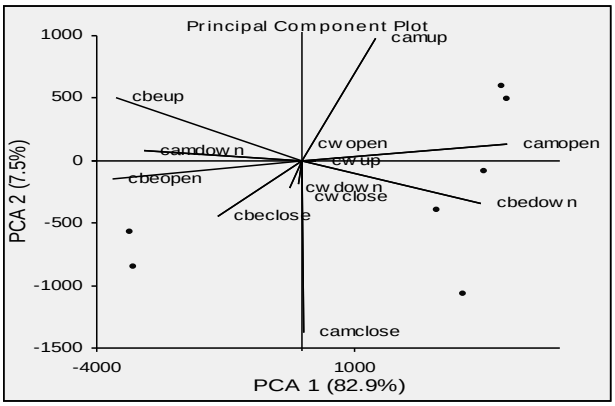

(b)

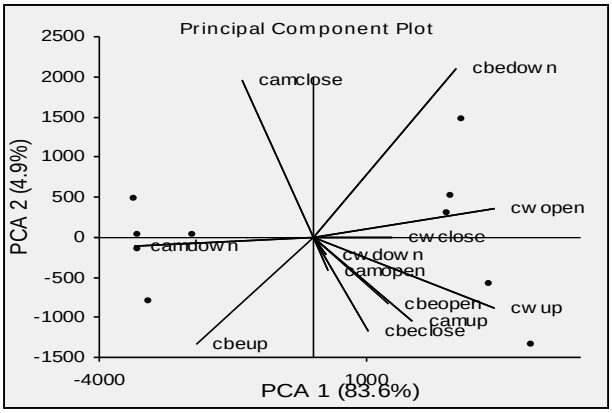

(c)

Fig. 5.6 PCA plot for two channel approach (a) subject 1 (b) subject 2 (c) subject 3

Table 5.10
Best selected combinations for a movement for 2-channel approach
(Based on the loading/score values of PC1)

	closing	opening	down	up
Subject 1	cam & camb	cam & camb	cbet & cbeb	cbet & cbeb
Subject 2	cbet & cbeb	cam & camb, cbet & cbeb	cbet & cbeb, cam & camb	cbet & cbeb
Subject 3	cbet & cbeb	cw & cwb, cbet & cbeb	cbet & cbeb, cam & camb	cbet & cbeb, cw & cwb

5.2.2 Three channel control strategy

In this study, two combinations were made as “cam, camb and cbet” (combination 1) and “cam, camb and cbeb” (combination 2). In 2-channel analysis “cw and cwb” showed lesser variations and hence neglected in 3-channel combinations. This is analogous to the three bipolar electrodes working as simultaneous three channels i.e. one bipolar at location “cam”, other at “camb” and another at “cbet”. Subject wise Tables 5.11- 5.13 shows the slope values arranged collectively for each chosen movement; say during opening of grip SEMG values of location “cw” and “cwb” put under the column heading “cwopen”. PCA was applied to the data sets of all the three subjects and the results are shown in Table A5.16 [appendix] subject-wise. Further, Table 5.14-5.15 presents the descriptive parameters in the reduced form extracted from the Tables A5.16 [appendix] with principal component plots of the three subjects. PC1 was showing around 60% of total variance in all the three subjects. Again, Table 5.16 shows best combination for 3-channel strategy for a movement was obtained by using Fig. 5.7 and component loading to PC1.

Considering contributions of variable to PC1 only, preference of locations for 3-channel strategy was firstly by combination 1 and secondly by combination 2. For example, as per Table 5.15 (subject 1), “cambetdown” contribute 0.53, -0.72 and 0.97 respectively to PC1 which is more discriminating than “cambebdown” -0.45, -0.88 and 0.83. The three channels showed difference in contribution to PC1 for good discrimination in Table 5.16. Another advantage of three channels over the two channels is increase in the degree of description i.e. all the four chosen movements were well detected.

5.2.3 Four channel control strategy

Similar Combinations of dataset were made of readings from all the four locations i.e. cam, camb, cbet and cbeb. This is analogous to the four bipolar electrodes working as simultaneous four channels i.e. a bipolar at each location “cam”, “camb” “cbet” and “cbeb”. Again, the similar type of PCA was applied and the outcomes are shown in Table A5.17 [appendix]. Table 5.18-5.20 presents the descriptive parameters in the reduced form extracted from the Tables A5.17 [appendix] with principal component plots of the three subjects as shown in Fig. 5.8. All the four movements are easily distinguished in terms of loading/scores as shown in Fig. 5.8 for all the three subjects.

Table 5.11
Slope values for three channel combination [Subject 1]

	Combination 1"cam, camb and cbet"					Combination 1"cam, camb and cbeb"			
	cambetclose	cambetopen	cambetdown	cambetup		cambebclose	cambebopen	cambebdown	cambebup
From"cam"	2467.6	1121.1	4018.3	2926.9	From"cam"	2467.6	1121.1	4018.3	2926.9
	4327.5	1300.2	3174.5	2292.6		4327.5	1300.2	3174.5	2292.6
	4382.8	2317.7	4632.3	1619.1		4382.8	2317.7	4632.3	1619.1
	4321.5	1065	4698.1	2007.7		4321.5	1065	4698.1	2007.7
	4870	1197.5	3259.7	1935.1		4870	1197.5	3259.7	1935.1
From"camb"	3259.4	4157.6	3501.4	3970.5	From"camb"	3259.4	4157.6	3501.4	3970.5
	2393.7	4517.8	3677.3	3451.4		2393.7	4517.8	3677.3	3451.4
	4024.6	5033.6	3677.3	3506.2		4024.6	5033.6	3677.3	3506.2
	2182.7	3982.8	3340.6	3728.7		2182.7	3982.8	3340.6	3728.7
	3047.1	4373.5	3563.3	4398.8		3047.1	4373.5	3563.3	4398.8
From "cbet"	2825.1	2145.1	822.5	3631.1	From "cbeb"	4375	1719.7	3731	1415.5
	2420.9	1414.1	757.6	3948.6		3205.1	1218.8	3825.2	2053.3
	3620.8	1181.3	555.4	3583.4		2957.1	998.3	4000.2	1244.1
	3363.1	1062.9	1590.1	3167.2		3709.7	1208.1	4668.2	1260.7
	3489.3	1013.7	552.4	3064.5		4126	1169.6	4457.3	999.28

Table 5.12
Slope values for three channel combination [Subject 2]

	Combination 1"cam, camb and cbet"					Combination 1"cam, camb and cbeb"			
	cambetclose	cambetopen	cambetdown	cambetup		cambebclose	cambebopen	cambebdown	cambebup
From"cam"	2657.1	1549.4	5069	3082.6	From"cam"	2657.1	1549.4	5069	3082.6
	3476.2	1329.6	3657.6	2063.8		3476.2	1329.6	3657.6	2063.8
	1977.7	1301	3350	4581.1		1977.7	1301	3350	4581.1
	4467	1143.3	4522.4	1965.7		4467	1143.3	4522.4	1965.7
	3784.8	1257.3	4374.9	2741.6		3784.8	1257.3	4374.9	2741.6
From"camb"	2452.8	5659.6	1440.1	3302.6	From"camb"	2452.8	5659.6	1440.1	3302.6
	4651.5	3988.6	1411.5	3925.4		4651.5	3988.6	1411.5	3925.4
	3513	3300	1943.1	3883.2		3513	3300	1943.1	3883.2
	3725.8	4945.4	1424.7	4292.8		3725.8	4945.4	1424.7	4292.8
	2814.8	4805	2193.1	4568.1		2814.8	4805	2193.1	4568.1
From "cbet"	2534.1	4286.1	763.8	4439.1	From "cbeb"	1334.8	1147	3179.7	628.6
	3930.1	4171.3	922.8	3673.1		2190	1170.2	3898.5	1307.2
	2957.1	3631.9	871.5	4709.6		2288.8	1332.9	4120.2	1292.9
	3693.5	4571.9	884.1	4166.7		1693.1	1580.3	3881.2	1377.8
	2932.4	4899.4	1379.9	3567.1		1845.9	1097.1	4438	858.9047

Table 5.13
Slope values for three channel combination [Subject 3]

	Combination 1"cam, camb and cbet"					Combination 1"cam, camb and cbeb"			
	cambetclose	cambetopen	cambetdown	cambetup		cambebclose	cambebopen	cambebdown	cambebup
From"cam"	2255.7	3241	3196.2	1995.6	From"cam"	2255.7	3241	3196.2	1995.6
	1760.1	2522.6	4015.5	2587.2		1760.1	2522.6	4015.5	2587.2
	2700.9	2440.8	4671.5	2023.5		2700.9	2440.8	4671.5	2023.5
	3537.1	3194.1	3710.7	2480.7		3537.1	3194.1	3710.7	2480.7
	2959.3	2872.8	5156.3	2580.8		2959.3	2872.8	5156.3	2580.8
From"camb"	2412.6	2785.6	1922.9	3153.9	From"camb"	2412.6	2785.6	1922.9	3153.9
	1665.8	3041.9	1137.3	3736.5		1665.8	3041.9	1137.3	3736.5
	1868.4	3049.6	1307.7	3771.1		1868.4	3049.6	1307.7	3771.1
	1637.1	3019.4	1681.6	4611.5		1637.1	3019.4	1681.6	4611.5

	674.3	3349.5	1220.1	3985		674.3	3349.5	1220.1	3985
From "cbet"	1218.9	710.5	578.31	2421.9	From "cbeb"	1510.3	1560.4	3862.4	805.0
	1317.5	1203.9	706.2	3041.6		1695.9	1560.4	2859	1295.3
	682.35	768.9	758.5	2379.1		1331.7	2872.9	2954.6	878.9
	945.1	1382.5	701.4	3564.2		2169.5	2508.9	2667.1	1099.2
	964.6	1200.2	623.4	3118.8		2340.9	2505.2	2427.1	1369

Table 5.14
Eigenvalues and variance of components for three channel combination

	Component	Eigenvalue	% of Variance	Cumulative %
Subject 1	PC 1	6696375.17	62.75	62.75
	PC 2	2519207.56	23.61	86.35
Subject 2	PC 1	6962179.44	51.29	51.29
	PC 2	4315737.47	31.79	83.08
Subject 3	PC 1	4661032.47	53.38	53.38
	PC 2	3198397.97	36.63	90.01

Table 5.15a
PCA component loadings for three channel combination

		Subject 1		Subject 2		Subject 3	
	Variable	PC 1	PC 2	PC 1	PC 2	PC 1	PC 2
Combination 1	cambetclose	-0.34	0.71	-0.07	0.19	0.84	0.30
	cambetopen	0.97	-0.10	0.87	-0.43	0.34	0.91
	cambetdown	0.53	0.81	-0.72	0.64	0.97	0.21
	cambetup	0.48	-0.83	0.60	-0.34	-0.66	0.60
Combination 2	cambebclose	-0.49	0.48	-0.06	0.77	0.74	-0.04
	cambebopen	0.98	-0.06	0.86	0.47	0.11	0.74
	cambebdown	-0.45	0.15	-0.88	-0.35	0.83	-0.52
	cambebup	0.93	0.03	0.38	0.84	-0.07	0.98

Table 5.15b
PCA component score coefficients for three channel combination

		Subject 1		Subject 2		Subject 3	
	Variable	PC 1	PC 2	PC 1	PC 2	PC 1	PC 2
Combination 1	cambetclose	-0.11	0.38	-0.02	0.07	0.33	0.15
	cambetopen	0.58	-0.09	0.53	-0.34	0.15	0.49
	cambetdown	0.31	0.76	-0.41	0.46	0.72	0.19
	cambetup	0.15	-0.44	0.20	-0.14	-0.24	0.26
Combination 2	cambebclose	-0.16	0.26	-0.02	0.38	0.24	-0.01
	cambebopen	0.58	-0.06	0.54	0.38	0.03	0.23
	cambebdown	-0.09	0.05	-0.42	-0.22	0.48	-0.37
	cambebup	0.40	0.02	0.20	0.56	-0.04	0.67

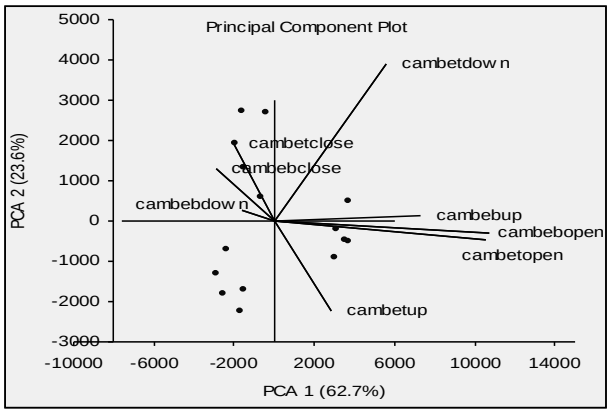

(a)

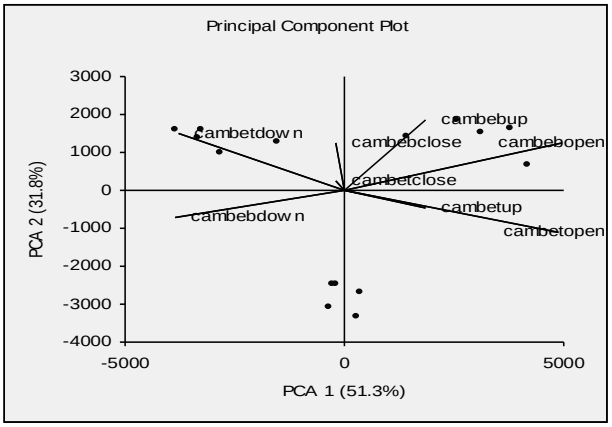

(b)

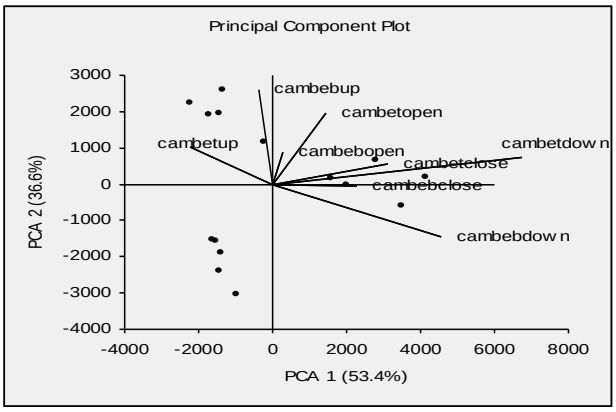

(c)

Fig. 5.7 PCA plot for three channel combination (a) subject 1 (b) subject 2 (c) subject 3

Table 5.16
Best selected combinations for a movement for 3-channel approach
(Based on the loading/score values of PC1)

	closing	opening	down	up
Subject 1	Combination II	Combination I & II are equally good	Combination I	Combination II
Subject 2	Combination I & II are equally good	Combination I & II are equally good	Combination II	Combination I
Subject 3	Combination I	Combination I	Combination I	Combination I

Table 5.17
Slope values from all the selected locations for a movement for four channel approach

	Subject 1				Subject 2				Subject 3			
	close	open	down	up	close	open	down	up	close	open	down	up
From "cam"	2467.6	1121.1	4018.3	2926.9	2657.1	1549.4	5069	3082.6	2255.7	3241	3196.2	1995.6
	4327.5	1300.2	3174.5	2292.6	3476.2	1329.6	3657.6	2063.8	1760.1	2522.6	4015.5	2587.2
	4382.8	2317.7	4632.3	1619.1	1977.7	1301	3350	4581.1	2700.9	2440.8	4671.5	2023.5
	4321.5	1065	4698.1	2007.7	4467	1143.3	4522.4	1965.7	3537.1	3194.1	3710.7	2480.7
	4870	1197.5	3259.7	1935.1	3784.8	1257.3	4374.9	2741.6	2959.3	2872.8	5156.3	2580.8
From "camb"	3259.4	4157.6	3501.4	3970.5	2452.8	5659.6	1440.1	3302.6	2412.6	2785.6	1922.9	3153.9
	2393.7	4517.8	3677.3	3451.4	4651.5	3988.6	1411.5	3925.4	1665.8	3041.9	1137.3	3736.5
	4024.6	5033.6	3677.3	3506.2	3513	3300	1943.1	3883.2	1868.4	3049.6	1307.7	3771.1
	2182.7	3982.8	3340.6	3728.7	3725.8	4945.4	1424.7	4292.8	1637.1	3019.4	1681.6	4611.5
	3047.1	4373.5	3563.3	4398.8	2814.8	4805	2193.1	4568.1	674.3	3349.5	1220.1	3985
From "cbet"	2825.1	2145.1	822.5	3631.1	2534.1	4286.1	763.8	4439.1	1218.9	710.5	578.31	2421.9
	2420.9	1414.1	757.6	3948.6	3930.1	4171.3	922.8	3673.1	1317.5	1203.9	706.2	3041.6
	3620.8	1181.3	555.4	3583.4	2957.1	3631.9	871.5	4709.6	682.35	768.9	758.5	2379.1
	3363.1	1062.9	1590.1	3167.2	3693.5	4571.9	884.1	4166.7	945.1	1382.5	701.4	3564.2
	3489.3	1013.7	552.4	3064.5	2932.4	4899.4	1379.9	3567.1	964.6	1200.2	623.4	3118.8
From "cbeb"	4375	1719.7	3731	1415.5	1334.8	1147	3179.7	628.6	1510.3	1560.4	3862.4	805.1
	3205.1	1218.8	3825.2	2053.3	2190	1170.2	3898.5	1307.2	1695.9	1560.4	2859	1295.3
	2957.1	998.3	4000.2	1244.1	2288.8	1332.9	4120.2	1292.9	1331.7	2872.9	2954.6	878.9
	3709.7	1208.1	4668.2	1260.7	1693.1	1580.3	3881.2	1377.8	2169.5	2508.9	2667.1	1099.2
	4126	1169.6	4457.3	999.28	1845.9	1097.1	4438	858.9	2340.9	2505.2	2427.1	1369

Table 5.18
Eigenvalues and variance of components for four channel approach

	Component	Eigenvalue	% of Variance	Cumulative %
Subject 1	PC 1	2878767.93	49.35	49.35
	PC 2	2378847.01	40.78	90.12
Subject 2	PC 1	6120611.50	78.30	78.30
	PC 2	874394.29	11.19	89.48
Subject 3	PC 1	2965294.91	63.61	63.61
	PC 2	1201516.73	25.77	89.38

Table 5.19
PCA component loadings for four channel approach

	Subject 1		Subject 2		Subject 3	
Variable	PC 1	PC 2	PC 1	PC 2	PC 1	PC 2
Close	-0.61	0.00	0.42	0.75	0.76	0.35
Open	0.63	0.76	0.96	-0.16	0.44	0.78
Down	-0.61	0.77	-0.94	0.19	0.98	0.06
Up	0.97	0.01	0.86	0.35	-0.62	0.74

Table 5.20
PCA component score coefficients (eigenvectors) for four channel approach

	Subject 1		Subject 2		Subject 3	
Variable	PC 1	PC 2	PC 1	PC 2	PC 1	PC 2
Close	-0.28	0.00	0.16	0.75	-0.03	0.91
Open	0.53	0.70	0.65	-0.30	0.71	-0.23
Down	-0.52	0.72	-0.57	0.30	-0.44	-0.34
Up	0.61	0.00	0.48	0.51	-0.54	-0.07

Control methodology on the basis of level/threshold has been proposed in Table 5.21 by taking into account the Fig.5.3 and Fig. 5.4. Slope value from each location has been classified as binary digit as mentioned below:

- High SEMG: Slope value >2000: Binary Digit “1”
- Low SEMG: Slope value <2000: Binary Digit “0”

Table 5.21
Excitation table for 2-channel and 3-channel methodology respectively

Two channel approach		
cbet	cbeb	Movement
1	1	close
1	0	open
0	1	down
1	0	up

Three channel approach			
cam	camb	cbet	Movement
1	1	1	close
0	1	1	open
1	0	0	down
1	1	0	up

The best combination will be of 3-channel combination in-terms of discrimination of four movements and complexity of acquisition. So the three channels behave as binary switches for a prosthetic device to perform the movements as per Table 5.21.

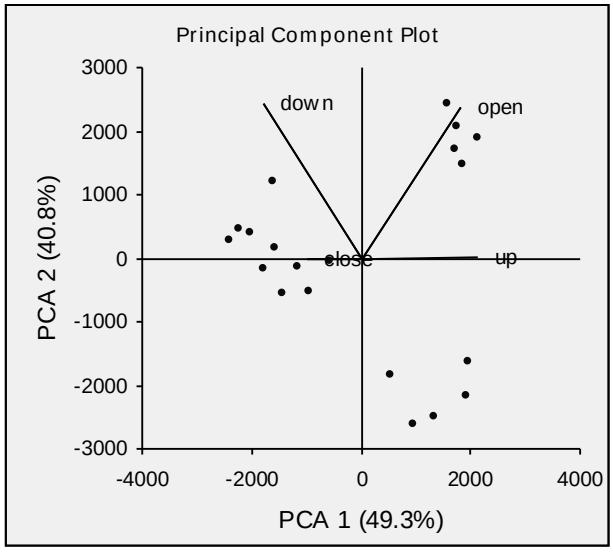

(a)

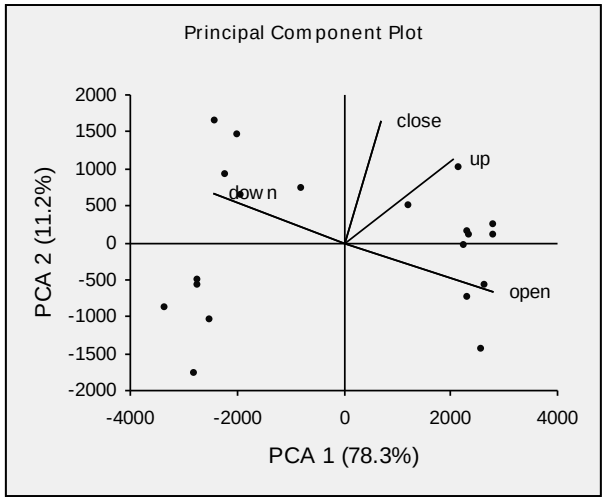

(b)

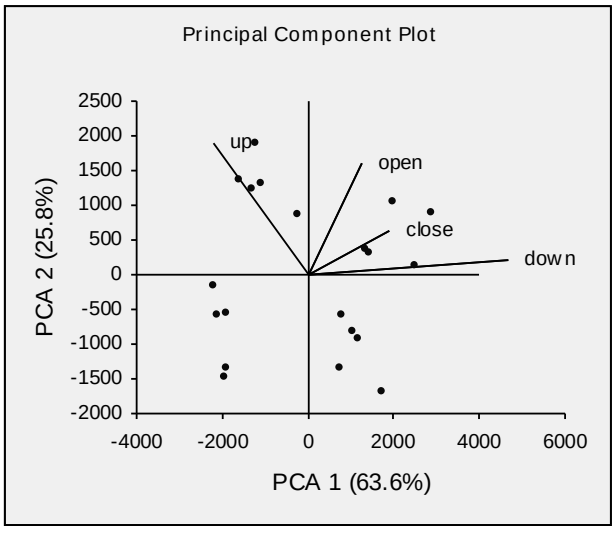

(c)

Fig. 5.8 PCA plot for four channel combination
(a) subject 1 (b) subject 2 (c) subject 3

All the movements can be well detected by using 2-channel or 3-channel control strategy. For SEMG applications, 4-channel control strategies are found to be advantageous for the selected movement discriminations but complexities in wrapping electrodes makes its priority lower than the other channels. Further percentage variance of PC1 reduces to 40-50% which make the discriminating explanation difficult using PC1 only. Electromyographic signals present an interesting solution to control artificial arm because (i) they are easy to record (non-invasive method) (ii) close to natural movements and (iii) offer more numbers of functions. This technique can also be extended to control different SEMG signal controlled robotic systems for remote and harsh area movements. This work presented a control strategy using single parameter (Slope) and multi-channel (preferably three) for prosthetic hand.

After the principal component analysis of data from different locations, it is found that in two channel locations namely “cbet and cbeb” and in three channel locations namely “cam”, “camb” and “cbet” will be best suited to discriminate the four chosen movements. Presently, 3-channel strategy takes the advantage among the other strategies studied for the selected movements. However the pressure points showed low performance w.r.t. the other locations. Best location can be related to the maximum loading percentage to PC1 and appropriate numbers of channel of the acquisition system to monitor movements depends again upon the loading percentage to PC1 but shall vary i.e. different movement shall have different contribution percentage for better discrimination.
The knowledge of SEMG signal at different locations and interpretations of parameters for a movement as done in this work will act as a helping tool for the researchers in understanding the behaviour of SEMG signal and arm/hand movement.

5.3 Interpretation of SEMG at acupressure points on wrist for hand movements
Graupe, 1994 used electrode sites for multifunctional approach where even very weak correlation between the measured signal and (more than one) limb functions may exist [Graupe, 1994]. This section is the study of section 4.2, chapter 4 with the help of PCA. The SEMG signal’s comparison between acupressure points and other SEMG locations below elbow arm have not given verdict in favour of acupressure points, but

they are needed to be examined independently. Again the two channel methodology was selected where “cw” and “cwb” collectively represents two channel systems. This was done to study the SEMG activities at these locations for discriminating chosen four movements.

5.3.1 Results and discussions

Table A5.18 shows the slope values rearranged for the four chosen movement respectively; say column “cwclose” means slope values during closing movement both from “cw’ and “cwb”. PCA was used to calculate which movement shows maximum variation. This investigation based on the internal variation was well demonstrated by PCA plot in Fig. 5.9. Five trials from the three subjects were put under one case. Considering PC1 which contribute 81% on screen plot, the interpretation of the four movements can be made very easily.

Observations made were, all the four movements were easily distinguished i.e. movement “open” was very easy to distinguish and prominent at this location. The observation made in this section is of similar fashion as depicted in section 4.2, chapter 4. Hence, writ muscle generates good SEMG for opening of hand-grip.

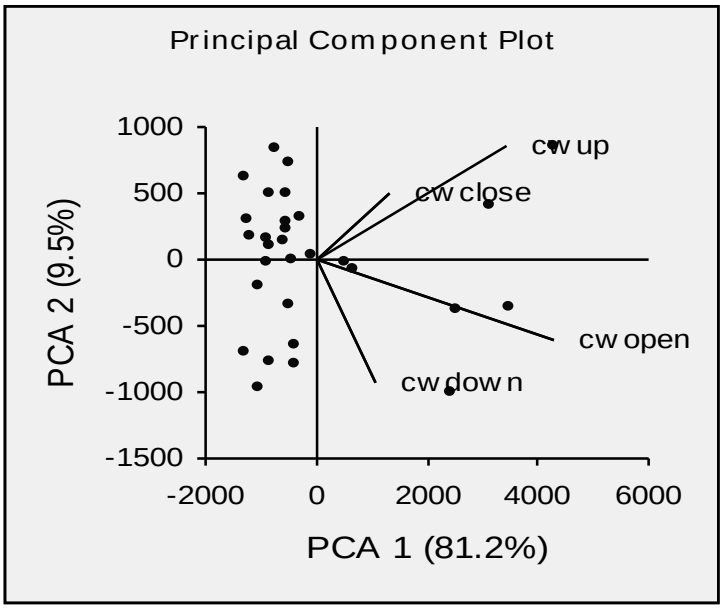

Fig. 5.9 PCA plot for two channel at “cw & cwb”

Table 5.22

Rearranged slope values from "cw" and "cwb"

cwclose	cwopen	cwdown	cwup
1348.8	1099.7	834.6	1241.4
1300.5	1931.2	1233.	1758.8
970.31	1793.5	944.5	1178.4
1201.8	1745	932.3	1656
1502.7	3296.1	721.1	1482.8
934.4	2484.6	589.8	1116
1265.2	2204.7	1389.7	998.3
1140	1619	525.2	824.0
1499.1	2248.8	639.4	931.2
1116.8	1890.9	973.8	677.8
622.2	2881.7	1068.7	743.6
1007.4	1348.9	2072.1	660.4
527.2	2182.5	1443.8	727.1
543.0	1848.6	1946.9	675.3
1198.4	2402.9	1631.8	904.1
779.9	1691.6	633.7	1548.4
1768.8	1627.2	970.6	1696.3
880.9	1807	1060	1675.5
724.5	3352.3	810.5	1959.5
820.0	1835.8	758.5	1192.1
1036.1	2163.9	531.7	738.5
1065.6	1698.9	644.4	837.8
1339.6	1488.8	678.1	1709.6
1519.9	2767.5	656.1	1124.9
790.3	2221.6	582.2	1409.2
2338	4619.7	1563.4	3579.9
1729.1	4605.1	1786.4	2817.2
1824.6	4721.8	2292.6	2281
1503.3	5010.1	2283.6	3783.2
2532	5296	1467.2	4629.5

Principal Component Results

Descriptive Statistics				
Variable	Mean	Std Dev.	Std Err	N
cwclose	1227.695	481.432	87.897	30
cwopen	2529.513	1177.853	215.046	30
cwdown	1122.232	541.051	98.782	30
cwup	1551.940	986.328	180.078	30
Covariance Matrix				
	cwclose	cwopen	cwdown	cwup
cwclose	231776.678	355164.043	70057.114	351363.558
cwopen	355164.043	1387337.533	329955.908	942671.128
cwdown	70057.114	329955.908	292736.216	215778.807
cwup	351363.558	942671.128	215778.807	972841.990
Explained Variance (Eigenvalues)				
Value	PC 1	PC 2	PC 3	PC 4
Eigenvalue	2343804.734	272794.676	178202.950	89890.056
% of Var.	81.250	9.457	6.178	3.116
Cum. %	81.250	90.706	96.884	100.000
Component Loadings				
Variable	PC 1	PC 2	PC 3	PC 4
cwclose	0.734	0.361	0.115	0.564
cwopen	0.965	-0.182	-0.189	0.010
cwdown	0.539	-0.599	0.591	0.039
cwup	0.931	0.306	0.155	-0.127
Component Score Coefficients (Eigenvectors)				
Variable	PC 1	PC 2	PC 3	PC 4
cwclose	0.231	0.333	0.131	0.905
cwopen	0.742	-0.411	-0.528	0.038
cwdown	0.190	-0.621	0.757	0.070
cwup	0.600	0.578	0.362	-0.418

Table 5.23
PCA results for wrist locations

Descriptive Statistics				
Variable	Mean	Std Dev.	Std Err	N
cw	1607.845	1006.884	91.916	120
cam	3068.758	1162.373	106.110	120
cbe	2239.686	1281.267	116.963	120
Covariance Matrix				
	cw	cam	cbe	
cw	1013815.478	10891.165	-258616.386	
cam	10891.165	1351111.007	-552111.093	
cbe	-258616.386	-552111.093	1641646.345	
Explained Variance (Eigenvalues)				
Value	PC 1	PC 2	PC 3	
Eigenvalue	2108833.644	1097352.882	800386.304	
% of Var.	52.634	27.389	19.977	
Cum. %	52.634	80.023	100.000	
Component Loadings				
Variable	PC 1	PC 2	PC 3	
cw	-0.278	-0.775	0.567	
cam	-0.724	0.551	0.414	
cbe	0.897	0.218	0.384	
Component Score Coefficients (Eigenvectors)				
Variable	PC 1	PC 2	PC 3	
cw	-0.193	-0.745	0.639	
cam	-0.580	0.612	0.538	
cbe	0.792	0.266	0.550	

Chapter's Summary:

Analysis proved linear relationship between muscle force and SEMG amplitude and it is also found that description of hand/wrist movements using parameter "slope" is possible. It has also been concluded that for 2-channel control strategy locations "cbet and cbeb" and for three channel control strategy locations ""cam, camb and cbet" are the best suited for four functions prosthetic devices.

Table A5.1a
Slope value for closing movement from the six locations

		cwcl	cwbcl	camcl	cambcl	cbetcl	cbebcl
Subject 1	trial 1	1348.8	779.9	2467.6	3259.4	2825.1	4375
	trial 2	1300.5	1768.8	4327.5	2393.7	2420.9	3205.1
	trial 3	970.31	880.9	4382.8	4024.6	3620.8	2957.1
	trial 4	1201.8	724.5	4321.5	2182.7	3363.1	3709.7
	trial 5	1502.7	820.0	4870	3047.1	3489.3	4126
	Av1	1264.8	994.8	4073.8	2981.5	3143.8	3674.5
Subject 2	trial 1	934.4	1036.1	2657.1	2452.8	2534.1	1334.8
	trial 2	1265.2	1065.6	3476.2	4651.5	3930.1	2190
	trial 3	1140	1339.6	1977.7	3513	2957.1	2288.8
	trial 4	1499.1	1519.9	4467	3725.8	3693.5	1693.1
	trial 5	1116.8	790.3	3784.8	2814.8	2932.4	1845.9
	Av2	1191.1	1150.3	3272.5	3431.5	3209.4	1870.5
Subject 3	trial 1	622.2	2338	2255.7	2412.6	1218.9	1510.3
	trial 2	1007.4	1729.1	1760.1	1665.8	1317.5	1695.9
	trial 3	527.2	1824.6	2700.9	1868.4	682.35	1331.7
	trial 4	543.0	1503.3	3537.1	1637.1	945.0	2169.5
	trial 5	1198.4	2532	2959.3	674.3	964.6	2340.9
	Av3	779.6	1985.4	2642.62	1651.6	1025.6	1809.6
	Av	1078.5	1376.8	3329.6	2688.2	2459.6	2451.5

Table A5.1b
V_{rms} value for closing movement from the six locations

		cwcl	cwbcl	camcl	cambcl	cbetcl	cbebcl
Subject 1	trial 1	0.10	0.07	0.22	0.27	0.23	0.37
	trial 2	0.13	0.14	0.42	0.20	0.28	0.31
	trial 3	0.10	0.08	0.41	0.43	0.40	0.32
	trial 4	0.09	0.07	0.47	0.23	0.32	0.39
	trial 5	0.12	0.08	0.48	0.28	0.39	0.46
	Av1	0.11	0.09	0.40	0.28	0.32	0.37
Subject 2	trial 1	0.08	0.09	0.25	0.26	0.25	0.15
	trial 2	0.11	0.12	0.37	0.48	0.34	0.17
	trial 3	0.12	0.14	0.19	0.33	0.29	0.22
	trial 4	0.13	0.13	0.29	0.39	0.37	0.15
	trial 5	0.12	0.09	0.30	0.28	0.30	0.20
	Av2	0.11	0.11	0.28	0.35	0.31	0.18
Subject 3	trial 1	0.05	0.22	0.22	0.27	0.13	0.18
	trial 2	0.10	0.18	0.17	0.13	0.13	0.17
	trial 3	0.05	0.17	0.27	0.18	0.06	0.13
	trial 4	0.06	0.19	0.28	0.19	0.10	0.20
	trial 5	0.11	0.23	0.25	0.08	0.10	0.24
	Av3	0.07	0.20	0.24	0.17	0.11	0.18

Table A5.2a
Slope value for opening movement from the six locations

		cwop	cwbop	camop	cambop	cbetop	cbebop
Subject 1	trial 1	1099.7	1691.6	1121.1	4157.6	2145.1	1719.7
	trial 2	1931.2	1627.2	1300.2	4517.8	1414.1	1218.8
	trial 3	1793.5	1807	2317.7	5033.6	1181.3	998.3
	trial 4	1745	3352.3	1065	3982.8	1062.9	1208.1
	trial 5	3296.1	1835.8	1197.5	4373.5	1013.7	1169.6
	Av1	1973.1	2062.7	1400.3	4413.1	1363.4	1262.9
Subject 2	trial 1	2484.6	2163.9	1549.4	5659.6	4286.1	1147
	trial 2	2204.7	1698.9	1329.6	3988.6	4171.3	1170.2
	trial 3	1619	1488.8	1301	3300	3631.9	1332.9
	trial 4	2248.8	2767.5	1143.3	4945.4	4571.9	1580.3
	trial 5	1890.9	2221.6	1257.3	4805	4899.4	1097.1
	Av2	2089.6	2068.1	1316.1	4539.7	4312.1	1265.5
Subject 3	trial 1	2881.7	4619.7	3241	2785.6	710.5	1560.4
	trial 2	1348.9	4605.1	2522.6	3041.9	1203.9	1560.4
	trial 3	2182.5	4721.8	2440.8	3049.6	768.9	2872.9
	trial 4	1848.6	5010.1	3194.1	3019.4	1382.5	2508.9
	trial 5	2402.9	5296	2872.8	3349.5	1200.2	2505.2
	Av3	2132.9	4850.5	2854.2	3049.2	1053.2	2201.5
	Av	2065.2	2993.8	1856.8	4000.6	2242.9	1576.6

Table A5.2b
V_{rms} value for opening movement from the six locations

		cwop	cwbop	camop	cambop	cbetop	cbebop
Subject 1	trial 1	0.11	0.16	0.12	0.47	0.19	0.12
	trial 2	0.14	0.17	0.13	0.54	0.12	0.13
	trial 3	0.17	0.18	0.22	0.52	0.11	0.10
	trial 4	0.16	0.26	0.11	0.48	0.11	0.13
	trial 5	0.25	0.16	0.11	0.54	0.09	0.11
	Av1	0.17	0.18	0.14	0.51	0.12	0.12
Subject 2	trial 1	0.22	0.22	0.14	0.55	0.35	0.11
	trial 2	0.24	0.15	0.12	0.46	0.43	0.10
	trial 3	0.14	0.14	0.11	0.39	0.36	0.11
	trial 4	0.19	0.23	0.11	0.57	0.51	0.15
	trial 5	0.20	0.22	0.13	0.58	0.47	0.11
	Av2	0.20	0.19	0.12	0.51	0.42	0.12
Subject 3	trial 1	0.20	0.48	0.30	0.25	0.07	0.17
	trial 2	0.11	0.42	0.29	0.32	0.11	0.17
	trial 3	0.17	0.54	0.21	0.34	0.09	0.22
	trial 4	0.16	0.56	0.29	0.30	0.15	0.27
	trial 5	0.20	0.52	0.29	0.38	0.13	0.30
	Av3	0.17	0.50	0.28	0.32	0.11	0.23

Table A5.3a
Slope value for down movement from the six locations

		cwd	cwbd	camd	cambd	cbetd	cbebd
Subject 1	trial 1	834.7	633.7	4018.3	3501.4	822.5	3731
	trial 2	1233.3	970.6	3174.5	3677.3	757.6	3825.2
	trial 3	944.5	1060	4632.3	3677.3	555.4	4000.2
	trial 4	932.3	810.5	4698.1	3340.6	1590.1	4668.2
	trial 5	721.1	758.5	3259.7	3563.3	552.4	4457.3
	Av1	933.2	846.7	3956.5	3551.9	855.6	4136.3
Subject 2	trial 1	589.8	531.7	5069	1440.1	763.8	3179.7
	trial 2	1389.7	644.4	3657.6	1411.5	922.8	3898.5
	trial 3	525.2	678.1	3350	1943.1	871.5	4120.2
	trial 4	639.4	656.1	4522.4	1424.7	884.1	3881.2
	trial 5	973.8	582.2	4374.9	2193.1	1379.9	4438
	Av2	823.6	618.5	4194.7	1682.5	964.4	3903.5
Subject 3	trial 1	1068.7	1563.4	3196.2	1922.9	578.31	3862.4
	trial 2	2072.1	1786.4	4015.5	1137.3	706.2	2859
	trial 3	1443.8	2292.6	4671.5	1307.7	758.5	2954.6
	trial 4	1946.9	2283.6	3710.7	1681.6	701.4	2667.1
	trial 5	1631.8	1467.2	5156.3	1220.1	623.4	2427.1
	Av3	1632.6	1878.6	4150.0	1453.9	673.5	2954.0
	Av	1129.8	1114.6	4100.4	2229.4	831.2	3664.6

Table A5.3b
V_{rms} value for down movement from the six locations

		cwd	cwbd	camd	cambd	cbetd	cbebd
Subject 1	trial 1	0.09	0.06	0.37	0.39	0.07	0.40
	trial 2	0.12	0.10	0.36	0.36	0.08	0.37
	trial 3	0.09	0.08	0.43	0.36	0.07	0.38
	trial 4	0.08	0.07	0.49	0.32	0.11	0.41
	trial 5	0.06	0.08	0.33	0.30	0.06	0.40
	Av1	0.09	0.08	0.40	0.35	0.08	0.39
Subject 2	trial 1	0.07	0.05	0.42	0.15	0.09	0.27
	trial 2	0.11	0.07	0.35	0.14	0.10	0.47
	trial 3	0.05	0.07	0.34	0.18	0.11	0.46
	trial 4	0.07	0.06	0.45	0.15	0.09	0.37
	trial 5	0.08	0.06	0.41	0.21	0.11	0.47
	Av2	0.08	0.06	0.39	0.17	0.10	0.41
Subject 3	trial 1	0.11	0.13	0.29	0.18	0.06	0.40
	trial 2	0.18	0.14	0.39	0.12	0.07	0.31
	trial 3	0.16	0.20	0.51	0.13	0.08	0.31
	trial 4	0.20	0.20	0.46	0.17	0.06	0.24
	trial 5	0.18	0.15	0.48	0.12	0.06	0.24
	Av3	0.16	0.17	0.42	0.14	0.07	0.30

Table A5.4a
Slope value for up movement from the six locations

		cwu	cwbu	camu	cambu	cbetu	cbebu
Subject 1	trial 1	1241.4	1548.4	2926.9	3970.5	3631.1	1415.5
	trial 2	1758.8	1696.3	2292.6	3451.4	3948.6	2053.3
	trial 3	1178.4	1675.5	1619.1	3506.2	3583.4	1244.1
	trial 4	1656	1959.5	2007.7	3728.7	3167.2	1260.7
	trial 5	1482.8	1192.1	1935.1	4398.8	3064.5	999.2
	Av1	1463.4	1614.3	2156.2	3811.1	3478.9	1394.5
Subject 2	trial 1	1116	738.5	3082.6	3302.6	4439.1	628.6
	trial 2	998.3	837.8	2063.8	3925.4	3673.1	1307.2
	trial 3	824.0	1709.6	4581.1	3883.2	4709.6	1292.9
	trial 4	931.2	1124.9	1965.7	4292.8	4166.7	1377.8
	trial 5	677.8	1409.2	2741.6	4568.1	3567.1	858.9
	Av2	909.4	1164.0	2886.9	3994.4	4111.1	1093.1
Subject 3	trial 1	743.6	3579.9	1995.6	3153.9	2421.9	805.0
	trial 2	660.4	2817.2	2587.2	3736.5	3041.6	1295.3
	trial 3	727.1	2281	2023.5	3771.1	2379.1	878.9
	trial 4	675.3	3783.2	2480.7	4611.5	3564.2	1099.2
	trial 5	904.0	4629.5	2580.8	3985	3118.8	1369
	Av3	742.1	3418.1	2333.5	3851.6	2905.1	1089.4
	Av	1038.3	2065.5	2458.9	3885.7	3498.4	1192.3

Table A5.4b
V_{rms} value for up movement from the six locations

		cwu	cwbu	camu	cambu	cbetu	cbebu
Subject 1	trial 1	0.12	0.15	0.27	0.44	0.31	0.15
	trial 2	0.16	0.17	0.18	0.37	0.39	0.15
	trial 3	0.10	0.16	0.14	0.42	0.31	0.10
	trial 4	0.15	0.16	0.17	0.29	0.28	0.12
	trial 5	0.16	0.13	0.15	0.40	0.32	0.11
	Av1	0.14	0.15	0.18	0.38	0.32	0.13
Subject 2	trial 1	0.10	0.08	0.28	0.36	0.38	0.07
	trial 2	0.09	0.09	0.19	0.40	0.46	0.12
	trial 3	0.09	0.13	0.37	0.44	0.48	0.12
	trial 4	0.09	0.13	0.19	0.51	0.38	0.12
	trial 5	0.06	0.11	0.23	0.49	0.42	0.08
	Av2	0.09	0.11	0.25	0.44	0.43	0.10
Subject 3	trial 1	0.09	0.35	0.20	0.26	0.26	0.09
	trial 2	0.08	0.33	0.26	0.30	0.31	0.11
	trial 3	0.06	0.25	0.17	0.34	0.25	0.10
	trial 4	0.06	0.43	0.23	0.48	0.36	0.12
	trial 5	0.08	0.52	0.29	0.40	0.33	0.11
	Av3	0.07	0.38	0.23	0.36	0.30	0.10

Table A5.5
Slope value and V_{rms} values from the location "cw" for four movements

		Slope Values					V_{rms} Values			
		cwcl	cwop	cwd	cwu		cwcl	cwop	cwd	cwu
Subject 1	trial 1	1348.8	1099.7	834.6	1241.4		0.10	0.11	0.09	0.12
	trial 2	1300.5	1931.2	1233.3	1758.8		0.13	0.14	0.12	0.16
	trial 3	970.31	1793.5	944.5	1178.4		0.10	0.17	0.09	0.10
	trial 4	1201.8	1745	932.3	1656		0.09	0.16	0.08	0.15
	trial 5	1502.7	3296.1	721.1	1482.8		0.12	0.25	0.06	0.16
	av1	1264.8	1973.1	933.2	1463.4		0.11	0.17	0.09	0.14
Subject 2	trial 1	934.4	2484.6	589.8	1116		0.08	0.22	0.07	0.10
	trial 2	1265.2	2204.7	1389.7	998.3		0.11	0.24	0.11	0.09
	trial 3	1140	1619	525.2	824.0		0.12	0.14	0.05	0.09
	trial 4	1499.1	2248.8	639.4	931.2		0.13	0.19	0.07	0.09
	trial 5	1116.8	1890.9	973.8	677.8		0.12	0.20	0.08	0.06
	av2	1191.1	2089.6	823.6	909.4		0.11	0.20	0.08	0.09
Subject 3	trial 1	622.2	2881.7	1068.7	743.6		0.05	0.20	0.11	0.09
	trial 2	1007.4	1348.9	2072.1	660.4		0.10	0.11	0.18	0.08
	trial 3	527.2	2182.5	1443.8	727.1		0.05	0.17	0.16	0.06
	trial 4	543.1	1848.6	1946.9	675.3		0.06	0.16	0.20	0.06
	trial 5	1198.4	2402.9	1631.8	904.1		0.11	0.20	0.18	0.08
	av3	779.6	2132.9	1632.6	742.1		0.07	0.17	0.16	0.07
	av	1078.5	2065.2	1129.8	1038.3					

Table A5.6
Slope value and V_{rms} values from the location "cwb" for four movements

		Slope Vlues					V_{rms} Values			
		cwbcl	cwbop	cwbd	cwbu		cwbcl	cwbop	cwbd	cwbu
Subject 1	trial 1	779.9	1691.6	633.7	1548.4		0.07	0.16	0.06	0.15
	trial 2	1768.8	1627.2	970.6	1696.3		0.14	0.17	0.10	0.17
	trial 3	880.9	1807	1060	1675.5		0.08	0.18	0.08	0.16
	trial 4	724.5	3352.3	810.5	1959.5		0.07	0.26	0.07	0.16
	trial 5	820.0	1835.8	758.5	1192.1		0.08	0.16	0.08	0.13
	av1	994.8	2062.7	846.7	1614.3		0.09	0.18	0.08	0.15
Subject 2	trial 1	1036.1	2163.9	531.7	738.5		0.09	0.22	0.05	0.08
	trial 2	1065.6	1698.9	644.4	837.8		0.12	0.15	0.07	0.09
	trial 3	1339.6	1488.8	678.1	1709.6		0.14	0.14	0.07	0.13
	trial 4	1519.9	2767.5	656.1	1124.9		0.13	0.23	0.06	0.13
	trial 5	790.3	2221.6	582.2	1409.2		0.09	0.22	0.06	0.11
	av2	1150.3	2068.1	618.5	1164.0		0.11	0.19	0.06	0.11
Subject 3	trial 1	2338	4619.7	1563.4	3579.9		0.22	0.48	0.13	0.35
	trial 2	1729.1	4605.1	1786.4	2817.2		0.18	0.42	0.14	0.33
	trial 3	1824.6	4721.8	2292.6	2281		0.17	0.54	0.20	0.25
	trial 4	1503.3	5010.1	2283.6	3783.2		0.19	0.56	0.20	0.43
	trial 5	2532	5296	1467.2	4629.5		0.23	0.52	0.15	0.52
	av3	1985.4	4850.5	1878.6	3418.1		0.20	0.50	0.17	0.38
	av	1376.8	2993.8	1114.6	2065.5					

Table A5.7
Slope value and V_{rms} values from the location "cam" for four movements

		Slope Values					V_{rms} Values			
		camcl	camop	camd	camu		camcl	camop	camd	camu
Subject 1	trial 1	2467.6	1121.1	4018.3	2926.9		0.22	0.12	0.37	0.27
	trial 2	4327.5	1300.2	3174.5	2292.6		0.42	0.13	0.36	0.18
	trial 3	4382.8	2317.7	4632.3	1619.1		0.41	0.22	0.43	0.14
	trial 4	4321.5	1065	4698.1	2007.7		0.47	0.11	0.49	0.17
	trial 5	4870	1197.5	3259.7	1935.1		0.48	0.11	0.33	0.15
	av1	4073.8	1400.3	3956.5	2156.2		0.25	0.14	0.42	0.28
Subject 2	trial 1	2657.1	1549.4	5069	3082.6		0.37	0.12	0.35	0.19
	trial 2	3476.2	1329.6	3657.6	2063.8		0.19	0.11	0.34	0.37
	trial 3	1977.7	1301	3350	4581.1		0.29	0.11	0.45	0.19
	trial 4	4467	1143.3	4522.4	1965.7		0.30	0.13	0.41	0.23
	trial 5	3784.8	1257.3	4374.9	2741.6		0.28	0.12	0.39	0.25
	av2	3272.5	1316.1	4194.7	2886.9		0.25	0.14	0.42	0.28
Subject 3	trial 1	2255.7	3241	3196.2	1995.6		0.22	0.30	0.29	0.20
	trial 2	1760.1	2522.6	4015.5	2587.2		0.17	0.29	0.39	0.26
	trial 3	2700.9	2440.8	4671.5	2023.5		0.27	0.21	0.51	0.17
	trial 4	3537.1	3194.1	3710.7	2480.7		0.28	0.29	0.46	0.23
	trial 5	2959.3	2872.8	5156.3	2580.8		0.25	0.29	0.48	0.29
	av3	2642.6	2854.2	4150.0	2333.5		0.24	0.28	0.42	0.23
	av	3329.6	1856.8	4100.4	2458.9					

Table A5.8
Slope value and V_{rms} values from the location "camb" for four movements

		Slope Values					V_{rms} Values			
		cambcl	cambop	cambd	cambu		cambcl	cambop	cambd	cambu
Subject 1	trial 1	3259.4	4157.6	3501.4	3970.5		0.27	0.47	0.39	0.44
	trial 2	2393.7	4517.8	3677.3	3451.4		0.20	0.54	0.36	0.37
	trial 3	4024.6	5033.6	3677.3	3506.2		0.43	0.52	0.36	0.42
	trial 4	2182.7	3982.8	3340.6	3728.7		0.23	0.48	0.32	0.29
	trial 5	3047.1	4373.5	3563.3	4398.8		0.28	0.54	0.30	0.40
	av1	2981.5	4413.0	3551.9	3811.1		0.28	0.51	0.35	0.38
Subject 2	trial 1	2452.8	5659.6	1440.1	3302.6		0.26	0.55	0.15	0.36
	trial 2	4651.5	3988.6	1411.5	3925.4		0.48	0.46	0.14	0.40
	trial 3	3513	3300	1943.1	3883.2		0.33	0.39	0.18	0.44
	trial 4	3725.8	4945.4	1424.7	4292.8		0.39	0.57	0.15	0.51
	trial 5	2814.8	4805	2193.1	4568.1		0.28	0.58	0.21	0.49
	av2	3431.5	4539.7	1682.5	3994.4		0.35	0.51	0.17	0.44
Subject 3	trial 1	2412.6	2785.6	1922.9	3153.9		0.27	0.25	0.18	0.26
	trial 2	1665.8	3041.9	1137.3	3736.5		0.13	0.32	0.12	0.30
	trial 3	1868.4	3049.6	1307.7	3771.1		0.18	0.34	0.13	0.34
	trial 4	1637.1	3019.4	1681.6	4611.5		0.19	0.30	0.17	0.48
	trial 5	674.3	3349.5	1220.1	3985		0.08	0.38	0.12	0.40
	av3	1651.6	3049.2	1453.9	3851.6		0.17	0.32	0.14	0.36
	av	2688.2	4000.6	2229.4	3885.7					

Table A5.9

Slope value and V_{rms} values from the location "cbet" for four movements

		Slope Values					V_{rms} Values			
		cbetcl	cbetop	cbetd	cbetu		cbetcl	cbetop	cbetd	cbetu
Subject 1	trial 1	2825.1	2145.1	822.5	3631.1		0.23	0.19	0.07	0.31
	trial 2	2420.9	1414.1	757.6	3948.6		0.28	0.12	0.08	0.39
	trial 3	3620.8	1181.3	555.4	3583.4		0.40	0.11	0.07	0.31
	trial 4	3363.1	1062.9	1590.1	3167.2		0.32	0.11	0.11	0.28
	trial 5	3489.3	1013.7	552.4	3064.5		0.39	0.09	0.06	0.32
	av1	3143.8	1363.4	855.6	3478.9		0.32	0.12	0.08	0.32
Subject 2	trial 1	2534.1	4286.1	763.8	4439.1		0.25	0.35	0.09	0.38
	trial 2	3930.1	4171.3	922.8	3673.1		0.34	0.43	0.10	0.46
	trial 3	2957.1	3631.9	871.5	4709.6		0.29	0.36	0.11	0.48
	trial 4	3693.5	4571.9	884.1	4166.7		0.37	0.51	0.09	0.38
	trial 5	2932.4	4899.4	1379.9	3567.1		0.30	0.47	0.11	0.42
	av2	3209.4	4312.1	964.4	4111.1		0.31	0.42	0.10	0.43
Subject 3	trial 1	1218.9	710.5	578.3	2421.9		0.13	0.07	0.06	0.26
	trial 2	1317.5	1203.9	706.2	3041.6		0.13	0.11	0.07	0.31
	trial 3	682.3	768.9	758.5	2379.1		0.06	0.09	0.08	0.25
	trial 4	945.0	1382.5	701.4	3564.2		0.10	0.15	0.06	0.36
	trial 5	964.6	1200.2	623.4	3118.8		0.10	0.13	0.06	0.33
	av3	1025.6	1053.2	673.5	2905.1		0.11	0.11	0.07	0.30
	av	2459.6	2242.9	831.2	3498.4					

Table A5.10

Slope value and V_{rms} values from the location "cbeb" for four movements

		Slope Values					V_{rms} Values			
		cbebcl	cbebop	cbebd	cbebu		cbebcl	cbebop	cbebd	cbebu
Subject 1	trial 1	4375	1719.7	3731	1415.5		0.37	0.12	0.40	0.15
	trial 2	3205.1	1218.8	3825.2	2053.3		0.31	0.13	0.37	0.15
	trial 3	2957.1	998.3	4000.2	1244.1		0.32	0.10	0.38	0.10
	trial 4	3709.7	1208.1	4668.2	1260.7		0.39	0.13	0.41	0.12
	trial 5	4126	1169.6	4457.3	999.2		0.46	0.11	0.40	0.11
	av1	3674.5	1262.9	4136.3	1394.5		0.37	0.12	0.39	0.13
Subject 2	trial 1	1334.8	1147	3179.7	628.6		0.15	0.11	0.27	0.07
	trial 2	2190	1170.2	3898.5	1307.2		0.17	0.10	0.47	0.12
	trial 3	2288.8	1332.9	4120.2	1292.9		0.22	0.11	0.46	0.12
	trial 4	1693.1	1580.3	3881.2	1377.8		0.15	0.15	0.37	0.12
	trial 5	1845.9	1097.1	4438	858.9		0.20	0.11	0.47	0.08
	av2	1870.5	1265.5	3903.5	1093.1		0.18	0.12	0.41	0.10
Subject 3	trial 1	1510.3	1560.4	3862.4	805.0		0.18	0.17	0.40	0.09
	trial 2	1695.9	1560.4	2859	1295.3		0.17	0.17	0.31	0.11
	trial 3	1331.7	2872.9	2954.6	878.9		0.13	0.22	0.31	0.10
	trial 4	2169.5	2508.9	2667.1	1099.2		0.20	0.27	0.24	0.12
	trial 5	2340.9	2505.2	2427.1	1369		0.24	0.30	0.24	0.11
	av3	1809.6	2201.5	2954.0	1089.4		0.18	0.23	0.30	0.10
	av	2451.5	1576.6	3664.6	1192.3					

Table A5.11
Av freq for closing movement from the six locations

	cwcl	cwbcl	camcl	cambcl	cbetcl	cbebcl
trial 1	174.15	146.48	168.13	174.80	182.29	156.90
trial 2	173.99	168.94	173.99	166.82	158.20	154.78
trial 3	156.73	133.95	170.41	136.88	180.82	146.80
trial 4	153.80	179.19	177.89	148.60	174.80	173.33
trial 5	178.71	156.73	173.66	172.03	140.46	153.48
av1	167.48	157.06	172.81	159.83	167.31	157.06
trial 1	163.89	172.36	164.55	188.31	174.64	171.87
trial 2	171.54	171.22	179.68	159.01	187.01	177.89
trial 3	148.76	152.01	189.29	172.20	166.50	160.15
trial 4	155.92	173.17	188.31	177.24	182.12	172.20
trial 5	191.56	164.22	193.19	171.87	167.48	180.98
av2	166.34	166.60	183.00	173.73	175.55	172.62
trial 1	152.34	158.37	185.71	178.06	166.99	154.62
trial 2	156.58	158.53	170.57	158.20	165.36	144.37
trial 3	162.11	150.72	174.15	168.29	159.67	170.90
trial 4	147.46	177.41	192.55	146.81	165.36	148.44
trial 5	164.23	153.65	170.57	153.48	144.37	163.90
av3	156.54	159.73	178.71	160.97	160.35	156.45
av	163.45	161.13	178.18	164.84	167.74	162.04

Table A5.12
Av freq for opening movement from the six locations

	cwop	cwbop	camop	cambop	cbetop	cbebop
trial 1	161.94	177.73	183.59	157.55	173.66	152.50
trial 2	167.96	150.87	188.31	159.66	155.92	167.15
trial 3	168.45	153.32	173.66	173.17	169.27	168.29
trial 4	170.89	152.50	156.90	178.54	152.83	174.31
trial 5	170.24	188.80	164.38	155.43	136.71	155.59
av1	167.90	164.64	173.37	164.87	157.68	163.57
trial 1	182.94	188.15	179.03	174.47	155.76	193.84
trial 2	176.26	194.98	180.82	175.78	121.90	193.84
trial 3	189.77	168.29	195.80	171.22	179.85	188.80
trial 4	186.03	162.76	165.36	179.19	156.73	202.79
trial 5	179.68	180.33	189.45	187.01	171.87	179.36
av2	182.94	178.90	182.09	177.53	157.22	191.73
trial 1	162.76	171.06	167.32	148.27	160.48	149.90
trial 2	163.25	148.60	180.83	167.48	164.88	140.14
trial 3	170.74	157.23	175.13	162.92	160.64	162.92
trial 4	151.04	175.13	133.46	158.69	161.78	137.53
trial 5	167.32	159.67	166.34	152.34	162.76	136.23
av3	163.02	162.34	164.62	157.94	162.11	145.35
av	171.29	168.63	173.36	166.79	159.01	166.88

Table A5.13
Av freq for down movement from the six locations

	cwd	cwbd	camd	cambd	cbetd	cbebd
trial 1	150.87	153.32	178.05	184.73	166.01	167.64
trial 2	141.76	156.25	156.90	178.38	153.32	152.34
trial 3	157.38	170.73	170.57	178.38	124.18	153.48
trial 4	154.94	145.34	180.50	184.40	156.57	161.29
trial 5	174.80	154.13	186.19	182.77	138.83	158.20
av1	155.95	155.95	174.44	181.73	147.78	158.59
trial 1	188.80	182.29	182.94	175.94	144.85	179.52
trial 2	196.61	172.36	160.48	185.05	161.78	199.86
trial 3	172.52	167.15	196.61	182.94	185.38	200.19
trial 4	187.5	188.80	205.56	186.19	180.82	192.38
trial 5	189.77	191.08	189.77	192.70	153.80	194.17
av2	187.04	180.33	187.07	184.57	165.33	193.22
trial 1	164.06	158.69	169.76	168.62	152.83	176.60
trial 2	179.52	156.90	187.34	181.64	160.32	153.48
trial 3	157.06	150.55	169.43	176.92	166.99	170.57
trial 4	176.76	175.46	173.99	164.55	175.94	178.06
trial 5	150.88	149.90	164.71	173.50	167.48	151.69
av3	165.66	158.30	173.05	173.05	164.71	166.08
av	169.55	164.87	178.19	179.79	159.28	172.63

Table A5.14
Av freq for up movement from the six locations

	cwu	cwbu	camu	cambu	cbetu	cbebu
trial 1	159.01	199.70	174.15	155.43	174.15	165.03
trial 2	173.99	170.08	176.26	152.99	171.54	149.41
trial 3	169.27	173.50	157.87	180.82	153.64	166.66
trial 4	192.87	178.05	187.33	176.26	189.61	168.29
trial 5	174.15	182.12	175.78	174.96	171.22	190.26
av1	173.86	180.69	174.28	168.09	172.03	167.93
trial 1	182.77	166.50	187.17	170.08	169.59	169.75
trial 2	178.38	183.59	184.40	188.63	162.59	176.26
trial 3	171.38	176.59	183.59	185.87	182.77	168.78
trial 4	130.69	167.48	178.54	187.17	167.31	175.78
trial 5	173.01	192.87	191.08	179.85	172.03	180.98
av2	167.25	177.40	184.96	182.32	170.86	174.31
trial 1	181.97	171.22	159.02	157.55	184.24	167.15
trial 2	171.06	128.91	161.78	187.83	194.34	162.43
trial 3	141.11	161.46	161.46	183.92	167.32	141.76
trial 4	188.64	155.76	181.80	167.48	180.34	157.06
trial 5	183.59	144.37	164.06	186.36	171.22	162.43
av3	173.27	152.34	165.63	176.63	179.49	158.17
av	171.46	170.15	174.96	175.68	174.13	166.81

Table A5.15a
Principal Component Results for two channels combination [Subject 1]

Descriptive Statistics												
Variable	cwclose	cwopen	cwdown	cwup	camclose	camopen	camdown	camup	cbeclose	cbeopen	cbedown	cbeup
Mean	1129.84	2017.94	889.97	1538.92	3527.69	2906.68	3754.28	2983.7	3409.21	1313.16	2496.01	2436.77
Std Dev.	349.54	724.69	176.01	263.39	975.9	1647.32	537.03	967.14	592	361.62	1773.45	1155.49
Std Err	110.53	229.17	55.66	83.29	308.61	520.93	169.82	305.84	187.21	114.36	560.81	365.4
N	10	10	10	10	10	10	10	10	10	10	10	10
Covariance Matrix												
	cwclose	cwopen	cwdown	cwup	camclose	camopen	camdown	camup	cbeclose	cbeopen	cbedown	cbeup
cwclose	122176.67	-32285.21	16631.77	1957.89	29475.51	-241008.69	-1379.04	-143411.07	-111492.64	5960.54	-287616.91	217147.58
cwopen	-32285.21	525179.32	-31603.33	84703.08	103312.19	-9827.95	-185259.53	-59351.33	91099.43	-133440.29	131952.20	-161663.08
cwdown	16631.77	-31603.33	30981.24	14708.56	46511.16	-42397.87	6799.81	-60479.00	-85531.23	-12964.57	-78236.85	83422.44
cwup	1957.89	84703.08	14708.56	69375.70	-34617.30	85603.43	-57454.99	30928.30	-37403.80	-26519.27	164219.93	-68335.18
camclose	29475.51	103312.19	46511.16	-34617.30	952380.85	-767762.72	95289.45	-673256.02	-102262.73	-162532.50	-1062123.13	526094.32
camopen	-241008.69	-9827.95	-42397.87	85603.43	-767762.72	2713660.58	-253270.87	1286862.00	416280.94	-137110.30	2668229.62	-1717883.21
camdown	-1379.04	-185259.53	6799.81	-57454.99	95289.45	-253270.87	288397.86	-235469.24	7391.45	-4796.81	-315016.61	218348.06
camup	-143411.07	-59351.33	-60479.00	30928.30	-673256.02	1286862.00	-235469.24	935352.60	249781.13	59145.59	1542972.45	-974351.64
cbeclose	-111492.64	91099.43	-85531.23	-37403.80	-102262.73	416280.94	7391.45	249781.13	350460.98	-22921.13	496774.00	-409465.18
cbeopen	5960.54	-133440.29	-12964.57	-26519.27	-162532.50	-137110.30	-4796.81	59145.59	-22921.13	130772.35	-123304.92	105628.26
cbedown	-287616.91	131952.20	-78236.85	164219.93	-1062123.13	2668229.62	-315016.61	1542972.45	496774.00	-123304.92	3145108.94	-1963620.96
cbeup	217147.58	-161663.08	83422.44	-68335.18	526094.32	-1717883.21	218348.06	-974351.64	-409465.18	105628.26	-1963620.96	1335156.55

Explained Variance (Eigenvalues)												
Value	PC 1	PC 2	PC 3	PC 4	PC 5	PC 6	PC 7	PC 8	PC 9	PC 10	PC 11	PC 12
Eigenvalue	8088480.29	932532.63	621241.47	390531.90	248217.59	178491.52	75428.59	41547.43	22532.22	0.00	0.00	0.00
% of Var.	76.31	8.80	5.86	3.68	2.34	1.68	0.71	0.39	0.21	0.00	0.00	0.00
Cum. %	76.31	85.11	90.97	94.66	97.00	98.68	99.40	99.79	100.00	100.00	100.00	100.00
Component Loadings												
(correlations between initial variables and principal components)												
Variable	PC 1	PC 2	PC 3	PC 4	PC 5	PC 6	PC 7	PC 8	PC 9	PC 10	PC 11	PC 12
cwclose	-0.47	-0.23	-0.05	-0.44	-0.11	0.14	0.70	-0.01	-0.08	0.10	0.12	-0.55
cwopen	0.07	0.67	-0.70	-0.05	-0.16	0.16	-0.06	0.05	0.00	-0.06	0.28	0.26
cwdown	-0.29	-0.03	0.34	-0.75	-0.18	-0.28	-0.21	-0.09	0.26	-0.05	0.29	-0.12
cwup	0.26	0.21	-0.39	-0.52	-0.30	-0.33	-0.10	-0.43	-0.26	-0.43	-0.09	0.21
camclose	-0.62	0.69	0.31	-0.01	0.18	-0.14	0.01	-0.02	-0.01	-0.02	0.51	-0.57
camopen	0.95	0.09	0.23	-0.12	-0.01	0.14	-0.02	0.00	0.00	-0.07	-0.28	0.82

camdown	-0.35	-0.17	0.55	0.46	-0.55	-0.12	-0.03	0.09	-0.04	-0.03	0.02	-0.28
camup	0.92	-0.25	-0.11	0.05	0.27	-0.07	0.01	0.03	0.03	-0.20	-0.44	0.72
cbeclose	0.50	0.25	-0.06	0.77	0.06	0.23	0.09	-0.16	0.04	-0.17	-0.49	0.41
cbeopen	-0.14	-0.82	-0.12	0.15	0.38	0.15	-0.21	-0.11	-0.23	0.37	-0.37	-0.29
cbedown	0.99	0.01	-0.05	0.00	-0.07	-0.12	0.01	-0.03	0.01	-0.35	-0.37	0.85
cbeup	-0.97	-0.18	0.04	-0.12	-0.06	0.06	-0.03	-0.08	0.06	0.27	0.25	-0.80
Component Score Coefficients (Eigenvectors)												
Variable	PC 1	PC 2	PC 3	PC 4	PC 5	PC 6	PC 7	PC 8	PC 9	PC 10	PC 11	PC 12
cwclose	-0.06	-0.08	-0.02	-0.25	-0.08	0.12	0.89	-0.02	-0.18	0.10	0.26	0.08
cwopen	0.02	0.50	-0.65	-0.06	-0.23	0.27	-0.15	0.18	0.01	0.07	0.28	0.26
cwdown	-0.02	-0.01	0.08	-0.21	-0.06	-0.12	-0.14	-0.08	0.30	-0.02	0.70	-0.57
cwup	0.02	0.06	-0.13	-0.22	-0.16	-0.20	-0.10	-0.55	-0.46	-0.58	0.04	0.04
camclose	-0.21	0.69	0.38	-0.01	0.36	-0.32	0.05	-0.11	-0.05	0.15	0.13	0.21
camopen	0.55	0.15	0.48	-0.30	-0.04	0.56	-0.12	-0.04	-0.03	-0.06	0.04	0.11
camdown	-0.07	-0.09	0.38	0.40	-0.59	-0.16	-0.06	0.25	-0.14	-0.10	0.33	0.33
camup	0.31	-0.25	-0.13	0.08	0.52	-0.17	0.03	0.17	0.22	-0.37	0.34	0.44
cbeclose	0.10	0.15	-0.04	0.73	0.07	0.33	0.20	-0.47	0.15	-0.09	0.09	-0.14
cbeopen	-0.02	-0.31	-0.06	0.09	0.27	0.13	-0.28	-0.19	-0.55	0.52	0.33	0.09
cbedown	0.62	0.02	-0.12	-0.01	-0.25	-0.49	0.07	-0.28	0.16	0.42	-0.08	0.09
cbeup	-0.39	-0.22	0.06	-0.22	-0.13	0.15	-0.11	-0.47	0.49	0.13	0.02	0.46

Table A5.15b
Principal Component Results for two channels combination [Subject 2]

Descriptive Statistics												
Variable	cwclose	cwopen	cwdown	cwup	camclose	camopen	camdown	camup	cbeclose	cbeopen	cbedown	cbeup
Mean	1170.71	2078.87	721.08	1036.76	3352.07	2927.92	2938.64	3440.69	2539.98	2788.81	2434	2602.11
Std Dev.	235.88	401.46	266.72	319.84	867.25	1807.3	1422.53	968.15	845.12	1641.66	1587.51	1638.6
Std Err	74.59	126.95	84.35	101.14	274.25	571.52	449.84	306.16	267.25	519.14	502.01	518.17
N	10	10	10	10	10	10	10	10	10	10	10	10
Covariance Matrix												
	cwclose	cwopen	cwdown	cwup	camclose	camopen	camdown	camup	cbeclose	cbeopen	cbedown	cbeup
cwclose	55640.22	12343.42	12911.16	3630.30	100829.28	-77469.44	-6261.39	-68458.29	66941.10	65497.75	-42087.69	53379.98
cwopen	12343.42	161168.04	3713.41	-6474.12	-1187.97	140602.44	72903.28	-74616.06	-44507.47	62316.69	-46653.57	27.04
cwdown	12911.16	3713.41	71141.03	-10124.89	63993.45	-205751.94	111068.91	-155014.26	141187.84	195714.01	-147006.18	114335.89
cwup	3630.30	-6474.12	-10124.89	102295.51	-9946.03	131978.96	-106580.82	102880.90	-53139.71	-218230.83	254973.96	-183036.90
camclose	100829.28	-1187.97	63993.45	-9946.03	752116.12	-109988.75	-59070.95	-322049.90	189362.22	52196.05	211594.07	-168653.78

camopen	-77469.44	140602.44	-205751.94	131978.96	-109988.75	3266318.75	-2279835.26	975122.99	-1374977.83	-2745615.46	2520614.33	-2785630.84
camdown	-6261.39	72903.28	111068.91	-106580.82	-59070.95	-2279835.26	2023601.73	-858685.70	882127.24	2206478.40	-1997036.35	2089509.28
camup	-68458.29	-74616.06	-155014.26	102880.90	-322049.90	975122.99	-858685.70	937320.48	-558947.68	-1080321.46	973923.03	-739383.22
cbeclose	66941.10	-44507.47	141187.84	-53139.71	189362.22	-1374977.83	882127.24	-558947.68	714227.57	1139806.50	-1043919.69	1105297.48
cbeopen	65497.75	62316.69	195714.01	-218230.83	52196.05	-2745615.46	2206478.40	-1080321.46	1139806.50	2695049.81	-2453795.46	2500561.98
cbedown	-42087.69	-46653.57	-147006.18	254973.96	211594.07	2520614.33	-1997036.35	973923.03	-1043919.69	-2453795.46	2520180.76	-2473561.15
cbeup	53379.98	27.04	114335.89	-183036.90	-168653.78	-2785630.84	2089509.28	-739383.22	1105297.48	2500561.98	-2473561.15	2685012.46
Explained Variance (Eigenvalues)												
Value	PC 1	PC 2	PC 3	PC 4	PC 5	PC 6	PC 7	PC 8	PC 9	PC 10	PC 11	PC 12
Eigenvalue	13253346.22	1199761.04	668812.85	337356.74	243501.34	125251.42	91514.64	45813.09	18715.14	0.00	0.00	0.00
% of Var.	82.92	7.51	4.18	2.11	1.52	0.78	0.57	0.29	0.12	0.00	0.00	0.00
Cum. %	82.92	90.42	94.61	96.72	98.24	99.02	99.60	99.88	100.00	100.00	100.00	100.00
Component Loadings												
(correlations between initial variables and principal components)												
Variable	PC 1	PC 2	PC 3	PC 4	PC 5	PC 6	PC 7	PC 8	PC 9	PC 10	PC 11	PC 12
cwclose	-0.15	-0.47	-0.16	-0.30	0.32	0.38	0.04	0.61	-0.16	-0.04	-0.40	0.31
cwopen	-0.01	-0.03	0.67	0.26	0.41	0.55	0.10	-0.06	0.08	-0.30	-0.12	-0.19
cwdown	-0.41	-0.47	0.04	-0.25	-0.32	0.19	0.54	-0.15	0.31	0.26	-0.30	0.34
cwup	0.36	0.00	-0.36	0.44	-0.45	0.52	-0.13	0.24	0.06	0.26	0.33	0.28
camclose	0.00	-0.92	-0.22	0.09	0.29	-0.05	-0.06	-0.03	0.02	0.07	0.04	0.10
camopen	0.97	0.04	0.25	-0.01	0.07	0.02	0.00	-0.02	-0.02	0.10	0.20	-0.45
camdown	-0.95	0.03	0.12	0.29	-0.06	-0.01	-0.05	-0.03	-0.01	-0.23	-0.09	0.25
camup	0.65	0.59	-0.43	0.11	0.19	0.00	0.08	-0.04	-0.01	0.10	-0.06	0.04
cbeclose	-0.86	-0.31	-0.22	-0.19	-0.14	0.19	0.03	-0.12	-0.09	-0.22	-0.11	0.27
cbeopen	-0.98	-0.05	0.09	0.05	0.05	-0.04	0.12	0.03	-0.02	-0.21	-0.32	0.31
cbedown	0.96	-0.12	-0.16	0.17	-0.04	0.02	0.04	0.01	-0.01	0.25	0.21	-0.18
cbeup	-0.97	0.18	-0.09	-0.03	0.11	0.05	-0.05	0.00	0.01	-0.24	-0.24	0.34
Component Score Coefficients (Eigenvectors)												
Variable	PC 1	PC 2	PC 3	PC 4	PC 5	PC 6	PC 7	PC 8	PC 9	PC 10	PC 11	PC 12
cwclose	-0.01	-0.10	-0.05	-0.12	0.15	0.25	0.03	0.67	-0.28	0.00	0.58	-0.14
cwopen	0.00	-0.01	0.33	0.18	0.33	0.62	0.13	-0.10	0.22	-0.50	-0.04	0.18
cwdown	-0.03	-0.11	0.01	-0.12	-0.17	0.14	0.47	-0.18	0.60	0.36	0.37	-0.17
cwup	0.03	0.00	-0.14	0.24	-0.29	0.47	-0.14	0.35	0.14	0.23	-0.51	-0.38
camclose	0.00	-0.73	-0.23	0.13	0.51	-0.12	-0.17	-0.11	0.11	0.06	-0.07	-0.23
camopen	0.48	0.07	0.54	-0.02	0.27	0.11	-0.02	-0.17	-0.29	0.50	-0.03	-0.15
camdown	-0.37	0.04	0.21	0.71	-0.17	-0.04	-0.23	-0.21	-0.12	0.06	0.37	-0.18
camup	0.17	0.52	-0.51	0.19	0.37	0.01	0.26	-0.19	-0.09	-0.10	0.06	-0.39

cbeclose	-0.20	-0.24	-0.22	-0.28	-0.24	0.44	0.10	-0.47	-0.53	0.01	0.01	-0.06
cbeopen	-0.44	-0.08	0.19	0.15	0.17	-0.17	0.67	0.21	-0.25	0.12	-0.33	0.01
cbedown	0.42	-0.18	-0.32	0.46	-0.13	0.08	0.23	0.04	-0.12	0.18	0.07	0.59
cbeup	-0.44	0.27	-0.19	-0.10	0.38	0.22	-0.28	-0.01	0.11	0.49	-0.01	0.40

Table A5.15c
Principal Component Results for two channels combination [Subject 3]

Descriptive Statistics												
Variable	cwclose	cwopen	cwdown	cwup	camclose	camopen	camdown	camup	cbeclose	cbeopen	cbedown	cbeup
Mean	1382.54	3491.73	1755.65	2080.14	2147.14	2951.73	2801.98	3092.58	1417.67	1627.39	1813.82	1997.31
Std Dev.	726.73	1496.26	395.72	1535.56	807.53	298.51	1528.48	895.69	530.18	753.31	1256.8	1027.18
Std Err	229.81	473.16	125.14	485.59	255.36	94.4	483.35	283.24	167.66	238.22	397.44	324.82
N	10	10	10	10	10	10	10	10	10	10	10	10
Covariance Matrix												
	cwclose	cwopen	cwdown	cwup	camclose	camopen	camdown	camup	cbeclose	cbeopen	cbedown	cbeup
cwclose	528131.73	914658.02	36565.24	1001670.82	-390915.37	63365.47	-842367.50	481867.63	288526.04	383695.26	782476.43	-585608.41
cwopen	914658.02	2238798.46	80988.85	2129190.46	-793459.37	217059.17	-2064824.86	1139067.80	631590.75	862488.58	1656927.82	-1421301.58
cwdown	36565.24	80988.85	156595.81	85967.01	-29384.00	-12310.87	-156371.27	198915.08	41675.36	184599.52	142939.63	-67255.08
cwup	1001670.82	2129190.46	85967.01	2357953.11	-876506.81	181391.61	-1956770.92	1184033.60	728922.91	852664.26	1633633.36	-1305360.71
camclose	-390915.37	-793459.37	-29384.00	-876506.81	652102.42	-60865.15	852132.47	-483720.74	-360382.83	-352608.85	-490940.85	517628.11
camopen	63365.47	217059.17	-12310.87	181391.61	-60865.15	89106.76	-242538.22	101101.55	77975.75	96142.69	72076.03	-57168.52
camdown	-842367.50	-2064824.86	-156371.27	-1956770.92	852132.47	-242538.22	2336238.83	-1117613.54	-643288.05	-863941.88	-1643215.90	1344513.16
camup	481867.63	1139067.80	198915.08	1184033.60	-483720.74	101101.55	-1117613.54	802259.55	407580.49	602912.41	861020.30	-682583.36
cbeclose	288526.04	631590.75	41675.36	728922.91	-360382.83	77975.75	-643288.05	407580.49	281094.82	278491.40	420862.60	-353700.77
cbeopen	383695.26	862488.58	184599.52	852664.26	-352608.85	96142.69	-863941.88	602912.41	278491.40	567474.93	643647.64	-514594.94
cbedown	782476.43	1656927.82	142939.63	1633633.36	-490940.85	72076.03	-1643215.90	861020.30	420862.60	643647.64	1579546.84	-1196192.31
cbeup	-585608.41	-1421301.58	-67255.08	-1305360.71	517628.11	-57168.52	1344513.16	-682583.36	-353700.77	-514594.94	-1196192.31	1055097.63

Explained Variance (Eigenvalues)												
Value	PC 1	PC 2	PC 3	PC 4	PC 5	PC 6	PC 7	PC 8	PC 9	PC 10	PC 11	PC 12
Eigenvalue	10568425.45	615462.53	468594.22	406679.95	244406.65	184152.36	110236.81	37855.96	8586.97	0.00	0.00	0.00
% of Var.	83.58	4.87	3.71	3.22	1.93	1.46	0.87	0.30	0.07	0.00	0.00	0.00
Cum. %	83.58	88.45	92.16	95.37	97.30	98.76	99.63	99.93	100.00	100.00	100.00	100.00
Component Loadings		(correlations between initial variables and principal components)										
Variable	PC 1	PC 2	PC 3	PC 4	PC 5	PC 6	PC 7	PC 8	PC 9	PC 10	PC 11	PC 12
cwclose	0.89	0.00	0.24	0.14	0.12	0.17	0.29	-0.10	0.00	0.08	0.25	-0.03

cwopen	0.98	0.05	0.05	-0.03	-0.13	-0.16	0.02	-0.04	-0.01	-0.02	0.44	-0.21
cwdown	0.25	-0.12	-0.73	0.55	0.27	0.05	-0.12	-0.01	0.02	0.02	0.00	-0.07
cwup	0.95	-0.12	0.22	0.11	-0.06	0.07	-0.05	0.06	-0.01	-0.15	0.21	-0.18
camclose	-0.72	0.50	-0.10	0.29	-0.36	0.06	-0.04	0.02	0.01	0.10	-0.27	0.22
camopen	0.42	-0.29	-0.18	-0.29	-0.73	0.07	0.25	-0.08	0.12	-0.08	0.23	-0.16
camdown	-0.94	-0.02	0.22	0.23	0.04	-0.11	0.01	-0.01	0.01	0.20	-0.24	0.22
camup	0.89	-0.24	-0.21	0.26	0.00	-0.05	-0.13	-0.10	-0.02	-0.06	0.28	-0.19
cbeclose	0.85	-0.46	0.09	-0.04	-0.02	0.11	-0.15	-0.04	0.14	-0.13	0.21	-0.34
cbeopen	0.81	-0.23	-0.36	0.30	-0.01	-0.12	0.22	0.12	0.01	-0.01	0.35	-0.17
cbedown	0.92	0.35	-0.01	0.11	0.10	0.11	-0.01	-0.02	0.01	-0.01	0.24	-0.14
cbeup	-0.92	-0.27	-0.03	0.08	-0.16	0.20	0.04	-0.05	-0.03	-0.02	-0.46	0.27
Component Score Coefficients (Eigenvectors)												
Variable	PC 1	PC 2	PC 3	PC 4	PC 5	PC 6	PC 7	PC 8	PC 9	PC 10	PC 11	PC 12
cwclose	0.20	0.00	0.26	0.16	0.17	0.28	0.64	-0.38	0.00	0.24	-0.01	-0.39
cwopen	0.45	0.09	0.12	-0.08	-0.38	-0.54	0.10	-0.31	-0.13	0.30	0.02	0.34
cwdown	0.03	-0.06	-0.42	0.34	0.21	0.05	-0.14	-0.03	0.06	0.49	0.61	0.09
cwup	0.45	-0.23	0.50	0.26	-0.19	0.24	-0.24	0.45	-0.17	0.00	0.19	-0.07
camclose	-0.18	0.52	-0.12	0.37	-0.60	0.12	-0.09	0.07	0.10	0.20	-0.18	-0.30
camopen	0.04	-0.11	-0.08	-0.14	-0.44	0.05	0.22	-0.12	0.39	-0.48	0.56	-0.07
camdown	-0.44	-0.03	0.48	0.55	0.13	-0.39	0.03	-0.11	0.18	-0.14	0.10	0.16
camup	0.25	-0.28	-0.27	0.37	0.00	-0.11	-0.36	-0.47	-0.19	-0.35	-0.18	-0.32
cbeclose	0.14	-0.31	0.07	-0.03	-0.02	0.14	-0.23	-0.12	0.77	0.26	-0.34	0.10
cbeopen	0.19	-0.22	-0.39	0.36	-0.01	-0.21	0.50	0.47	0.10	-0.12	-0.27	0.13
cbedown	0.36	0.56	-0.01	0.21	0.25	0.31	-0.03	-0.13	0.13	-0.34	-0.03	0.46
cbeup	-0.29	-0.35	-0.05	0.13	-0.34	0.47	0.12	-0.24	-0.30	0.05	-0.11	0.51

Table A5.16a
Principal Component Results for three channel combination [Subject 1]

Descriptive Statistics								
Variable	cambetclose	cambetopen	cambetdown	cambetup	cambebclose	cambebopen	cambebdown	cambebup
Mean	3399.74	2392.26	2788.06	3148.79	3576.65	2358.76	3881.65	2453.99
Std Dev.	848.6	1540.43	1496.07	834.92	848.28	1552	517.4	1116.98
Std Err	219.11	397.74	386.28	215.58	219.03	400.72	133.59	288.4
N	15	15	15	15	15	15	15	15
Covariance Matrix								
	cambetclose	cambetopen	cambetdown	cambetup	cambebclose	cambebopen	cambebdown	cambebup
cambetclose	720122.11	-392473.20	325780.04	-517337.58	594362.47	-363629.36	63243.06	-339042.21
cambetopen	-392473.20	2372939.96	895782.51	671170.15	-512824.46	2380783.34	-344638.45	1429439.26
cambetdown	325780.04	895782.51	2238211.29	-506444.35	-31036.82	975689.22	-51303.52	945471.43
cambetup	-517337.58	671170.15	-506444.35	697097.79	-443122.23	638929.56	-143519.68	449795.99
cambebclose	594362.47	-512824.46	-31036.82	-443122.23	719581.47	-516305.17	83436.01	-514798.37
cambebopen	-363629.36	2380783.34	975689.22	638929.56	-516305.17	2408707.81	-326254.94	1453821.41
cambebdown	63243.06	-344638.45	-51303.52	-143519.68	83436.01	-326254.94	267698.70	-323876.13
cambebup	-339042.21	1429439.26	945471.43	449795.99	-514798.37	1453821.41	-323876.13	1247647.87
Explained Variance (Eigenvalues)								
Value	PC 1	PC 2	PC 3	PC 4	PC 5	PC 6	PC 7	PC 8
Eigenvalue	6696375.17	2519207.56	912712.45	314901.28	119243.21	95045.32	13552.48	969.54
% of Var.	62.75	23.61	8.55	2.95	1.12	0.89	0.13	0.01
Cum. %	62.75	86.35	94.91	97.86	98.97	99.86	99.99	100.00
Component Loadings		(correlations between initial variables and principal components)						
Variable	PC 1	PC 2	PC 3	PC 4	PC 5	PC 6	PC 7	PC 8
cambetclose	-0.34	0.71	0.54	-0.15	0.10	-0.26	0.01	0.00
cambetopen	0.97	-0.10	0.20	0.06	-0.04	0.01	0.04	-0.01
cambetdown	0.53	0.81	-0.24	0.03	0.02	0.03	0.02	0.01
cambetup	0.48	-0.83	-0.04	-0.11	0.25	0.01	0.07	0.02
cambebclose	-0.49	0.48	0.67	-0.11	0.09	0.25	-0.01	0.00
cambebopen	0.98	-0.06	0.19	0.08	-0.02	-0.02	-0.04	0.01
cambebdown	-0.45	0.15	-0.07	0.78	0.40	-0.02	-0.05	-0.02
cambebup	0.93	0.03	-0.22	-0.27	0.11	0.01	-0.05	-0.01
Component Score Coefficients (Eigenvectors)								
Variable	PC 1	PC 2	PC 3	PC 4	PC 5	PC 6	PC 7	PC 8
cambetclose	-0.11	0.38	0.48	-0.23	0.24	-0.70	0.10	-0.03
cambetopen	0.58	-0.09	0.33	0.17	-0.16	0.06	0.47	-0.52

cambetdown	0.31	0.76	-0.38	0.08	0.08	0.13	0.29	0.24
cambetup	0.15	-0.44	-0.04	-0.17	0.61	0.02	0.47	0.41
cambebclose	-0.16	0.26	0.59	-0.17	0.23	0.68	-0.08	0.03
cambebopen	0.58	-0.06	0.31	0.22	-0.09	-0.10	-0.47	0.52
cambebdown	-0.09	0.05	-0.04	0.72	0.60	-0.04	-0.21	-0.27
cambebup	0.40	0.02	-0.26	-0.54	0.35	0.03	-0.44	-0.40

Table A5.16b
Principal Component Results for three channel combination [Subject 2]

Descriptive Statistics								
Variable	cambetclose	cambetopen	cambetdown	cambetup	cambebclose	cambebopen	cambebdown	cambebup
Mean	3304.53	3389.32	2280.59	3664.17	2858.22	2373.78	3260.27	2658.16
Std Dev.	764.71	1618.62	1498.41	881.99	1024.06	1663.99	1258.48	1394.99
Std Err	197.45	417.93	386.89	227.73	264.41	429.64	324.94	360.18
N	15	15	15	15	15	15	15	15
Covariance Matrix								
	cambetclose	cambetopen	cambetdown	cambetup	cambebclose	cambebopen	cambebdown	cambebup
cambetclose	584787.99	-114086.34	27280.83	-266268.32	562917.36	-439.43	-51337.24	-83008.88
cambetopen	-114086.34	2619939.82	-2094994.17	800747.66	-585849.40	1548571.45	-1134737.09	-162373.45
cambetdown	27280.83	-2094994.17	2245222.50	-890972.98	662650.11	-689475.82	872291.36	547556.06
cambetup	-266268.32	800747.66	-890972.98	777914.04	-447939.05	372379.35	-426387.07	229019.83
cambebclose	562917.36	-585849.40	662650.11	-447939.05	1048698.95	516391.79	-344935.95	646510.47
cambebopen	-439.43	1548571.45	-689475.82	372379.35	516391.79	2768866.26	-1847248.63	1568728.73
cambebdown	-51337.24	-1134737.09	872291.36	-426387.07	-344935.95	-1847248.63	1583770.35	-1073700.74
cambebup	-83008.88	-162373.45	547556.06	229019.83	646510.47	1568728.73	-1073700.74	1945987.39
Explained Variance (Eigenvalues)								
Value	PC 1	PC 2	PC 3	PC 4	PC 5	PC 6	PC 7	PC 8
Eigenvalue	6962179.44	4315737.47	1298476.97	633385.86	246381.77	69049.17	26738.66	23237.95
% of Var.	51.29	31.79	9.57	4.67	1.81	0.51	0.20	0.17
Cum. %	51.29	83.08	92.64	97.31	99.12	99.63	99.83	100.00
Component Loadings								
(correlations between initial variables and principal components)								
Variable	PC 1	PC 2	PC 3	PC 4	PC 5	PC 6	PC 7	PC 8

cambetclose	-0.07	0.19	-0.88	0.30	0.24	0.13	-0.07	-0.09
cambetopen	0.87	-0.43	-0.09	-0.18	0.12	0.03	0.05	0.00
cambetdown	-0.72	0.64	0.11	-0.23	0.06	-0.01	0.04	-0.05
cambetup	0.60	-0.34	0.51	0.44	0.22	-0.15	0.01	-0.07
cambebclose	-0.06	0.77	-0.59	0.17	0.07	-0.12	0.06	0.05
cambebopen	0.86	0.47	-0.04	-0.20	0.01	-0.05	-0.05	0.00
cambebdown	-0.88	-0.35	0.06	-0.16	0.26	-0.02	-0.04	0.05
cambebup	0.38	0.84	0.33	0.15	0.10	0.09	0.01	0.03
Component Score Coefficients (Eigenvectors)								
Variable	PC 1	PC 2	PC 3	PC 4	PC 5	PC 6	PC 7	PC 8
cambetclose	-0.02	0.07	-0.59	0.29	0.36	0.37	-0.32	-0.43
cambetopen	0.53	-0.34	-0.13	-0.36	0.39	0.20	0.51	-0.02
cambetdown	-0.41	0.46	0.14	-0.43	0.17	-0.04	0.33	-0.53
cambetup	0.20	-0.14	0.40	0.49	0.38	-0.50	0.04	-0.39
cambebclose	-0.02	0.38	-0.53	0.22	0.14	-0.47	0.40	0.35
cambebopen	0.54	0.38	-0.05	-0.42	0.03	-0.33	-0.53	-0.05
cambebdown	-0.42	-0.22	0.07	-0.25	0.66	-0.12	-0.31	0.40
cambebup	0.20	0.56	0.40	0.26	0.29	0.47	0.06	0.32

Table A5.16c
Principal Component Results for three channel combination [Subject 3]

Descriptive Statistics								
Variable	cambetclose	cambetopen	cambetdown	cambetup	cambebclose	cambebopen	cambebdown	cambebup
Mean	1773.32	2318.89	2092.52	3030.09	2034.64	2701.67	2852.67	2424.89
Std Dev.	858.23	969.81	1606.84	772.12	706.67	543.62	1262.01	1220.09
Std Err	221.59	250.4	414.88	199.36	182.46	140.36	325.85	315.03
N	15	15	15	15	15	15	15	15
Covariance Matrix								
	cambetclose	cambetopen	cambetdown	cambetup	cambebclose	cambebopen	cambebdown	cambebup
cambetclose	736550.40	470645.02	1113447.42	-256562.31	510148.04	119405.56	521689.91	228137.02
cambetopen	470645.02	940537.24	807262.67	191454.60	143270.26	401959.42	-260203.56	987058.42
cambetdown	1113447.42	807262.67	2581923.92	-622506.41	716504.52	230702.07	1419726.01	296771.32
cambetup	-256562.31	191454.60	-622506.41	596167.46	-243670.26	108235.08	-779103.96	629600.37

cambebclose	510148.04	143270.26	716504.52	-243670.26	499375.58	36571.04	489540.75	-127559.79
cambebopen	119405.56	401959.42	230702.07	108235.08	36571.04	295523.98	-238025.76	422548.35
cambebdown	521689.91	-260203.56	1419726.01	-779103.96	489540.75	-238025.76	1592669.63	-821567.29
cambebup	228137.02	987058.42	296771.32	629600.37	-127559.79	422548.35	-821567.29	1488613.40
Explained Variance (Eigenvalues)								
Value	PC 1	PC 2	PC 3	PC 4	PC 5	PC 6	PC 7	PC 8
Eigenvalue	4661032.47	3198397.97	424597.70	248820.93	118639.17	40702.33	33742.11	5428.94
% of Var.	53.38	36.63	4.86	2.85	1.36	0.47	0.39	0.06
Cum. %	53.38	90.01	94.88	97.73	99.09	99.55	99.94	100.00
Component Loadings								
(correlations between initial variables and principal components)								
Variable	PC 1	PC 2	PC 3	PC 4	PC 5	PC 6	PC 7	PC 8
cambetclose	0.84	0.30	0.41	-0.10	0.16	0.07	0.03	0.05
cambetopen	0.34	0.91	0.03	0.16	0.06	-0.11	0.10	-0.01
cambetdown	0.97	0.21	-0.13	0.01	-0.04	-0.03	-0.05	0.01
cambetup	-0.66	0.60	-0.05	-0.38	-0.23	-0.07	0.05	0.04
cambebclose	0.74	-0.04	0.63	-0.14	-0.18	-0.03	-0.05	-0.05
cambebopen	0.11	0.74	0.08	0.50	-0.37	0.19	0.06	0.02
cambebdown	0.83	-0.52	-0.15	-0.11	-0.03	0.04	0.08	-0.01
cambebup	-0.07	0.98	-0.11	-0.13	0.05	0.07	-0.02	-0.02
Component Score Coefficients (Eigenvectors)								
Variable	PC 1	PC 2	PC 3	PC 4	PC 5	PC 6	PC 7	PC 8
cambetclose	0.33	0.15	0.54	-0.18	0.40	0.29	0.16	0.53
cambetopen	0.15	0.49	0.05	0.31	0.17	-0.52	0.55	-0.19
cambetdown	0.72	0.19	-0.32	0.05	-0.17	-0.23	-0.46	0.23
cambetup	-0.24	0.26	-0.05	-0.58	-0.52	-0.25	0.23	0.39
cambebclose	0.24	-0.01	0.68	-0.19	-0.37	-0.12	-0.18	-0.50
cambebopen	0.03	0.23	0.07	0.55	-0.58	0.50	0.17	0.15
cambebdown	0.48	-0.37	-0.29	-0.29	-0.10	0.26	0.57	-0.24
cambebup	-0.04	0.67	-0.21	-0.33	0.17	0.45	-0.15	-0.38

Table A5.17a
Principal Component Results for four channel combination [Subject 1]

Descriptive Statistics				
Variable	Mean	Std Dev.	Std Err	N
close	3468.45	787.93	176.19	20.00
open	2109.92	1419.72	317.46	20.00
down	3125.14	1429.35	319.61	20.00
up	2710.23	1074.35	240.23	20.00
Covariance Matrix				
	close	open	down	up
close	620829.69	-324850.27	319682.76	-495815.17
open	-324850.27	2015599.01	349274.79	888954.74
down	319682.76	349274.79	2043043.35	-860571.65
up	-495815.17	888954.74	-860571.65	1154223.97
Explained Variance (Eigenvalues)				
Value	PC 1	PC 2	PC 3	PC 4
Eigenvalue	2878767.93	2378847.01	453757.49	122323.59
% of Var.	49.35	40.78	7.78	2.10
Cum. %	49.35	90.12	97.90	100.00
Component Loadings				
Variable	PC 1	PC 2	PC 3	PC 4
close	-0.61	0.00	0.78	0.13
open	0.63	0.76	0.14	-0.10
down	-0.61	0.77	-0.13	0.09
up	0.97	0.01	-0.04	0.26
Component Score Coefficients (Eigenvectors)				
Variable	PC 1	PC 2	PC 3	PC 4
close	-0.28	0.00	0.91	0.29
open	0.53	0.70	0.29	-0.39
down	-0.52	0.72	-0.28	0.38
up	0.61	0.00	-0.06	0.79

Table A5.17b
Principal Component Results for four channel combination [Subject 2]

Descriptive Statistics				
Variable	Mean	Std Dev.	Std Err	N
close	2946.03	931.74	208.34	20.00
open	2858.37	1681.93	376.09	20.00
down	2686.32	1489.74	333.12	20.00
up	3021.40	1378.73	308.29	20.00
Covariance Matrix				
	close	open	down	up
close	868133.90	517537.32	-414623.35	550223.23
open	517537.32	2828898.68	-2223772.26	1677075.75
down	-414623.35	-2223772.26	2219334.65	-1467068.90
up	550223.23	1677075.75	-1467068.90	1900898.99
Explained Variance (Eigenvalues)				
Value	PC 1	PC 2	PC 3	PC 4
Eigenvalue	6120611.50	874394.29	544848.97	277411.45
% of Var.	78.30	11.19	6.97	3.55
Cum. %	78.30	89.48	96.45	100.00
Component Loadings				
Variable	PC 1	PC 2	PC 3	PC 4
close	0.42	0.75	0.51	-0.04
open	0.96	-0.16	0.11	0.20
down	-0.94	0.19	-0.06	0.27
up	0.86	0.35	-0.38	0.01
Component Score Coefficients (Eigenvectors)				
Variable	PC 1	PC 2	PC 3	PC 4
close	0.16	0.75	0.64	-0.07
open	0.65	-0.30	0.26	0.65
down	-0.57	0.30	-0.12	0.76
up	0.48	0.51	-0.71	0.04

Table A5.17c
Principal Component Results for four channel combination [Subject 3]

Descriptive Statistics				
Variable	Mean	Std Dev.	Std Err	N
close	1782.40	762.94	170.60	20.00
open	2289.56	878.95	196.54	20.00
down	2307.90	1453.21	324.95	20.00
up	2544.94	1093.38	244.49	20.00
Covariance Matrix				
	close	open	down	up
close	582071.72	357312.71	792689.89	-186420.70
open	357312.71	772561.61	534386.07	185849.09
down	792689.89	534386.07	2111811.54	-811195.53
up	-186420.70	185849.09	-811195.53	1195489.45
Explained Variance (Eigenvalues)				
Value	PC 1	PC 2	PC 3	PC 4
Eigenvalue	2965294.91	1201516.73	287996.66	207126.01
% of Var.	63.61	25.77	6.18	4.44
Cum. %	63.61	89.38	95.56	100.00
Component Loadings				
Variable	PC 1	PC 2	PC 3	PC 4
close	0.76	0.35	-0.02	0.54
open	0.44	0.78	0.44	-0.12
down	0.98	0.06	-0.16	-0.11
up	-0.62	0.74	-0.27	-0.03
Component Score Coefficients (Eigenvectors)				
Variable	PC 1	PC 2	PC 3	PC 4
close	0.34	0.24	-0.03	0.91
open	0.22	0.62	0.71	-0.23
down	0.83	0.08	-0.44	-0.34
up	-0.39	0.74	-0.54	-0.07

Table A5.18
Two channel analogy slope value

cw	cam	cbe
1348.8	2467.6	2825.1
1300.5	4327.5	2420.9
970.3	4382.8	3620.8
1201.8	4321.5	3363.1
1502.7	4870	3489.3
934.4	2657.1	2534.1
1265.2	3476.2	3930.1
1140	1977.7	2957.1
1499.1	4467	3693.5
1116.8	3784.8	2932.4
622.2	2255.7	1218.9
1007.4	1760.1	1317.5
527.2	2700.9	682.3
543.1	3537.1	945.0
1198.4	2959.3	964.6
779.9	3259.4	4375
1768.8	2393.7	3205.1
880.9	4024.6	2957.1
724.5	2182.7	3709.7
820.0	3047.1	4126
1036.1	2452.8	1334.8
1065.6	4651.5	2190
1339.6	3513	2288.8
1519.9	3725.8	1693.1
790.3	2814.8	1845.9
2338	2412.6	1510.3
1729.1	1665.8	1695.9
1824.6	1868.4	1331.7
1503.3	1637.1	2169.5
2532	674.3	2340.9
1099.7	1121.1	2145.1
1931.2	1300.2	1414.1
1793.5	2317.7	1181.3
1745	1065	1062.9
3296.1	1197.5	1013.7
2484.6	1549.4	4286.1
2204.7	1329.6	4171.3
1619	1301	3631.9
2248.8	1143.3	4571.9
1890.9	1257.3	4899.4
2881.7	3241	710.5
1348.9	2522.6	1203.9
2182.5	2440.8	768.9
1848.6	3194.1	1382.5
2402.9	2872.8	1200.2
1691.6	4157.6	1719.7
1627.2	4517.8	1218.8
1807	5033.6	998.3
3352.3	3982.8	1208.1
1835.8	4373.5	1169.6
2163.9	5659.6	1147
1698.9	3988.6	1170.2
1488.8	3300	1332.9
2767.5	4945.4	1580.3

2221.6	4805	1097.1
4619.7	2785.6	1560.4
4605.1	3041.9	1560.4
4721.8	3049.6	2872.9
5010.1	3019.4	2508.9
5296	3349.5	2505.2
834.6	4018.3	822.5
1233.3	3174.5	757.6
944.5	4632.3	555.4
932.3	4698.1	1590.1
721.1	3259.7	552.4
589.8	5069	763.8
1389.7	3657.6	922.8
525.2	3350	871.5
639.4	4522.4	884.1
973.8	4374.9	1379.9
1068.7	3196.2	578.3
2072.1	4015.5	706.2
1443.8	4671.5	758.5
1946.9	3710.7	701.4
1631.8	5156.3	623.4
633.7	3501.4	3731
970.6	3677.3	3825.2
1060	3677.3	4000.2
810.5	3340.6	4668.2
758.5	3563.3	4457.3
531.7	1440.1	3179.7
644.4	1411.5	3898.5
678.1	1943.1	4120.2
656.1	1424.7	3881.2
582.2	2193.1	4438
1563.4	1922.9	3862.4
1786.4	1137.3	2859
2292.6	1307.7	2954.6
2283.6	1681.6	2667.1
1467.2	1220.1	2427.1
1241.4	2926.9	3631.1
1758.8	2292.6	3948.6
1178.4	1619.1	3583.4
1656	2007.7	3167.2
1482.8	1935.1	3064.5
1116	3082.6	4439.1
998.3	2063.8	3673.1
824.0	4581.1	4709.6
931.2	1965.7	4166.7
677.8	2741.6	3567.1
743.6	1995.6	2421.9
660.4	2587.2	3041.6
727.1	2023.5	2379.1
675.3	2480.7	3564.2
904.1	2580.8	3118.8
1548.4	3970.5	1415.5
1696.3	3451.4	2053.3
1675.5	3506.2	1244.1
1959.5	3728.7	1260.7
1192.1	4398.8	999.2
738.5	3302.6	628.6
837.8	3925.4	1307.2

1709.6	3883.2	1292.9
1124.9	4292.8	1377.8
1409.2	4568.1	858.9
3579.9	3153.9	805.1
2817.2	3736.5	1295.3
2281	3771.1	878.9
3783.2	4611.5	1099.2
4629.5	3985	1369

CHAPTER 6

DEVELOPMENTS OF ELECTRONIC PROSTHETIC ELBOW

This chapter includes design of electronics elbow based on the analysis performed in previous chapters. Above-elbow analysis was done and prototype model was realized.

The elbow joint is made up of three bones: the humerus bone of the upper arm and the ulna and radius bones of the forearm. The ulna and the humerus meet at the elbow and form a hinge. This hinge allows the arm to straighten and bend. The large triceps muscle in the back of the arm attaches to the point of the ulna which when contracts, it straightens out the elbow. The biceps muscles in the front of the arm contracts to bend the elbow. There is more than one kind of artificial elbow joint (also called prosthesis). The most common types are like a hinge. Elbow prosthesis has two parts as shown in Fig. 6.1[Online ref.17]. The humeral component replaces the lower end of the humerus in the upper arm. The humeral component has a long stem that anchors it into the hollow center of the humerus. The ulnar component replaces the upper end of the ulna in the lower arm. The ulnar component has a shorter metal stem that anchors it into the hollow center of the ulna.

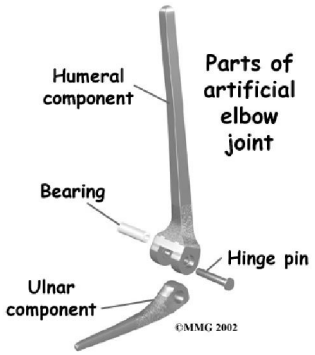

Fig. 6.1 Parts of mechanical artificial elbow [Online ref.17]

The hinge between the two components is made of metal and plastic. The plastic part of the hinge is tough and slick. It allows the two pieces of the new joint to glide easily against each other as elbow moved. The hinge allows the elbow to bend and straighten smoothly. There are two different ways to hold the artificial elbow in place. A cemented prosthesis uses a special type of epoxy cement to glue it to the bone. An

uncemented prosthesis has a fine mesh of holes on the surface. Over time, the bone grows into the mesh, anchoring the prosthesis to the bone. Upper-arm deficient individuals are now widely accepting prosthetic devices employing myoelectric control systems. Prosthetics are quite successfully fitted to below-elbow amputees for controlling a single function i.e. opening and closing a prosthetic hand. The controlling myoelectric signal is derived from the muscles of the residual arm. In an investigation, the use of the orthogonal method for elbow induced wrist force estimation was done while arm motion is restricted to elbow extension and flexion in horizontal plane and under three operating conditions: isometric, isotonic and light load. These results are evaluated with different nonlinear basis functions. The EMG electrodes were attached to the bicep brachii proximal to the elbow, tricep brachii long head, and brachioradialis muscles [Mobasser et al., 2007]. This very work of Mobasser et al. encouraged that electrodes position for proper elbow movement is needed to be investigated at all the muscles group as per the elbow anatomy. It is not at all necessary that elbow movement means that the electrode site should be above elbow.

In this chapter four electrode positions have been selected for discrimination of four movements of elbow and arm. The combination of two best electrode locations has been identified using principal component analysis. The prototype elbow was deigned utilizing SEMG acquition circuit as discussed in chapter 3. The strategies for operation of elbow were developed for single/two channel for two/four movements. The strategies thus developed have been tested on healthy subject. The single channel scheme has been tested on amputee also.

6.1 SEMG signal analysis for elbow movement

In the present research work, SEMG analysis for four elbow/arm movements has been carried out using SEMG parameters like RMS value and slope. To realize microcontroller based artificial elbow RMS value was chosen, as wide ranges of RMS to DC converters are easily available. In above-elbow amputees the multifunctional control of artificial prosthetic device using myoelectric signals is of major importance. A good prosthesis design has to take into account all the problems related with the interaction between human and machines. Microcontroller based artificial elbow was designed to carter the four selected elbow movements. Myoelectric signals were recorded using Ag-AgCl surface electrodes from biceps and triceps branchii, as these

muscle groups are related to the elbow movements of interest i.e. elbow flexion, extension, pronation and supination movements. It has been an endeavor to develop suitable control strategies so as to provide stable and smooth operation.

6.1.1 Single channel approach

Three healthy male subjects of age 27-33 years were selected for SEMG recording. Location selected for the placement of the electrodes was on the upper arm. The point is located at above elbow thumb side as shown in the Fig. 6.2.

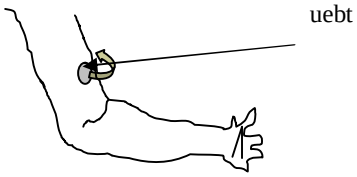

Fig. 6.2 Selected location

The SEMG signal is acquired in similar fashion as discussed in previous chapters for four movements i.e. elbow flexion, extension, pronation and supination movements. Parameters: RMS value (V_{rms}) and slope were calculated as mentioned in chapter 3. Total 87 trials were done from the three subjects at different time in a day. No limit was placed on the voluntary contraction levels. Fig. 6.3 shows the V_{rms} plot of all the repetitions done for the four specified movements. Table 6.1 shows the interpretation of the V_{rms} value for realizing a control methodology. It was observed that V_{rms} for extension mostly attained higher value than that of others. Supination and Pronation could not be well differentiated by the values whereas Flexion was easily distinguished. This analysis suggests that single location acquisition discriminates extension and flexion using threshold approach. Moreover, to discriminate supination and pronation some other suitable location is needed.

Table 6.1
Inter-relation observed for the chosen locations

Movement	Description of SEMG
Extension	V_{rms} value of SEMG is highest
Flexion	V_{rms} value is of moderate range
Supination	Lower values of SEMG
Pronation	Lower values of SEMG

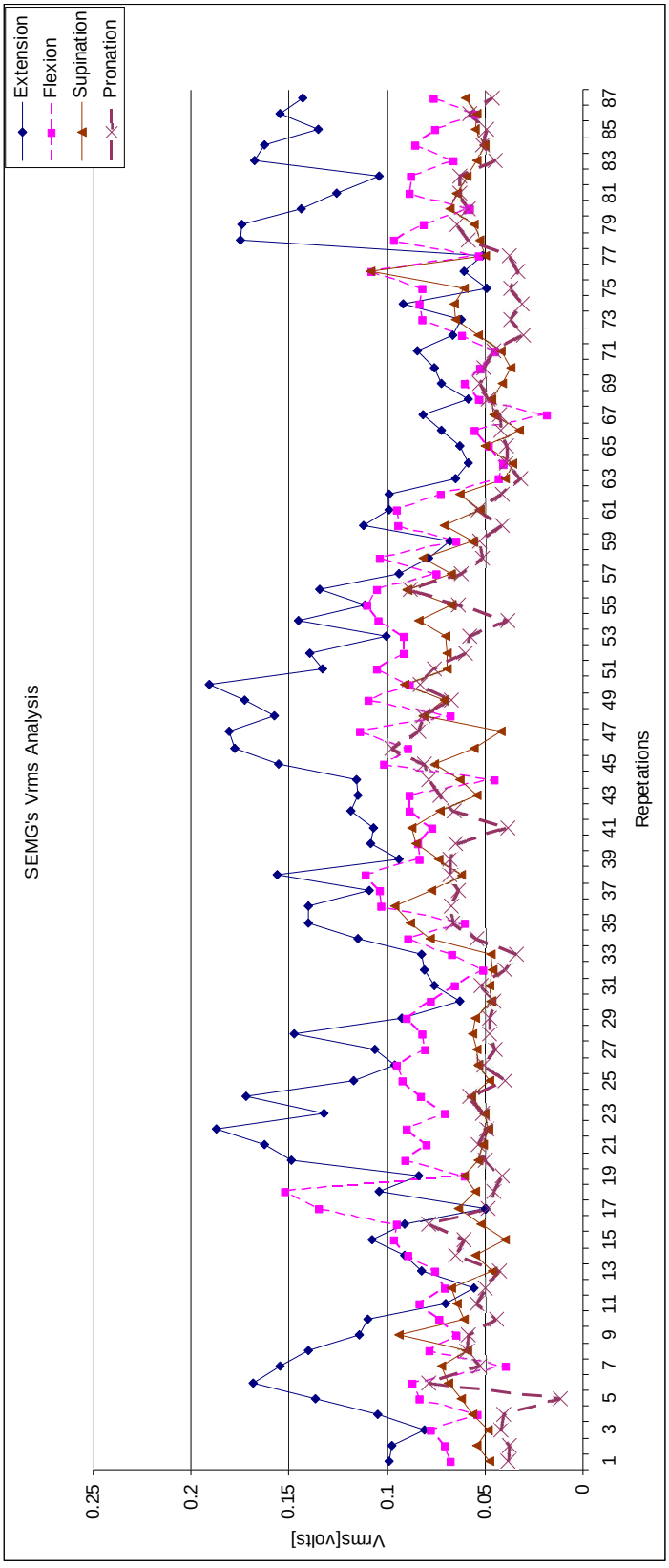

Fig. 6.3 SEMG-V_{rms} Analysis

6.1.2 Two channel approach

In the present study three healthy male subjects in the age group 27-33 years were selected for SEMG recording. The observations were taken as per the methodology explained in section 3.4. Four set of trials were conducted for analysis. They were stored as Trials 1- 4 as: Trial 1 and Trial 2 were from same subject 1, Trial 3 was from subject 2 and Trial 4 was from the subject 3. Each trial was conducted for four times for four chosen movements for a subject. For the SEMG analysis "V_{rms}" and "slope" were used as parameters as discussed in section 3.4. All the recorded SEMG were taken of same duration. The study was carried out to find out the muscles segments; firstly, muscles act to flex at the elbow, secondly muscles act to extend at the elbow, thirdly muscles that act to pronate and finally muscles act to supinate. Anatomy of elbow muscles helped in identifying the muscles groups for the four selected movements. The selected elbow joint movements were:

- Flexion (u): bending at the elbow
- Extension (d): straightening at the elbow
- Pronation (p): moving the arm in a palms down position
- Supination (s): moving the arm in a palms up position

Using the anatomy of active muscles helped in finding the location for the placement of electrodes. Along with these locations, two acupressure points near the elbow joint were also selected for the placement of electrode on left arm as shown in Table 6.2 and Fig. 6.4.

Table 6.2
Selective pressure points on human arm

Description	Figure
Location: On the side of the elbow, on the outer side of the arm. Bend forearm with hand towards neck, the point is located at the end of the crease at the elbow. This is halfway up the side of the arm.	
Location: On the upper arm, one hand width under the armpit. The point is located in the depression between the muscles from the shoulder and the biceps (under the shoulder muscle).	

For SEMG analysis following combinations of 2-chennels (electrode positions)were selected and are shown in Fig. 6.4:

1. Combination I- above the elbow thumb side (uebt) and below the elbow thumb side (bebt)
2. Combination II- "uebt" and below the elbow little finger side (beblf)
3. Combination III- " uebt" and above the elbow little finger side (ueblf)

In the three selected combinations, location "uebt (above the elbow thumb side)" was kept common as posterior side muscles are always in action in all the four chosen movements. This location is very much close to pressure points as mentioned in Table 6.1. Similarly "bebt(below the elbow thumb side)" is closer to the pressure points.

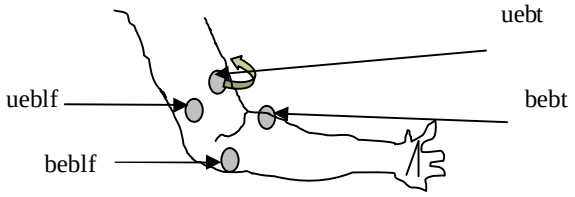

Fig. 6.4 Selective locations near elbow for analysis

Study has been carried out to find the best combination of electrode position from where one can distinguish the four chosen movements and to explore the inter variation/relation of SEMG at all the four chosen locations. Left channel (0) was always kept at "uebt (above the elbow thumb side)" in all the three chosen combinations. Only the right channel (1) was kept varied at different locations and selected as:

- For Combination-I, at "bebt(below the elbow thumb side)".
- For Combination-II, at "beblf(below the elbow little finger side)".
- For Combination-III, at "ueblf (above the elbow little finger side)".

Table A6.1a (appendix) shows V_{rms} values and Table A6.1b(appendix) shows slope values from each channel for extension movement respectively. Fig. 6.5(a) shows the plot of V_{rms} values and Fig. 6.5(b) shows plot of slope values, where combinations were represented by right channel only for proper representation. For extension movement Combination I and II, channel 0 (uebt; above the elbow thumb side; yellow line) has higher V_{rms} and slope values than their channel 1. Combination III was not giving any differentiation. Hence, both Combination I and II can be good locations for the movement extension. On a secondary outlook, comparison of SEMG of all the four location "ueblf" was apparently dominating over "bebt(below the elbow thumb side)" and "beblf(below the elbow little finger side)". Similarly, V_{rms} values

were recorded for flexion movement as shown in Table A6.2a and Table A6.2b (appendix). Fig. 6.6(a) and (b) shows the plots of V_{rms} and slope values of each combination where these values for different combinations do not show a definite pattern, so it was difficult to identify the flexion movement from the chosen combinations.

Again, the V_{rms} and slope values were calculated for pronation movement as shown in Table A6.3a and Table A6.3b (appendix) respectively. Fig. 6.7(a) and (b) shows the plots. In Combination II, the channel 0(uebt; above the elbow thumb side; yellow line) acquires the higher values than its channel 1(beblf; below the elbow little finger side; pink line). In other combinations, V_{rms} and slope values couldn't interpretate this movement. Hence, combination II can be good location for the movement pronation. Comparing all the four, "uebt(above the elbow thumb side)" dominated the others.

Lastly, again both the values were recorded for supination movement as shown in Table A6.4a and Table A6.4b (appendix) respectively. Fig. 6.8 shows the plots. In combination II the channel 1(beblf; below the elbow little finger side; pink line) acquires the higher values than its channel 0 (uebt; above the elbow thumb side; yellow line) which is just opposite result that of other movements as discussed above. V_{rms} and slope values in other channels couldn't interpretate the supination movement. Hence, again combination II can be good location for the movement supination. Table 6.3 gives the outcome of the above investigation, which gives SEMG for elbow movement considering the V_{rms} and slope values from all the locations as shown in Fig. 6.5-6.8.

Table 6.3
Inter-relation observed for the chosen locations

Movement	Description of SEMG
Extension	"ueblf(above the elbow little finger side)" generates stronger SEMG signal than "bebt(below the elbow thumb side)" and "beblf(below the elbow little finger side)". "uebt(above the elbow thumb side)" generates same as of "ueblf(above the elbow little finger side)"
Flexion	All location generate about same SEMG signals
Pronation	"uebt(above the elbow thumb side)" generates stronger than "ueblf(above the elbow little finger side)" and "ueblf(above the elbow little finger side)" generates stronger than "beblf(below the elbow little finger side)"
Supination	"beblf(below the elbow little finger side)" generates much stronger than other three locations

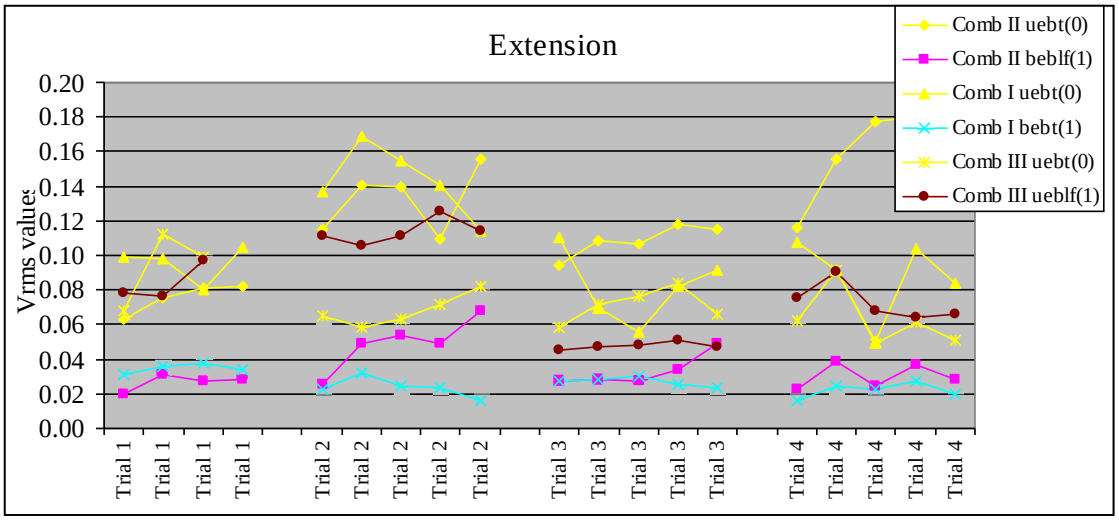

Fig.6.5 (a) Extension plots using V_{rms} values

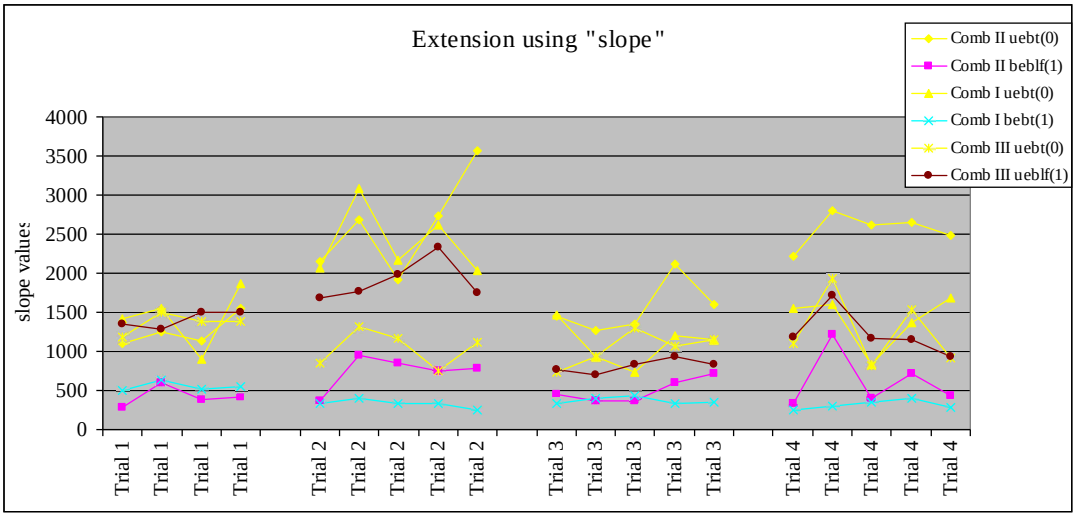

Fig.6.5 (b) Extension plots using slope values

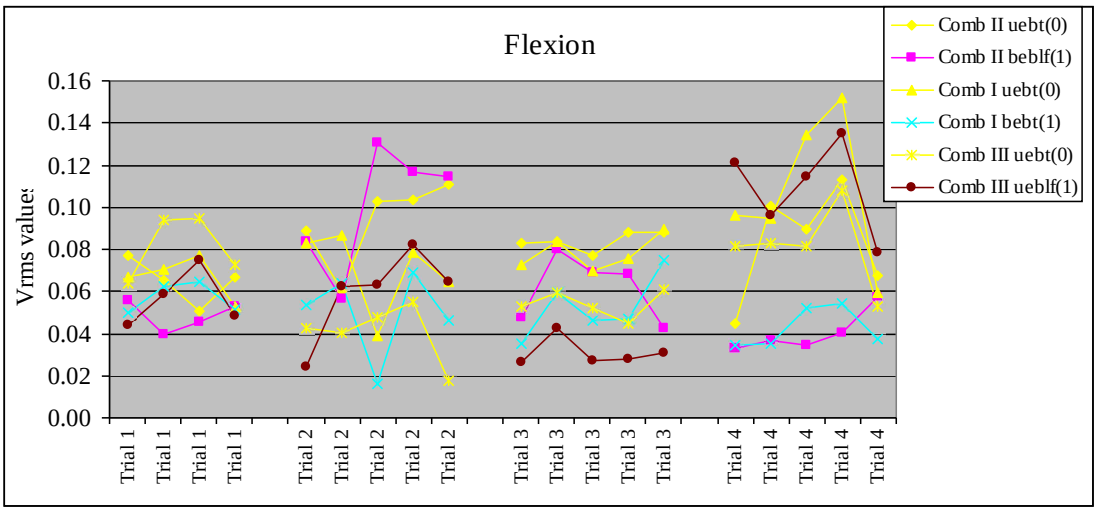

Fig. 6.6(a) Flexion plots using V_{rms} values

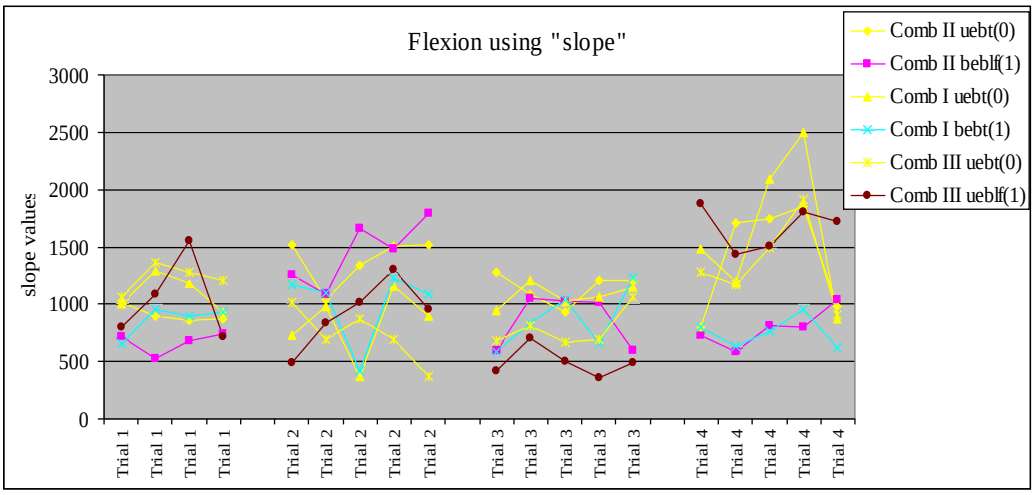

Fig. 6.6(b) Flexion plots using slope values

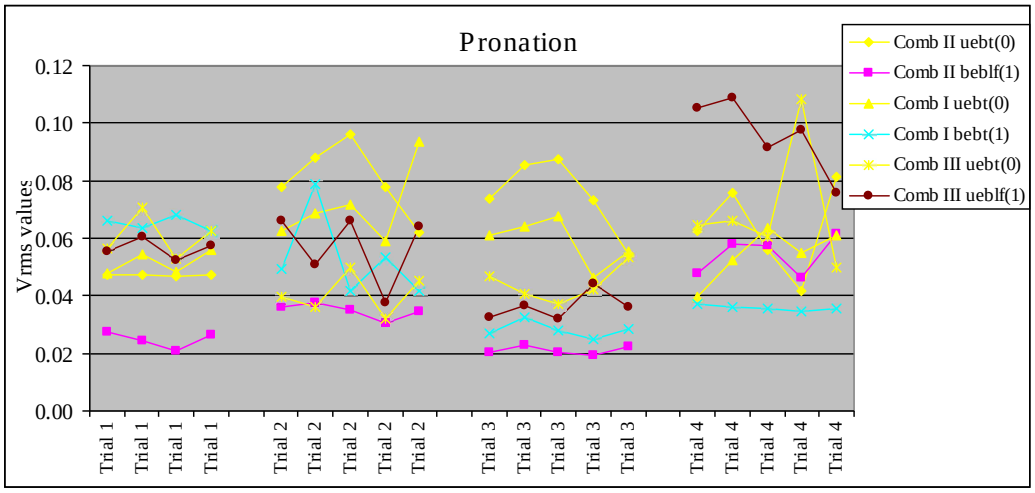

Fig. 6.7(a) Pronation plots using V_{rms} values

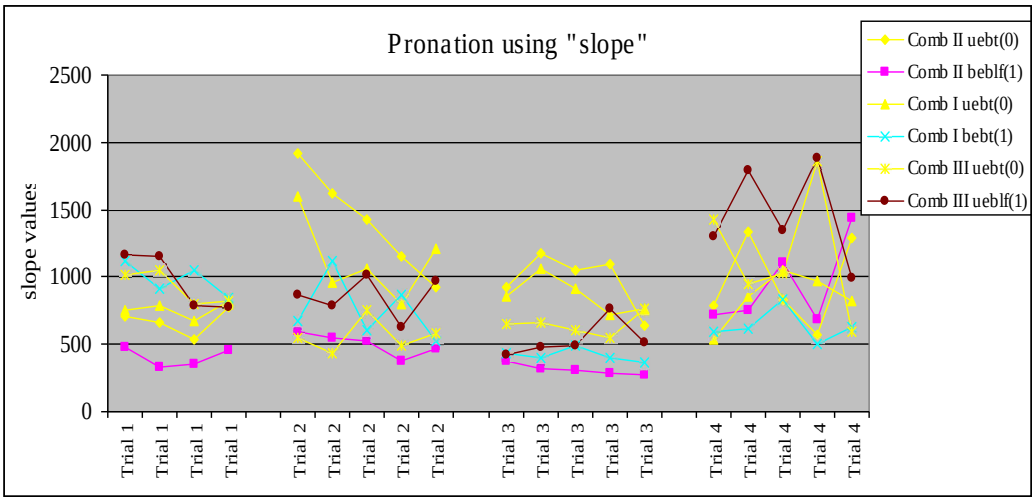

Fig. 6.7(b) Pronation plots using slope values

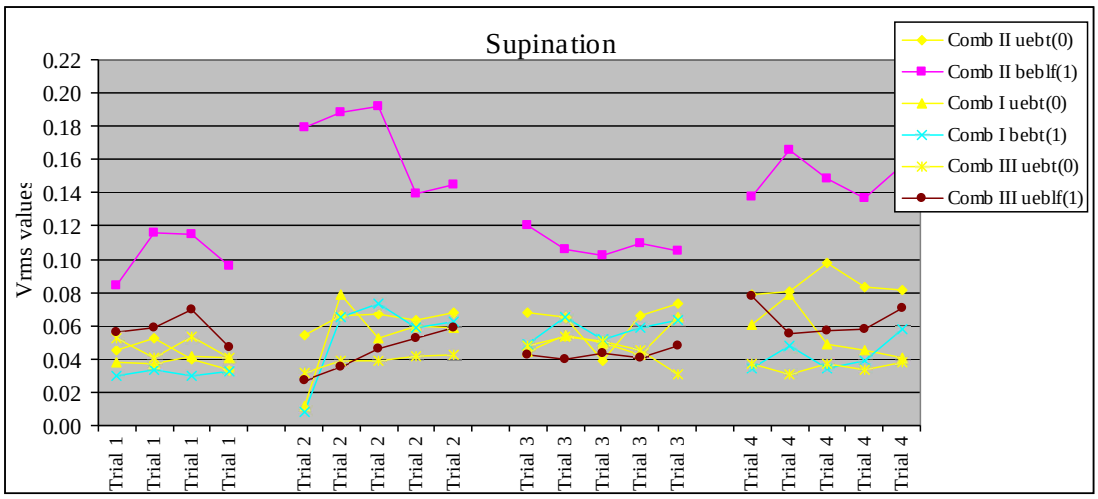

Fig. 6.8(a) Supination plots using V_{rms} values

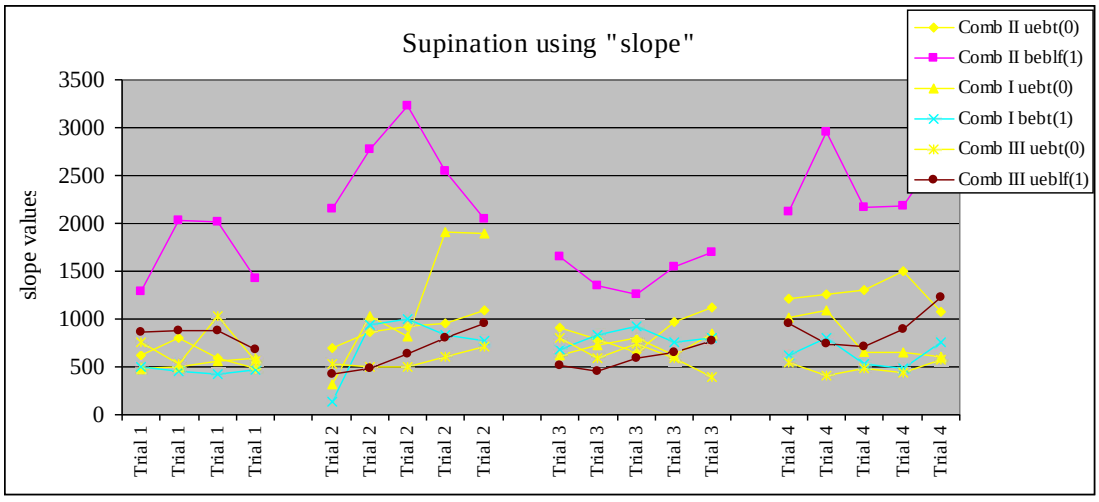

Fig. 6.8(b) Supination plots using slope values

In the present investigation, Combination II was found to be the best combination where maximum movements can be realized as two channel system. For the interpretation of all the four chosen movements, there is a need of control methodology which enables the proper interpretation of elbow movement. Both the parameters behaved in the same manner and could be considered for control methodology for prosthetic devices. Combination II is locations above elbow thumb side (uebt) and below elbow little finger side (beblf). So for the selected four movements considering above elbow points (i.e. uebt and ueblf) will not prototype multifunctional elbow as per the investigation. Combination I which represents pressure points again observed to be the second preference in the investigation.

6.1.3 Principal component analysis for suitable locations for elbow movements

After obtaining the best combination of electrode placement through observation in the last section, Principal component analysis has been used for validation of our observations i.e. verification of Table 6.3. The three chosen combinations for the detection of elbow movement were analyzed using PCA. Table A6.5a and Table A6.5b (appendix) represents the rearranged data from all the subjects collectively both for V_{rms} and slope values respectively. For each movement, the recordings from "uebt(above the elbow thumb side)" are grouped together with the other locations i.e. left and right channel values are grouped together. For extension, combination I was converted into "bebtd", for flexion into "bebtu", for pronation/supination as "bebtp" and "bebts" respectively. Similarly, other combinations were transformed. This is done to check the two channel variations w.r.t. movements.

Table 6.3 presents the visual outcome of the two channel system for depicting the four selected elbow movement. For the validity of the table PCA was done were the data were grouped for the comparison of which two channel combination is the best. In Table A6.5 (appendix) "bebt" represents the Combination I. Similarly "beblf(below the elbow little finger side)", "ueblf(above the elbow little finger side)" represents Combination II and Combination III respectively and last letter is for the representation of movement. PCA results were shown in Table A6.9-A6.12 (appendix) individually, for each movement. Each movement was displayed by the PCA score plot as shown in Fig. 6.9-6.12. Again two principal components (PC1 and PC2) were found to be sufficient for the interpretation. Component loading contributions of each variables to component one i.e. PC1 helped in deciding which combination is the best. Component loading contribution to PC1 for extension of "bebtd" is 0.91366, "beblfd" is 0.95068 and "ueblfd" is -0.14652 as per Table 6.4a. Combination "beblf (below the elbow little finger side)" or "combination-II" takes the advantage. Here, "bebt(below the elbow thumb side)" also shows the promising variation and could be selected.

In Table 6.5a the contributions of "bebtu" is -0.81084, "beblfu" is 0.66412 and "ueblfu" is -0.73212 for flexion. Now, location "bebt(below the elbow thumb side)" contribute 80% but location "beblf(below the elbow little finger side)" showed least variation. Similarly, in Table 6.6a the contributions of "bebtp" is 0.66765, "beblfp" is 0.89921 and "ueblfp" is -0.40954 for pronation. Clearly, location "beblf (below the

elbow little finger side)" is most suitable. In Table 6.7a the contributions of "bebts" is 0.05952, "beblfs" is 0.99982 and "ueblfs" is 0.26939 for supination. Again, best location is "beblf (below the elbow little finger side)". Hence, statistically, Combination II is the most dominant location for two channel system for two channel elbow prosthetics considering the V_{rms} values.

Table 6.4(a)
Principal component results for extension using V_{rms} values

Descriptive Statistics			
Variable	Mean	Std Dev.	Std Err
bebtd	0.06433	0.04425	0.00718
beblfd	0.07787	0.05021	0.00814
ueblfd	0.07135	0.02750	0.00446
Covariance Matrix			
	bebtd	beblfd	ueblfd
bebtd	0.00196	0.00165	-0.00020
beblfd	0.00165	0.00252	-0.00010
ueblfd	-0.00020	-0.00010	0.00076
Explained Variance (Eigenvalues)			
Value	PC 1	PC 2	PC 3
Eigenvalue	0.00393	0.00078	0.00053
% of Var.	75.04912	14.86546	10.08542
Cum. %	75.04912	89.91458	100.00000
Component Loadings			
Variable	PC 1	PC 2	PC 3
bebtd	0.91366	-0.15563	0.37551
beblfd	0.95068	0.15963	-0.26596
ueblfd	-0.14652	0.93876	0.31187
Component Score Coefficients (Eigenvectors)			
Variable	PC 1	PC 2	PC 3
bebtd	0.64503	-0.24687	0.72318
beblfd	0.76145	0.28727	-0.58110
ueblfd	-0.06429	0.92549	0.37328

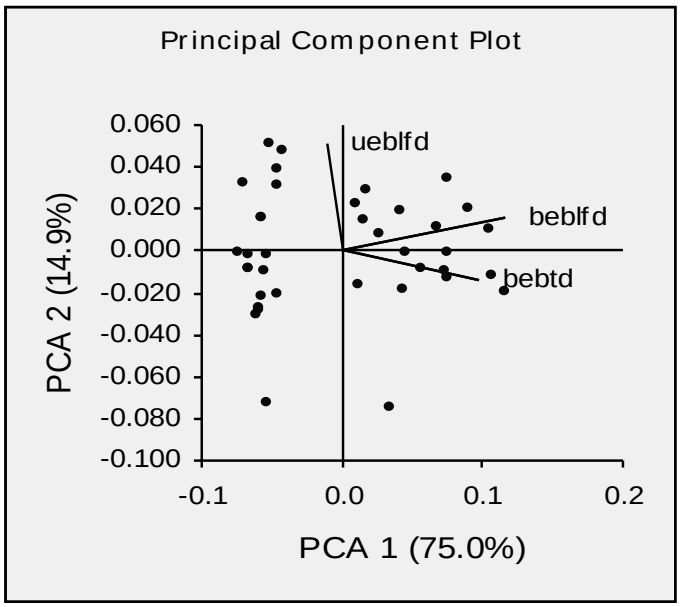

Fig. 6.9(a) PCA plot for extension using V_{rms} values

Table 6.4(b)
Principal component results for extension using Slope values

Descriptive Statistics			
Variable	Mean	Std Dev.	Std Err
beblfd	1306.161	903.507	146.568
bebtd	985.805	749.504	121.586
ueblfd	1249.299	390.712	63.382
Covariance Matrix			
	beblfd	bebtd	ueblfd
beblfd	816324.864	549251.385	-37392.365
bebtd	549251.385	561756.804	-57722.702
ueblfd	-37392.365	-57722.702	152655.891
Explained Variance (Eigenvalues)			
Value	PC 1	PC 2	PC 3
Eigenvalue	1256698.275	161877.826	112161.457
% of Var.	82.098	10.575	7.327
Cum. %	82.098	92.673	100.000
Component Loadings			
Variable	PC 1	PC 2	PC 3
beblfd	0.969	0.160	-0.190
bebtd	0.930	-0.198	0.308
ueblfd	-0.169	0.883	0.439
Component Score Coefficients (Eigenvectors)			
Variable	PC 1	PC 2	PC 3
beblfd	0.781	0.359	-0.511
bebtd	0.622	-0.370	0.690
ueblfd	-0.059	0.857	0.512

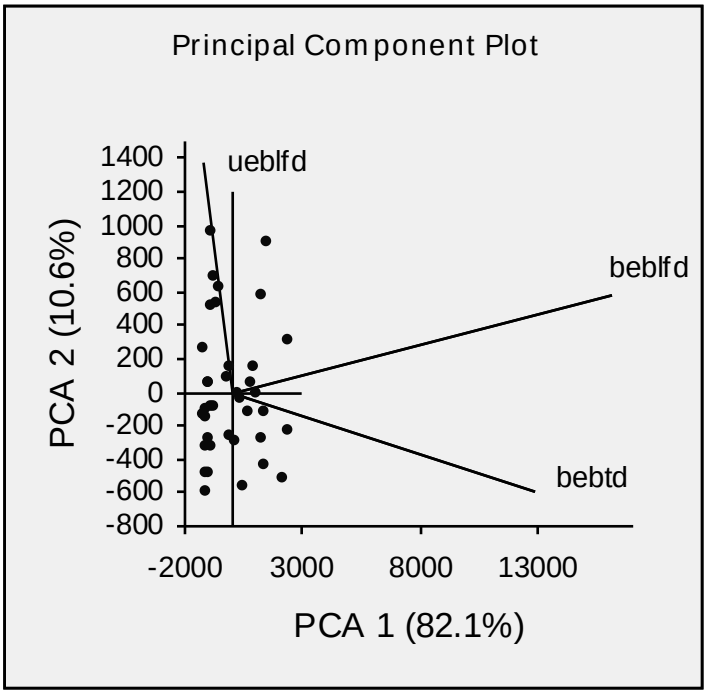

Fig. 6.9(b) PCA plot for extension using slope values

Table 6.5(a)
Principal component results for flexion using V_{rms} values

Descriptive Statistics			
Variable	Mean	Std Dev.	Std Err
bebtu	0.08142	0.02565	0.00416
beblfu	0.07281	0.02634	0.00427
ueblfu	0.05755	0.02128	0.00345
Covariance Matrix			
	bebtu	beblfu	ueblfu
bebtu	0.00066	-0.00014	0.00028
beblfu	-0.00014	0.00069	-0.00014
ueblfu	0.00028	-0.00014	0.00045
Explained Variance (Eigenvalues)			
Value	PC 1	PC 2	PC 3
Eigenvalue	0.00098	0.00057	0.00026
% of Var.	54.37937	31.46028	14.16034
Cum. %	54.37937	85.83966	100.00000
Component Loadings			
Variable	PC 1	PC 2	PC 3
bebtu	-0.81084	0.47753	-0.33837
beblfu	0.66412	0.74529	0.05900
ueblfu	-0.73212	0.26722	0.62658
Component Score Coefficients (Eigenvectors)			
Variable	PC 1	PC 2	PC 3
bebtu	-0.66397	0.51410	-0.54299
beblfu	0.55839	0.82386	0.09722
ueblfu	-0.49733	0.23865	0.83409

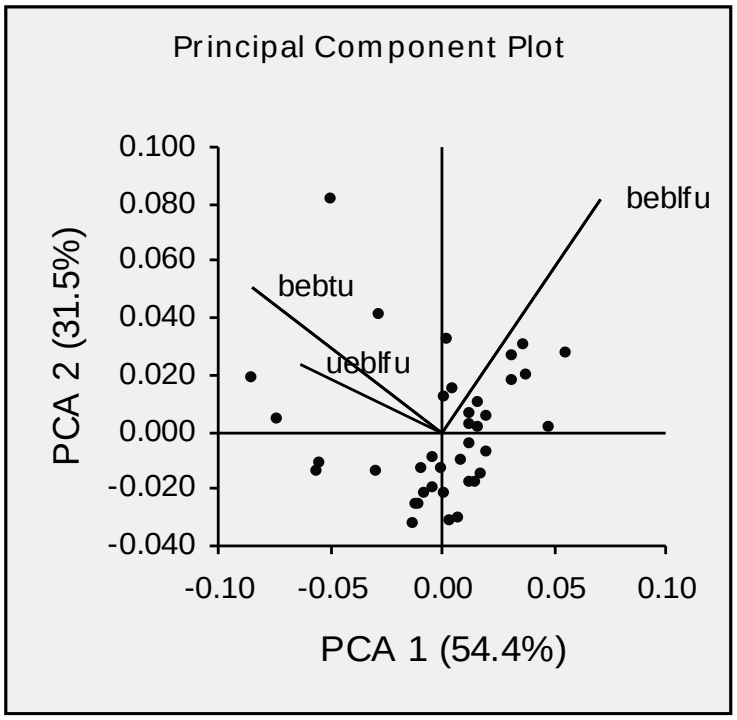

Fig. 6.10(a) PCA plot for flexion using V_{rms} values

Table 6.5(b)
Principal component results for flexion using slope values

Descriptive Statistics			
Variable	Mean	Std Dev.	Std Err
beblfu	1093.850	372.559	60.437
bebtu	1017.528	393.032	63.758
ueblfu	1021.427	432.007	70.081
Covariance Matrix			
	beblfu	bebtu	ueblfu
beblfu	138800.231	55627.010	522.561
bebtu	55627.010	154473.885	50922.537
ueblfu	522.561	50922.537	186629.637
Explained Variance (Eigenvalues)			
Value	PC 1	PC 2	PC 3
Eigenvalue	237454.703	163404.400	79044.649
% of Var.	49.480	34.049	16.471
Cum. %	49.480	83.529	100.000
Component Loadings			
Variable	PC 1	PC 2	PC 3
beblfu	0.487	-0.726	0.485
bebtu	0.811	-0.311	-0.496
ueblfu	0.743	0.635	0.212
Component Score Coefficients (Eigenvectors)			
Variable	PC 1	PC 2	PC 3
beblfu	0.372	-0.670	0.643
bebtu	0.654	-0.303	-0.694
ueblfu	0.659	0.678	0.325

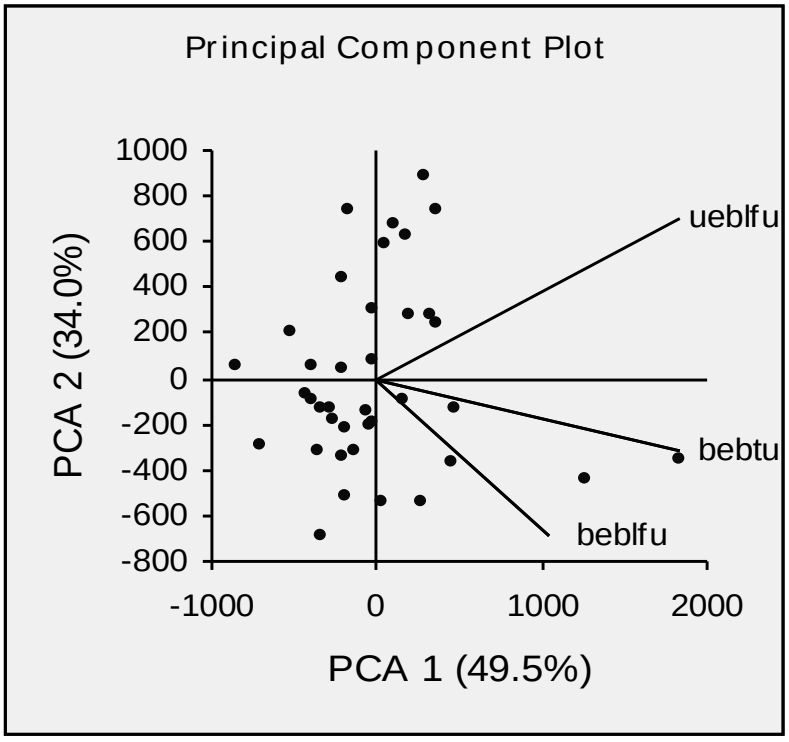

Fig. 6.10(b) PCA plot for flexion using slope values

Table 6.6(a)
Principal component results for pronation using V_{rms} values

Descriptive Statistics			
Variable	Mean	Std Dev.	Std Err
bebtp	0.05194	0.01589	0.00258
beblfp	0.05077	0.02279	0.00370
ueblfp	0.05755	0.02128	0.00345
Covariance Matrix			
	bebts	beblfs	ueblfs
bebtp	0.00025	0.00015	-0.00008
beblfp	0.00015	0.00052	-0.00003
ueblfp	-0.00008	-0.00003	0.00045
Explained Variance (Eigenvalues)			
Value	PC 1	PC 2	PC 3
Eigenvalue	0.00061	0.00045	0.00017
% of Var.	49.67827	36.36476	13.95697
Cum. %	49.67827	86.04303	100.00000
Component Loadings			
Variable	PC 1	PC 2	PC 3
bebtp	0.66765	-0.06216	0.74188
beblfp	0.89921	0.38098	-0.21510
ueblfp	-0.40954	0.90261	0.13257
Component Score Coefficients (Eigenvectors)			
Variable	PC 1	PC 2	PC 3
bebtp	0.43007	-0.04680	0.90158
beblfp	0.83077	0.41140	-0.37493
ueblfp	-0.35336	0.91025	0.21581

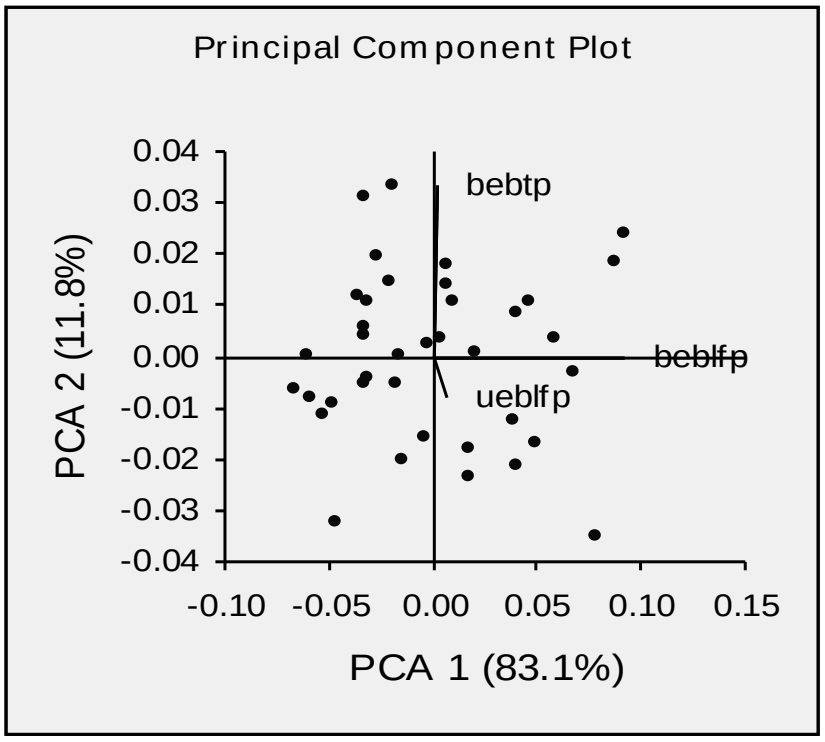

Fig. 6.11(a) PCA plot for pronation using V_{rms} values

Table 6.6(b)
Principal component results for pronation using slope values

Descriptive Statistics			
Variable	Mean	Std Dev.	Std Err
beblfp	784.193	412.309	66.885
bebtp	794.257	259.984	42.175
ueblfp	886.974	384.155	62.318
Covariance Matrix			
	beblfp	bebtp	ueblfp
beblfp	169998.424	55909.141	-21862.201
bebtp	55909.141	67591.915	-11261.166
ueblfp	-21862.201	-11261.166	147574.789
Explained Variance (Eigenvalues)			
Value	PC 1	PC 2	PC 3
Eigenvalue	205087.066	137118.188	42959.874
% of Var.	53.247	35.600	11.154
Cum. %	53.247	88.846	100.000
Component Loadings			
Variable	PC 1	PC 2	PC 3
beblfp	0.923	0.328	-0.201
bebtp	0.651	0.206	0.730
ueblfp	-0.463	0.886	0.008
Component Score Coefficients (Eigenvectors)			
Variable	PC 1	PC 2	PC 3
beblfp	0.840	0.365	-0.401
bebtp	0.374	0.145	0.916
ueblfp	-0.393	0.920	0.015

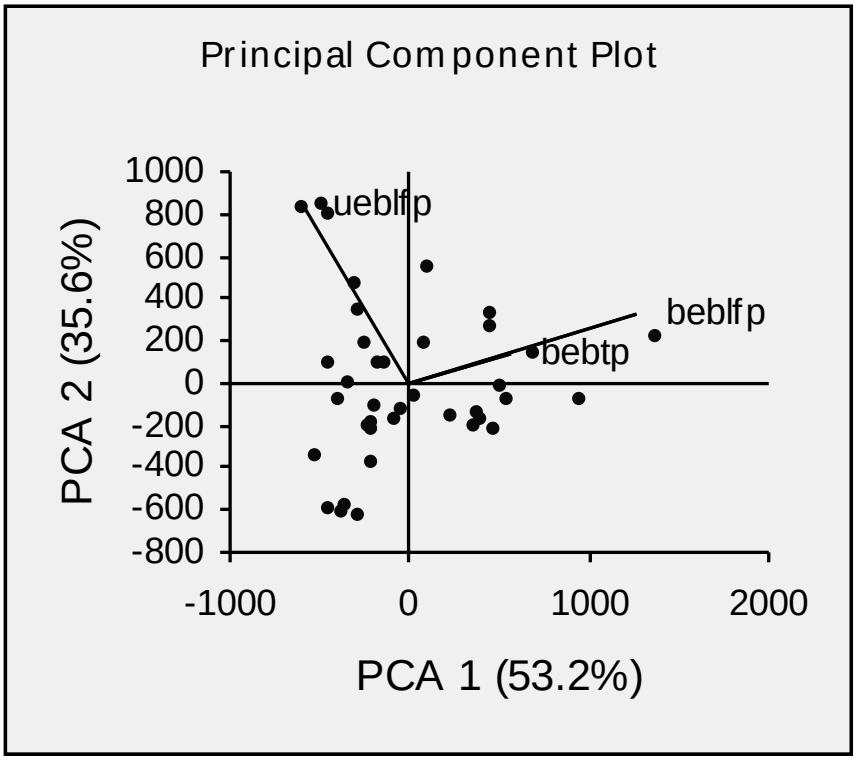

Fig. 6.11(b) PCA plot for pronation using slope values

Table 6.7(a)
Principal component results for supination using V_{rms} values

Descriptive Statistics			
Variable	Mean	Std Dev.	Std Err
bebts	0.04850	0.01609	0.00261
beblfs	0.09912	0.04323	0.00701
ueblfs	0.04659	0.01159	0.00188
Covariance Matrix			
	bebtp	beblfp	ueblfp
bebts	0.00026	0.00004	-0.00003
beblfs	0.00004	0.00187	0.00013
ueblfs	-0.00003	0.00013	0.00013
Explained Variance (Eigenvalues)			
Value	PC 1	PC 2	PC 3
Eigenvalue	0.00188	0.00027	0.00012
% of Var.	83.05937	11.76359	5.17704
Cum. %	83.05937	94.82296	100.00000
Component Loadings			
Variable	PC 1	PC 2	PC 3
bebts	0.05952	0.98592	0.15629
beblfs	0.99982	-0.00177	-0.01883
ueblfs	0.26939	-0.32839	0.90531
Component Score Coefficients (Eigenvectors)			
Variable	PC 1	PC 2	PC 3
bebts	0.02209	0.97238	0.23235
beblfs	0.99716	-0.00468	-0.07521
ueblfs	0.07204	-0.23335	0.96972

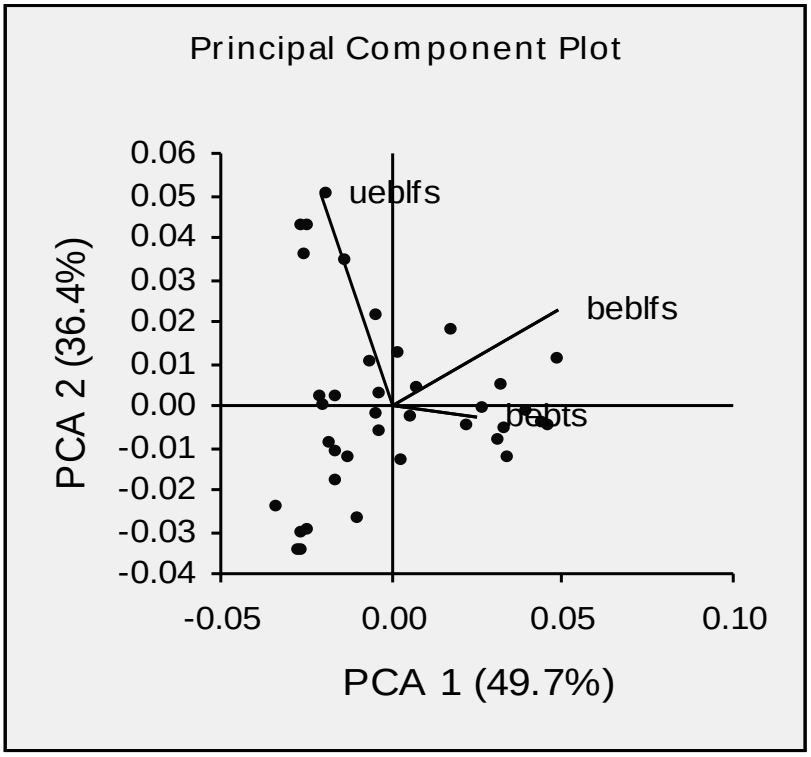

Fig. 6.12(a) PCA plot for supination using V_{rms} values

Table 6.7(b)
Principal component results for supination using slope values

Descriptive Statistics			
Variable	Mean	Std Dev.	Std Err
beblfs	1498.818	724.602	117.546
bebts	749.825	344.044	55.811
ueblfs	668.853	192.876	31.289
Covariance Matrix			
	beblfs	bebts	ueblfs
beblfs	525048.598	-13955.522	42333.880
bebts	-13955.522	118366.163	-8867.210
ueblfs	42333.880	-8867.210	37201.294
Explained Variance (Eigenvalues)			
Value	PC 1	PC 2	PC 3
Eigenvalue	529218.549	118528.196	32869.310
% of Var.	77.756	17.415	4.829
Cum. %	77.756	95.171	100.000
Component Loadings			
Variable	PC 1	PC 2	PC 3
beblfs	1.000	0.020	-0.021
bebts	-0.075	0.996	0.047
ueblfs	0.326	-0.154	0.933
Component Score Coefficients (Eigenvectors)			
Variable	PC 1	PC 2	PC 3
beblfs	0.996	0.043	-0.083
bebts	-0.036	0.995	0.089
ueblfs	0.086	-0.086	0.993

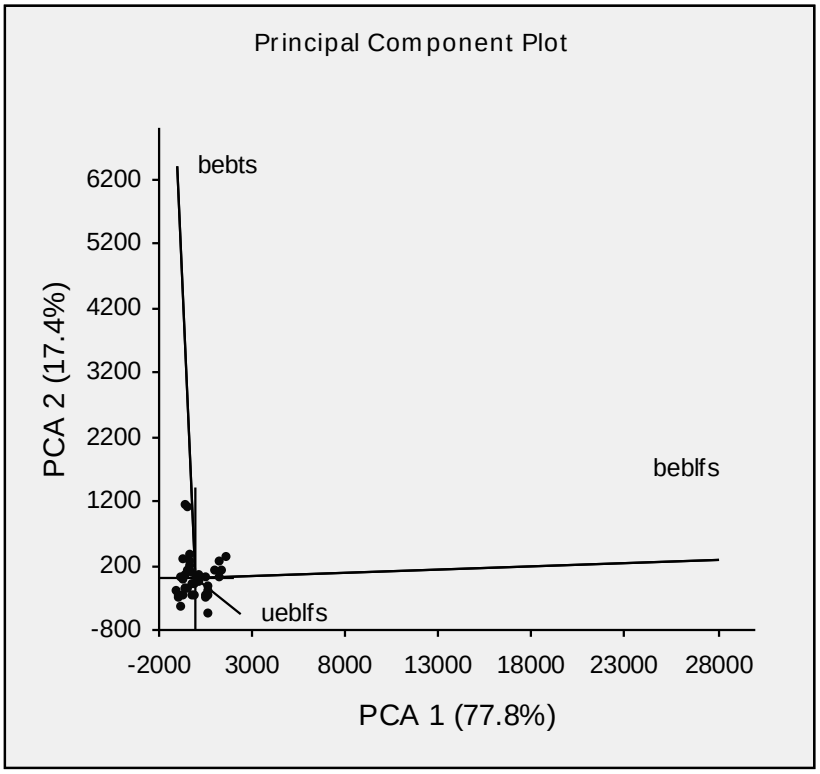

Fig. 6.12(b) PCA plot for supination using slope values

A similar outcome was observed considering slope values. Component loading contribution to PC1 of “beblfd” is 0.969, “bebtd” is 0.930 and “ueblfd” is -0.169 for extension as per Table 6.4b. Both “combination-I” and “combination-II” takes the advantage. In Table 6.5b the contributions of “beblfu” is 0.487, “bebtu” is 0.811 and “ueblfu” is 0.743 for flexion. Now, location “bebt (below the elbow thumb side)” contribute 80% but location “beblf (below the elbow little finger side)” showed least variation. Similarly, in Table 6.6b the contributions of “beblfp” 0.923, “bebtp” is 0.651 and “ueblfp” is -0.463 for pronation. Clearly, location “beblf (below the elbow little finger side)” is most suitable. In Table 6.7b the contributions of “beblfs” is 1.000, “bebts” is -0.075 and “ueblfs” is 0.326 for supination. Again best location is “beblf (below the elbow little finger side)”.

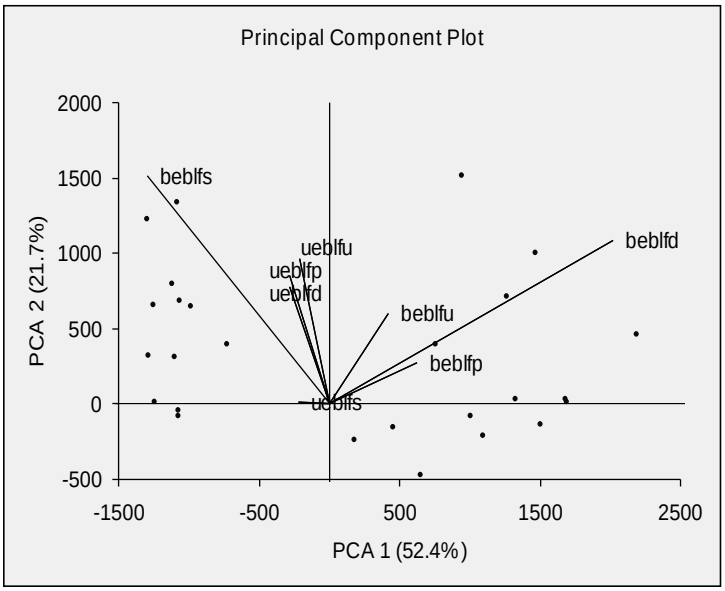

Fig. 6.13 PCA plot for comparing combination II and III

Again, it is concluded, Combination II is the best location for two channel elbow prosthetics. The next preferable combination is observed to be combination I which are acupressure points. The analysis of elbow movement suggested that combination II is the best which has one location at “uebt (above elbow thumb side)” and other at “beblf (below elbow little finger side)”. The result can be very helpful for exoskeleton type of elbow design but upper elbow amputees are not having the advantage of location “beblf (below the elbow little finger side)”.

This becomes important that combination III, which have both the points available for above elbow prosthesis needed to be compared with combination II. Table A6.6

shows the result of PCA for comparing the two locations i.e. combination II and combination III for the four chosen movements. Fig. 6.13 shows the related component loading. From the Fig.6.13 it was observed that the variations in the dataset of combination II is much more appealing for discriminating movements. Extension and supination are the most easier to discriminate in comparison to other movements. Combination III was found to be not proper combination for the elbow prosthesis and would be able to discriminate at the most two movements.

Table 6.8
Behavior observed of SEMG parameters (chosen) related to selected movements

Movement	Channel 0 [uebt(above the elbow thumb side)]	Channel 1[beblf(below the elbow little finger side)]
Extension	High V_{rms}/slope values	Don't care
Flexion	Low V_{rms}/slope values	Low/ Moderate V_{rms}/slope values
Pronation	Moderate V_{rms}/slope values	Moderate V_{rms}/slope values
Supination	Moderate V_{rms}/slope values	High V_{rms}/slope values

Table 6.8 was an attempt to define the values of the two chosen parameters for the two channel methodology. This will help in deciding the levels of threshold during the microcontrolled prosthetic applications. All the four movements were well discriminated using combination II. Another aspect of the discussion was to observe the selected acupressure points. The selected pressure points were covered under combination I which was found to be the second best location for the chosen movements.

6.2 Prototype elbow design

The elbow joint allows two main different movements:

- The hinge-like bending and straightening of the elbow (flexion and extension) happens at the articulation ("joint") between the humerus and the ulna.
- The complex action of turning the forearm over (pronation or supination) happens at the articulation between the radius and the ulna (this movement also occurs at the wrist joint).

In the anatomical position (with the forearm supine), the radius and ulna lie parallel to each other. During pronation, the ulna remains fixed, and the radius rolls around it at both the wrist and the elbow joints. In the prone position, the radius and ulna appear crossed [Casolo et al., 2008]. The different prostheses developed by the main prosthetic societies: UTAH, OTTO BOCK and PROTEOR concentrate 90% of the market. Three kinds of mechanical elbow products are currently offered to the patients. The first is the elbow with toothed rack, which is released thanks to a pushbutton actuated by the valid hand or by a cable. Many drawbacks are attached to this mechanical elbow: noise of the toothed rack, the limited number of positions of the front arm and the bad aesthetic of the pushbutton. The second elbow is the elbow with friction, which moves thanks to the friction of a spiral spring on the axis of the elbow. A cable ordered by the other shoulder actuates blocking: one traction locks it, another unbolts it. It is more functional than the previous one, but maintains the position less firmly. In addition, it needs a double order from the amputee, which is not always easy to carry out. Lastly, there is an automatic elbow from OTTO BOCK. The front arm is manufactured out of plastic and is not very solid. Its distal part (near to the wrist) is cylindrical and is simply cut to the length of the healthy member. Unfortunately, prosthetic arm will not resemble to the healthy member. The consequences of the Viet Nam war were at the origin of the development of the UTAH products. This society was the first to propose the SEMG technology to control the prosthesis. The OTTO BOCK society also proposes prosthesis of hand coupled with a myoelectric elbow. Unfortunately, the whole system proposed by this society is too expensive for patient [Artigue et al., 2009]. A parallel engineering mission to develop a humanoid can be of great help in developing prosthetic structures. A humanoid robot should have humanlike appearance, dexterity and manipulation. These requirements lead to a complex design process and a design which has to be highly spatially integrated as well as functionally integrated. ARMAR

III is the current Humanoid Robot. The elbow joint of ARMAR III has two degrees of freedom. Thus bending as well as a rotation of the forearm is possible [Albers et al., 2006].

In this work the same concept was adopted to realize the mechanical structure as shown in Fig. 6.14. The elbow joint has two degrees of freedom. Thus, bending as well as a rotation of the forearm is possible. The present microcontroller based prototype elbow is aimed at improving the functionality of the myoelectric prostheses using cost effective technologies. Two small dc geared motors of 12 volts,10 rpm were used for the two movements as shown in Fig. 6.14b. Elbow motor will perform extension and flexion whereas wrist motor will perform supination and pronation. The required elbow movement is less than 180 degree movement so each motor is made position controlled using limit switches to have the desired range of movement. SEMG is sensed by electrode, amplified, filtered, converted to DC voltage by RMS to DC converter and then converted to digital 8 bit data by ADC which was acquired by microcontroller in its register. The basic building block and photograph of experimental setup of the prototype is shown in Fig. 6.14a.

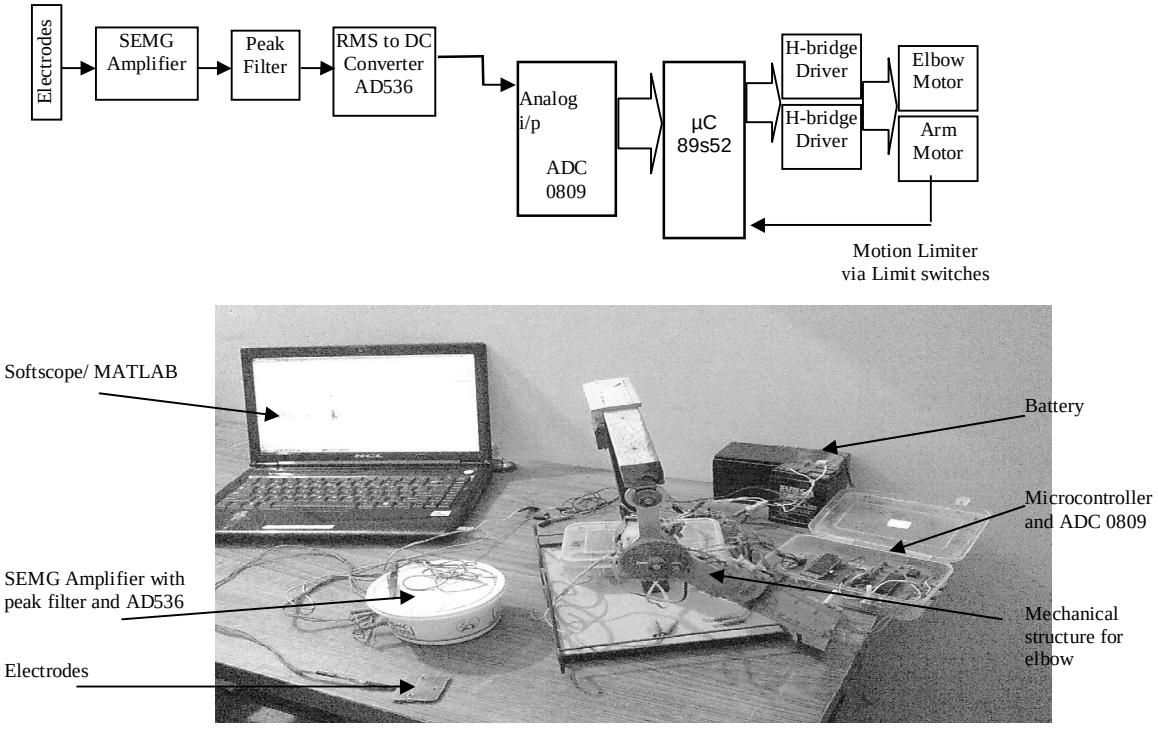

(a)

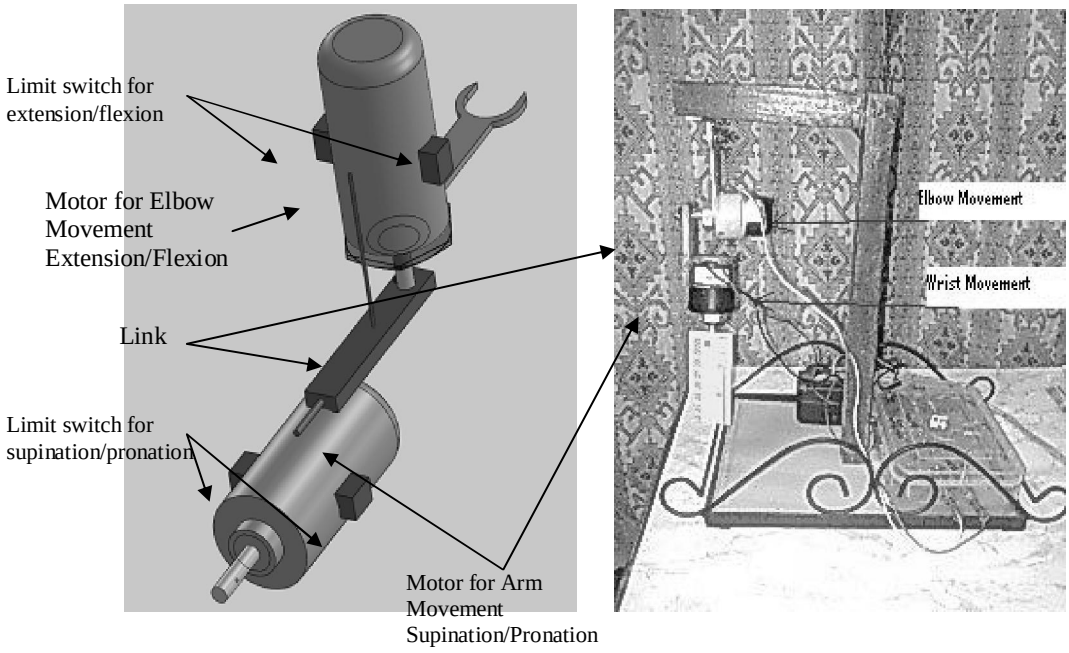

(b)

Fig. 6.14(a) Block diagram and photograph of prototype elbow (b) Prototype artificial elbow with solid-works model

The AD536A computes the true root-mean-square level of a complex ac (or ac plus dc) input signal and gives an equivalent dc output level which is generated by the peak filter. The true RMS value of a waveform is a more useful quantity than the average rectified value, since it relates directly to the power of the signal [Annexure 2]. The output of the AD536 was given to ADC 0809 interfaced to microcontroller. In this research work microcontroller 89s52 was used [Annexure 3]. As per the datasheet of the AD 536 a low-pass filter formed by internal resistance and the externally connected capacitor, C_{AV}. The time constant must be kept much greater than the longest period of the input signal to get effective average. The only external component required is the capacitor which sets the averaging period. The averaging time constant should be at least ten times the signal period. For example, a 100 Hz pulse rate requires a 100 ms time constant, which corresponds to a 4 µF capacitor (time constant = 25 ms per µF).

For the present investigation, SEMG RMS to DC conversion was done by using the 4.7 microfarad capacitor value. Large value of C_{AV} helped in controlling the ripple in the DC output. The primary disadvantage in using a large C_{AV} to remove ripple is that the settling time for a step change in input level is increased proportionately. But for

ADC working this helps as a holding circuit. SEMG peaks are fast moving so this feature of increased settling time was proved to be advantageous.

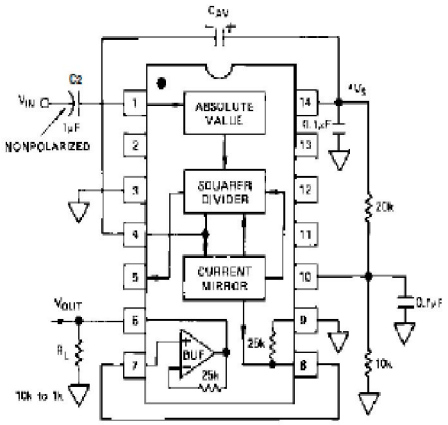

Fig. 6.15 AD 536, Vrms to DC voltage circuit arrangement [Datasheet AD536]

Analogue-to-digital converter (ADC 0809) was used to interface through a microcontroller 89s52 to convert analogue signal received from AD536 into digital format. The circuit of A-to-D converter shown in the Fig. 6.16 is in free-running mode i.e. avoiding the use of a microcontroller. The ADC 0809 is an 8-bit A-to-D converter, having data lines D0-D7. It works on the principle of successive approximation. It has a total of eight analogue input channels, out of which any one can be selected using address lines A, B and C. Here, in this investigation, input channel IN0 and input channel IN1 were selected by connecting A, B and C address lines as shown in Table 6.9. Usually the control signals EOC (end of conversion), SC (start conversion), ALE (address latch enable) and OE (output enable) are interfaced by means of a microcontroller. However, the circuit shown here was built to operate in its continuous mode. Therefore, the input control signals ALE and OE, being active-high, were tied to Vcc (+5 volts). The input control signal SC being active-low initiate start of conversion at falling edge of the pulse. The output signal EOC becomes high after completion of digitization. This EOC output is coupled to SC input, where falling edge of EOC output acts as SC input to direct the ADC to start the conversion. As the conversion starts, EOC signal goes high. At next clock pulse EOC output again goes low and hence SC is enabled to start the next conversion. Thus, it provides continuous 8-bit digital output corresponding to instantaneous value

of analogue input from AD536. The maximum level of analogue input voltage was scaled down below positive reference (+5V) level using V_{ref} of ADC 0809. This was done by using a potentiometer. This very control was used to full scale the maximum SEMG signal manually. The ADC 0809 was operated by clock signal which was derived from an astable multivibrator constructed using 555 timer IC. In order to visualize the digital output, the row of eight LEDs (LED1 through LED8) were used, where in each LED is connected to respective data lines D0 through D7. The same were connected to Port 0 of microcontroller 89s52 in parallel. Since ADC was working in the continuous mode, it displayed digital output as soon as analogue input was applied which is SEMG signal in DC form from AD536.

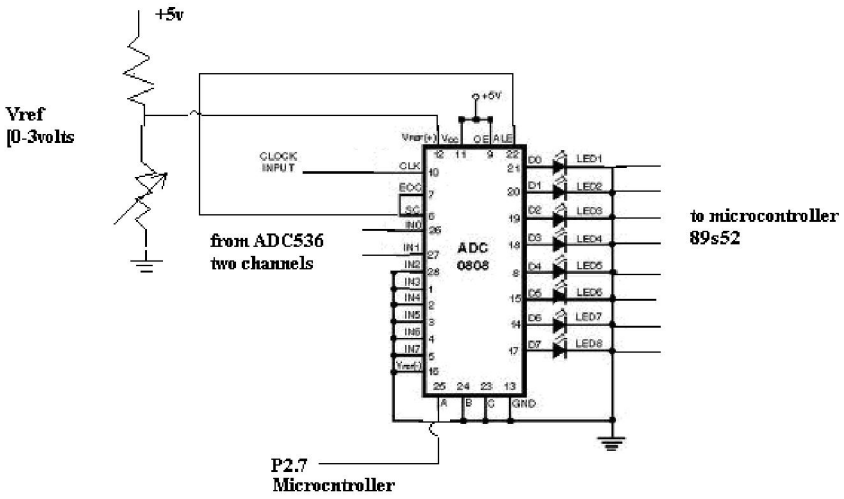

Fig. 6.16 Schematic diagram for the ADC0809

AT89S52 is a low power, high-performance CMOS 8-bit microcontroller with 8K bytes of in-system programmable flash memory. The device is manufactured using ATMEL's high-density nonvolatile memory technology and is compatible with the industry- standard 80C51 instruction set and pin out. The on-chip flash allows the program memory to be reprogrammed in-system or by a conventional nonvolatile memory programmer. By combining a versatile 8-bit CPU with in-system programmable flash on a monolithic chip, the Atmel 89S52 is a powerful microcontroller, which provides a highly flexible and cost- effective solution to many

embedded control applications. If the value stored in the register of microcontroller is greater than a predefined threshold value then the driver subroutine is called for movement. The driver subroutine checks the SEMG value and then sends the control bit to enable the H-bridge motor operation. Controlling the DC motor is done using the principle of the H-bridge.

Connections of microcontroller:-

Port P1 and P2.1 were programmed to work as input whereas Port P2.2 and Port P2.3 were programmed to work as output ports.

P1 was connected to data line of ADC0809.

P2.1 is used to check the limit switches for flexion-extension.

P2.2 and P2.3 were connected to motor driver h-bridge circuit for elbow movement.

P2.4 is used to check the limit switches for pronation-supination.

P2.5 and P2.6 were connected to motor drive h-bridge circuit for wrist movement.

P2.7 was used to select analog input channel of ADC. Channel selection was done by ADDA, ADDB and ADDC of ADC. ADDA is connected to P2.7 while other to were grounded as Table 6.9.

Table 6.9
Analog channel selection

Selected analog channel	Address line C B A
IN0	L L L
IN1	L L H

6.3 Control methodology for elbow movement

A prosthesis control system based on microcontroller hardware has been described whereby control of an artificial elbow for above-elbow amputees is prototyped. The design employs running RMS identification techniques for single parameter discrimination. With proper synchronizing of the arm position and the muscle contraction the specific sequence of movements are achieved successfully. The user is required to be trained to contract the muscle group where electrodes are placed. The user must also understand the force level to be exerted. After few repetitions the user gets used to the prototype. For single channel methodology location selected was "uebt(above the elbow thumb side)" and for two channel methodology locations selected were "uebt(above the elbow thumb side)" and "beblf(below the elbow little finger side)" as discussed in section 6.1. Although, the development of externally powered upper-limb prostheses has been an engineering challenge and the effort has a significant payoff. Advantage of the design presented is microcontroller based elbow prototype actuator being the SEMG signal. The current system had the features that would be feasible for any improvements to control and enhancement.

6.3.1 Methodology for single channel prosthetic elbow

Fig. 6.17 (a) shows the block diagram for signal channel and two movements. SEMG signal was acquired from location as shown in Fig. 6.4. The acquired SEMG was converted to 8-bit digital data by the ADC and stored in register R7 of microcontroller. The microcontroller was programmed as per the flowchart shown in Fig. 6.17 (b). Multi- threshold values were kept. If R7 value goes greater than 6Fh then controller make the prototype to extend and if between 0Fh and 6Fh then makes it to flex. User needs little training to exert force during extension. Success rate is shown via operation Table 6.10. Each movement was done after confirming SEMG signals on softscope-MATLB. Degree of operation can be increased by enhancing the programming of microcontroller for all the four movement.

Fig. 6.18 (a) shows the block diagram for single channel four movements using the concept of strategic triggering. R7 was loaded first time to perform extension or flexion and then microcontroller waits for second contraction. Again R7 was loaded with new value of SEMG to decide upon pronation and supination as described by flow chart shown in Fig. 6.18(b). User is made to understand the force level to be exerted to achieve the specific movement. The success rate is shown via Table 6.11

but a compromise had to be made considering the natural movement. Pronation and supination were achieved purely in robotic nature. This specific prosthetic action can be very good for the applications of pick and place jobs.

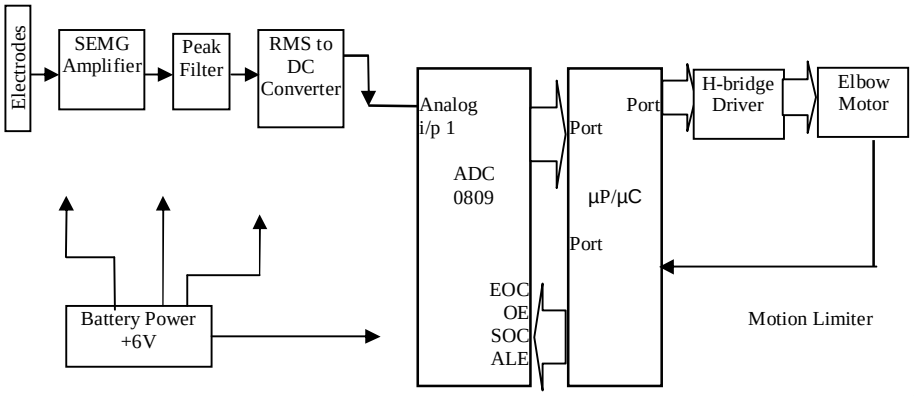

(a)

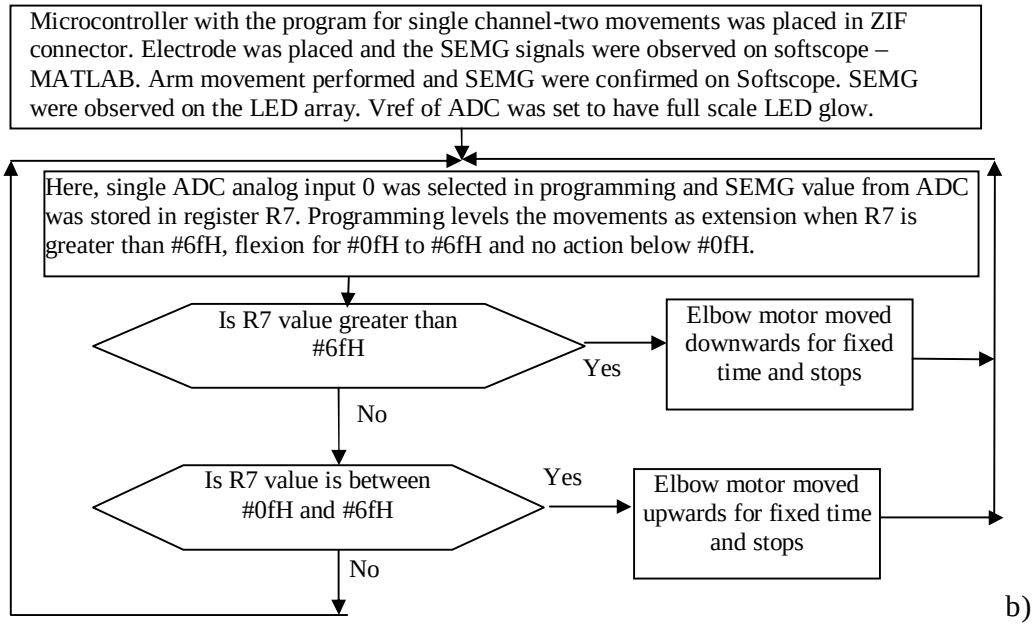

b)

Fig. 6.17 (a) Block diagram for single channel two movements approach (b) Flowchart for Microcontroller programming

Table 6.10
Testing of the prototype (single channel-two movement)

Intended movement	No. of trials	Controller response		Success percentage
		True	False	
Extension	25	24	01	96%
Flexion	25	25	Nil	100%

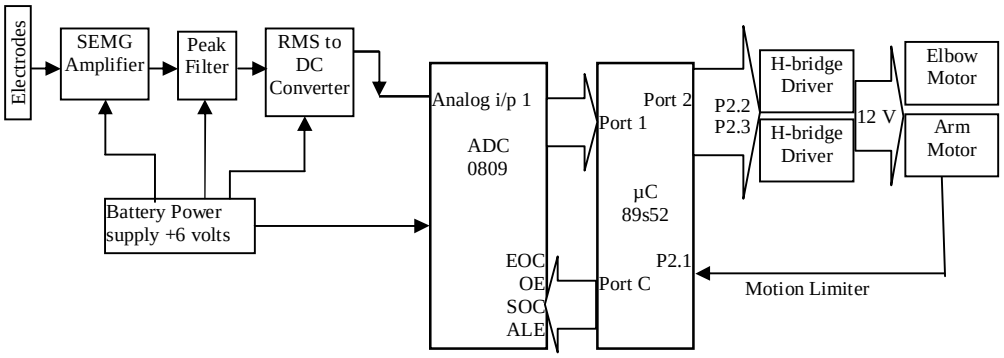

(a)

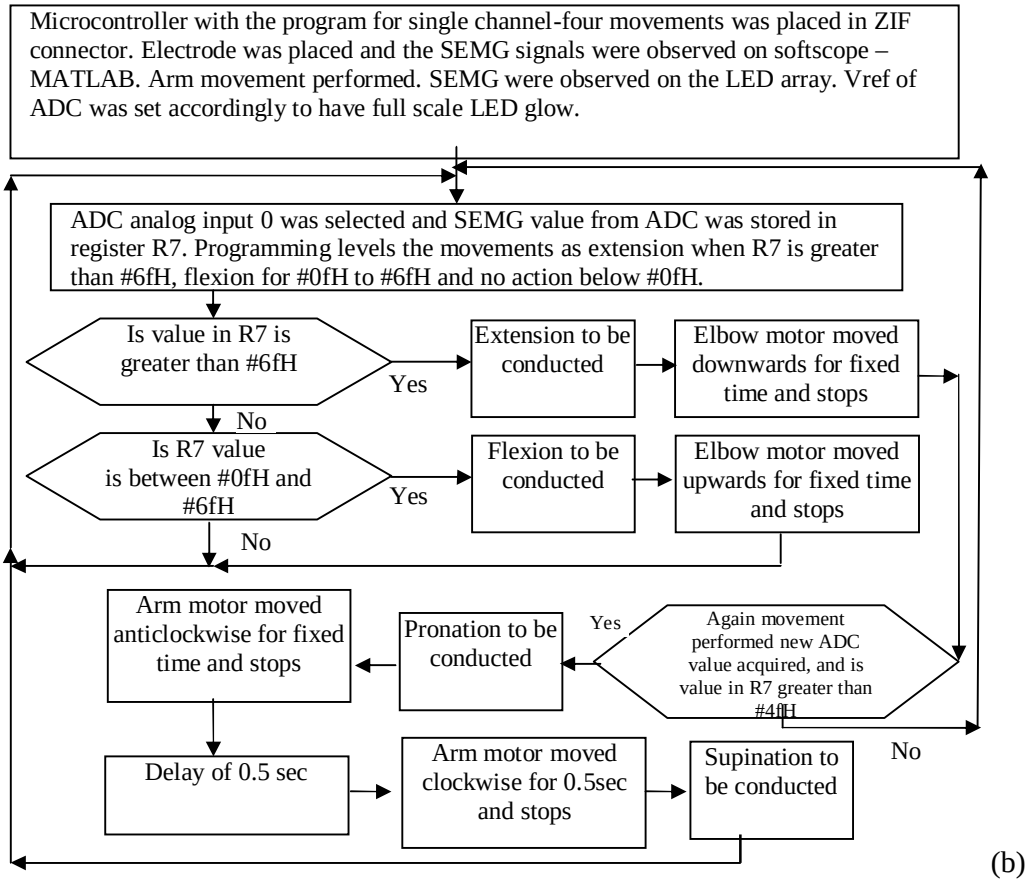

(b)

Fig. 6.18 (a) Block diagram for single channel four movements approach (b) Flowchart for Microcontroller programming

Table 6.11
Testing of the prototype (single channel-four movement)

Intended movement	No. of trials	Controller response		Success percentage
		True	False	
Extension	25	23	02	92%
Flexion	25	24	01	96%
Pronation-Supination	25	25	Nil	100%

6.3.2 Methodology for two channel prosthetic elbow

Table 6.3 concludes the two channel approach which helps in deciding the threshold levels for performing the movements. Fig. 6.19 (a) shows the block diagram. The two sets of electrodes and acquisition circuits were used with ADC running its two analog channels and storing their data in register R7 and R6. Flow chart as shown in Fig. 6.19 (b) narrates the sequence of movement for achieving two movements i.e. extension and flexion. Again the success rate is shown in Table 6.12. This very methodology has no advantage over single channel two movements but increased complexity of wrapping two electrode sets.

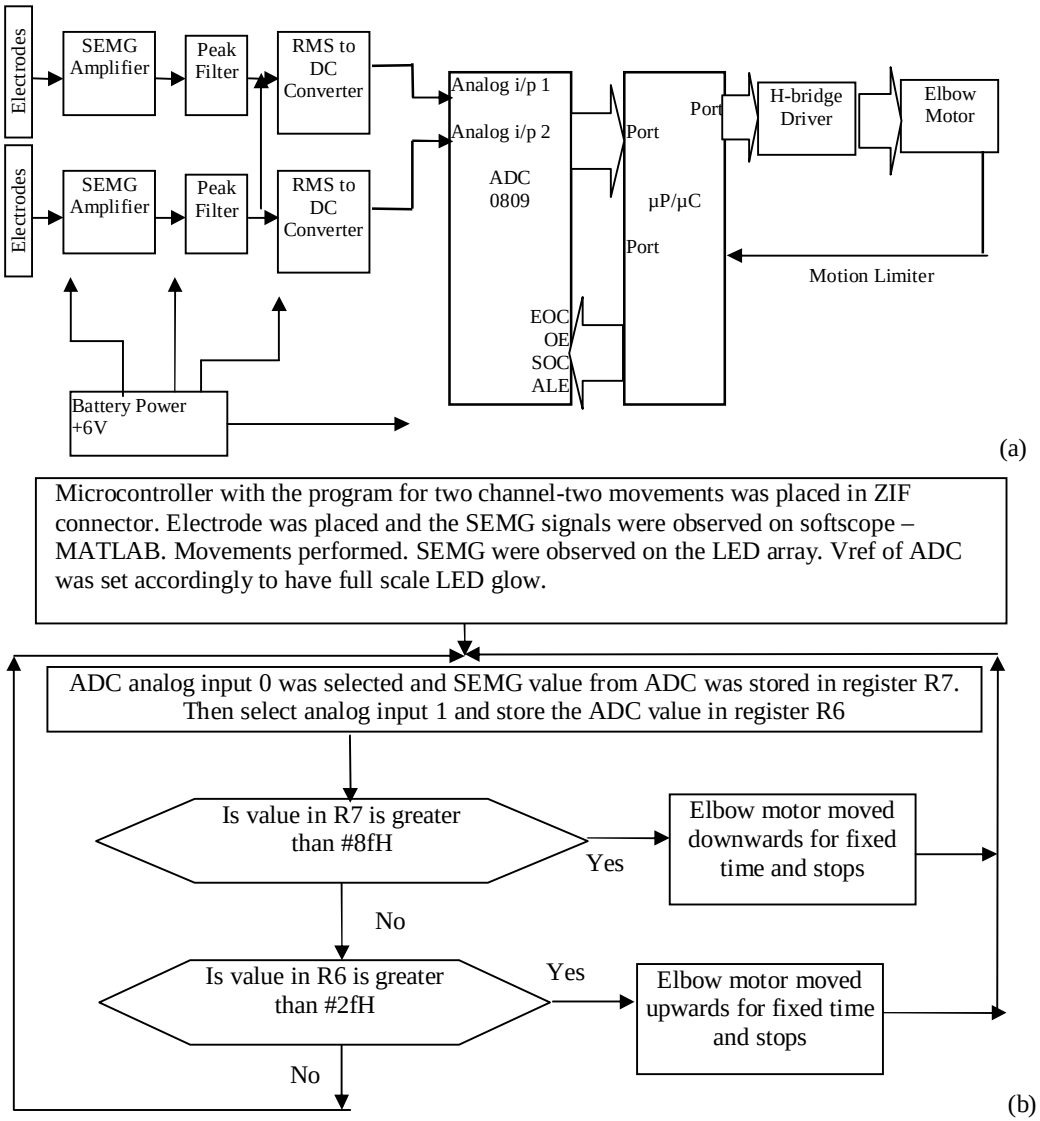

Fig. 6.19(a) Block diagram for two channel two movements approach (b) Flowchart for Microcontroller programming

Table 6.12
Testing of the prototype (two channel-two movement)

Intended movement	No. of trials	Controller response		Success percentage
		True	False	
Extension	25	25	Nil	100%
Flexion	25	24	01	96%

To distinguish all the four movement with ease two channel four movement approaches were selected. Figure 6.20(a) shows two channel control of elbow where both the channel were stored in two different registers R6 and R7 of 89s52. Comparison of two was used to trigger the H-bridge circuit as depicted in the flowchart of Fig. 6.20(b). In Fig.6.5-6.8 or Table 6.8, the variation of V_{rms} for extension (d) and flexion (u) are reciprocal in nature i.e. channel 0 goes low then channel 1 goes high. Similarly, for pronation (p) and supination (s) the variation is the same but if pronation is compared to extension or supination is compared to flexion then differentiation is a problem. Accordingly the level control was derives as:

- R7 value is more than #8fH then extension will be realized. For this user is required to exert maximum force while performing extension movement at his elbow.
- R7 value is between #6fH and #8fH and R6 value is greater than #6fH then supination is performed by prototype elbow. For this user needs to understand the force exertion level while performing supination at his elbow. This requires lot of training.
- R7 value is between #6fH and #8fH and R6 value is between #2fH and #6fH then pronation is performed by prototype elbow. Again user needs to be trained to overcome the malfunction.
- R7 value is between #2fH and #6fH then flexion of prototype elbow takes place. User needs to exert low force.

The success rate is shown by Table 6.20. This very methodology is an attempt to give the prototype movement natural look but is complicated in performance and control for the user.

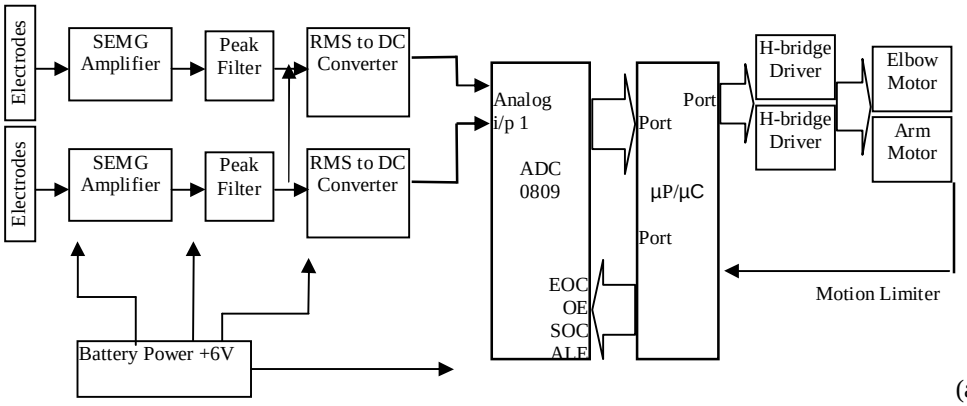

(a)

Microcontroller with the program for two channel-four movements was placed in ZIF connector. Electrode was placed and the SEMG signals were observed on softscope – MATLAB. Movements performed. SEMG were observed on the LED array. V_{ref} of ADC was set accordingly to have full scale LED glow.

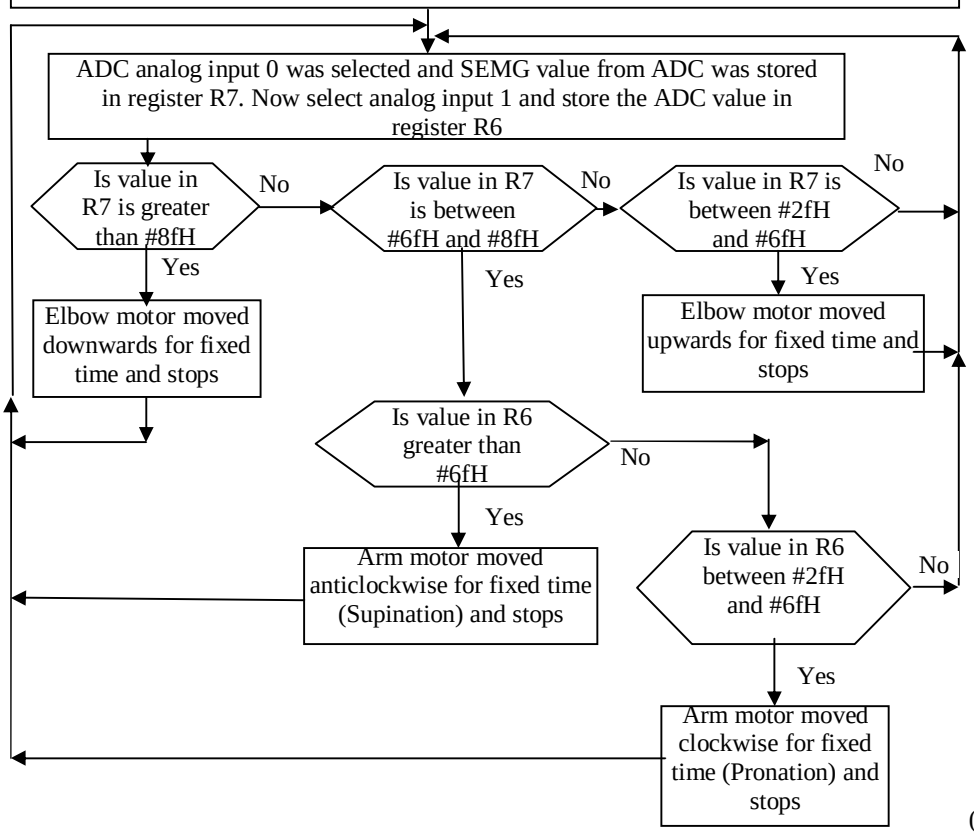

(b)

Fig. 6.20 (a) Block diagram for two channel four movements approach (b) Flowchart for Microcontroller programming

Table 6.13
Testing of the prototype (two channel-four movement)

Intended movement	No. of trials	Controller response		Success percentage
		True	False	
Extension	25	22	03	88%
Supination	25	23	02	92%
Pronation	25	22	03	88%
Flexion	25	23	02	92%

In all the above movements the arm was allowed to move for 160 degrees. It was limited by using limit switches. Whenever these switches got pressed, motor was commanded to do reverse action for a while and then stopped till the next cycle starts based on the SEMG level.

The aim was to develop prosthetic elbow in accordance with the amputees' needs at a reasonable cost. But the main advantages are the low cost of instrumentation and easy customization of the product. The success of this work mainly results from the control strategy proposed and the structure developed for understanding the same. The single channel-two movements (extension/ flexion) found to be the best suited solution considering comfort of operation and natural response of the prototype. Moreover, above elbow amputee does not have location "beblf (below the elbow little finger side)", so the locations "uebt" and "ueblf" [above elbow locations] are available which are found to give best performance for two movements [extension/flexion].

6.4 Single channel SEMG analysis of an elbow amputee

In this section the SEMG analysis were done from the stump muscles of an amputee as shown in the Fig.6.21. The amputation was done from the elbow (elbow disarticulation). Upper elbow muscles were available for the prosthetic uses. The amputee is a male subject of age 33 years old and belongs from a village near Mohali and has lost his left arm partially. The accident happened at his age of around 6 years while using an agriculture machine. The single channel acquisition observations are presented in the Fig.6.23 and the values of the selected parameters are shown in Table 6.14. Location selected is shown in Fig.6.22. Fig.6.23 clearly defines the difference in the wave shape of the two movements i.e. extension and flexion performed by the amputee. The amputee was instructed to copy the action of a healthy subject in his mind and the residue part of the arm. Healthy subject was asked to perform extension and to exert force. Amputee was also trained to do the same with electrode wrapped as per Fig. 6.22. Similarly the other movements were studied. Single channel acquisition was recorded using softscope in the workspace [as explained in section 3.1]

Fig.6.21 Photograph of an elbow amputee

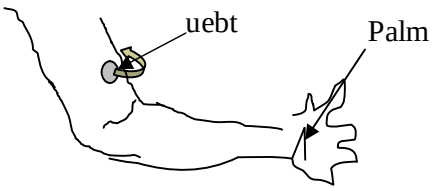

Fig.6.22 Selected location of SEMG acquisition

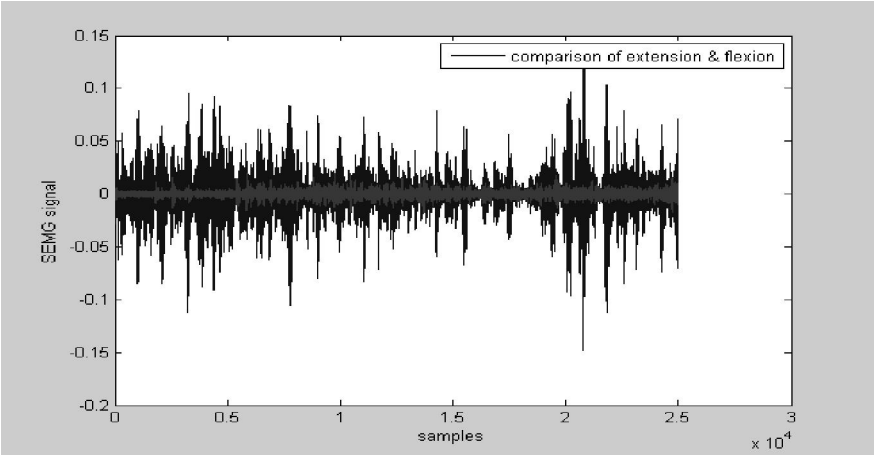

Fig.6.23 MATLAB plot for the comparison of SEMG signal acquired while performing extension (black colour) and flexion (gray colour)

Table 6.14
Calculated values of selected parameters

	Vrms				Slope				Av freq			
	Extension	Flexion	Supination	Pronation	Extension	Flexion	Supination	Pronation	Extension	Flexion	Supination	Pronation
trial 1	0.0293	0.0022	0.0027	0.0042	427.01	51.43	38.83	57.85	158.53	151.11	76.99	159.02
trial 2	0.0479	0.0046	0.0032	0.0028	822.97	59.99	46.24	41.25	161.13	159.02	166.83	83.98
trial 3	0.0375	0.0043	0.0028	0.0043	570.56	68.32	37.07	65.33	156.58	163.41	80.73	164.23
trial 4	0.0465	0.0036	0.0028	0.0044	598.55	54.15	35.71	59.71	163.90	163.09	141.93	160.32
trial 5	0.0331	0.0043	0.0028	0.0019	403.64	66.05	41.82	24.78	160.16	161.13	163.41	24.25

Selected parameters V_{rms}, Slope and Av freq were calculated explained earlier in section 3.4. Reading of five trials flexion and ten trials of extension were recorded in Table 6.14. The comparison was made using plots of the parameters as show in Fig. 6.24-6.26. Fig. 6.26 shows the validity of acquired SEMG signal for extension and flexion as they remain in the selected band nea 180 Hz but supination and pronation plots shows very low or probably no SEMG activity. This is the advantage of calculating Av freq.

It was observed that Extension movement in the amputee achieved higher values of V_{rms} and Slope and Flexion movement was observed to have lower values of V_{rms} and Slope than extension. However for Pronation and Supination no significant changes in SEMG were observed. These observations were similar which is observed for healthy subject in Table 6.1. But the manual observation and the above study suggested that there could be the discrimination of the two movements only. Hence, the prototype elbow having single channel (two movements) can be the best solution.

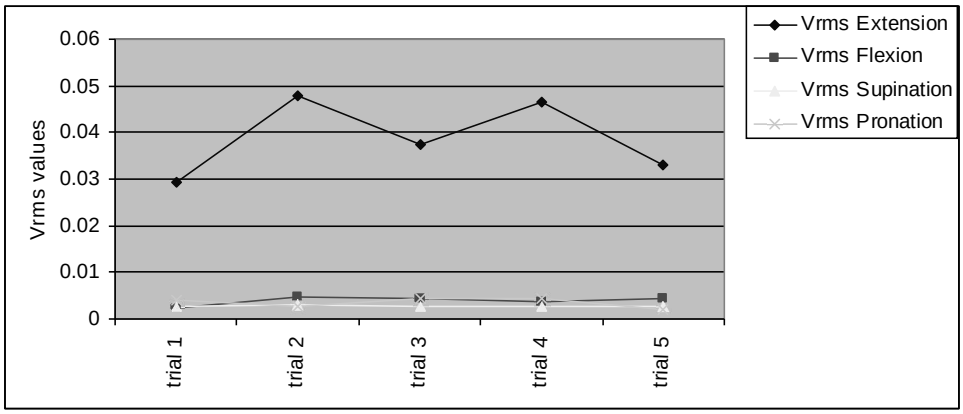

Fig. 6.24 Amputee's SEM-Vrms for elbow movements

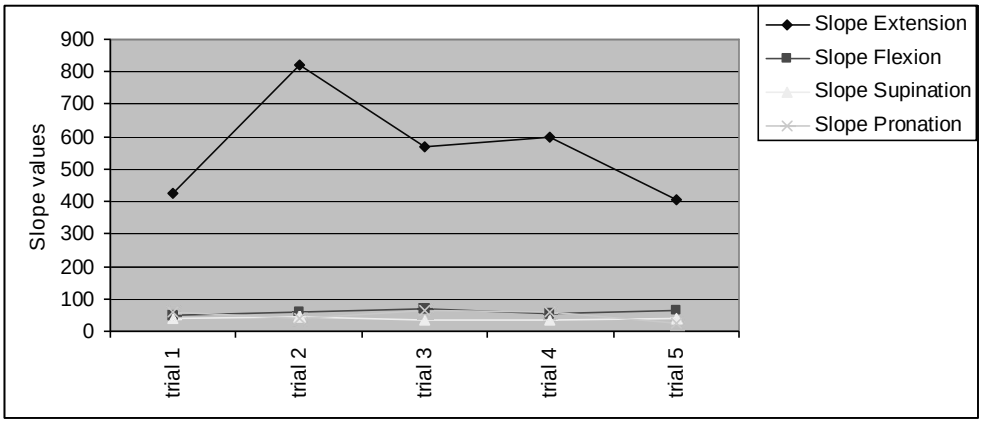

Fig.6.25 Amputee's SEM-Slope for elbow movements

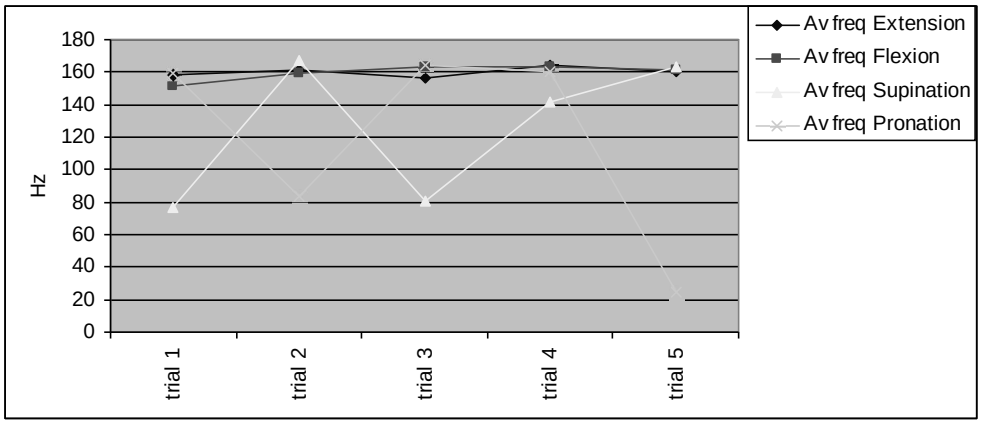

Fig.6.26 Amputee's SEM-Av freq for elbow movements

Chapter's Summary:

Degree of operation of the prosthetic device can be improved or optimized by using proper set of electrodes on proper muscle group. Prototype elbow was developed which will contribute to the developing SEMG based prosthetic devices.

Table A6.1a
2-channel V_{rms} values for extension

	Combination I		Combination II		Combination III	
	channel 0	channel 1	channel 0	channel 1	channel 0	channel 1
Trial 1	0.0992	0.0311	0.0632	0.02	0.0676	0.0785
Trial 1	0.0979	0.0362	0.0756	0.0308	0.1123	0.076
Trial 1	0.0806	0.0374	0.0807	0.0274	0.0991	0.097
Trial 1	0.1045	0.034	0.0823	0.0286	0.0990	0.090
Trial 2	0.1364	0.0223	0.1151	0.0256	0.065	0.1115
Trial 2	0.1685	0.0319	0.1401	0.0489	0.0586	0.1053
Trial 2	0.1545	0.0249	0.1399	0.0539	0.0631	0.1109
Trial 2	0.1402	0.0235	0.1091	0.049	0.072	0.1253
Trial 2	0.114	0.0157	0.1561	0.0675	0.082	0.1137
Trial 3	0.1101	0.0278	0.0942	0.0275	0.0586	0.0449
Trial 3	0.0702	0.0281	0.1086	0.0284	0.0719	0.0472
Trial 3	0.0558	0.0298	0.1068	0.0273	0.076	0.0478
Trial 3	0.0821	0.0255	0.1182	0.0335	0.0842	0.051
Trial 3	0.0913	0.024	0.1147	0.0488	0.0662	0.0469
Trial 4	0.1076	0.0165	0.1158	0.0228	0.0624	0.0751
Trial 4	0.0912	0.0245	0.1553	0.0385	0.0917	0.0901
Trial 4	0.0496	0.0223	0.1777	0.0248	0.0488	0.0681
Trial 4	0.1038	0.0278	0.1803	0.0367	0.061	0.0641
Trial 4	0.0836	0.0201	0.1574	0.028	0.0512	0.0663

Table A6.1b
2-channel Slope values for extension

	Combination I		Combination II		Combination III	
	channel 0	channel 1	channel 0	channel 0	channel 1	channel 0
Trial 1	1096.70	283.47	1416.20	508.25	1178.80	1345.90
Trial 1	1257.00	606.13	1553.70	630.76	1505.40	1280.40
Trial 1	1131.00	376.73	903.66	514.96	1388.20	1496.30
Trial 1	1557.80	411.48	1873.30	546.29	1388.20	1496.30
Trial 2	2147.30	362.86	2058.70	337.62	847.70	1676.70
Trial 2	2676.60	958.19	3089.20	401.97	1315.40	1766.00
Trial 2	1912.00	842.97	2163.00	338.52	1172.80	1977.90
Trial 2	2740.70	753.04	2613.20	331.83	752.70	2326.00
Trial 2	3564.40	787.87	2025.70	248.23	1115.70	1743.10
Trial 3	1444.60	457.56	1467.4	327.4117	741.5655	763.1168
Trial 3	1266.90	364.00	926.0415	391.9991	933.82	697.03
Trial 3	1356.90	367.83	732.76	440.56	1297.90	840.94
Trial 3	2115.40	596.68	1202.00	339.41	1071.10	941.50
Trial 3	1602.10	723.81	1143.90	357.34	1153.00	836.88
Trial 4	2219.4	333.3482	1543.4	242.2753	1093.2	1178.2
Trial 4	2802.10	1219.70	1595.60	299.46	1929.6	1717.3
Trial 4	2619.80	405.60	832.97	351.33	809.80	1171.40
Trial 4	2647.90	711.24	1364.00	396.68	1529.70	1149.70
Trial 4	2480.00	433.05	1675.80	275.16	909.44	934.67

Table A6.2a
2-Channel V_{rms} values for flexion

	Combination I		Combination II		Combination III	
	channel 0	channel 1	channel 0	channel 1	channel 0	channel 1
Trial 1	0.067	0.0498	0.077	0.0558	0.0641	0.0444
Trial 1	0.0704	0.0627	0.065	0.0395	0.0941	0.0589
Trial 1	0.0771	0.0648	0.0505	0.0455	0.0945	0.0747
Trial 1	0.0532	0.0511	0.0668	0.0531	0.0726	0.0483
Trial 2	0.0833	0.0534	0.0889	0.0839	0.0426	0.0239
Trial 2	0.0867	0.0636	0.0602	0.0563	0.0406	0.0627
Trial 2	0.0392	0.0159	0.1027	0.1307	0.0477	0.0633
Trial 2	0.0783	0.0687	0.1036	0.117	0.0551	0.0819
Trial 2	0.0645	0.0459	0.1109	0.1142	0.0178	0.0647
Trial 3	0.0727	0.0355	0.0828	0.0479	0.0526	0.0265
Trial 3	0.0834	0.0595	0.0839	0.0801	0.0597	0.0428
Trial 3	0.0699	0.0465	0.0769	0.0692	0.0518	0.0271
Trial 3	0.0753	0.0472	0.0878	0.0683	0.0449	0.0278
Trial 3	0.0892	0.0746	0.0878	0.0429	0.0612	0.0306
Trial 4	0.096	0.0347	0.0449	0.0331	0.0814	0.1209
Trial 4	0.0947	0.035	0.1009	0.0366	0.0831	0.0959
Trial 4	0.1346	0.0519	0.0892	0.0348	0.0815	0.1144
Trial 4	0.1516	0.0541	0.1131	0.0404	0.108	0.1352
Trial 4	0.0598	0.0374	0.0672	0.0574	0.053	0.0785

Table A6.2b
2-Channel Slope values for flexion

	Combination I		Combination II		Combination III	
	channel 0	channel 1	channel 0	channel 1	channel 0	channel 1
Trial 1	1011.10	718.89	999.43	661.61	1058.90	803.25
Trial 1	891.23	523.15	1289.60	956.28	1360.70	1086.10
Trial 1	856.34	676.30	1185.00	896.74	1280.30	1548.10
Trial 1	872.29	746.60	931.74	930.27	1204.90	721.30
Trial 2	1519.80	1253.40	726.95	1172.60	1017.00	494.43
Trial 2	1038.50	1086.70	980.60	1102.20	689.87	837.81
Trial 2	1338.80	1667.20	366.25	423.78	874.47	1010.00
Trial 2	1506.80	1478.80	1159.10	1226.60	697.14	1302.00
Trial 2	1523.90	1797.00	901.40	1084.20	376.24	957.94
Trial 3	1280.50	601.90	948.11	588.13	676.73	423.36
Trial 3	1086.80	1049.90	1208.30	839.62	807.80	708.56
Trial 3	927.92	1022.90	1029.60	1039.00	667.18	496.05
Trial 3	1206.40	1020.30	1067.60	651.88	698.15	352.61
Trial 3	1206.40	602.54	1148.70	1225.30	1063.80	491.97
Trial 4	795.68	731.57	1477.90	806.22	1282.30	1877.40
Trial 4	1707.20	585.16	1198.20	630.79	1172.80	1428.80
Trial 4	1748.90	813.74	2086.20	762.85	1495.90	1508.10
Trial 4	1852.90	802.45	2501.30	959.95	1917.80	1804.30
Trial 4	974.96	1041.40	874.86	627.24	902.94	1717.20

Table A6.3a
2-Channel V_{rms} values for pronation

	Combination I		Combination II		Combination III	
	channel 0	channel 1	channel 0	channel 1	channel 0	channel 1
Trial 1	0.048	0.0663	0.0473	0.0274	0.0566	0.0555
Trial 1	0.0545	0.0636	0.0475	0.0242	0.0709	0.0603
Trial 1	0.0484	0.0683	0.0466	0.021	0.0528	0.0524
Trial 1	0.0561	0.0623	0.0473	0.0262	0.0627	0.0573
Trial 2	0.0623	0.0495	0.0778	0.0361	0.0398	0.0662
Trial 2	0.0686	0.0788	0.0881	0.0375	0.036	0.0507
Trial 2	0.0719	0.0416	0.0961	0.0352	0.05	0.0662
Trial 2	0.0591	0.0535	0.0776	0.0303	0.0322	0.0377
Trial 2	0.0938	0.0419	0.0618	0.0345	0.0454	0.0641
Trial 3	0.0609	0.0272	0.0737	0.0203	0.0467	0.0325
Trial 3	0.0643	0.0327	0.0853	0.0228	0.0409	0.0365
Trial 3	0.0674	0.0282	0.0876	0.0205	0.037	0.0322
Trial 3	0.0465	0.0247	0.0733	0.0191	0.042	0.0441
Trial 3	0.0552	0.0283	0.0542	0.0222	0.0533	0.0362
Trial 4	0.0397	0.0372	0.0627	0.0476	0.0648	0.1051
Trial 4	0.0523	0.036	0.0757	0.0578	0.0659	0.1089
Trial 4	0.0636	0.0358	0.0557	0.0574	0.0606	0.0917
Trial 4	0.0547	0.0344	0.0416	0.0464	0.1085	0.0978
Trial 4	0.0609	0.0354	0.0813	0.0614	0.0497	0.0757

Table A6.3b
2-Channel Slope values for pronation

	Combination I		Combination II		Combination III	
	channel 0	channel 1	channel 0	channel 0	channel 1	channel 0
Trial 1	703.77	476.99	748.85	1118.10	1021.60	1160.60
Trial 1	657.12	333.81	785.85	910.75	1046.30	1151.30
Trial 1	539.20	353.06	678.85	1046.80	801.40	790.12
Trial 1	771.13	452.47	824.08	844.86	817.98	773.11
Trial 2	1913.40	589.51	1592.70	677.25	543.05	863.64
Trial 2	1626.60	550.78	957.60	1114.10	436.57	791.66
Trial 2	1425.40	530.51	1056.60	601.01	749.66	1017.60
Trial 2	1150.40	376.49	798.64	864.69	492.83	631.87
Trial 2	922.57	469.62	1211.60	526.73	576.49	971.42
Trial 3	921.31	380.61	857.26	432.89	649.19	420.22
Trial 3	1173.00	314.14	1059.70	400.45	667.64	474.04
Trial 3	1051.60	306.79	918.74	488.18	601.70	495.78
Trial 3	1093.20	281.36	717.41	401.41	547.15	767.74
Trial 3	637.72	269.08	767.14	368.60	761.03	517.59
Trial 4	782.36	724.19	539.79	598.63	1428.70	1306.80
Trial 4	1332.60	755.64	851.10	617.55	946.15	1786.90
Trial 4	838.51	1109.60	1052.10	835.41	1023.10	1348.40
Trial 4	574.92	680.37	967.62	498.54	1856.90	1878.20
Trial 4	1287.60	1441.90	821.40	628.78	591.74	998.85

Table A6.4a
2-Channel V_{rms} values for supination

	Combination I		Combination II		Combination III	
	channel 0	channel 1	channel 0	channel 1	channel 0	channel 1
Trial 1	0.0382	0.0302	0.0455	0.0845	0.0528	0.0558
Trial 1	0.0374	0.0332	0.0521	0.116	0.0409	0.0584
Trial 1	0.0416	0.0298	0.0401	0.1151	0.0536	0.0693
Trial 1	0.0404	0.0325	0.0337	0.0956	0.041	0.047
Trial 2	0.0114	0.0082	0.0544	0.1796	0.0321	0.0273
Trial 2	0.0787	0.065	0.0665	0.1881	0.0388	0.0351
Trial 2	0.0524	0.0734	0.0673	0.1915	0.0388	0.0462
Trial 2	0.0595	0.0588	0.0638	0.1393	0.0416	0.0523
Trial 2	0.0586	0.0629	0.0681	0.1447	0.0429	0.0589
Trial 3	0.0444	0.0485	0.0682	0.1201	0.0484	0.0428
Trial 3	0.0542	0.0652	0.065	0.1055	0.053	0.0394
Trial 3	0.0495	0.0515	0.0385	0.1023	0.0505	0.0434
Trial 3	0.0426	0.0584	0.0661	0.1096	0.0456	0.0405
Trial 3	0.0649	0.0633	0.0731	0.1052	0.0306	0.0481
Trial 4	0.061	0.0345	0.0785	0.1377	0.0371	0.078
Trial 4	0.0789	0.0477	0.0806	0.1661	0.0308	0.0553
Trial 4	0.0485	0.0341	0.0976	0.1484	0.0369	0.057
Trial 4	0.0457	0.0386	0.0836	0.1369	0.0334	0.0582
Trial 4	0.0409	0.0583	0.0815	0.1563	0.0376	0.071

Table A6.4b
2-Channel Slope values for supination

	Combination I		Combination II		Combination III	
	channel 0	channel 1	channel 0	channel 0	channel 1	channel 0
Trial 1	615.93	1282.80	491.82	504.02	754.30	864.11
Trial 1	808.85	2028.70	505.78	458.72	533.94	871.67
Trial 1	595.63	2021.70	562.12	428.91	1027.20	878.38
Trial 1	490.36	1424.90	587.78	471.70	566.34	682.26
Trial 2	694.78	2148.60	315.55	143.77	537.61	425.48
Trial 2	867.38	2766.00	1037.60	936.95	502.35	480.14
Trial 2	929.53	3222.30	817.65	995.37	502.35	632.69
Trial 2	947.62	2539.80	1913.90	834.77	607.71	801.75
Trial 2	1088.30	2037.90	1889.50	769.01	706.82	954.11
Trial 3	908.71	1656.90	623.18	682.23	796.04	515.03
Trial 3	782.64	1344.90	730.99	826.68	597.17	453.50
Trial 3	649.13	1252.19	809.13	925.61	743.20	589.01
Trial 3	962.62	1539.20	615.57	757.09	596.59	653.20
Trial 3	1114.80	1690.40	850.26	809.54	391.48	777.51
Trial 4	1219.30	2122.80	1018.10	621.62	545.94	949.49
Trial 4	1251.90	2951.30	1087.60	806.95	415.98	744.80
Trial 4	1309.50	2173.30	652.88	523.19	484.25	711.61
Trial 4	1500.30	2178.90	648.90	477.39	435.74	887.89
Trial 4	1078.00	2757.20	600.75	760.77	575.29	1223.50

Table A6.5(a)
Inter-relation of the chosen locations using V_{rms} values

Extension			Flexion			Pronation			Supination		
bebtd	beblfd	ueblfd	bebtu	beblfu	ueblfu	bebtp	beblfp	ueblfp	bebts	beblfs	ueblfs
0.0992	0.0632	0.0676	0.067	0.077	0.0566	0.048	0.0473	0.0566	0.0382	0.0455	0.0528
0.0979	0.0756	0.1123	0.0704	0.065	0.0709	0.0545	0.0475	0.0709	0.0374	0.0521	0.0409
0.0806	0.0807	0.0991	0.0771	0.0505	0.0528	0.0484	0.0466	0.0528	0.0416	0.0401	0.0536
0.1045	0.0823	0	0.0532	0.0668	0.0627	0.0561	0.0473	0.0627	0.0404	0.0337	0.041
0.1364	0.1151	0.065	0.0833	0.0889	0.0398	0.0623	0.0778	0.0398	0.0114	0.0544	0.0321
0.1685	0.1401	0.0586	0.0867	0.0602	0.036	0.0686	0.0881	0.036	0.0787	0.0665	0.0388
0.1545	0.1399	0.0631	0.0392	0.1027	0.05	0.0719	0.0961	0.05	0.0524	0.0673	0.0388
0.1402	0.1091	0.072	0.0783	0.1036	0.0322	0.0591	0.0776	0.0322	0.0595	0.0638	0.0416
0.114	0.1561	0.082	0.0645	0.1109	0.0454	0.0938	0.0618	0.0454	0.0586	0.0681	0.0429
0.1101	0.0942	0.0586	0.0727	0.0828	0.0467	0.0609	0.0737	0.0467	0.0444	0.0682	0.0484
0.0702	0.1086	0.0719	0.0834	0.0839	0.0409	0.0643	0.0853	0.0409	0.0542	0.065	0.053
0.0558	0.1068	0.076	0.0699	0.0769	0.037	0.0674	0.0876	0.037	0.0495	0.0385	0.0505
0.0821	0.1182	0.0842	0.0753	0.0878	0.042	0.0465	0.0733	0.042	0.0426	0.0661	0.0456
0.0913	0.1147	0.0662	0.0892	0.0878	0.0533	0.0552	0.0542	0.0533	0.0649	0.0731	0.0306
0.1076	0.1158	0.0624	0.096	0.0449	0.0648	0.0397	0.0627	0.0648	0.061	0.0785	0.0371
0.0912	0.1553	0.0917	0.0947	0.1009	0.0659	0.0523	0.0757	0.0659	0.0789	0.0806	0.0308
0.0496	0.1777	0.0488	0.1346	0.0892	0.0606	0.0636	0.0557	0.0606	0.0485	0.0976	0.0369
0.1038	0.1803	0.061	0.1516	0.1131	0.1085	0.0547	0.0416	0.1085	0.0457	0.0836	0.0334
0.0836	0.1574	0.0512	0.0598	0.0672	0.0497	0.0609	0.0813	0.0497	0.0409	0.0815	0.0376
0.0311	0.02	0.0785	0.067	0.0558	0.0555	0.0663	0.0274	0.0555	0.0302	0.0845	0.0558
0.0362	0.0308	0.076	0.0704	0.0395	0.0603	0.0636	0.0242	0.0603	0.0332	0.116	0.0584
0.0374	0.0274	0.097	0.0771	0.0455	0.0524	0.0683	0.021	0.0524	0.0298	0.1151	0.0693
0.034	0.0286	0	0.0532	0.0531	0.0573	0.0623	0.0262	0.0573	0.0325	0.0956	0.047
0.0223	0.0256	0.1115	0.0833	0.0839	0.0662	0.0495	0.0361	0.0662	0.0082	0.1796	0.0273
0.0319	0.0489	0.1053	0.0867	0.0563	0.0507	0.0788	0.0375	0.0507	0.065	0.1881	0.0351
0.0249	0.0539	0.1109	0.0392	0.1307	0.0662	0.0416	0.0352	0.0662	0.0734	0.1915	0.0462
0.0235	0.049	0.1253	0.0783	0.117	0.0377	0.0535	0.0303	0.0377	0.0588	0.1393	0.0523
0.0157	0.0675	0.1137	0.0645	0.1142	0.0641	0.0419	0.0345	0.0641	0.0629	0.1447	0.0589
0.0278	0.0275	0.0449	0.0727	0.0479	0.0325	0.0272	0.0203	0.0325	0.0485	0.1201	0.0428
0.0281	0.0284	0.0472	0.0834	0.0801	0.0365	0.0327	0.0228	0.0365	0.0652	0.1055	0.0394
0.0298	0.0273	0.0478	0.0699	0.0692	0.0322	0.0282	0.0205	0.0322	0.0515	0.1023	0.0434
0.0255	0.0335	0.051	0.0753	0.0683	0.0441	0.0247	0.0191	0.0441	0.0584	0.1096	0.0405
0.024	0.0488	0.0469	0.0892	0.0429	0.0362	0.0283	0.0222	0.0362	0.0633	0.1052	0.0481
0.0165	0.0228	0.0751	0.096	0.0331	0.1051	0.0372	0.0476	0.1051	0.0345	0.1377	0.078
0.0245	0.0385	0.0901	0.0947	0.0366	0.1089	0.036	0.0578	0.1089	0.0477	0.1661	0.0553
0.0223	0.0248	0.0681	0.1346	0.0348	0.0917	0.0358	0.0574	0.0917	0.0341	0.1484	0.057
0.0278	0.0367	0.0641	0.1516	0.0404	0.0978	0.0344	0.0464	0.0978	0.0386	0.1369	0.0582
0.0201	0.028	0.0663	0.0598	0.0574	0.0757	0.0354	0.0614	0.0757	0.0583	0.1563	0.071

Table A6.5(b)
Inter-relation of the chosen locations using slope values

Extension			Flexion			Pronation			Supination		
bebtd	beblfd	ueblfd	bebtu	beblfu	ueblfu	bebtp	beblfp	ueblfp	bebts	beblfs	ueblfs
1096.70	1416.20	1178.80	1011.10	999.43	1058.90	703.77	748.85	1021.60	615.93	491.82	754.30
1257.00	1553.70	1505.40	891.23	1289.60	1360.70	657.12	785.85	1046.30	808.85	505.78	533.94
1131.00	903.66	1388.20	856.34	1185.00	1280.30	539.20	678.85	801.40	595.63	562.12	1027.20
1557.80	1873.30	1388.20	872.29	931.74	1204.90	771.13	824.08	817.98	490.36	587.78	566.34
2147.30	2058.70	847.70	1519.80	726.95	1017.00	1913.40	1592.70	543.05	694.78	315.55	537.61
2676.60	3089.20	1315.40	1038.50	980.60	689.87	1626.60	957.60	436.57	867.38	1037.60	502.35
1912.00	2163.00	1172.80	1338.80	366.25	874.47	1425.40	1056.60	749.66	929.53	817.65	502.35
2740.70	2613.20	752.70	1506.80	1159.10	697.14	1150.40	798.64	492.83	947.62	1913.90	607.71
3564.40	2025.70	1115.70	1523.90	901.40	376.24	922.57	1211.60	576.49	1088.30	1889.50	706.82
1444.60	1467.4	741.5655	1280.50	948.11	676.73	921.31	857.26	649.19	908.71	623.18	796.04
1266.90	926.0415	933.82	1086.80	1208.30	807.80	1173.00	1059.70	667.64	782.64	730.99	597.17
1356.90	732.76	1297.90	927.92	1029.60	667.18	1051.60	918.74	601.70	649.13	809.13	743.20
2115.40	1202.00	1071.10	1206.40	1067.60	698.15	1093.20	717.41	547.15	962.62	615.57	596.59
1602.10	1143.90	1153.00	1206.40	1148.70	1063.80	637.72	767.14	761.03	1114.80	850.26	391.48
2219.4	1543.4	1093.2	795.68	1477.90	1282.30	782.36	539.79	1428.70	1219.30	1018.10	545.94
2802.10	1595.60	1929.6	1707.20	1198.20	1172.80	1332.60	851.10	946.15	1251.90	1087.60	415.98
2619.80	832.97	809.80	1748.90	2086.20	1495.90	838.51	1052.10	1023.10	1309.50	652.88	484.25
2647.90	1364.00	1529.70	1852.90	2501.30	1917.80	574.92	967.62	1856.90	1500.30	648.90	435.74
2480.00	1675.80	909.44	974.96	874.86	902.94	1287.60	821.40	591.74	1078.00	600.75	575.29
283.47	508.25	1345.90	718.89	661.61	803.25	476.99	1118.10	1160.60	1282.80	504.02	864.11
606.13	630.76	1280.40	523.15	956.28	1086.10	333.81	910.75	1151.30	2028.70	458.72	871.67
376.73	514.96	1496.30	676.30	896.74	1548.10	353.06	1046.80	790.12	2021.70	428.91	878.38
411.48	546.29	1496.30	746.60	930.27	721.30	452.47	844.86	773.11	1424.90	471.70	682.26
362.86	337.62	1676.70	1253.40	1172.60	494.43	589.51	677.25	863.64	2148.60	143.77	425.48
958.19	401.97	1766.00	1086.70	1102.20	837.81	550.78	1114.10	791.66	2766.00	936.95	480.14
842.97	338.52	1977.90	1667.20	423.78	1010.00	530.51	601.01	1017.60	3222.30	995.37	632.69
753.04	331.83	2326.00	1478.80	1226.60	1302.00	376.49	864.69	631.87	2539.80	834.77	801.75
787.87	248.23	1743.10	1797.00	1084.20	957.94	469.62	526.73	971.42	2037.90	769.01	954.11
457.56	327.4117	763.1168	601.90	588.13	423.36	380.61	432.89	420.22	1656.90	682.23	515.03
364.00	391.9991	697.03	1049.90	839.62	708.56	314.14	400.45	474.04	1344.90	826.68	453.50
367.83	440.56	840.94	1022.90	1039.00	496.05	306.79	488.18	495.78	1252.19	925.61	589.01
596.68	339.41	941.50	1020.30	651.88	352.61	281.36	401.41	767.74	1539.20	757.09	653.20
723.81	357.34	836.88	602.54	1225.30	491.97	269.08	368.60	517.59	1690.40	809.54	777.51
333.3482	242.2753	1178.2	731.57	806.22	1877.40	724.19	598.63	1306.80	2122.80	621.62	949.49
1219.70	299.46	1717.3	585.16	630.79	1428.80	755.64	617.55	1786.90	2951.30	806.95	744.80
405.60	351.33	1171.40	813.74	762.85	1508.10	1109.60	835.41	1348.40	2173.30	523.19	711.61
711.24	396.68	1149.70	802.45	959.95	1804.30	680.37	498.54	1878.20	2178.90	477.39	887.89
433.05	275.16	934.67	1041.40	627.24	1717.20	1441.90	628.78	998.85	2757.20	760.77	1223.50

Table A6.6

Principal component results for comparison of above elbow locations vs. best locations using slope values

Descriptive Statistics			
Variable	Mean	Std Dev.	Std Err
ueblfd	1249.299	390.712	63.382
ueblfu	1021.427	432.007	70.081
ueblfp	886.974	384.155	62.318
ueblfs	668.853	192.876	31.289
beblfd	1306.161	903.507	146.568
beblfu	1093.850	372.559	60.437
beblfp	784.193	412.309	66.885
beblfs	1498.818	724.602	117.546

Covariance Matrix								
	ueblfd	ueblfu	ueblfp	ueblfs	beblfd	beblfu	beblfp	beblfs
ueblfd	152655.891	45529.727	45773.731	2952.461	-37392.365	29881.821	-33474.643	130019.804
ueblfu	45529.727	186629.637	123313.576	26239.636	-14817.426	522.561	13939.071	96716.111
ueblfp	45773.731	123313.576	147574.789	15497.897	-33704.109	-12985.423	-21862.201	114051.534
ueblfs	2952.461	26239.636	15497.897	37201.294	-76959.082	-23388.415	-10992.704	42333.880
beblfd	-37392.365	-14817.426	-33704.109	-76959.082	816324.864	182611.019	217857.071	-311056.894
beblfu	29881.821	522.561	-12985.423	-23388.415	182611.019	138800.231	44450.577	-14300.407
beblfp	-33474.643	13939.071	-21862.201	-10992.704	217857.071	44450.577	169998.424	-98528.779
beblfs	130019.804	96716.111	114051.534	42333.880	-311056.894	-14300.407	-98528.779	525048.598

Explained Variance (Eigenvalues)								
Value	PC 1	PC 2	PC 3	PC 4	PC 5	PC 6	PC 7	PC 8
Eigenvalue	1139006.666	471786.484	214172.799	128359.147	93543.985	69211.929	35139.898	23012.819
% of Var.	52.387	21.699	9.850	5.904	4.302	3.183	1.616	1.058
Cum. %	52.387	74.086	83.936	89.840	94.142	97.325	98.942	100.000

Component Loadings								
Variable	PC 1	PC 2	PC 3	PC 4	PC 5	PC 6	PC 7	PC 8
ueblfd	-0.297	0.550	-0.207	0.547	0.386	0.343	0.001	0.014
ueblfu	-0.201	0.618	0.698	0.019	0.130	-0.129	-0.210	-0.114
ueblfp	-0.302	0.615	0.583	0.153	-0.213	-0.016	0.332	0.108
ueblfs	-0.466	0.014	0.289	-0.194	0.111	0.020	-0.395	0.702
beblfd	0.932	0.332	-0.058	0.008	-0.116	0.048	-0.034	0.007
beblfu	0.465	0.448	-0.389	0.165	0.298	-0.554	0.075	0.052
beblfp	0.627	0.184	0.131	-0.572	0.437	0.142	0.133	0.005
beblfs	-0.743	0.577	-0.265	-0.187	-0.095	0.015	-0.018	-0.011

Component Score Coefficients (Eigenvectors)								
Variable	PC 1	PC 2	PC 3	PC 4	PC 5	PC 6	PC 7	PC 8
ueblfd	-0.109	0.313	-0.175	0.597	0.493	0.509	0.003	0.036
ueblfu	-0.081	0.389	0.651	0.023	0.184	-0.211	-0.483	-0.325
ueblfp	-0.109	0.344	0.484	0.164	-0.267	-0.024	0.680	0.273
ueblfs	-0.084	0.004	0.120	-0.104	0.070	0.015	-0.406	0.893
beblfd	0.789	0.437	-0.114	0.021	-0.342	0.166	-0.163	0.040
beblfu	0.162	0.243	-0.313	0.172	0.363	-0.785	0.148	0.129
beblfp	0.242	0.110	0.117	-0.658	0.589	0.223	0.292	0.013
beblfs	-0.504	0.609	-0.414	-0.377	-0.226	0.041	-0.069	-0.053

CHAPTER 7
CONCLUSION AND FUTURE SCOPE

This chapter outlines the conclusions of the research done and the scope of the technology in 21st century.

Prosthetics are important to improve amputees' lifestyles and in order to do so there have been many studies aimed at allowing control over the prosthetic appendage. Surface Electromyogram (SEMG) is used for the study of muscle activities and to develop myoelectric prosthesis in the present investigation.

This thesis presents development of a control methodology to use myoelectric signals from muscles as the control signals to operate the elbow prosthesis. Implementation of the SEMG amplifier device, SEMG recording technique and development of artificial elbow were discussed in details. SEMG recording technique was developed to measure and record the signals from the SEMG amplifier with the aim to use the same circuit later to drive elbow-prototype. The study of different parameters in relation to SEMG variations with force level was carried out and found that both amplitude related parameters and selected statistical parameters gave good view of force level exerted by muscles. The SEMG amplitude based parameter resulted into linear variations up to around 80% of the maximum voluntary contraction of a subject. Proposed function slope gives good representation of the SEMG. SEMG frequency based variation remains constant in a narrow band. The effect of prolong use of the device was studied and found to result in lower level of SEMG signals. Therefore, the design and method of acquisition systems was developed with the capability of adjusting SEMG level to get proper degree of controllability.

As an additional study, electrode locations to have multifunctional prosthesis, acupressure points were considered. The study explored that electrode sites can be considered where even very weak correlation between the measured signal (SEMG) and limb functions (more than one) existed. In this work selection of acupressure point were chosen from the anatomically valid locations. At four pressure points on arm, SEMG signal behaviour was studied and the similar linear relationship was observed during forced-grasping as that of studies done in chapter 3(with non pressure point). Hence, it is concluded that acupressure points shows SEMG activities useful for multifunctional prosthetics. SEMG parameters have also been experimented with

variable force exerted by the muscles both for above-elbow and below elbow and it was observed that above elbow showed higher level of SEMG activities.

The analysis has been done on the SEMG signals from six locations on arm for discriminating four movements of hand (taken from three male subjects). Hand movements chosen were opening and closing of grip, up and down movement of wrist. Six locations also included two pressure points on wrist to study the comparison among the locations. Analysis resulted into classification of these locations with respect to specific movement and numbers of acquisition channels. To understand the optimum requirement of number of channels for such interpretations, principal component analysis was done. After the principal component analysis from different locations, it is found that in two channel locations namely "cbet (below elbow thumb side) and cbeb (below elbow little finger side)" and in three channel locations namely "cam (below arm middle palm side)", "camb (opposite side of cam)" and "cbet (below elbow thumb side)" were best suited to discriminate the four chosen movements. However, the selected pressure points showed low performance *w.r.t.* the other locations. Best location was related to the maximum loading percentage to PC1 and appropriate numbers of channel of the acquisition system to monitor movements again depended upon the loading percentage to PC1 but shall vary within *i.e.* different movements had different contribution percentages for better discrimination.

Further, SEMG analysis on the elbow movement for the four operations (extension, flexion, supination and pronation) was discussed which resulted into control methodology for single-channel and two-channel prototype elbow. Principal component analyses from four different locations were analyzed to discriminate the four chosen operations with two channel approach. The analysis of elbow movement suggested that combination II was the best which had one location at "uebt (above elbow thumb side)" and other at "beblf (below elbow little finger side)". However, elbow amputees' does not have location "beblf (below the elbow little finger side)" available. A compromising solution is needed with the existing locations *i.e.* "uebt (above elbow thumb side)" and "ueblf (above elbow locations)" to give best performance for elbow movements.

A prototype above elbow based on SEMG analysis had been developed using microcontroller based hardware. The prototype elbow had been developed using single channel and two channel acquisition circuits respectively to realize two movement controls (extension/flexion) and four movement controls

(extension/flexion/pronation/supination). The single channel-two movements (extension/ flexion) found to be the best suited solution considering operational success and natural response of the prototype model. Although all the mentioned studies were conducted on healthy subjects but additionally, a study was also conducted on an amputee for the single channel-two movement elbow prototype. The SEMG results for the four selected elbow movements from the amputee found to be the same as of the healthy subject.

This work presents a successful creation of inexpensive SEMG platform. Ultimate goal is to realize the artificial limb whose functionality is close to human arm where this work is an effort. The effort to achieve this goal will always was encouraging the researchers into the field of SEMG technologies.

For the future development of the SEMG technologies, following suggestion are made:

1. Although the value of SEMG has been proven in fundamental researches and for specific diagnostic questions, there is as yet no broad clinical application. This is partly due to limitations of construction principles and application techniques of conventional electrode systems. Multi-electrode grid can be the better solution for movement discrimination.

1) The material used as electrode carrier *e.g.* polyimid allows grids to be cut out in any required shape or size. The high mechanical flexibility can be allowed in electrode grid to follow the skin surface even in areas with very uneven contours, resulting in good electrical connections in the whole recording area.
2) The processors with high programming capabilities can be used to handle large data from SEMG electrodes (multi-electrode) and to analyze these data for future use. The system's sensitivity needs to be further improved the low functional arm/hand movements.
3) To remove the motion artifacts from wired electrode systems, wireless sensor network technologies are likely to produce better results.
4) More study on reliability of acupressure or other similar points *e.g* acupuncture points may be carried out. This will help in establishing SEMG sites on the skin for specific movements.
5) Evolutionary classification techniques can be explored for better discrimination of large number of movements.

6) Prosthetic devices can be developed by using newly discovered alloys or composite materials as they are light weight and hard enough to meet the requirements. The greatest advantage is the ease of machining which can fulfill the laws of biomechanics of human arm.
7) The study on energy efficient motors, driving circuits and couplings can further improve the degree of functionalities of prosthetic devices.

Practical medical applications involves SEMG use in pre/post surgical assessment and treatment, prevention or retardation of muscle atrophy, increasing local blood circulation, relaxation of muscle spasms, maintaining or increasing range of motion, and muscle re-education and rehabilitation through biofeedback. Extending beyond the traditional use of SEMG in physiological and biomechanical research, SEMG has well established value as an evaluation tool used in applied research, physiotherapy, rehabilitation, sports medicine/training, bio-feedback and ergonomics research.

References

1. Abul-Haj Cary and Hogan Neville, “An Emulator System for Developing Improved Elbow-Prosthesis Designs”, IEEE Trans. on Biomedical Engineering, vol. BME-34, no. 9, pp. 724-737, Sep. 1987
2. Ajiboye AB and Weir F ff, “A heuristic fuzzy logic approach to EMG pattern recognition to multifunctional prosthesis control” IEEE Transaction on Neural Systems and Rehabilitation Engineering, pp: 1678-1681, September 2005
3. Agarwal Gyan C and Gottlieb Gerald L, “An analysis of the electromyogram by Fourier, simulation and experimental techniques”, IEEE Trans. Biomedical Engineering, vol. BME-22, no. 3, pp. 225 – 229, May 1975
4. Agarabi Mina,“ An SEMG based method for assessing the design of computer mice”, The 26th International Conference of the IEEE Engineering in Medicine and Biology Society, San Francisco, pp:301-302, September 2004
5. Al-Assaf Y, “Surface myoelectric signal analysis: dynamic approaches for change detection and classification”, IEEE Trans. Biomedical Engineering, vol. 53, no.11, pp.2248 – 2256, Nov. 2006
6. Albers A, Brudniok S, Ottnad J, Sauter C and Sedchaicharn K, “Upper body of a new humanoid robot - the design of ARMAR, 6th IEEE-RAS International Conference Humanoid robots, Genova, pp. 308 – 313, Dec. 4-6, 2006, DOI: 10.1109/ICHR.2006.321289
7. Alberts, Bray, Johnson, Lewis, Raff, Roberts & Walter, “Propagation of an action potential”, 1998, http://www.essentialcellbiology.com
8. Alberts, Bray, Johnson, Lewis, Raff, Roberts, Walter, “Propagation of an action potential” http://www.essentialcellbiology.com, 1998
9. Anctil B and Slawnych MP, “An efficient method for modelling EMG potentials as recorded using surface electrodes”, Proceedings 20th Annual International Conference Engineering in Medicine and Biology Society, IEEE, vol. 5, pp. 2613 – 2615, Oct. 29 - Nov. 1,1998
10. Arora AS, “Development of control strategies for EMG based control of multifunction prosthetic hand” Ph.D. Thesis, IIT, Roorkee, 2002
11. Arora AS, “Modified adaptive resonance theory based control strategy for EMG operated prosthesis for below-elbow amputee”, Journal of Medical Engineering & Technology, vol. 31, no. 3, pp.191 – 201, 2007
12. Artemiadis PK and Kyriakopoulos KJ, “EMG-based position and force control of a robot arm: Application to teleoperation and orthosis”, International conference on Advanced intelligent mechatronics, IEEE/ASME , pp. 1-6, 2007, DOI: 10.1109/AIM.2007.4412420
13. Artigue V and Thomann G, “Development of a prosthetic arm: experimental validation with the user and adapted software”, IEEE International Conference on Robotic and Automation, ICRA09, Kobe, Japan, hal-00400808, version 1 – 1, Jul 2009
14. Beck Sebastian, Mikut Ralf, Lehmann Arne and Bretthauer Georg, “Model-based control and object contact detection for a fluidic actuated robotic hand” Proceedings, 42nd IEEE Conference Decision and Control, Maui, Hawaii USA, p.6369, Dec. 2003
15. Bergamasco M and Scattareggia Marchese S, “The mechanical design of the MARCUS prosthetic hand”, Proceedings 4th IEEE International Workshop Robot and Human Communication, , pp. 95 – 100, July 5-7, 1995
16. Bonato P, D'alessio T and Knaflitz M, “A statistical method for the measurement of muscle activation intervals from surface myoelectric signal during gait”, IEEE Trans. Biomedical Engineering, vol. 45, no.3, pp.287 – 299, March 1998, DOI-10.1109/10.661154
17. Bonato P, Gagliati G and Knaflitz M, “Analysis of myoelectric signals recorded during dynamic contractions”, IEEE Magazine Engineering in Medicine and Biology, vol. 15, no. 6, pp.102 – 111, 1996

18. Bonivento C and Fantuzzi C, “Supervisory system of myoelectric prostheses”, Proceedings of the 1998 IEEE International Conference Control Applications, vol. 1, pp. 61-65, Sept. 1-4 1998, DOI:10.1109/CCA.1998.728245

19. Bouchard S, Rancourt D and Clancy EA, “EMG-to-torque dynamic relationship for elbow constant angle contractions”, Proceedings Conference BMES/EMBS, vol.1, p.573, Oct. 13-16 1999, DOI:10.1109/IEMBS.1999.802651

20. Bowen RC, Seliktar R, Rahman T and Alexander M, “Surface EMG and motor control of the upper extremity in muscular dystrophy: a pilot study”, Proceedings of the 23rd Annual International Conference of the Engineering in Medicine and Biology Society, IEEE, vol.2, pp.1220 – 1223, 2001

21. Boyd JD, Clark Wilfred Le Gros, Hamilton WJ, Yoffey JM, Zuckerman Solly and Appleton AB, “Textbook of Human Anatomy”, London, Macmillan and Co. Ltd. 1956

22. Bruce Lori M, “Bioelectric Potential” IEEE potentials,pp.5-8, Jan 1999

23. Buchenrieder Klaus, “Dimensionality Reduction for the Control of Powered Upper Limb Prostheses”, Proceedings 14th annual IEEE International Conference and Workshops Engineering of Computer-Based Systems (ECBS'07), 2007

24. Cao Thanh D, “Acupressure point treating system” USA Patent No. :US6,299,586B1, Oct. 9, 2001

25. Caohua Hua, Hajj Dib I El, Antoni J and Marque C, “Analysis of muscular fatigue during cyclic dynamic movement”, 29th Annual International Conference Engineering in Medicine and Biology Society, EMBS 2007, IEEE, pp.1880 – 1883, Aug. 22-26, 2007

26. Casolo Federico, Cinquemani Simone and Cocetta Matteo “Functional design of a transmission for a myoelectric elbow prosthesis” Proceedings World Congress on Engineering London, U.K., vol.3, pp. 978-988, July 2008

27. Cattin E, Roccella S, Vitiello N, Vecchi F, and Carrozza MC, “NEUROExos elbow module: a new exoskeleton for elbow rehabilitation”

28. Chapman Arthur, “Book: Biomechanical Analysis of Fundamental Human Movements” ISBN: 0-7360-6402-8, edition 1, Human Kinetics Publication, 2008

29. Chan FH, Yang YS, Lam FK, Zhang YT and Parker PA, “Fuzzy EMG classification for prosthesis control”, IEEE Trans. Rehabil. Eng., vol.8, pp.305-311, Sep. 2000

30. Chauvet E, Fokapu O, Hogrel JY, Gamet D, and Duchene, “A method of EMG decomposition based on fuzzy logic” Engineering in Medicine and Biology Society, IEEE Proceedings of the 23rd Annual International Conference of the UMR CNRS, vol 2, pp:1948-1950, 2001

31. Chen Xiang, Zhang Xu, Zhao Zhang-Yan, Yang Ji-Hai, Lantz Vuokko and Wang Kong-Qiao, “Multiple hand gesture recognition based on surface EMG signal”, 1st International Conference on Bioinformatics and Biomedical Engineering, ICBBE 2007, no. 6, pp. 506 – 509, July 2007

32. Chunling Liu and Xu Wang, “Development of the system to detect and process electromyogram signals”, 27th Annual International Conference Engineering in Medicine and Biology Society, IEEE-EMBS 2005, pp. 6627 – 6630, 2005

33. Cipriani Christian, Zaccone Franco, Micera Silvestro, and Carrozza M Chiara, “On the Shared Control of an EMG-Controlled Prosthetic Hand: Analysis of User–Prosthesis Interaction, IEEE Trans. on robotics, vol. 24, no. 1, pp. 170-184, 2008

34. Cram Jeffrey R, “Massage: A Surface EMG Comparison of the Effects of a body cushion Versus a Standard Massage Table” Journal of Myofascial Tharapy, vol.1, no.3, Oct. 1994

35. Cram JR, Kasman GS and Holtz J, “Introduction to Surface Electromyography,” Gaithersburg, Maryland, Aspen Publication, 1998

36. De Luca Carlo J, “Physiology and mathematics of myoelectric signals”, IEEE Trans. on Biomedical Engineering, vol. BME-26, no. 6, pp.313-325, 1979

37. De Luca CJ, “Surface electromyography: detection and recording,” www.delsys.com/emg.shtml, Delsys Inc., 1996

38. De Luca CJ, “The use of surface electromyography in biomechanics,” www.delsys.com/emg.shtml, Neuromuscular Research Centre and Biomedical Engineering Dept. and Neurology Dept., Boston University, Delsys Inc., 1997

39. Delis Alberto Lopez, Rocha Adson Ferreira da, Santos Icaro dos, Sene Iwens Gervásio Jr, Salomoni Sauro and Borges Geovany Araujo, “Development of a microcontrolled bioinstrumentation system for active control of leg prostheses”, 30th Annual International IEEE EMBS Conference, Vancouver, Canada, pp.2393-2396, August 20-24, 2008

40. Dingwell JB, Joubert JE, Diefenthaeler F and Trinity JD,“Changes in muscle activity and kinematics of highly trained cyclists during fatigue”, IEEE Trans. on Biomedical Engineering, vol. 55, no. 11, pp. 2666 - 2674, Nov. 2008, DOI:10.1109/TBME.2008.2001130

41. Doringer JA and Hogan N, “Performance of above elbow body-powered prostheses in visually guided unconstrained motion tasks” IEEE Transactions on Biomedical Engineering, vol. 42, no. 6, pp. 621-631, 1995

42. Englehart KB and Parker PA, “Single motor unit myoelectric signal analysis with nonstationary data”, IEEE Trans. on Biomedical Engineering, vol. 41, no. 2, pp. 168 – 180, Feb. 1994, DOI:10.1109/10.284928

43. Farina Dario, Pozzo Marco, Merlo Enrico, Bottin Andrea and Merletti Roberto," Assessment of average muscle fiber conduction velocity from surface EMG signals during fatiguing dynamic contractions, IEEE Trans. Biomedical Engineering, vol. 51,no. 8, pp. 1383-1392, 2004

44. Farnsworth Troy, “The call to arms” BSME, CP, FAAOP, Active Living Magazine, Aug 3, 2004

45. Farrell Stephanie, Kadlowec Jennifer, Marchese Anthony, Schmalze John, and Mandayam Shreekanth, “A unique learning system for engineering: technology of the human body”, Proceedings American Society for Engineering Education, 2002

46. Fermo De Vincenzo, Bastos-Filho and Dynnikov, “Development of an adaptive framework for the control of upper limb myoelectric prosthesis”, Proceedings, 22nd Annual International Conference Engineering in Medicine and Biology Society IEEE, vol.4, pp.2402 – 2405, July 23-28, 2000

47. Finat J and Lcipez- Coronado J, “A hybrid model for the hand preconfiguration in rehabilitation grasping tasks” IEEE, p.3448, 1998

48. Gaur AM, Kumar Amod and Rana Dinesh Singh, “Microcontroller based myo trainer system for displaying EMG signal on graphical liquid crystal display”, Proceedings of the World Congress on Engineering, WCE 2010, vol. 2, London, U.K., June 30 - July 2, 2010

49. Georgakis A, Stergioulas LK and Giakas G, “Fatigue Analysis of the Surface EMG Signal in Isometric Constant Force Contractions Using the Averaged Instantaneous Frequency” IEEE Transactions On Biomedical Engineering, Vol. 50, No. 2, pp.262-265, February 2003

50. Gerber Andreas, Roland M, De Figureueiredo Rui JP and Moschytz George S, “A new framework and computer program for quantitative EMG signal analysis”, IEEE Trans. Biomedical Engineering, vol. BME-31, p.12, December 1988

51. Gibbons David T, O'riain Micheal D and Philippe-Auguste Sebastien, “An above-elbow prosthesis employing programmed linkages”, IEEE Trans. Biomedical Engineering, vol. BME-34, pp.493–498, 1987

52. Giuffrida JP and Crago PE, “Reciprocal EMG control of elbow extension by FES”, IEEE Trans. on Neural Systems and Rehabilitation Engineering, vol.9, no.4, pp.338-345, 2001, DOI: 10.1109/7333.1000113

53. Goehler Craig M, PhD thesis, “design of a humanoid shoulder-elbow complex”, Aerospace and Mechanical Engineering, Notre Dame, Indiana, July 2007

54. Gopura RARC and Kiguchi Kazuo, “A Human forearm and wrist motion assist exoskeleton robot with EMG based neuro fuzzy control” IEEE RAS & EMBS International Conference on Biomedical Robotics and Biomechatronics, Saga University, Saga, Japan, , pp: 550-555, October 19-22, 2008

55. Graupe D and Monlux WJ, “Multifunctional control of artificial upper limbs based on parameter identification of myoelectric signals”, IEEE Conference on Decision and Control including the 14th Symposium on Adaptive Processes, vol. 14, pp. 105 – 110, 1975

56. Graupe Daniel, Magnussen Jan and Beex Aloysius A, “A microprocessor system for multifunctional control of upper-limb prostheses via myoelectric signal identification”, BME Trans. Rehabilitation Engineering, vol. 2, no. 4, pp. 538-544, 1994

57. Gray Henry, Anatomy of the Human Body, 20th edision, 1918

58. Han-Panghuang and Nchen Churrye, “Development of a Myoelectric Discrimination System for a Multi-Degree Prosthetic Hand”, Proceedings IEEE International Conference on Robotics & Automation Detroit, Michigan, p. 2392, May 1999

59. Hargrove L, Englehart K and Hudgins B, “The effect of electrode displacements on pattern recognition based myoelectric control”, 28th Annual International Conference of the IEEE Engineering in Medicine and Biology Society, EMBS '06, pp. 2203 – 2206, Aug. 2006, DOI:10.1109/IEMBS.2006.260681

60. Hargrove Levi J, Englehart Kevin, and Hudgins Bernard, “A Comparison of Surface and Intramuscular Myoelectric Signal Classification”, IEEE trans. Biomedical Engineering, vol. 54, no. 5, pp. 847-853, May 2007

61. Helal JN and Duchene J, “A pseudoperiodic model for myoelectric signal during dynamic exercise”, IEEE Trans. Biomedical Engineering, vol. 36, no.11, pp. 1092 –1097, Nov. 1989

62. Huang Han-Pang and Chen Churryen, “Development of a Myoelectric Discrimination System for a Multi-Degree Prosthetic Hand”, Proceedings of the 1999 IEEE International Conference on Robotics & Automation, Detroit, Michigan, pp. 2392-2397, May 1999

63. Huang Han-Pang and Chiang Chun-Ying, “DSP-Based Controller for a Multi-Degree Prosthetic Hand”, Proceedings of the 2000 IEEE International Conference on Robotics 8 Automation, p.1378, April 2000

64. Hudgins B, Parker P, Scott RN, “A new strategy for multifunction myoelectric control” IEEE Trans Biomed Engg, vol 40(1), pp: 82-94, Jan 1993

65. Ishikawa Y, Yu W, Yokoi H and Kakazu Y, “Development of robotic hands with an adjustable power transmitting mechanism,” Intelligent Engineering Systems Through Neural Networks, vol. 10, pp. 631–636, 2000

66. Jarc M, Kimes AB, Pearson ME and Peck MA, “The design and control of a low-power, upper-limb prosthesis” Sibley School of Mechanical Engineering, Cornell University, Ithaca, NY, IEEE, pp. 165-166, 2006

67. Joshi Deepak, Atreya Sonal, Arora AS and Anand Sneh “Trends in EMG based prosthetic hand development: A Review”, Indian Journal of Biomechanics: special issue (NCBM), pp. 228-232, March 2009

68. Karlsson JS, Gerdle B and Akay M, “Analyzing surface myoelectric signals recorded during isokinetic contractions”, Engineering in Medicine and Biology IEEE Magazine, vol. 20, no. 6, pp. 97 - 105 , Nov.-Dec. 2001, DOI:10.1109/51.982281

69. Karlsson S and Gerdle B, “Mean frequency and signal amplitude of the surface EMG of the quadriceps muscles increase with increasing torque—a study using the continuous wavelet transform”, J. Electromyogr Kinesiol, vol.11, pp.131–140, 2001

70. Kelly MF, Parker PA and Scott RN, “Myoelectric signal analysis using neural networks”, Engineering in Medicine and Biology IEEE Magazine, vol. 9, no. 1, pp. 61 – 64, March 1990, DOI:10.1109/51.62909

71. Khezri M, Jahed M and Sadati N, “Neuro-Fuzzy surface EMG pattern recognition for multifunctional hand prosthesis control”, International Symposium on Industrial Electronics, ISIE 2007, IEEE no. 4-7, pp. 269 – 274, June 2007

72. Kiguchi K, Esaki R, Tsuruta T, Watanabe K and Fukuda T, “An exoskeleton for human elbow and forearm motion assist”, Proceedings International Conference on Intelligent Robots and Systems, IROS 2003, IEEE/RSJ, vol. 4, pp.3600 - 3605 2003, DOI: 10.1109/IROS.2003.1249714,

73. Kiguchi Kazuo, Kariya Shingo, Watanabe Keigo, Izumi Kiyotaka and Fukuda Toshio, “An Exoskeletal Robot for Human Elbow Motion Support—Sensor Fusion, Adaptation, and Control”, IEEE Trans. on Systems, Man, and Cybernetics—Part b: Cybernetics, vol. 31, no. 3, pp. 353-361, June 2001

74. Knaflitz M and Balestra G, “Computer analysis of the myoelectric signal”, Micro, IEEE, vol. 11, no.5, pp.48-58, Oct. 1991

75. Knaflitz M and Bonato P, “Time–frequency methods applied to muscle fatigue assessment during dynamic contractions”, Journal Electromyography Kinesiol, vol. 9, pp.337–350, 1999

76. Knox RR, Brooks DH, Manolakos E and Markogiannakis S, “Time-series based features for EMG pattern recognition: preliminary results” Proceedings Bioengineering Conference IEEE Nineteenth Annual Northeast, pp. 1 – 2, March 18-19,1993

77. Kuba Y, Wada M and Endo H, “An interfacing method between an artificial hand and human”, Proceedings IEEE International Workshop on Robot and Human Communication, pp. 194 – 198, Sep 1-3, 1992

78. Kundu, Kumar Subrata, Kiguchi and Kazuo, “EMG controlled robotic elbow prosthesis as an inner skeleton power assist system”, 4th IEEE International Conference on Mechatronics, ICM2007, pp.1-6, May 8-10, 2007

79. Kuribayashi Katsutoshi, Takahashi Makoto and Taniguchi Takao, “An Upper Extremity Prosthesis Using SMA Actuator” IEEE International Workshop on Robot and Human Communication, p. 52, 1992

80. Kuruganti U, Hudgins B and Scott RN, “Two-channel enhancement of a multifunction control system”, IEEE Transactions on Biomedical Engineering, vol. 42, no. 1, pp. 109 – 111, Jan. 1995, DOI:10.1109/10.362912

81. Kyberd Peter, “The intelligent hand” IEEE reviews, p.31, September 2000

82. Latif Rhonira, Sanei Saeid, and Nazarpour Kianoush, “Classification of elbow electromyography signals based on directed transfer functions”, International Conference on BioMedical Engineering and Informatics, Centre of Digital Signal Processing, School of Engineering, Cardiff University, Wales, UK, pp. 371-374, 2008, DOI: 10.1109/BMEI.2008.135

83. Lee YK and Shimoyama I, “A skeletal framework artificial hand actuated by pneumatic artificial muscles”, Proceedings IEEE International Conference on Robotics & Automation, Detroit, Michigan, p. 926, May 1999

84. Light CM and Chappell PH, “Development of a lightweight and adaptable multiple-axis hand prosthesis,” Med. Eng. Phys., vol. 22, pp. 679–684, Feb. 2001

85. Lindstrom LH and Magnusson RI, “Interpretation of myoelectric power spectra: A model and its applications”, Proceedings IEEE, vol. 65, no. 5, pp.653 – 662, May 1977

86. Lowery MM and O'Malley MJ, “Analysis and Simulation of changes in EMG amplitude during high-level fatiguing contractions” IEEE Trans. on Biomedical Engineering, vol. 50, no. 9, pp. 1052 – 1062, Sept. 2003, DOI:10.1109/TBME.2003.816078

87. Matrone Giulia C, Cipriani Christian, Secco Emanuele L, Magenes Giovanni and Carrozza Maria Chiara, “Principal components analysis based control of a multi-dof underactuated prosthetic hand” Journal of NeuroEngineering and Rehabilitation, pp: 7-16, 2010

88. Masuda and Tadashi, “A reliable myoelectric signal detector based on the propagation characteristics of motor unit action potentials”, IEEE Trans. on Biomedical Engineering, vol. BME-33, no. 9, pp. 876 – 878, Sept. 1986, DOI:10.1109/TBME.1986.325782

89. Meanley S, “Different approaches and cultural considerations in third world prosthetics”, Journal of the International Society for Prosthetics and Orthotics, vol. 19, pp. 176-180, 1995

90. Media.wiley.com, “Introduction to Biomedical Signals” media.wiley.com/product_data/excerpt/16/.../0471208116.pdf

91. Meier Robert H, “Book: Functional Restoration of Adults and Children with Upper Extremity” (ISBN13 9781888799736), Demos Medical Publishing, LLC, 1st Edition Jan 28, 2005

92. Merletti R and Lo Conte LR, “Advances in processing of surface myoelectric signals: Part 2,” Medical & Biological Eng. & Computing, vol.33, pp. 373-384, May 1995

93. Merletti R, Roy SH, Kupa E, Roatta S and Granata A, “Modeling of surface myoelectric signals. II. Model-based signal interpretation”, IEEE Trans. Biomedical Engineering, vol. 46, no. 7, pp. 821 – 829, July 1999, DOI:10.1109/10.771191

94. Merlettit R, Balestrat G and Knaflitzt M, “Effect of FFT based algorithms on estimation of myoelectric signal spectral parameters”, IEEE 11th Annual International Conference Engineering in Medicine Biology Society, pp. 1022-23, 1989

95. Micera S, Carpaneto J and Raspopovic S, “Control of hand prostheses using peripheral information”, IEEE Reviews in Biomedical Engineering, vol. PP, no. 99, p.1, DOI: 10.1109/RBME.2010.2085429, Oct. 11, 2010

96. Mobasser E, Eklund JM and Hashtrudi-Zaad K, “Estimation of elbow-induced wrist force with EMG signals using fast orthogonal search” IEEE Trans. Biomedical Engineering, vol.54, no.4, pp. 683 – 693, April 2007

97. Morita Satoshi, Kondo Toshiyuki and Ito Koji, “Estimation of forearm movement from EMG signal and application to prosthetic hand control”, IEEE Proceedings International Conference on Robotics & Automation, Seoul, Korea, p.3692, May 21-26, 2001

98. Moshoua Dimitrios, Hostensa Ivo, Papaioannoub George and Ramona Herman, “Dynamic muscle fatigue detection using self-organizing maps”, Elsevier Applied Soft Computing, vol.5, pp.391–398, 2005

99. Netter Frank H, “Netter's Atlas of Human Anatomy”, Publisher: Saunders, ISBN-10: 1416033858, edition 4 June 23, 2006

100. O’neill Patricia A, Morin Evelyn L and Scott Robert N, “Myoelectric signal characteristics from muscles in residual upper limbs”, Biomedical Engineering Trans. Rehabilitation Engineering, vol. 2, no. 4, pp. 266-270, Dec.1994

101. Ogino K and Kozak W, “Spectrum analysis of surface electromyogram (EMG)”, IEEE International Conference on Acoustics, Speech, and Signal Processing, ICASSP '83, vol. 8, pp.1114 – 1117, April 1983

102. Okuno R., Yoshida M. and Akazawa K., “Development of biomimetic prosthetic hand controlled by electromyogram”, vol. 1, no. 18-21, pp.103 – 108, March 1996

103. Park E, Meek SG, “Fatigue compensation of the electromyographic signal for prosthetic control and force estimation”, IEEE Trans. on Biomedical Engineering, vol 40, no. 10, pp.1019 – 1023, Oct. 1993, DOI: 10.1109/10.247800

104. Patterson PE and Katz JA, “A sensory feedback system for grasping pressure in a myoelectric hand”, IEEE Proceedings of the Annual International Conference of the Engineering in Medicine and Biology Society, vol.4, pp. 1564-1565, Nov 4-7 1988, DOI: 10.1109/IEMBS.1988.94698

105. Patterson PE and Katz JA, “Design and evolution of a sensory feedback systems that provides grasping pressure in a myoelectric hand,” Journal of Rehabilitation Research and Development, vol. 29, no. 1, pp. 1-8, 1992

106. Pau James WL, Saini Harnoor, Xie Shane SQ, Pullan Andrew J and Mallinson Gordon, “An EMG-Driven Neuromuscular Interface for Human Elbow Joint”, Proceedings of the 3rd International Conference on Biomedical Robotics and Biomechatronics, IEEE RAS & EMBS, pp. 156-161University of Tokyo, Japan, Sep. 26-29, 2010

107. Pfeiffer F, “Grasping with hydraulic fingers-an example of mechatronics”, IEEE/ASME Trans. on Mechatronics, vol.1, no. 2, pp.158 – 167, June 1996

108. Quach Jee Hong, “Surface electromyography: use, design & technological overview”, Concordia University, 2007

109. Quanjun Song, Bingyu Sun, Jianhe Lei, Zhen Gao, Yong Yu, Ming Liu and Yunjian Ge, “ Prediction of Human Elbow Torque from EMG Using SVM Based on AWR Information Acquisition Platform”, IEEE International Conference on Information Acquisition, 2006, pp.1274 – 1278, DOI: 10.1109/ICIA.2006.305933

110. Quanjun Song, Huanghuan Shen, Shuangwei Xie, Zhen Gao, Ming Liu, Yu Yong and Yunjian Ge, “A Study of real-time EMG-driven Arm Wrestling Robot”, IEEE International Conference on Robotics and Biomimetics, ROBIO '06, pp.1610 – 1615, 2006, DOI: 10.1109/ROBIO.2006.340185

111. Ray GC and Guha SK, “Relationship between the surface-EMG and muscular force” Medical and Biological Engineering and Computing (Great Britain), vol. 21, no. 5, p. 579, Sep. 1983

112. Ray GC, Saxena SC and Mukhopadhyay P, “Myoelectric control of an artificial hand for sequential movement in a tropical climate”, Journal of Medical and Biological Engineering and Computing, Springer, vol. 17, no.6, pp. 724-728, 2006

113. Reaz MBI, Hussain MS and Mohd-Yasin F, “Techniques of EMG signal analysis: detection, processing, classification and applications”, Biol. Proceeding Online 2006, p.11, March 23, 2006

114. Ryait Hardeep S, Arora AS and Agarwal Ravinder, “Interpretation of wrist operations from SEMG signals at different locations on arm”, IEEE Trans. Biomedical Circuits and Systems, vol. 4, no. 2, pp.101-111, 2010

115. Ryait Hardeep S, Arora AS and Agarwal Ravinder, “Study of issues in the development of surface emg controlled human hand”, Journal of Materials Science: Materials in Medicine, Springer, vol. 20, pp.107-114, 2009

116. Saito Yukio, Ogawa Atsuo, Negoto Hiroshi and Ohnishi Kengo, “Development of intelligent prosthetic hand adapted to age and body shape”, IEEE Proceedings 9th International Conference on Rehabilitation Robotics, Chicago, IL, USA, p.384, June28 - July1, 2005

117. Saridis George N and Thomas P, “EMG Pattern Analysis and Classification for a Prosthetic Arm”, IEEE Trans. on Biomedical Engineering, vol. BME-29, no. 6, pp. 403 – 412, 1982

118. Saxena SC and Mukhopadhyay P, “EMG operated electronic artificial-leg controller” Journal of Medical and Biological Engineering and Computing, Springer, vol. 15, no. 5, pp. 553-557, Sep. 1977

119. Saxena SC and Wadhwani AK, “A comparative study of the techniques for decomposition of EMG signals”, IETE Journal of Research, vol. 50, no.1, pp. 87-102, 2004

120. Saxena SC, Kumar V and Giri VK “Quality assurance in cardiac disease diagnostic using computerized feature extraction of ECG signal”, The Institution of Electronics and Telecommunication, IETE Technical Review, vol. 20, no.4, pp.377-386, 2003

121. Schauer T, Salbert RC, Negard N-O and Raisch J, “Detection and filtering of SEMG for assessing voluntary muscle activity during FES”, 9th Annual Conference of the International FES Society Bournemouth, UK, September 2004

122. Schulz S, Pylatiuk C and Bretthauer G, “A new ultra light anthropomorphic hand”, Proceedings of the 2001 IEEE International Conference on Robotics and Automation, Seoul, Korea, vol. 3, pp. 2437 – 2441, May 21-26, 2001

123. Schulz S, Pylatiuk C, Reischl M, Martin J, Mikut R, and Bretthauer G, “A hydraulically driven multifunctional prosthetic hand,” Robotica, vol. 23, pp. 293–299, 2005

124. Shahid Shahjahan, Walker Jacqueline, Lyons Gerard M, Byrne Ciaran A, and Nene Anand Vishwanath, “Application of higher order statistics techniques to EMG signals to characterize the motor unit action potential”, IEEE Trans. Biomedical Engineering, vol. 52, no. 7,July 2005

125. Shwedyk Edward, Balasubramanian R and Scott RN, “A nonstationary model for the electromyogram”, IEEE Trans. on Biomedical Engineering, vol. BME-24, no. 5, pp. 417 – 424, Sep. 1977

126. Singh Harpreet and Lal M “Computational procedure for the minimum realizations of linear time-varying systems”, IEEE Trans. Automatic Controls, vol. AC 16, no. 1, p. 93, Feb. 1971

127. Singh Harpreet, Bawa HS, Barada S, Bryant B and Anneberg “Fuzzy Logic Approach in determining the range of electric vehicle”, Proceeding of 37th Midwest Symposium on Circuits and Systems, Louisiana, pp. 1519-1522, Aug. 1994

128. Singh Harsimrat, Li Xu Qin, Hines Evor and Stocks Nigel, “Classification and feature extraction strategies for multi channel multi trial BCI data”, International Journal of Bio electromagnetism, vol. 9, no. 4, pp. 233 - 236, 2007

129. Smith Ryan J, Tenore Francesco, Huberdeau David, Etienne-Cummings Ralph, and Thakor Nitish V, “Continuous Decoding of Finger Position from Surface EMG Signals for the Control of Powered Prostheses”, 30th Annual International IEEE EMBS Conference, Vancouver, British Columbia, Canada, pp:197-200, Aug. 20-24, 2008

130. Standridge RK, Kondraske GV, Mooney V, Carmichael TW and Mayer TG, “Temporal characterization of myoelectric spectral moments changes: analysis of common parameters”, IEEE Trans. on Biomedical Engineering, vol. 35, no. 10, pp. 789 – 797, Oct. 1988, DOI:10.1109/10.7285

131. Stashuk Daniel William, “Decomposition and quantitative analysis of clinical electromyographic signals” Elsevier Journal Medical Engineering & Physics, vol.21, pp. 389–404, 1999

132. Staudenmann Didier, Kingma Idsart, Daffertshofer Andreas, Stegeman Dick F and Dieën Jaap H. van, “Improving EMG-based muscle force estimation by using a high-density EMG grid and principal component analysis”, IEEE trans. on Biomedical Engineering, vol. 53, no. 4, pp.712-718, April 2006

133. Stein A, “Myoelectric-control system for arm-hand prosthesis”, Electronics Letters, vol. 7, no. 10, p. 238, May 20 1971, DOI:10.1049/el:19710161

134. Stencel JE, “Using algorithms in solving synapse transmission problems: Teaching difficult concepts through a problem-solving approach” Journal of College Science Teaching, pp.55-57, Sept/Oct, 1992

135. Stoykov NS, Lowery MM, Heckman CJ, Taflove A and Kuiken TA, “Recording intramuscular EMG signals using surface electrodes”, 9th International Conference on Rehabilitation Robotics, ICORR, pp. 291 – 294, June 28- July 1, 2005, DOI:10.1109/ICORR.2005.1501104

136. Stulen Foster B and De Luca Carlo J, “Frequency parameters of the myoelectric signal as a measure of muscle conduction velocity”, IEEE Trans. on Biomedical Engineering, vol. BME-28, no. 7, pp. 515-523, July 1981

137. Texas Instruments, “Filter design in thirty seconds”, Application report- SLOA093, Dec.2001

138. Tomovic R and Boni G, “An adaptive artificial hand”, IRE Trans. Automatic Control, p.3, April 1962

139. Tsuji Toshio, Fukuda Osamu, Shigeyoshi Hiroki and Kaneko Makoto, “Bio-mimetic impedance control of an EMG-controlled prosthetic hand”, Proceedings International Conference on Intelligent Robots and Systems, IEEE/RSJ, p.377, 2000

140. Ullah K and Jung-Hoon Kim, “A mathematical model for mapping EMG signal to joint torque for the human elbow joint using nonlinear regression”, 4th International Conference on Autonomous Robots and Agents, ICARA 2009, pp.103-108, 2009, DOI: 10.1109/ICARA.2000.4803995

141. Vanderwerker Earl E, “A brief review of the history of amputations and prostheses”, Journal of the Association of Children's Prosthetic & Orthotic Clinics (JACPOC), ACPOC News, vol. 15, no. 5, pp. 15-16, 1976

142. Villasenor-Herrera Alejandro, De Serres Sophie J, Wagner Ross, Kearney Robert E, “Exploring the Human Grip Force System: A Preliminary Study” 30th Annual International IEEE EMBS Conference Vancouver, British Columbia, Canada, p:5362, 2008

143. Voge KR and Dingwell JB, “Relative timing of changes in muscle fatigue and movement coordination during a repetitive one-hand lifting task”, Proceedings of the 25th Annual International Conference of the IEEE Engineering in Medicine and Biology Society, vol. 2, pp. 1807 – 1810, Sept. 17-21, 2003, DOI:10.1109/IEMBS.2003.1279767

144. Wadhwani AK and Wadhwani S, “Techniques for decomposition of EMG signals”, Biomedical Engineering and Information Systems: Technologies, Tools and Applications, pp.187-197

145. Weirl RF and Ajiboye AB, “A Multifunction prosthesis controller based on Fuzzy-Logic techniques”, Proceedings 25th Annual International Conference IEEE EMBS, Cancun, Mexico, pp.1678-1681, Sep.17-21, 2003

146. Weir F ff Richard and Grahn C Edward, “Development of Externally-Powered Prostheses for Persons with Partial Hand Amputations” IEEE Proceedings of the 22nd Annual EMBS International Conference, Chicago, pp: 427-430, July 23-28,2000

147. Wongsiri S and Laksanacharoen S, "Design and Construction of an Artificial Limb Driven by Artificial Muscles for Amputees", PSU-UNS International Conference 2003: Energy and the Environment, Prince of Songkla University, Hat Yai, Songkla, Thailand, Dec. 11-12, 2003

148. Xiong, Fuqin Q and Shwedyk Ed, “Some aspects of non-stationary myoelectric signal processing”, IEEE Trans. on Biomedical Engineering, vol. BME-34, no. 2, pp. 166 – 172, Feb. 1987, DOI:10.1109/TBME.1987.326041

149. Yazama Y, Mitsukura Y, Fukumi M and Akamatsu N, “Analysis and recognition of wrist motions by using multidimensional directed information and EMG signal”, IEEE International Conference of the North American Fuzzy Information Processing Society, pp. 867-870, 2004

150. Zajdlik Jakub, “The Preliminary Design and Motion Control of a Five-fingered Prosthetic Hand”, 10th International Conference on Intelligent Engineering Systems (INES), p.202, 2006

151. Zaman Abdullah Al, Sharmin T, Ali Khan Mohammad Ashraf and Ferdjallah M, “Muscle fatigue analysis in young adults at different MVC levels using EMG metrics”, Proceedings IEEE, SoutheastCon, pp.390 – 394, March 22-25, 2007, DOI:10.1109/SECON.2007.342930

152. Zardoshti-Kermani M, Wheeler BC, Badie K and Hashemi RM, “EMG feature evaluation for movement control of upper extremity prostheses”, IEEE Transactions on Rehabilitation Engineering, vol. 3 ,no. 4, pp. 324 –333, 1995, DOI: 10.1109/86.481972

153. Zardoshti-Kermani Mahyar, Wheeler Bruce C, Badie Kambiz and Hashemi Reza M, “EMG feature evaluation for movement control of upper extremity prostheses”, IEEE trans. on rehabilitation engineering, vol. 3, no. 4, Dec. 1995

154. Zhang YT, Herzog W and Liu MM, “A mathematical model of myoelectric signals obtained during locomotion”, IEEE 17th Annual Conference Engineering in Medicine and Biology Society, vol. 2,no. 20-23, pp.1403 – 1404, Sep. 1995

Online References

Online 1:	Andrews Dennis R, http://expertpages.com/news/ concepts_in_human_factors_engineering_5.htm, 2009
Online 2:	http://www.amputee-coalition.org/nllic_faq.html#2, 2009
Online 3:	http://www.aboutonehandtyping.com/statistics.html, 2007
Online 4:	health.indianetzone.com/acupressure/, 2007
Online 5:	http://www.eclecticenergies.com/acupressure/points.php, 2007
Online 6:	http://www.geocities.com/jrh_iii/acupressure/acupoints.html, 2007
Online 7:	The Online Acupressure Guide, http://pointfinder.org/, 2007
Online 8:	http://www.innerbody.com/image_musfov/musc47-new.html
Online 9:	http://www.dartmouth.edu/~humananatomy/index.html, 2010
Online 10:	http://www.pianoperceptions.com/pdf/NCKPWorkshop07.pdf, 2009
Online 11:	Sellers Bill, "Functional Anatomy of the Upper Limb", http://homepage.mac.com/wis/Personal/lectures/musculoskeletal/UpperLib.pdf, 2009
Online 12:	Beldholm Bernard, http://www.healthyintentions.com.au/files/ Fact_sheet_Flexor%20muscles%20of%20the%20forearm.pdf, 2009
Online 13:	http://www.hper.txstate.edu/hper/faculty/pankey/3320/4325tut/elb/ bicep.html
Online 14:	Adams Mary Jo, http://www.castonline.ilstu.edu/mjadams/181/ knr_181_anatomy_lab.htm, Horton, 227-G, 2010
Online 15:	http://www.statistixl.com, 2008
Online 16:	http://www.taxonomy.delrieu.org/methods_pca.php, 2009
Online 17:	http://www.orthogate.org/patient-education/elbow/artificial-joint-replacement-of-the-elbow.html, 2009
Online 18:	Kelly Brian M, http://emedicine.medscape.com/article/317234, 2010
Online 19:	http://en.wikipedia.org/wiki/List_of_muscles_of_the_human_body

Publications in refereed journals

1. "Study of Issues in the Development of Surface EMG Controlled Human Hand", Hardeep S. Ryait, A.S. Arora and Ravinder Agarwal, Journal of Materials Science: Materials in Medicine, Springer, vol. 20, pp. 107-114, 2009.

2. "Interpretation of Wrist Operations from SEMG Signals at Different Locations on Arm", Hardeep S. Ryait, A.S.Arora and Ravinder Agarwal, IEEE Transactions on Biomedical Circuits and Systems, vol. 4, no. 2, pp. 101-111, 2010.

3. "SEMG Signal Analysis at Acupressure Points for Elbow Movement", Hardeep S. Ryait, A.S.Arora and Ravinder Agarwal, Journal of Electromyography and Kinesiology, vol. 21(5), pp: 868–876, 2011.

4. "SEMG-Prosthetic Elbow Controlled with RMS Identification" Hardeep S. Ryait, A.S. Arora and Ravinder Agarwal, Journal of Bioinformatics and its Applications, vol. 5(3 & 4), pp: 72-79, 2010.

5. "Realization of SEMG Based Multifunctional Prototype Elbow Prosthesis" Hardeep S. Ryait, A.S.Arora and Ravinder Agarwal, Int. J. Biomedical Engineering and Technology, Jan 2011 (accepted).

Papers/abstract published in conferences proceeding

1. "Development of Computer Aided System for SEMG Signal Analysis for Muscle Fatigue", Hardeep S. Ryait, A.S. Arora and Ravinder Agarwal, National Conference on "Technological Advances and Computational Techniques (TACT-2009)", March 16-17, 2009, NIT, Hamirpur

2. "Development of Computer Aided System for SEMG Signal Analysis for Grip-Force", Hardeep S. Ryait, A.S. Arora and Ravinder Agarwal, International Conference on Innovative Technologies (ICIT-09), June 18-19, 2009, PDM Engineering College, Bahadurgarh

3. "SEMG Signal Analysis for Forced Gripping and Elbow Movement at Acupressure Points on Arm", Hardeep S. Ryait, A.S. Arora and Ravinder Agarwal, Proceeding National Conference on Emerging Trends in Electronics Engineering and Computing (E3C 2010), pp. 1323-1328, Feb 9-10, 2010, JD College of Engg. Nagpur

4. "Development of Single Channel SEMG Prosthetic Elbow", Hardeep S. Ryait, A.S. Arora and Ravinder Agarwal, National Conference Emerging Medical Instrumentation (CEMI-2010), May 11–12, 2010, CSIO, Chandigarh

List of annexure

National Semiconductor

August 2000

LM124/LM224/LM324/LM2902
Low Power Quad Operational Amplifiers

General Description

The LM124 series consists of four independent, high gain, internally frequency compensated operational amplifiers which were designed specifically to operate from a single power supply over a wide range of voltages. Operation from split power supplies is also possible and the low power supply current drain is independent of the magnitude of the power supply voltage.

Application areas include transducer amplifiers, DC gain blocks and all the conventional op amp circuits which now can be more easily implemented in single power supply systems. For example, the LM124 series can be directly operated off of the standard +5V power supply voltage which is used in digital systems and will easily provide the required interface electronics without requiring the additional ±15V power supplies.

Unique Characteristics

- In the linear mode the input common-mode voltage range includes ground and the output voltage can also swing to ground, even though operated from only a single power supply voltage
- The unity gain cross frequency is temperature compensated
- The input bias current is also temperature compensated

Advantages

- Eliminates need for dual supplies
- Four internally compensated op amps in a single package
- Allows directly sensing near GND and V_{OUT} also goes to GND
- Compatible with all forms of logic
- Power drain suitable for battery operation

Features

- Internally frequency compensated for unity gain
- Large DC voltage gain 100 dB
- Wide bandwidth (unity gain) 1 MHz (temperature compensated)
- Wide power supply range:
  Single supply 3V to 32V
  or dual supplies ±1.5V to ±16V
- Very low supply current drain (700 µA)—essentially independent of supply voltage
- Low input biasing current 45 nA (temperature compensated)
- Low input offset voltage 2 mV and offset current: 5 nA
- Input common-mode voltage range includes ground
- Differential input voltage range equal to the power supply voltage
- Large output voltage swing 0V to V^+ – 1.5V

Connection Diagrams

Dual-In-Line Package

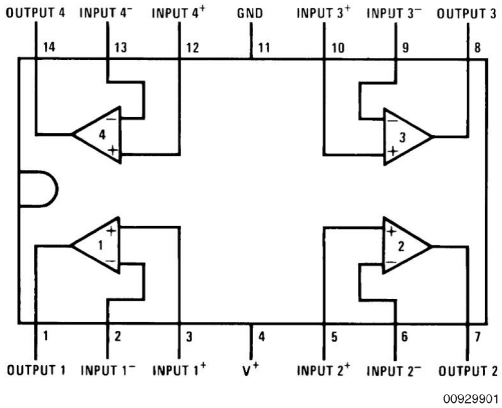

00929901

Top View

Order Number LM124J, LM124AJ, LM124J/883 (Note 2), **LM124AJ/883** (Note 1), **LM224J, LM224AJ, LM324J, LM324M, LM324MX, LM324AM, LM324AMX, LM2902M, LM2902MX, LM324N, LM324AN, LM324MT, LM324MTX or LM2902N LM124AJRQML and LM124AJRQMLV**(Note 3)
See NS Package Number J14A, M14A or N14A

Connection Diagrams (Continued)

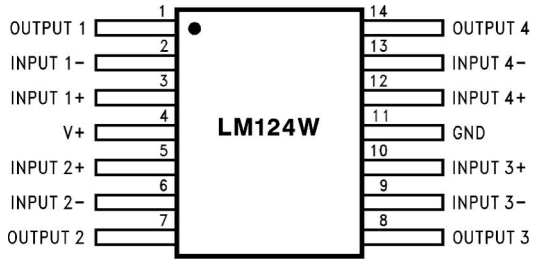

00929933

Order Number LM124AW/883, LM124AWG/883, LM124W/883 or LM124WG/883
LM124AWRQML and LM124AWRQMLV(Note 3)
See NS Package Number W14B
LM124AWGRQML and LM124AWGRQMLV(Note 3)
See NS Package Number WG14A

Note 1: LM124A available per JM38510/11006

Note 2: LM124 available per JM38510/11005

Note 3: See STD Mil DWG 5962R99504 for Radiation Tolerant Device

Schematic Diagram (Each Amplifier)

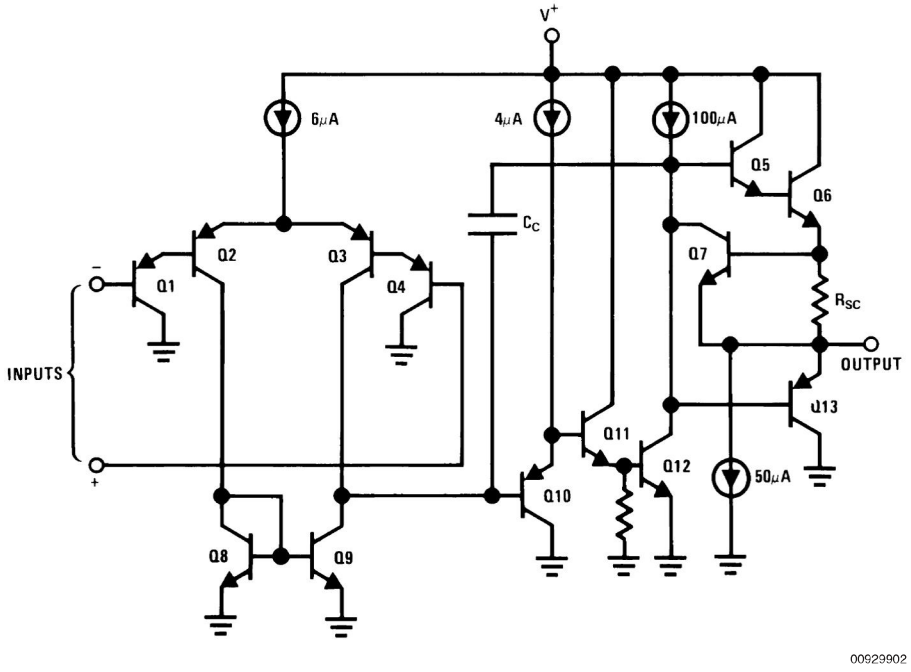

00929902

Absolute Maximum Ratings (Note 12)

If Military/Aerospace specified devices are required, please contact the National Semiconductor Sales Office/ Distributors for availability and specifications.

	LM124/LM224/LM324 LM124A/LM224A/LM324A	LM2902
Supply Voltage, V^+	32V	26V
Differential Input Voltage	32V	26V
Input Voltage	−0.3V to +32V	−0.3V to +26V
Input Current		
(V_{IN} < −0.3V) (Note 6)	50 mA	50 mA
Power Dissipation (Note 4)		
Molded DIP	1130 mW	1130 mW
Cavity DIP	1260 mW	1260 mW
Small Outline Package	800 mW	800 mW
Output Short-Circuit to GND		
(One Amplifier) (Note 5)		
$V^+ \leq 15V$ and $T_A = 25^\circ C$	Continuous	Continuous
Operating Temperature Range		−40°C to +85°C
LM324/LM324A	0°C to +70°C	
LM224/LM224A	−25°C to +85°C	
LM124/LM124A	−55°C to +125°C	
Storage Temperature Range	−65°C to +150°C	−65°C to +150°C
Lead Temperature (Soldering, 10 seconds)	260°C	260°C
Soldering Information		
Dual-In-Line Package		
Soldering (10 seconds)	260°C	260°C
Small Outline Package		
Vapor Phase (60 seconds)	215°C	215°C
Infrared (15 seconds)	220°C	220°C
See AN-450 "Surface Mounting Methods and Their Effect on Product Reliability" for other methods of soldering surface mount devices.		
ESD Tolerance (Note 13)	250V	250V

Electrical Characteristics

$V^+ = +5.0V$, (Note 7), unless otherwise stated

Parameter	Conditions	LM124A			LM224A			LM324A			Units
		Min	Typ	Max	Min	Typ	Max	Min	Typ	Max	
Input Offset Voltage	(Note 8) $T_A = 25^\circ C$		1	2		1	3		2	3	mV
Input Bias Current (Note 9)	$I_{IN(+)}$ or $I_{IN(-)}$, $V_{CM} = 0V$, $T_A = 25^\circ C$		20	50		40	80		45	100	nA
Input Offset Current	$I_{IN(+)}$ or $I_{IN(-)}$, $V_{CM} = 0V$, $T_A = 25^\circ C$		2	10		2	15		5	30	nA
Input Common-Mode Voltage Range (Note 10)	$V^+ = 30V$, (LM2902, $V^+ = 26V$), $T_A = 25^\circ C$	0		$V^+-1.5$	0		$V^+-1.5$	0		$V^+-1.5$	V
Supply Current	Over Full Temperature Range $R_L = \infty$ On All Op Amps										mA
	$V^+ = 30V$ (LM2902 $V^+ = 26V$)		1.5	3		1.5	3		1.5	3	
	$V^+ = 5V$		0.7	1.2		0.7	1.2		0.7	1.2	
Large Signal Voltage Gain	$V^+ = 15V$, $R_L \geq 2k\Omega$, ($V_O = 1V$ to $11V$), $T_A = 25^\circ C$	50	100		50	100		25	100		V/mV
Common-Mode	DC, $V_{CM} = 0V$ to $V^+ - 1.5V$,	70	85		70	85		65	85		dB

Electrical Characteristics (Continued)

V^+ = +5.0V, (Note 7), unless otherwise stated

Parameter		Conditions		LM124A			LM224A			LM324A			Units
				Min	Typ	Max	Min	Typ	Max	Min	Typ	Max	
Rejection Ratio		T_A = 25˚C											
Power Supply Rejection Ratio		V^+ = 5V to 30V (LM2902, V^+ = 5V to 26V), T_A = 25˚C		65	100		65	100		65	100		dB
Amplifier-to-Amplifier Coupling (Note 11)		f = 1 kHz to 20 kHz, T_A = 25˚C (Input Referred)			−120			−120			−120		dB
Output Current	Source	V_{IN}^+ = 1V, V_{IN}^- = 0V, V^+ = 15V, V_O = 2V, T_A = 25˚C		20	40		20	40		20	40		mA
	Sink	V_{IN}^- = 1V, V_{IN}^+ = 0V, V^+ = 15V, V_O = 2V, T_A = 25˚C		10	20		10	20		10	20		mA
		V_{IN}^- = 1V, V_{IN}^+ = 0V, V^+ = 15V, V_O = 200 mV, T_A = 25˚C		12	50		12	50		12	50		µA
Short Circuit to Ground		(Note 5) V^+ = 15V, T_A = 25˚C			40	60		40	60		40	60	mA
Input Offset Voltage		(Note 8)				4			4			5	mV
V_{OS} Drift		R_S = 0Ω			7	20		7	20		7	30	µV/˚C
Input Offset Current		$I_{IN(+)} - I_{IN(-)}$, V_{CM} = 0V				30			30			75	nA
I_{OS} Drift		R_S = 0Ω			10	200		10	200		10	300	pA/˚C
Input Bias Current		$I_{IN(+)}$ or $I_{IN(-)}$			40	100		40	100		40	200	nA
Input Common-Mode Voltage Range (Note 10)		V^+ = +30V (LM2902, V^+ = 26V)		0		V^+–2	0		V^+–2	0		V^+–2	V
Large Signal Voltage Gain		V^+ = +15V (V_OSwing = 1V to 11V) $R_L \geq 2$ kΩ		25			25			15			V/mV
Output Voltage Swing	V_{OH}	V^+ = 30V (LM2902, V^+ = 26V)	R_L = 2 kΩ	26			26			26			V
			R_L = 10 kΩ	27	28		27	28		27	28		
	V_{OL}	V^+ = 5V, R_L = 10 kΩ			5	20		5	20		5	20	mV
Output Current	Source	V_O = 2V	V_{IN}^+ = +1V, V_{IN}^- = 0V, V^+ = 15V	10	20		10	20		10	20		mA
	Sink		V_{IN}^- = +1V, V_{IN}^+ = 0V, V^+ = 15V	10	15		5	8		5	8		

Electrical Characteristics

V^+ = +5.0V, (Note 7), unless otherwise stated

Parameter	Conditions	LM124/LM224			LM324			LM2902			Units
		Min	Typ	Max	Min	Typ	Max	Min	Typ	Max	
Input Offset Voltage	(Note 8) T_A = 25˚C		2	5		2	7		2	7	mV
Input Bias Current (Note 9)	$I_{IN(+)}$ or $I_{IN(-)}$, V_{CM} = 0V, T_A = 25˚C		45	150		45	250		45	250	nA
Input Offset Current	$I_{IN(+)}$ or $I_{IN(-)}$, V_{CM} = 0V, T_A = 25˚C		3	30		5	50		5	50	nA
Input Common-Mode Voltage Range (Note 10)	V^+ = 30V, (LM2902, V^+ = 26V), T_A = 25˚C	0		V^+–1.5	0		V^+–1.5	0		V^+–1.5	V

Electrical Characteristics (Continued)

V^+ = +5.0V, (Note 7), unless otherwise stated

Parameter		Conditions		LM124/LM224			LM324			LM2902			Units
				Min	Typ	Max	Min	Typ	Max	Min	Typ	Max	
Supply Current		Over Full Temperature Range $R_L = \infty$ On All Op Amps V^+ = 30V (LM2902 V^+ = 26V) V^+ = 5V			1.5 0.7	3 1.2		1.5 0.7	3 1.2		1.5 0.7	3 1.2	mA
Large Signal Voltage Gain		V^+ = 15V, $R_L \geq 2k\Omega$, (V_O = 1V to 11V), T_A = 25˚C		50	100		25	100		25	100		V/mV
Common-Mode Rejection Ratio		DC, V_{CM} = 0V to V^+ − 1.5V, T_A = 25˚C		70	85		65	85		50	70		dB
Power Supply Rejection Ratio		V^+ = 5V to 30V (LM2902, V^+ = 5V to 26V), T_A = 25˚C		65	100		65	100		50	100		dB
Amplifier-to-Amplifier Coupling (Note 11)		f = 1 kHz to 20 kHz, T_A = 25˚C (Input Referred)			−120			−120			−120		dB
Output Current	Source	V_{IN}^+ = 1V, V_{IN}^- = 0V, V^+ = 15V, V_O = 2V, T_A = 25˚C		20	40		20	40		20	40		mA
	Sink	V_{IN}^- = 1V, V_{IN}^+ = 0V, V^+ = 15V, V_O = 2V, T_A = 25˚C		10	20		10	20		10	20		mA
		V_{IN}^- = 1V, V_{IN}^+ = 0V, V^+ = 15V, V_O = 200 mV, T_A = 25˚C		12	50		12	50		12	50		µA
Short Circuit to Ground		(Note 5) V^+ = 15V, T_A = 25˚C			40	60		40	60		40	60	mA
Input Offset Voltage		(Note 8)				7			9			10	mV
V_{OS} Drift		R_S = 0Ω			7			7			7		µV/˚C
Input Offset Current		$I_{IN(+)} - I_{IN(-)}$, V_{CM} = 0V				100			150		45	200	nA
I_{OS} Drift		R_S = 0Ω			10			10			10		pA/˚C
Input Bias Current		$I_{IN(+)}$ or $I_{IN(-)}$			40	300		40	500		40	500	nA
Input Common-Mode Voltage Range (Note 10)		V^+ = +30V (LM2902, V^+ = 26V)		0		V^+–2	0		V^+–2	0		V^+–2	V
Large Signal Voltage Gain		V^+ = +15V (V_OSwing = 1V to 11V) $R_L \geq$ 2 kΩ		25			15			15			V/mV
Output Voltage Swing	V_{OH}	V^+ = 30V	R_L = 2 kΩ	26			26			22			V
		(LM2902, V^+ = 26V)	R_L = 10 kΩ	27	28		27	28		23	24		
	V_{OL}	V^+ = 5V, R_L = 10 kΩ			5	20		5	20		5	100	mV
Output Current	Source	V_O = 2V	V_{IN}^+ = +1V, V_{IN}^- = 0V, V^+ = 15V	10	20		10	20		10	20		mA
	Sink		V_{IN}^- = +1V, V_{IN}^+ = 0V, V^+ = 15V	5	8		5	8		5	8		

Note 4: For operating at high temperatures, the LM324/LM324A/LM2902 must be derated based on a +125˚C maximum junction temperature and a thermal resistance of 88˚C/W which applies for the device soldered in a printed circuit board, operating in a still air ambient. The LM224/LM224A and LM124/LM124A can be derated based on a +150˚C maximum junction temperature. The dissipation is the total of all four amplifiers—use external resistors, where possible, to allow the amplifier to saturate of to reduce the power which is dissipated in the integrated circuit.

Note 5: Short circuits from the output to V^+ can cause excessive heating and eventual destruction. When considering short circuits to ground, the maximum output current is approximately 40 mA independent of the magnitude of V^+. At values of supply voltage in excess of +15V, continuous short-circuits can exceed the power dissipation ratings and cause eventual destruction. Destructive dissipation can result from simultaneous shorts on all amplifiers.

Note 6: This input current will only exist when the voltage at any of the input leads is driven negative. It is due to the collector-base junction of the input PNP transistors becoming forward biased and thereby acting as input diode clamps. In addition to this diode action, there is also lateral NPN parasitic transistor action

Electrical Characteristics (Continued)

on the IC chip. This transistor action can cause the output voltages of the op amps to go to the V^+voltage level (or to ground for a large overdrive) for the time duration that an input is driven negative. This is not destructive and normal output states will re-establish when the input voltage, which was negative, again returns to a value greater than −0.3V (at 25˚C).

Note 7: These specifications are limited to $-55^\circ C \le T_A \le +125^\circ C$ for the LM124/LM124A. With the LM224/LM224A, all temperature specifications are limited to $-25^\circ C \le T_A \le +85^\circ C$, the LM324/LM324A temperature specifications are limited to $0^\circ C \le T_A \le +70^\circ C$, and the LM2902 specifications are limited to $-40^\circ C \le T_A \le +85^\circ C$.

Note 8: $V_O \approx 1.4V$, $R_S = 0\Omega$ with V^+ from 5V to 30V; and over the full input common-mode range (0V to $V^+ - 1.5V$) for LM2902, V^+ from 5V to 26V.

Note 9: The direction of the input current is out of the IC due to the PNP input stage. This current is essentially constant, independent of the state of the output so no loading change exists on the input lines.

Note 10: The input common-mode voltage of either input signal voltage should not be allowed to go negative by more than 0.3V (at 25˚C). The upper end of the common-mode voltage range is $V^+ - 1.5V$ (at 25˚C), but either or both inputs can go to +32V without damage (+26V for LM2902), independent of the magnitude of V^+.

Note 11: Due to proximity of external components, insure that coupling is not originating via stray capacitance between these external parts. This typically can be detected as this type of capacitance increases at higher frequencies.

Note 12: Refer to RETS124AX for LM124A military specifications and refer to RETS124X for LM124 military specifications.

Note 13: Human body model, 1.5 kΩ in series with 100 pF.

Typical Performance Characteristics

Input Voltage Range

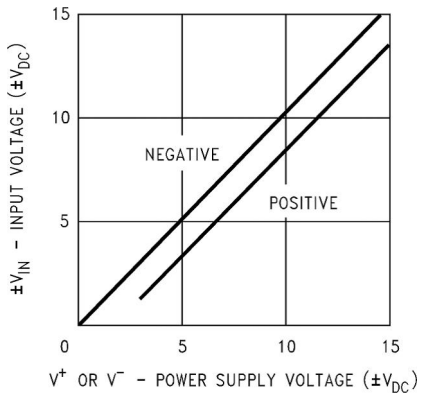

00929934

Input Current

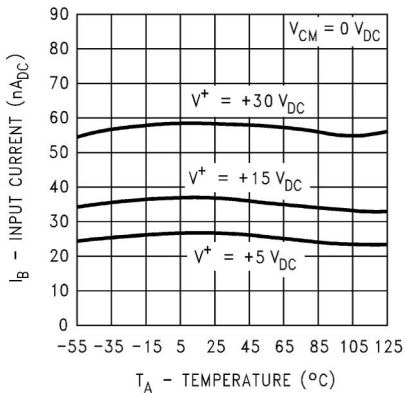

00929935

Supply Current

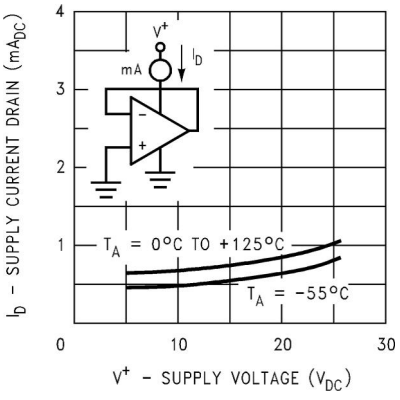

00929936

Voltage Gain

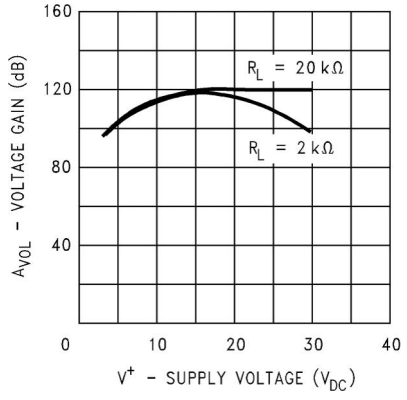

00929937

Typical Performance Characteristics (Continued)

Open Loop Frequency Response

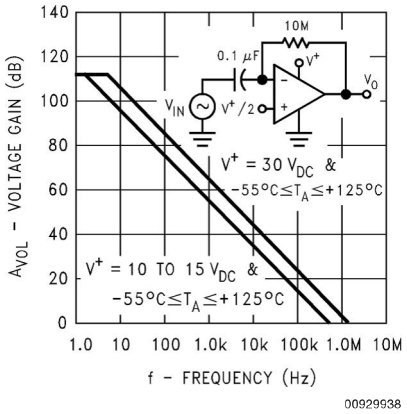

00929938

Common Mode Rejection Ratio

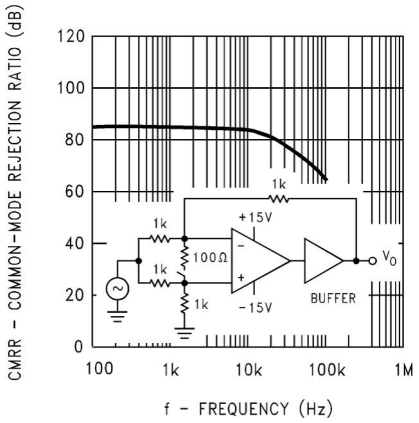

00929939

Voltage Follower Pulse Response

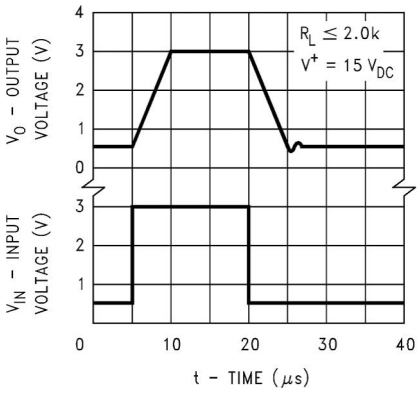

00929940

Voltage Follower Pulse Response (Small Signal)

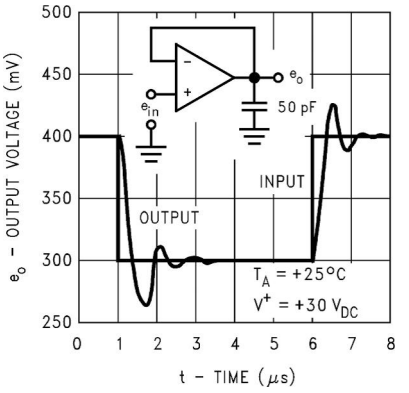

00929941

Large Signal Frequency Response

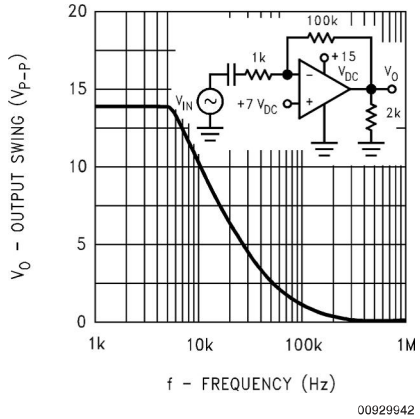

00929942

Output Characteristics Current Sourcing

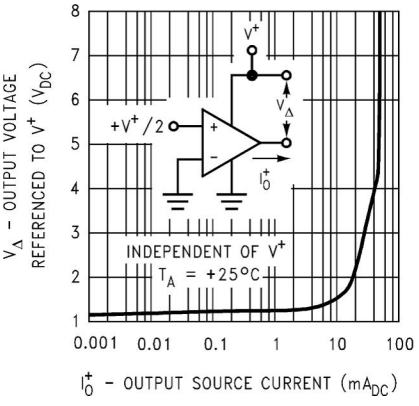

00929943

Typical Performance Characteristics (Continued)

Output Characteristics Current Sinking

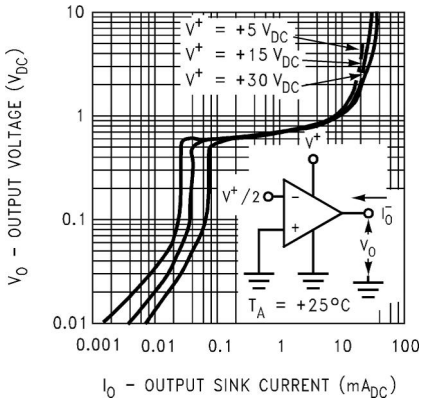

00929944

Current Limiting

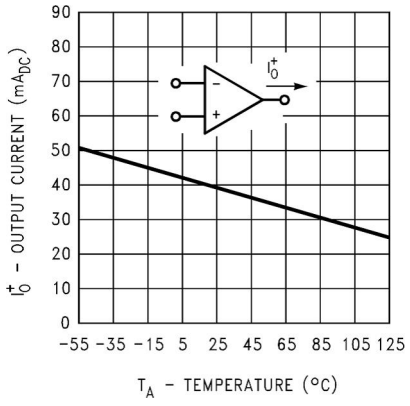

00929945

Input Current (LM2902 only)

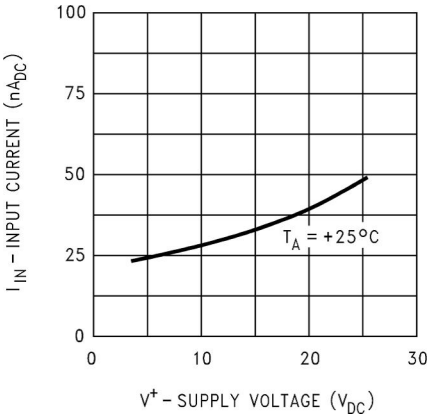

00929946

Voltage Gain (LM2902 only)

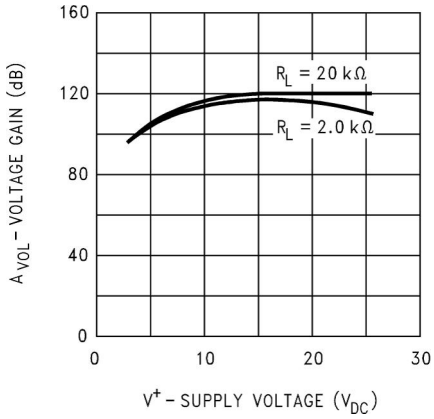

00929947

Application Hints

The LM124 series are op amps which operate with only a single power supply voltage, have true-differential inputs, and remain in the linear mode with an input common-mode voltage of 0 V_{DC}. These amplifiers operate over a wide range of power supply voltage with little change in performance characteristics. At 25˚C amplifier operation is possible down to a minimum supply voltage of 2.3 V_{DC}.

The pinouts of the package have been designed to simplify PC board layouts. Inverting inputs are adjacent to outputs for all of the amplifiers and the outputs have also been placed at the corners of the package (pins 1, 7, 8, and 14).

Precautions should be taken to insure that the power supply for the integrated circuit never becomes reversed in polarity or that the unit is not inadvertently installed backwards in a test socket as an unlimited current surge through the resulting forward diode within the IC could cause fusing of the internal conductors and result in a destroyed unit.

Large differential input voltages can be easily accommodated and, as input differential voltage protection diodes are not needed, no large input currents result from large differential input voltages. The differential input voltage may be larger than V^+ without damaging the device. Protection should be provided to prevent the input voltages from going negative more than –0.3 V_{DC} (at 25˚C). An input clamp diode with a resistor to the IC input terminal can be used.

To reduce the power supply drain, the amplifiers have a class A output stage for small signal levels which converts to class B in a large signal mode. This allows the amplifiers to both source and sink large output currents. Therefore both NPN and PNP external current boost transistors can be used to extend the power capability of the basic amplifiers. The output voltage needs to raise approximately 1 diode drop above ground to bias the on-chip vertical PNP transistor for output current sinking applications.

For ac applications, where the load is capacitively coupled to the output of the amplifier, a resistor should be used, from the output of the amplifier to ground to increase the class A bias current and prevent crossover distortion.

Where the load is directly coupled, as in dc applications, there is no crossover distortion.

Capacitive loads which are applied directly to the output of the amplifier reduce the loop stability margin. Values of 50 pF can be accommodated using the worst-case non-inverting unity gain connection. Large closed loop gains or resistive isolation should be used if larger load capacitance must be driven by the amplifier.

Application Hints (Continued)

The bias network of the LM124 establishes a drain current which is independent of the magnitude of the power supply voltage over the range of from 3 V_{DC} to 30 V_{DC}.

Output short circuits either to ground or to the positive power supply should be of short time duration. Units can be destroyed, not as a result of the short circuit current causing metal fusing, but rather due to the large increase in IC chip dissipation which will cause eventual failure due to excessive junction temperatures. Putting direct short-circuits on more than one amplifier at a time will increase the total IC power dissipation to destructive levels, if not properly protected with external dissipation limiting resistors in series with the output leads of the amplifiers. The larger value of output source current which is available at 25˚C provides a larger output current capability at elevated temperatures (see typical performance characteristics) than a standard IC op amp.

The circuits presented in the section on typical applications emphasize operation on only a single power supply voltage. If complementary power supplies are available, all of the standard op amp circuits can be used. In general, introducing a pseudo-ground (a bias voltage reference of $V^+/2$) will allow operation above and below this value in single power supply systems. Many application circuits are shown which take advantage of the wide input common-mode voltage range which includes ground. In most cases, input biasing is not required and input voltages which range to ground can easily be accommodated.

Typical Single-Supply Applications (V^+ = 5.0 V_{DC})

Non-Inverting DC Gain (0V Input = 0V Output)

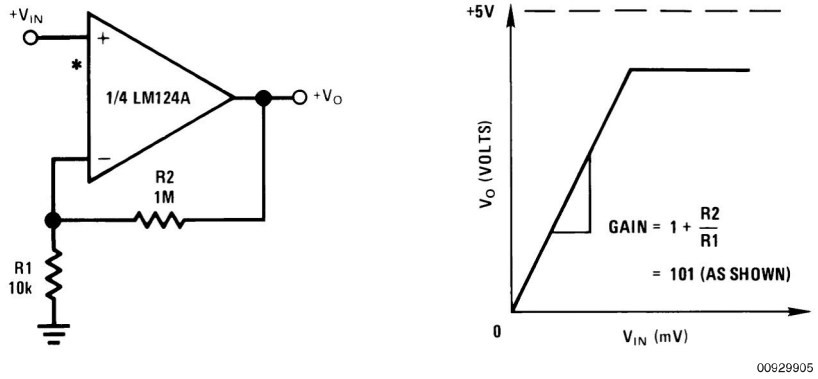

00929905

*R not needed due to temperature independent I_{IN}

DC Summing Amplifier
($V_{IN'S} \geq 0\ V_{DC}$ and $V_O \geq V_{DC}$)

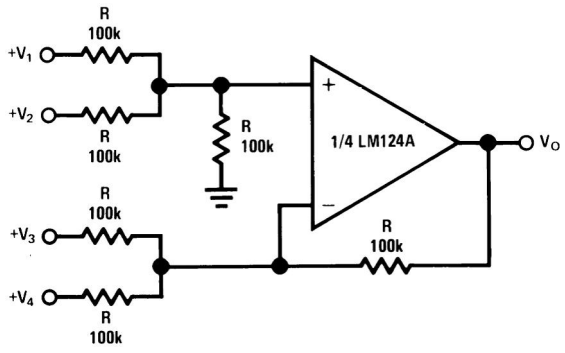

00929906

Where: $V_0 = V_1 + V_2 - V_3 - V_4$

$(V_1 + V_2) \geq (V_3 + V_4)$ to keep $V_O > 0\ V_{DC}$

Power Amplifier

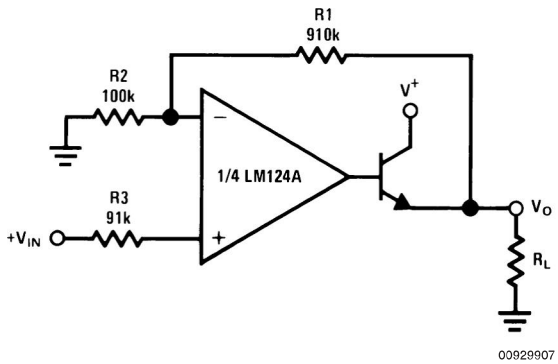

00929907

$V_0 = 0\ V_{DC}$ for $V_{IN} = 0\ V_{DC}$

$A_V = 10$

Typical Single-Supply Applications (V^+ = 5.0 V_{DC}) (Continued)

LED Driver

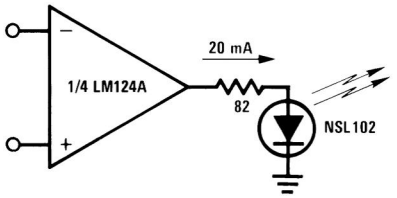

00929908

"BI-QUAD" RC Active Bandpass Filter

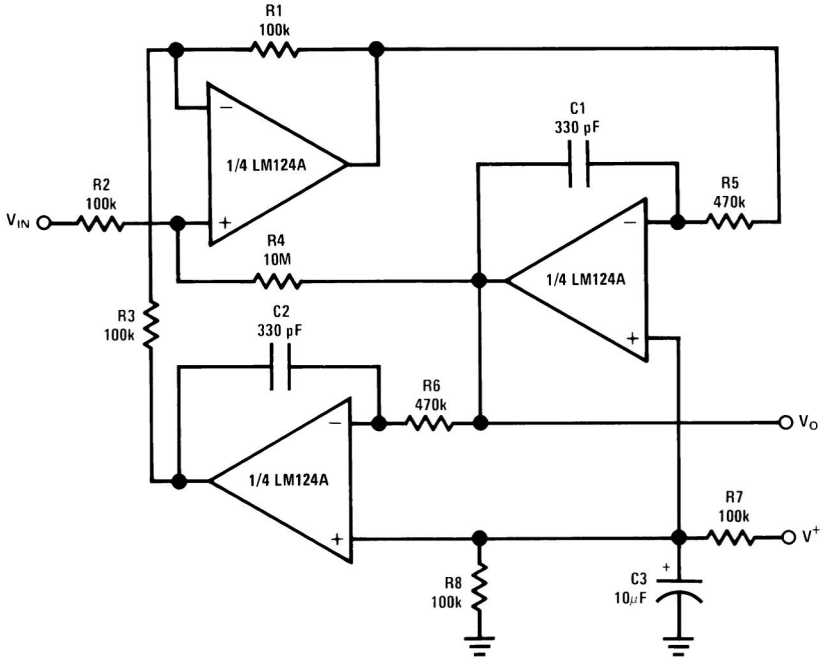

00929909

f_o = 1 kHz
Q = 50
A_V = 100 (40 dB)

Fixed Current Sources

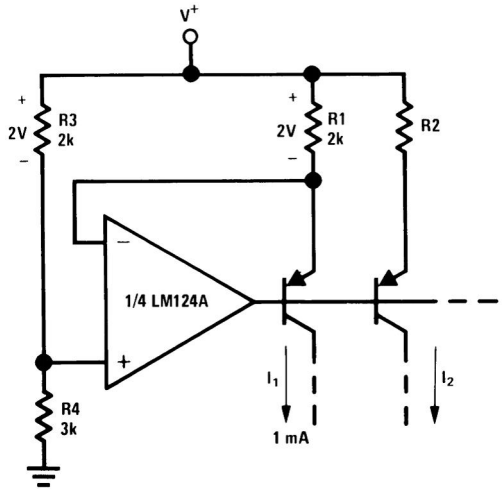

00929910

$$I_2 = \left(\frac{R1}{R2}\right) I_1$$

Lamp Driver

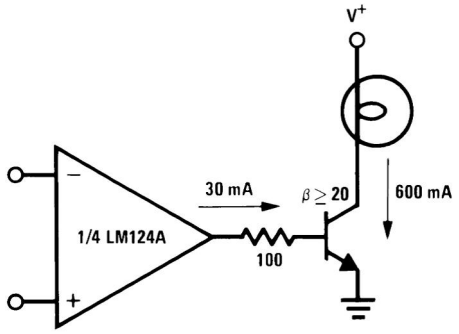

00929911

Typical Single-Supply Applications

(V^+ = 5.0 V_{DC}) (Continued)

Current Monitor

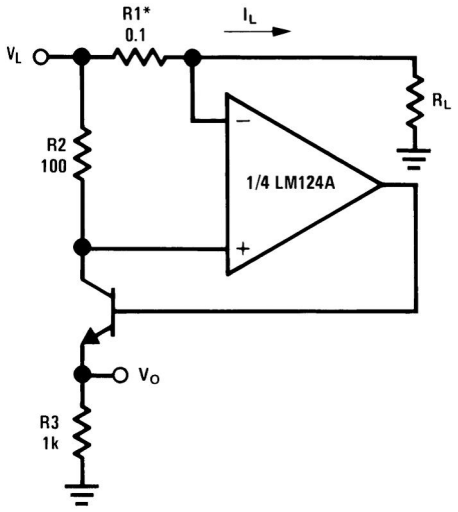

00929912

$$V_O = \frac{1V(I_L)}{1A}$$

$$V_L \leq V^+ - 2V$$

*(Increase R1 for I_L small)

Driving TTL

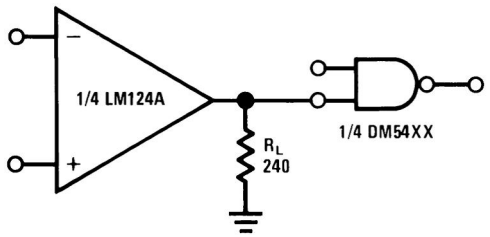

00929913

Voltage Follower

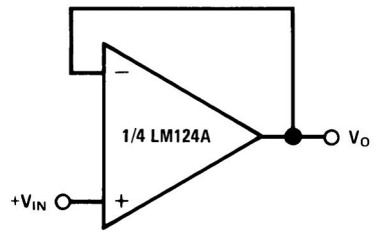

00929914

Pulse Generator

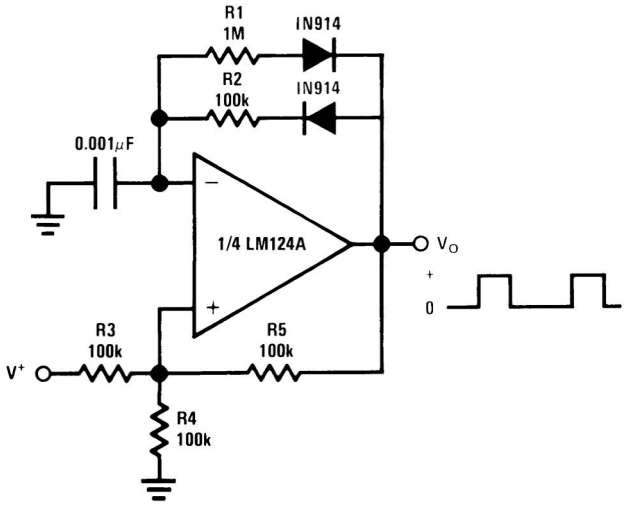

00929915

Squarewave Oscillator

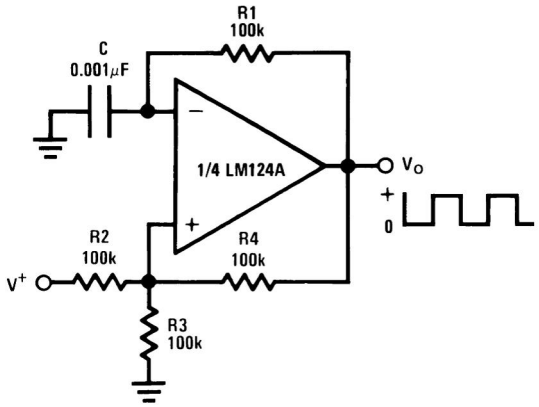

00929916

Pulse Generator

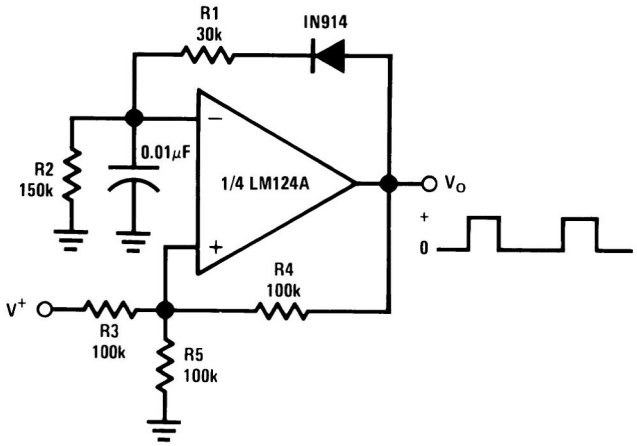

00929917

Typical Single-Supply Applications (V^+ = 5.0 V_{DC}) (Continued)

High Compliance Current Sink

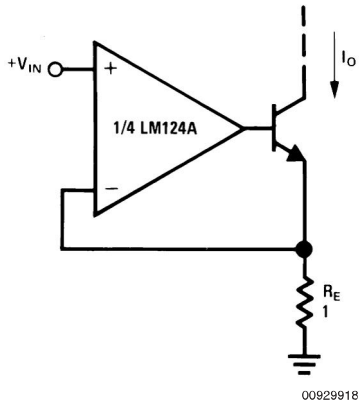

I_O = 1 amp/volt V_{IN}
(Increase R_E for I_o small)

Low Drift Peak Detector

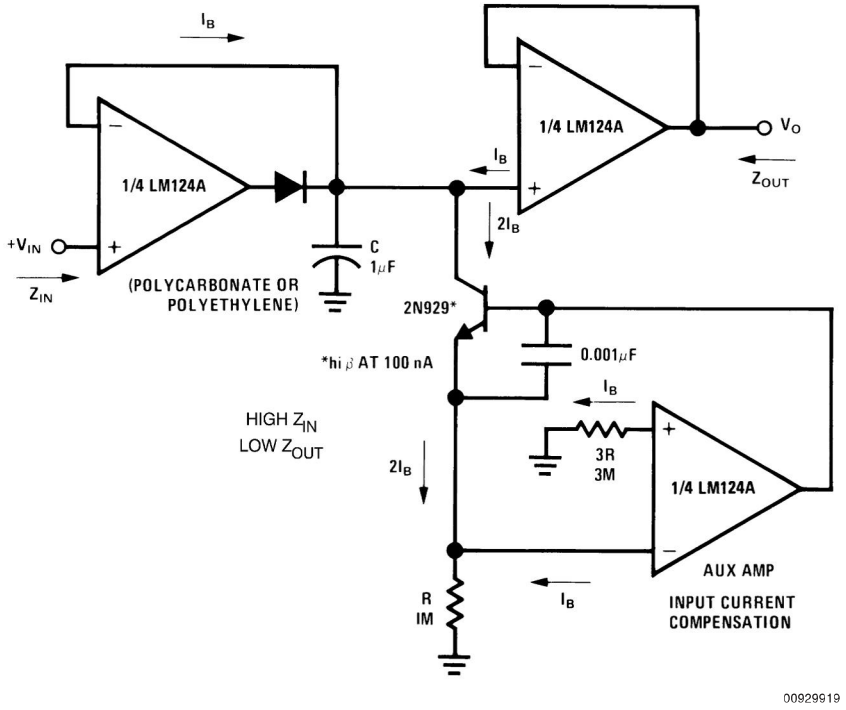

Typical Single-Supply Applications (V^+ = 5.0 V_{DC}) (Continued)

Comparator with Hysteresis

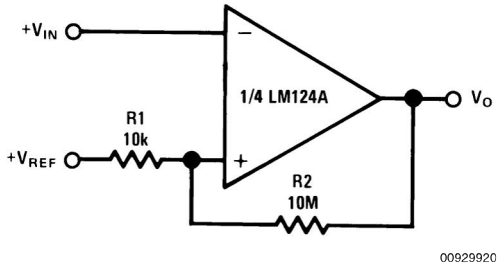

00929920

Ground Referencing a Differential Input Signal

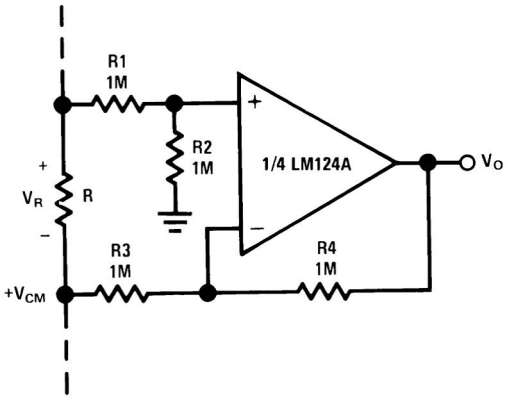

00929921

$V_O = V_R$

Voltage Controlled Oscillator Circuit

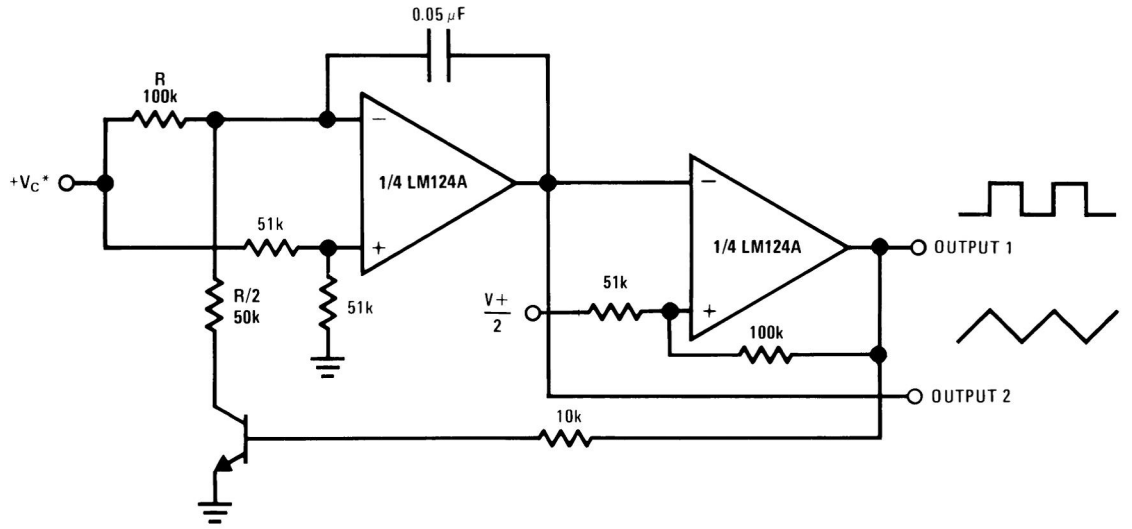

00929922

*Wide control voltage range: 0 $V_{DC} \leq V_C \leq 2$ ($V^+ - 1.5$ V_{DC})

Photo Voltaic-Cell Amplifier

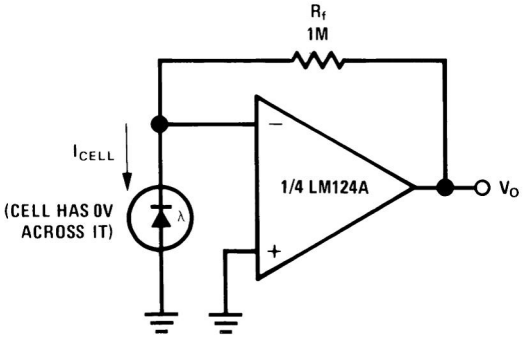

00929923

Integrated Circuit True RMS-to-DC Converter

AD536A

FEATURES

True RMS-to-DC Conversion
Laser-Trimmed to High Accuracy
0.2% Max Error (AD536AK)
0.5% Max Error (AD536AJ)
Wide Response Capability:
Computes RMS of AC and DC Signals
450 kHz Bandwidth: V rms > 100 mV
2 MHz Bandwidth: V rms > 1 V
Signal Crest Factor of 7 for 1% Error
dB Output with 60 dB Range
Low Power: 1.2 mA Quiescent Current
Single or Dual Supply Operation
Monolithic Integrated Circuit
–55°C to +125°C Operation (AD536AS)

PIN CONFIGURATIONS AND FUNCTIONAL BLOCK DIAGRAMS

TO-116 (D-14) and Q-14 Package

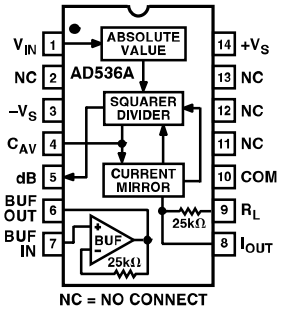

NC = NO CONNECT

TO-100 (H-10A) Package

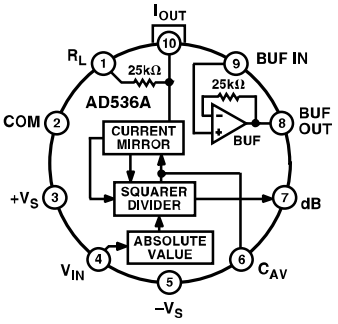

LCC (E-20A) Package

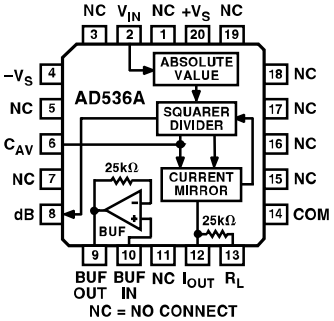

NC = NO CONNECT

PRODUCT DESCRIPTION

The AD536A is a complete monolithic integrated circuit which performs true rms-to-dc conversion. It offers performance which is comparable or superior to that of hybrid or modular units costing much more. The AD536A directly computes the true rms value of any complex input waveform containing ac and dc components. It has a crest factor compensation scheme which allows measurements with 1% error at crest factors up to 7. The wide bandwidth of the device extends the measurement capability to 300 kHz with 3 dB error for signal levels above 100 mV.

An important feature of the AD536A not previously available in rms converters is an auxiliary dB output. The logarithm of the rms output signal is brought out to a separate pin to allow the dB conversion, with a useful dynamic range of 60 dB. Using an externally supplied reference current, the 0 dB level can be conveniently set by the user to correspond to any input level from 0.1 to 2 volts rms.

The AD536A is laser trimmed at the wafer level for input and output offset, positive and negative waveform symmetry (dc reversal error), and full-scale accuracy at 7 V rms. As a result, no external trims are required to achieve the rated unit accuracy.

There is full protection for both inputs and outputs. The input circuitry can take overload voltages well beyond the supply levels. Loss of supply voltage with inputs connected will not cause unit failure. The output is short-circuit protected.

The AD536A is available in two accuracy grades (J, K) for commercial temperature range (0°C to +70°C) applications, and one grade (S) rated for the –55°C to +125°C extended range. The AD536AK offers a maximum total error of ±2 mV ±0.2% of reading, and the AD536AJ and AD536AS have maximum errors of ±5 mV ±0.5% of reading. All three versions are available in either a hermetically sealed 14-lead DIP or 10-pin TO-100 metal can. The AD536AS is also available in a 20-leadless hermetically sealed ceramic chip carrier.

PRODUCT HIGHLIGHTS

1. The AD536A computes the true root-mean-square level of a complex ac (or ac plus dc) input signal and gives an equivalent dc output level. The true rms value of a waveform is a more useful quantity than the average rectified value since it relates directly to the power of the signal. The rms value of a statistical signal also relates to its standard deviation.
2. The crest factor of a waveform is the ratio of the peak signal swing to the rms value. The crest factor compensation scheme of the AD536A allows measurement of highly complex signals with wide dynamic range.
3. The only external component required to perform measurements to the fully specified accuracy is the capacitor which sets the averaging period. The value of this capacitor determines the low frequency ac accuracy, ripple level and settling time.
4. The AD536A will operate equally well from split supplies or a single supply with total supply levels from 5 to 36 volts. The one milliampere quiescent supply current makes the device well-suited for a wide variety of remote controllers and battery powered instruments.
5. The AD536A directly replaces the AD536 and provides improved bandwidth and temperature drift specifications.

REV. B

One Technology Way, P.O. Box 9106, Norwood, MA 02062-9106, U.S.A.
Tel: 781/329-4700 World Wide Web Site: http://www.analog.com
Fax: 781/326-8703

AD536A–SPECIFICATIONS (@ +25°C, and ±15 V dc unless otherwise noted)

Model	AD536AJ			AD536AK			AD536AS			Units
	Min	Typ	Max	Min	Typ	Max	Min	Typ	Max	
TRANSFER FUNCTION		$V_{OUT} = \sqrt{avg.(V_{IN})^2}$			$V_{OUT} = \sqrt{avg.(V_{IN})^2}$			$V_{OUT} = \sqrt{avg.(V_{IN})^2}$		
CONVERSION ACCURACY										
Total Error, Internal Trim[1] (Figure 1)			**±5 ±0.5**			**±2 ±0.2**			**±5 ±0.5**	mV ± % of Reading
vs. Temperature, T_{MIN} to +70°C			±0.1 ±0.01			±0.05 ±0.005			**±0.1 ±0.005**	mV ± % of Reading/°C
+70°C to +125°C									**±0.3 ±0.005**	mV ± % of Reading/°C
vs. Supply Voltage		±0.1 ±0.01			±0.1 ±0.01			±0.1 ±0.01		mV ± % of Reading/V
dc Reversal Error		±0.2			**±0.1**			±0.2		± % of Reading
Total Error, External Trim[1] (Figure 2)		±3 ±0.3			±2 ±0.1			±3 ±0.3		mV ± % of Reading
ERROR VS. CREST FACTOR[2]										
Crest Factor 1 to 2		Specified Accuracy			Specified Accuracy			Specified Accuracy		
Crest Factor = 3		–0.1			–0.1			–0.1		% of Reading
Crest Factor = 7		–1.0			–1.0			–1.0		% of Reading
FREQUENCY RESPONSE[3]										
Bandwidth for 1% Additional Error (0.09 dB)										
V_{IN} = 10 mV		5			5			5		kHz
V_{IN} = 100 mV		45			45			45		kHz
V_{IN} = 1 V		120			120			120		kHz
±3 dB Bandwidth										
V_{IN} = 10 mV		90			90			90		kHz
V_{IN} = 100 mV		450			450			450		kHz
V_{IN} = 1 V		2.3			2.3			2.3		MHz
AVERAGING TIME CONSTANT (Figure 5)		25			25			25		ms/µF CAV
INPUT CHARACTERISTICS										
Signal Range, ±15 V Supplies										
Continuous rms Level		0 to 7			0 to 7			0 to 7		V rms
Peak Transient Input			±20			±20			±20	V peak
Continuous rms Level, ±5 V Supplies		0 to 2			0 to 2			0 to 2		V rms
Peak Transient Input, ±5 V Supplies			±7			±7			±7	V peak
Maximum Continuous Nondestructive Input Level (All Supply Voltages)			±25			±25			±25	V peak
Input Resistance	13.33	16.67	20	13.33	16.67	20	13.33	16.67	20	kΩ
Input Offset Voltage		0.8	±2		0.5	±1		0.8	±2	mV
OUTPUT CHARACTERISTICS										
Offset Voltage, V_{IN} = COM (Figure 1)		±1	**±2**		±0.5	**±1**			**±2**	mV
vs. Temperature		±0.1			±0.1				**±0.2**	mV/°C
vs. Supply Voltage		±0.1			±0.1			±0.2		mV/V
Voltage Swing, ±15 V Supplies	**0 to +11**	+12.5		**0 to +11**	+12.5		**0 to +11**	+12.5		V
±5 V Supply	0 to +2			0 to +2			0 to +2			V
dB OUTPUT (Figure 13)										
Error, V_{IN} 7 mV to 7 V rms, 0 dB = 1 V rms		±0.4	**±0.6**		±0.2	**±0.3**		±0.5	**±0.6**	dB
Scale Factor		–3			–3			–3		mV/dB
Scale Factor TC (Uncompensated, see Figure 1 for Temperature Compensation)		–0.033			–0.033			–0.033		dB/°C
		+0.33			+0.33			+0.33		% of Reading/°C
I_{REF} for 0 dB = 1 V rms	**5**	20	**80**	**5**	20	**80**	**5**	20	**80**	µA
I_{REF} Range	**1**		100	**1**		100	**1**		100	µA
I_{OUT} TERMINAL										
I_{OUT} Scale Factor		40			40			40		µA/V rms
I_{OUT} Scale Factor Tolerance		±10	±20		±10	±20		±10	±20	%
Output Resistance	20	25	30	20	25	30	20	25	30	kΩ
Voltage Compliance		$–V_S$ to ($+V_S$ –2.5 V)			$–V_S$ to ($+V_S$ –2.5 V)			$–V_S$ to ($+V_S$ –2.5 V)		V
BUFFER AMPLIFIER										
Input and Output Voltage Range	$–V_S$ to ($+V_S$ –2.5 V)			$–V_S$ to ($+V_S$ –2.5 V)			$–V_S$ to ($+V_S$ –2.5 V)			V
Input Offset Voltage, R_S = 25 k		±0.5	**±4**		±0.5	**±4**		±0.5	**±4**	mV
Input Bias Current		20	**60**		20	**60**		20	**60**	nA
Input Resistance		10^8			10^8			10^8		Ω
Output Current	(+5 mA, –130 µA)			(+5 mA, –130 µA)			(+5 mA, –130 µA)			
Short Circuit Current		20			20			20		mA
Output Resistance			0.5			0.5			0.5	Ω
Small Signal Bandwidth		1			1			1		MHz
Slew Rate[4]		5			5			5		V/µs
POWER SUPPLY										
Voltage Rated Performance		±15			±15			±15		V
Dual Supply	±3.0		±18	±3.0		±18	±3.0		±18	V
Single Supply	+5		+36	+5		+36	+5		+36	V
Quiescent Current										
Total V_S, 5 V to 36 V, T_{MIN} to T_{MAX}		1.2	**2**		1.2	**2**		1.2	**2**	mA
TEMPERATURE RANGE										
Rated Performance	0		+70	0		+70	–55		+125	°C
Storage	–55		+150	–55		+150	–55		+150	°C
NUMBER OF TRANSISTORS		65			65			65		

NOTES

[1]Accuracy is specified for 0 V to 7 V rms, dc or 1 kHz sine wave input with the AD536A connected as in the figure referenced.

[2]Error vs. crest factor is specified as an additional error for 1 V rms rectangular pulse input, pulsewidth = 200 µs.

[3]Input voltages are expressed in volts rms, and error is percent of reading.

[4]With 2k external pull-down resistor.

Specifications subject to change without notice.

Specifications shown in **boldface** are tested on all production units at final electrical test. Results from those tests are used to calculate outgoing quality levels. All min and max specifications are guaranteed, although only those shown in boldface are tested on all production units.

ABSOLUTE MAXIMUM RATINGS[1]

Supply Voltage
- Dual Supply ..... ±18 V
- Single Supply ..... +36 V

Internal Power Dissipation[2] ..... 500 mW
Maximum Input Voltage ..... ±25 V Peak
Buffer Maximum Input Voltage ..... $\pm V_S$
Maximum Input Voltage ..... ±25 V Peak
Storage Temperature Range ..... –55°C to +150°C
Operating Temperature Range
- AD536AJ/K ..... 0°C to +70°C
- AD536AS ..... –55°C to +125°C

Lead Temperature Range
- (Soldering 60 sec) ..... +300°C

ESD Rating ..... 1000 V

NOTES

[1]Stresses above those listed under Absolute Maximum Ratings may cause permanent damage to the device. This is a stress rating only; functional operation of the device at these or any other conditions above those indicated in the operational section of this specification is not implied. Exposure to absolute maximum rating conditions for extended periods may affect device reliability.

[2]10-Pin Header: θ_{JA} = 150°C/W; 20-Leadless LCC: θ_{JA} = 95°C/W; 14-Lead Size Brazed Ceramic DIP: θ_{JA} = 95°C/W.

CHIP DIMENSIONS AND PAD LAYOUT

Dimensions shown in inches and (mm).

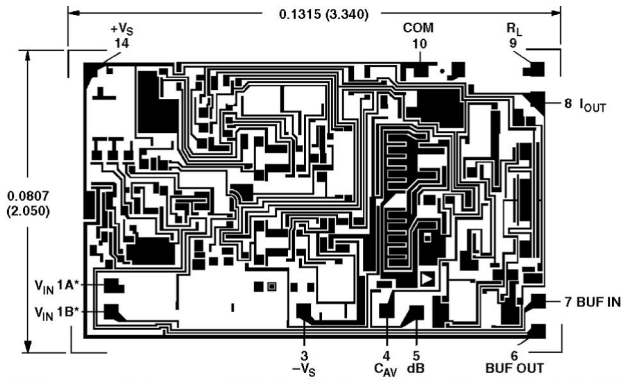

PAD NUMBERS CORRESPOND TO PIN NUMBERS FOR THE TO-166 14-LEAD CERAMIC DIP PACKAGE.
NOTE
*BOTH PADS SHOWN MUST BE CONNECTED TO V_{IN}.
THE AD536A IS AVAILABLE IN LASER TRIMMED CHIP FORM.
SUBSTRATE CONNECTED TO $-V_S$.

ORDERING GUIDE

Model	Temperature Range	Package Description	Package Option
AD536AJD	0°C to +70°C	Side Brazed Ceramic DIP	D-14
AD536AKD	0°C to +70°C	Side Brazed Ceramic DIP	D-14
AD536AJH	0°C to +70°C	Header	H-10A
AD536AKH	0°C to +70°C	Header	H-10A
AD536AJQ	0°C to +70°C	Cerdip	Q-14
AD536AKQ	0°C to +70°C	Cerdip	Q-14
AD536ASD	–55°C to +125°C	Side Brazed Ceramic DIP	D-14
AD536ASD/883B	–55°C to +125°C	Side Brazed Ceramic DIP	D-14
AD536ASE/883B	–55°C to +125°C	LCC	E-20A
AD536ASH	–55°C to +125°C	Header	H-10A
AD536ASH/883B	–55°C to +125°C	Header	H-10A
AD536AJCHIPS	0°C to +70°C	Die	
AD536AKH/+	0°C to +70°C	Header	H-10A
AD536ASCHIPS	–55°C to +125°C	Die	
5962-89805012A	–55°C to +125°C	LCC	E-20A
5962-8980501CA	–55°C to +125°C	Side Brazed Ceramic DIP	D-14
5962-8980501IA	–55°C to +125°C	Header	H-10A

STANDARD CONNECTION

The AD536A is simple to connect for the majority of high accuracy rms measurements, requiring only an external capacitor to set the averaging time constant. The standard connection is shown in Figure 1. In this configuration, the AD536A will measure the rms of the ac and dc level present at the input, but will show an error for low frequency inputs as a function of the filter capacitor, C_{AV}, as shown in Figure 5. Thus, if a 4 µF capacitor is used, the additional average error at 10 Hz will be 0.1%, at 3 Hz it will be 1%. The accuracy at higher frequencies will be according to specification. If it is desired to reject the dc input, a capacitor is added in series with the input, as shown in Figure 3, the capacitor must be nonpolar. If the AD536A is driven with power supplies with a considerable amount of high frequency ripple, it is advisable to bypass both supplies to ground with 0.1 µF ceramic discs as near the device as possible.

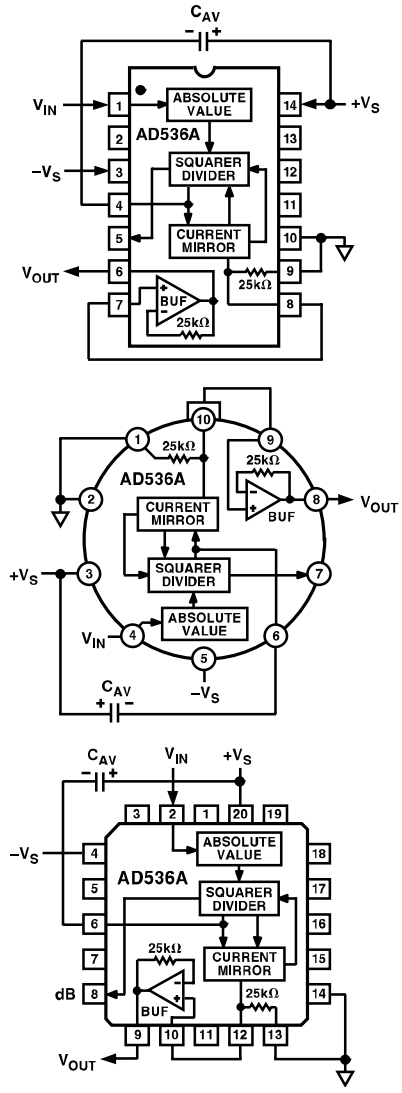

Figure 1. Standard RMS Connection

The input and output signal ranges are a function of the supply voltages; these ranges are shown in Figure 14. The AD536A can also be used in an unbuffered voltage output mode by disconnecting the input to the buffer. The output then appears unbuffered across the 25 kΩ resistor. The buffer amplifier can then be used for other purposes. Further the AD536A can be used in a current output mode by disconnecting the 25 kΩ resistor from ground. The output current is available at Pin 8 (Pin 10 on the "H" package) with a nominal scale of 40 μA per volt rms input positive out.

OPTIONAL EXTERNAL TRIMS FOR HIGH ACCURACY

If it is desired to improve the accuracy of the AD536A, the external trims shown in Figure 2 can be added. R4 is used to trim the offset. Note that the offset trim circuit adds 365 Ω in series with the internal 25 kΩ resistor. This will cause a 1.5% increase in scale factor, which is trimmed out by using R1 as shown. Range of scale factor adjustment is ±1.5%.

The trimming procedure is as follows:

1. Ground the input signal, V_{IN}, and adjust R4 to give zero volts output from Pin 6. Alternatively, R4 can be adjusted to give the correct output with the lowest expected value of V_{IN}.
2. Connect the desired full scale input level to V_{IN}, either dc or a calibrated ac signal (1 kHz is the optimum frequency); then trim R1, to give the correct output from Pin 6, i.e., 1000 V dc input should give 1.000 V dc output. Of course, a ±1.000 V peak-to-peak sine wave should give a 0.707 V dc output. The remaining errors, as given in the specifications are due to the nonlinearity.

The major advantage of external trimming is to optimize device performance for a reduced signal range; the AD536A is internally trimmed for a 7 V rms full-scale range.

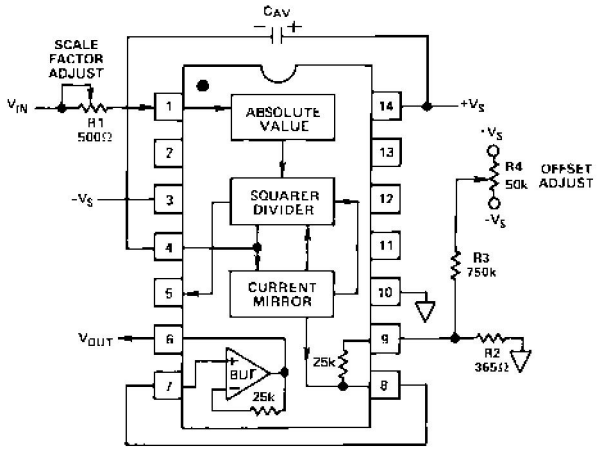

Figure 2. Optional External Gain and Output Offset Trims

SINGLE SUPPLY CONNECTION

The applications in Figures 1 and 2 require the use of approximately symmetrical dual supplies. The AD536A can also be used with only a single positive supply down to +5 volts, as shown in Figure 3. The major limitation of this connection is that only ac signals can be measured since the differential input stage must be biased off ground for proper operation. This biasing is done at Pin 10; thus it is critical that no extraneous signals be coupled into this point. Biasing can be accomplished by using a resistive divider between $+V_S$ and ground. The values of the resistors can be increased in the interest of lowered power consumption, since only 5 mA of current flows into Pin 10 (Pin 2 on the "H" package). AC input coupling requires only capacitor C2 as shown; a dc return is not necessary as it is provided internally. C2 is selected for the proper low frequency break point with the input resistance of 16.7 kΩ; for a cutoff at 10 Hz, C2 should be 1 μF. The signal ranges in this connection are slightly more restricted than in the dual supply connection. The input and output signal ranges are shown in Figure 14. The load resistor, R_L, is necessary to provide output sink current.

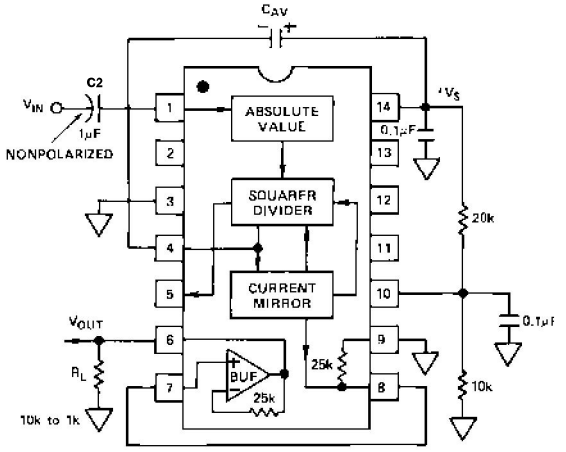

Figure 3. Single Supply Connection

CHOOSING THE AVERAGING TIME CONSTANT

The AD536A will compute the rms of both ac and dc signals. If the input is a slowly-varying dc signal, the output of the AD536A will track the input exactly. At higher frequencies, the average output of the AD536A will approach the rms value of the input signal. The actual output of the AD536A will differ from the ideal output by a dc (or average) error and some amount of ripple, as demonstrated in Figure 4.

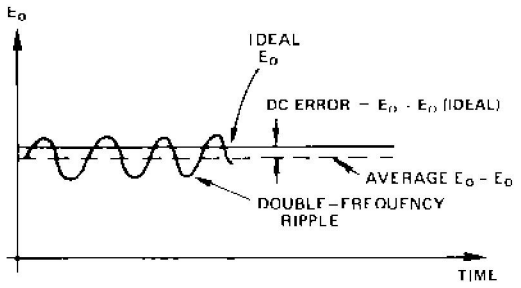

Figure 4. Typical Output Waveform for Sinusoidal Input

The dc error is dependent on the input signal frequency and the value of C_{AV}. Figure 5 can be used to determine the minimum value of C_{AV} which will yield a given percent dc error above a given frequency using the standard rms connection.

The ac component of the output signal is the ripple. There are two ways to reduce the ripple. The first method involves using a large value of C_{AV}. Since the ripple is inversely proportional to C_{AV}, a tenfold increase in this capacitance will affect a tenfold reduction in ripple. When measuring waveforms with high crest

factors, (such as low duty cycle pulse trains), the averaging time constant should be at least ten times the signal period. For example, a 100 Hz pulse rate requires a 100 ms time constant, which corresponds to a 4 µF capacitor (time constant = 25 ms per µF).

The primary disadvantage in using a large C_{AV} to remove ripple is that the settling time for a step change in input level is increased proportionately. Figure 5 shows that the relationship between C_{AV} and 1% settling time is 115 milliseconds for each microfarad of C_{AV}. The settling time is twice as great for decreasing signals as for increasing signals (the values in Figure 5 are for decreasing signals). Settling time also increases for low signal levels, as shown in Figure 6.

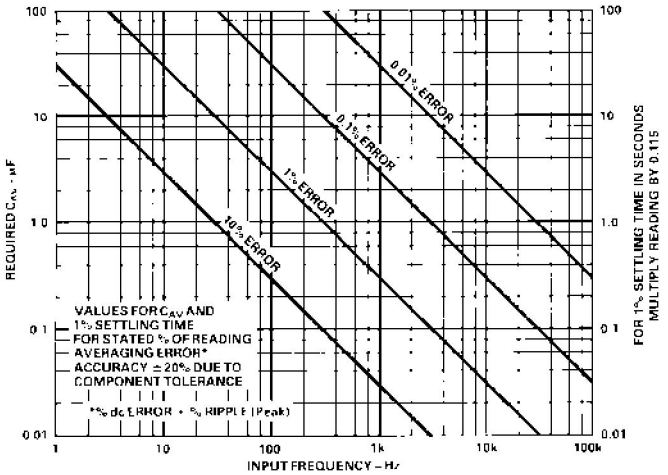

Figure 5. Error/Settling Time Graph for Use with the Standard rms Connection in Figure 1

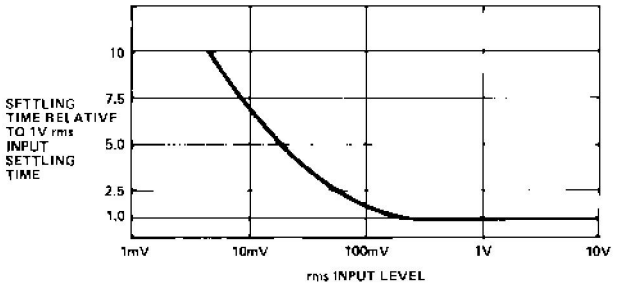

Figure 6. Settling Time vs. Input Level

A better method for reducing output ripple is the use of a "post-filter." Figure 7 shows a suggested circuit. If a single-pole filter is used (C3 removed, R_X shorted), and C2 is approximately twice the value of C_{AV}, the ripple is reduced as shown in Figure 8 and settling time is increased. For example, with C_{AV} = 1 µF and C2 = 2.2 µF, the ripple for a 60 Hz input is reduced from 10% of reading to approximately 0.3% of reading. The settling time, however, is increased by approximately a factor of 3. The values of C_{AV} and C2, can, therefore, be reduced to permit faster settling times while still providing substantial ripple reduction.

The two-pole post-filter uses an active filter stage to provide even greater ripple reduction without substantially increasing the settling times over a circuit with a one-pole filter. The values of C_{AV}, C2, and C3 can then be reduced to allow extremely fast settling times for a constant amount of ripple. Caution should be exercised in choosing the value of C_{AV}, since the dc error is dependent upon this value and is independent of the post filter.

For a more detailed explanation of these topics refer to the *RMS to DC Conversion Application Guide 2nd Edition*, available from Analog Devices.

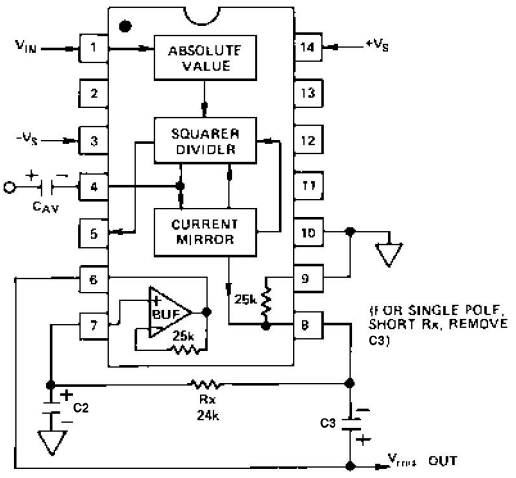

Figure 7. 2-Pole "Post" Filter

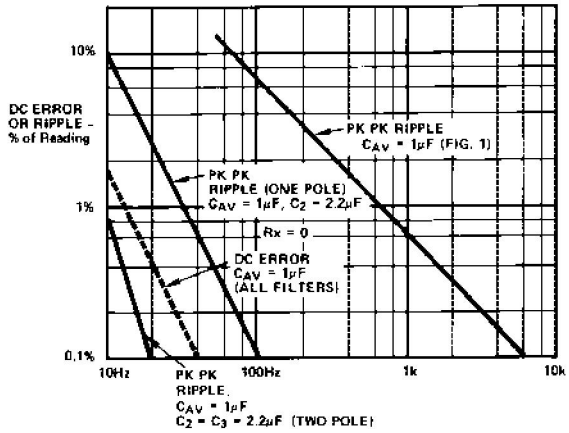

Figure 8. Performance Features of Various Filter Types

AD536A PRINCIPLE OF OPERATION

The AD536A embodies an implicit solution of the rms equation that overcomes the dynamic range as well as other limitations inherent in a straightforward computation of rms. The actual computation performed by the AD536A follows the equation:

$$V\,rms = Avg.\left[\frac{V_{IN}^{\,2}}{V\,rms}\right]$$

Figure 9 is a simplified schematic of the AD536A; it is subdivided into four major sections: absolute value circuit (active rectifier), squarer/divider, current mirror, and buffer amplifier. The input voltage, V_{IN}, which can be ac or dc, is converted to a unipolar current I_1, by the active rectifier A_1, A_2. I_1 drives one input of the squarer/divider, which has the transfer function:

$$I_4 = I_1^2/I_3$$

The output current, I_4, of the squarer/divider drives the current mirror through a low-pass filter formed by R1 and the externally connected capacitor, C_{AV}. If the R1, C_{AV} time constant is much greater than the longest period of the input signal, then I_4 is effectively averaged. The current mirror returns a current I_3, which equals Avg. [I_4], back to the squarer/divider to complete the implicit rms computation. Thus:

$$I_4 = Avg.\left[I_1^2/I_4\right] = I_1\ rms$$

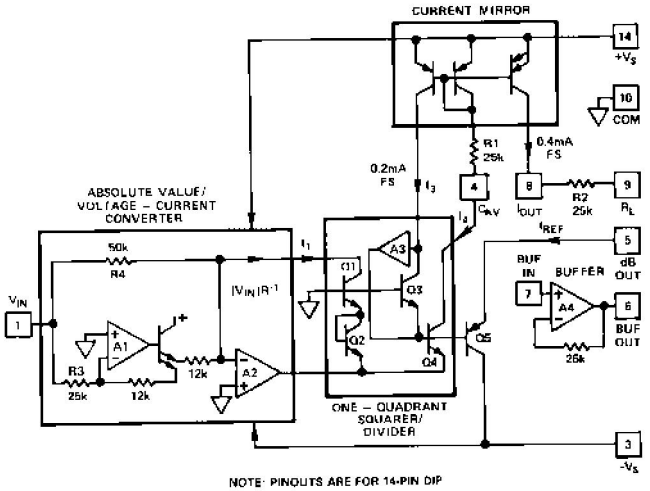

Figure 9. Simplified Schematic

The current mirror also produces the output current, I_{OUT}, which equals $2I_4$. I_{OUT} can be used directly or converted to a voltage with R2 and buffered by A4 to provide a low impedance voltage output. The transfer function of the AD536A thus results:

$$V_{OUT} = 2R2\ I\ rms = V_{IN}\ rms$$

The dB output is derived from the emitter of Q3, since the voltage at this point is proportional to –log V_{IN}. Emitter follower, Q5, buffers and level shifts this voltage, so that the dB output voltage is zero when the externally supplied emitter current (I_{REF}) to Q5 approximates I_3.

CONNECTIONS FOR dB OPERATION

A powerful feature added to the AD536A is the logarithmic or decibel output. The internal circuit computing dB works accurately over a 60 dB range. The connections for dB measurements are shown in Figure 10. The user selects the 0 dB level by adjusting R1, for the proper 0 dB reference current (which is set to exactly cancel the log output current from the squarer-divider at the desired 0 dB point). The external op amp is used to provide a more convenient scale and to allow compensation of the +0.33%/°C scale factor drift of the dB output pin. The special T.C. resistor, R2, is available from Tel Labs in Londonderry, N.H. (model Q-81) or from Precision Resistor Inc., Hillside, N.J. (model PT146). The averaged temperature coefficients of resistors R2 and R3 develop the +3300 ppm needed to reverse compensate the dB output. The linear rms output is available at Pin 8 on DIP or Pin 10 on header device with an output impedance of 25 kΩ; thus some applications may require an additional buffer amplifier if this output is desired.

dB Calibration:

1. Set V_{IN} = 1.00 V dc or 1.00 V rms
2. Adjust R1 for dB out = 0.00 V
3. Set V_{IN} = +0.1 V dc or 0.10 V rms
4. Adjust R5 for dB out = –2.00 V

Any other desired 0 dB reference level can be used by setting V_{IN} and adjusting R1, accordingly. Note that adjusting R5 for the proper gain automatically gives the correct temperature compensation.

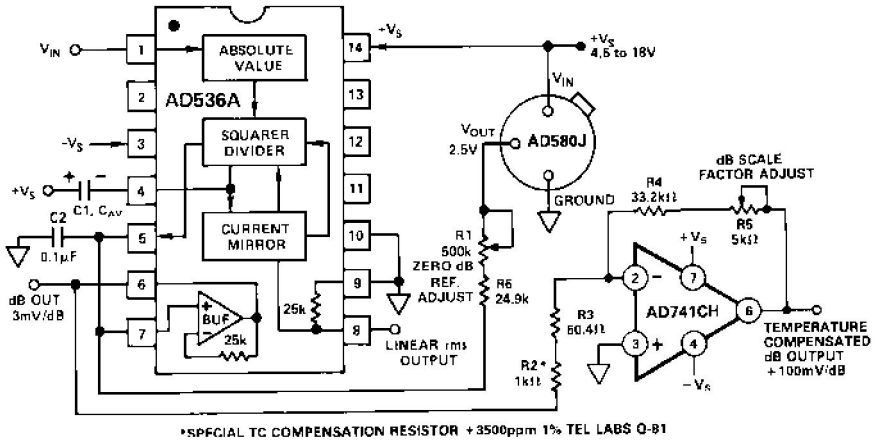

Figure 10. dB Connection

Features

- Compatible with MCS®-51 Products
- 8K Bytes of In-System Programmable (ISP) Flash Memory
  - Endurance: 10,000 Write/Erase Cycles
- 4.0V to 5.5V Operating Range
- Fully Static Operation: 0 Hz to 33 MHz
- Three-level Program Memory Lock
- 256 x 8-bit Internal RAM
- 32 Programmable I/O Lines
- Three 16-bit Timer/Counters
- Eight Interrupt Sources
- Full Duplex UART Serial Channel
- Low-power Idle and Power-down Modes
- Interrupt Recovery from Power-down Mode
- Watchdog Timer
- Dual Data Pointer
- Power-off Flag
- Fast Programming Time
- Flexible ISP Programming (Byte and Page Mode)
- Green (Pb/Halide-free) Packaging Option

8-bit Microcontroller with 8K Bytes In-System Programmable Flash

AT89S52

1. Description

The AT89S52 is a low-power, high-performance CMOS 8-bit microcontroller with 8K bytes of in-system programmable Flash memory. The device is manufactured using Atmel's high-density nonvolatile memory technology and is compatible with the industry-standard 80C51 instruction set and pinout. The on-chip Flash allows the program memory to be reprogrammed in-system or by a conventional nonvolatile memory programmer. By combining a versatile 8-bit CPU with in-system programmable Flash on a monolithic chip, the Atmel AT89S52 is a powerful microcontroller which provides a highly-flexible and cost-effective solution to many embedded control applications.

The AT89S52 provides the following standard features: 8K bytes of Flash, 256 bytes of RAM, 32 I/O lines, Watchdog timer, two data pointers, three 16-bit timer/counters, a six-vector two-level interrupt architecture, a full duplex serial port, on-chip oscillator, and clock circuitry. In addition, the AT89S52 is designed with static logic for operation down to zero frequency and supports two software selectable power saving modes. The Idle Mode stops the CPU while allowing the RAM, timer/counters, serial port, and interrupt system to continue functioning. The Power-down mode saves the RAM contents but freezes the oscillator, disabling all other chip functions until the next interrupt or hardware reset.

1919D–MICRO–6/08

2. Pin Configurations

2.1 40-lead PDIP

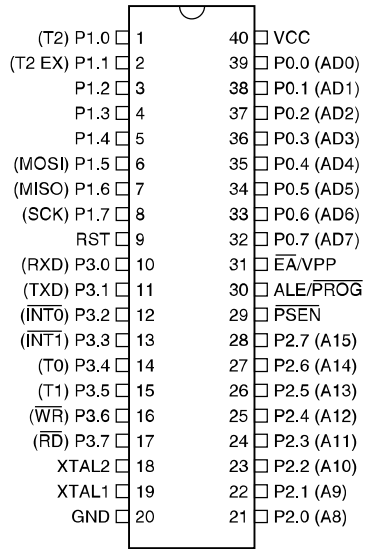

2.2 44-lead TQFP

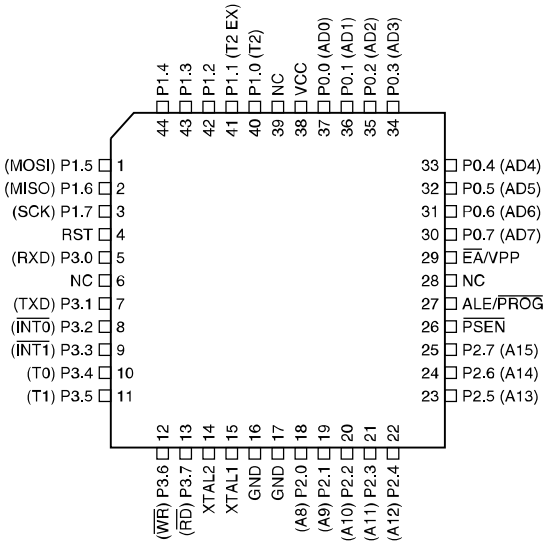

2.3 44-lead PLCC

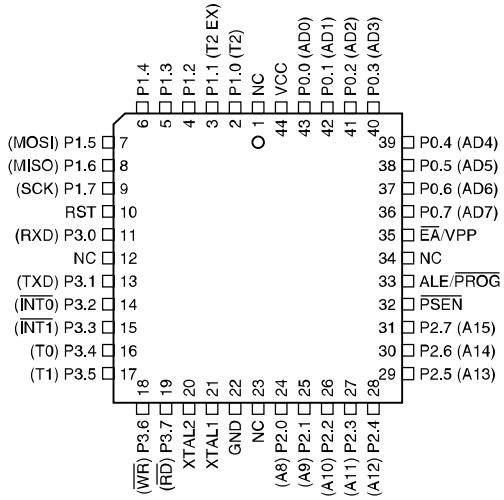

3. Block Diagram

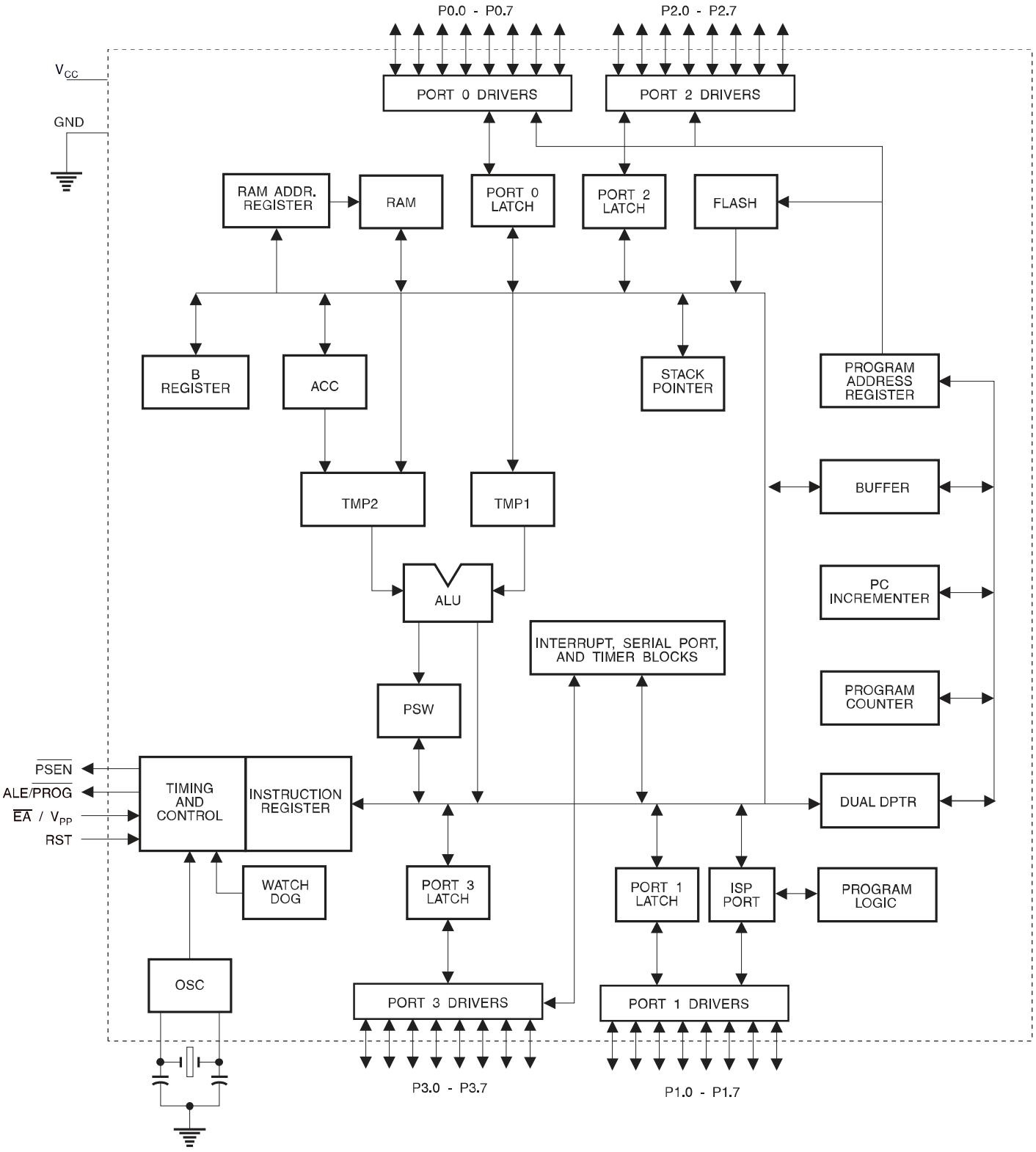

4. Pin Description

4.1 VCC

Supply voltage.

4.2 GND

Ground.

4.3 Port 0

Port 0 is an 8-bit open drain bidirectional I/O port. As an output port, each pin can sink eight TTL inputs. When 1s are written to port 0 pins, the pins can be used as high-impedance inputs.

Port 0 can also be configured to be the multiplexed low-order address/data bus during accesses to external program and data memory. In this mode, P0 has internal pull-ups.

Port 0 also receives the code bytes during Flash programming and outputs the code bytes during program verification. **External pull-ups are required during program verification.**

4.4 Port 1

Port 1 is an 8-bit bidirectional I/O port with internal pull-ups. The Port 1 output buffers can sink/source four TTL inputs. When 1s are written to Port 1 pins, they are pulled high by the internal pull-ups and can be used as inputs. As inputs, Port 1 pins that are externally being pulled low will source current (I_{IL}) because of the internal pull-ups.

In addition, P1.0 and P1.1 can be configured to be the timer/counter 2 external count input (P1.0/T2) and the timer/counter 2 trigger input (P1.1/T2EX), respectively, as shown in the following table.

Port 1 also receives the low-order address bytes during Flash programming and verification.

Port Pin	Alternate Functions
P1.0	T2 (external count input to Timer/Counter 2), clock-out
P1.1	T2EX (Timer/Counter 2 capture/reload trigger and direction control)
P1.5	MOSI (used for In-System Programming)
P1.6	MISO (used for In-System Programming)
P1.7	SCK (used for In-System Programming)

4.5 Port 2

Port 2 is an 8-bit bidirectional I/O port with internal pull-ups. The Port 2 output buffers can sink/source four TTL inputs. When 1s are written to Port 2 pins, they are pulled high by the internal pull-ups and can be used as inputs. As inputs, Port 2 pins that are externally being pulled low will source current (I_{IL}) because of the internal pull-ups.

Port 2 emits the high-order address byte during fetches from external program memory and during accesses to external data memory that use 16-bit addresses (MOVX @ DPTR). In this application, Port 2 uses strong internal pull-ups when emitting 1s. During accesses to external data memory that use 8-bit addresses (MOVX @ RI), Port 2 emits the contents of the P2 Special Function Register.

Port 2 also receives the high-order address bits and some control signals during Flash programming and verification.

4.6 Port 3

Port 3 is an 8-bit bidirectional I/O port with internal pull-ups. The Port 3 output buffers can sink/source four TTL inputs. When 1s are written to Port 3 pins, they are pulled high by the internal pull-ups and can be used as inputs. As inputs, Port 3 pins that are externally being pulled low will source current (I_{IL}) because of the pull-ups.

Port 3 receives some control signals for Flash programming and verification.

Port 3 also serves the functions of various special features of the AT89S52, as shown in the following table.

Port Pin	Alternate Functions
P3.0	RXD (serial input port)
P3.1	TXD (serial output port)
P3.2	$\overline{\text{INT0}}$ (external interrupt 0)
P3.3	$\overline{\text{INT1}}$ (external interrupt 1)
P3.4	T0 (timer 0 external input)
P3.5	T1 (timer 1 external input)
P3.6	$\overline{\text{WR}}$ (external data memory write strobe)
P3.7	$\overline{\text{RD}}$ (external data memory read strobe)

4.7 RST

Reset input. A high on this pin for two machine cycles while the oscillator is running resets the device. This pin drives high for 98 oscillator periods after the Watchdog times out. The DISRTO bit in SFR AUXR (address 8EH) can be used to disable this feature. In the default state of bit DISRTO, the RESET HIGH out feature is enabled.

4.8 ALE/$\overline{\text{PROG}}$

Address Latch Enable (ALE) is an output pulse for latching the low byte of the address during accesses to external memory. This pin is also the program pulse input ($\overline{\text{PROG}}$) during Flash programming.

In normal operation, ALE is emitted at a constant rate of 1/6 the oscillator frequency and may be used for external timing or clocking purposes. Note, however, that one ALE pulse is skipped during each access to external data memory.

If desired, ALE operation can be disabled by setting bit 0 of SFR location 8EH. With the bit set, ALE is active only during a MOVX or MOVC instruction. Otherwise, the pin is weakly pulled high. Setting the ALE-disable bit has no effect if the microcontroller is in external execution mode.

4.9 $\overline{\text{PSEN}}$

Program Store Enable ($\overline{\text{PSEN}}$) is the read strobe to external program memory.

When the AT89S52 is executing code from external program memory, $\overline{\text{PSEN}}$ is activated twice each machine cycle, except that two $\overline{\text{PSEN}}$ activations are skipped during each access to external data memory.

4.10 $\overline{\text{EA}}$/VPP

External Access Enable. $\overline{\text{EA}}$ must be strapped to GND in order to enable the device to fetch code from external program memory locations starting at 0000H up to FFFFH. Note, however, that if lock bit 1 is programmed, $\overline{\text{EA}}$ will be internally latched on reset.

$\overline{\text{EA}}$ should be strapped to V_{CC} for internal program executions.

This pin also receives the 12-volt programming enable voltage (V_{PP}) during Flash programming.

4.11 XTAL1

Input to the inverting oscillator amplifier and input to the internal clock operating circuit.

4.12 XTAL2

Output from the inverting oscillator amplifier.

5. Special Function Registers

A map of the on-chip memory area called the Special Function Register (SFR) space is shown in Table 5-1.

Note that not all of the addresses are occupied, and unoccupied addresses may not be implemented on the chip. Read accesses to these addresses will in general return random data, and write accesses will have an indeterminate effect.

User software should not write 1s to these unlisted locations, since they may be used in future products to invoke new features. In that case, the reset or inactive values of the new bits will always be 0.

Timer 2 Registers: Control and status bits are contained in registers T2CON (shown in Table 5-2) and T2MOD (shown in Table 10-2) for Timer 2. The register pair (RCAP2H, RCAP2L) are the Capture/Reload registers for Timer 2 in 16-bit capture mode or 16-bit auto-reload mode.

Interrupt Registers: The individual interrupt enable bits are in the IE register. Two priorities can be set for each of the six interrupt sources in the IP register.

National Semiconductor

July 8, 2009

ADC0808/ADC0809

8-Bit µP Compatible A/D Converters with 8-Channel Multiplexer

General Description

The ADC0808, ADC0809 data acquisition component is a monolithic CMOS device with an 8-bit analog-to-digital converter, 8-channel multiplexer and microprocessor compatible control logic. The 8-bit A/D converter uses successive approximation as the conversion technique. The converter features a high impedance chopper stabilized comparator, a 256R voltage divider with analog switch tree and a successive approximation register. The 8-channel multiplexer can directly access any of 8-single-ended analog signals.

The device eliminates the need for external zero and full-scale adjustments. Easy interfacing to microprocessors is provided by the latched and decoded multiplexer address inputs and latched TTL TRI-STATE outputs.

The design of the ADC0808, ADC0809 has been optimized by incorporating the most desirable aspects of several A/D conversion techniques. The ADC0808, ADC0809 offers high speed, high accuracy, minimal temperature dependence, excellent long-term accuracy and repeatability, and consumes minimal power. These features make this device ideally suited to applications from process and machine control to consumer and automotive applications. For 16-channel multiplexer with common output (sample/hold port) see ADC0816 data sheet. (See AN-247 for more information.)

Features

- Easy interface to all microprocessors
- Operates ratiometrically or with 5 V_{DC} or analog span adjusted voltage reference
- No zero or full-scale adjust required
- 8-channel multiplexer with address logic
- 0V to V_{CC} input range
- Outputs meet TTL voltage level specifications
- ADC0808 equivalent to MM74C949
- ADC0809 equivalent to MM74C949-1

Key Specifications

Resolution	8 Bits
Total Unadjusted Error	±½ LSB and ±1 LSB
Single Supply	5 V_{DC}
Low Power	15 mW
Conversion Time	100 µs

Block Diagram

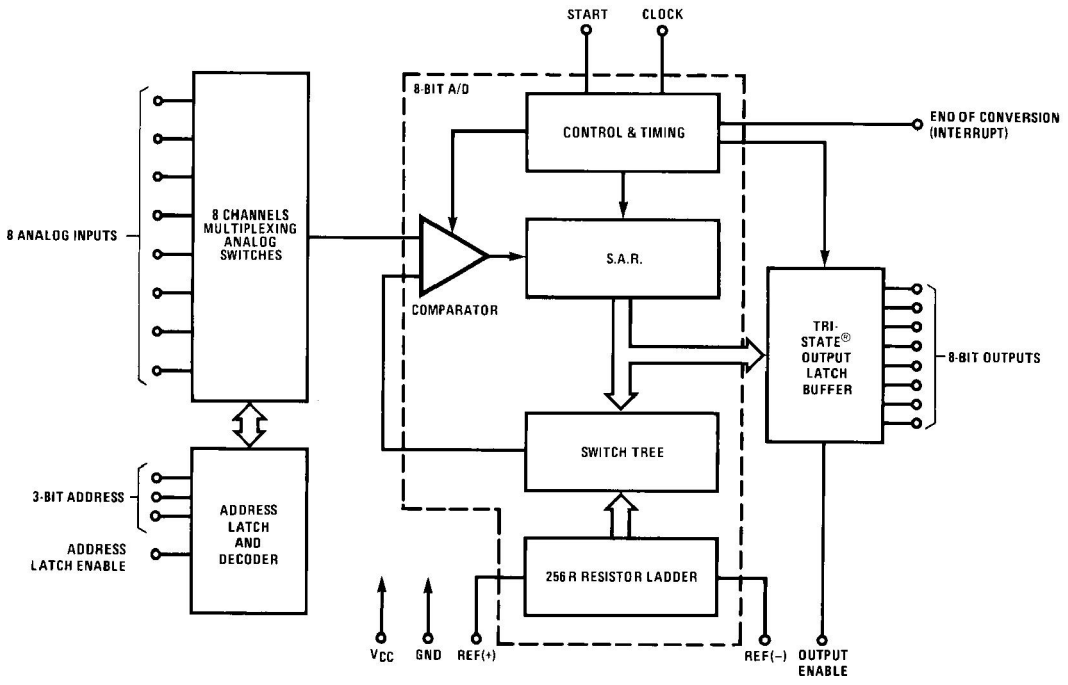

See Ordering Information

Connection Diagrams

Dual-In-Line Package

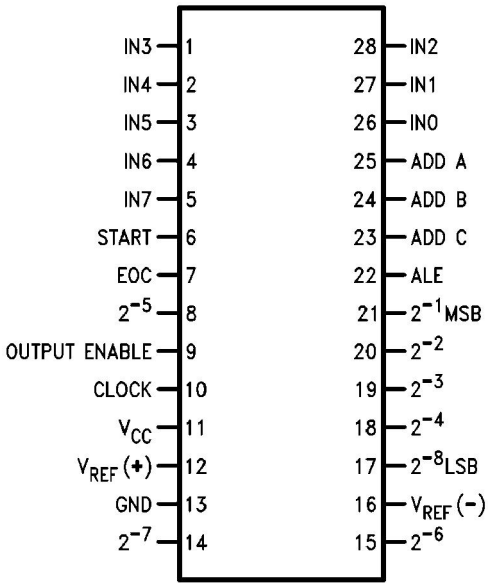

567211

Order Number ADC0808CCN or ADC0809CCN
See NS Package NA28E

Molded Chip Carrier Package

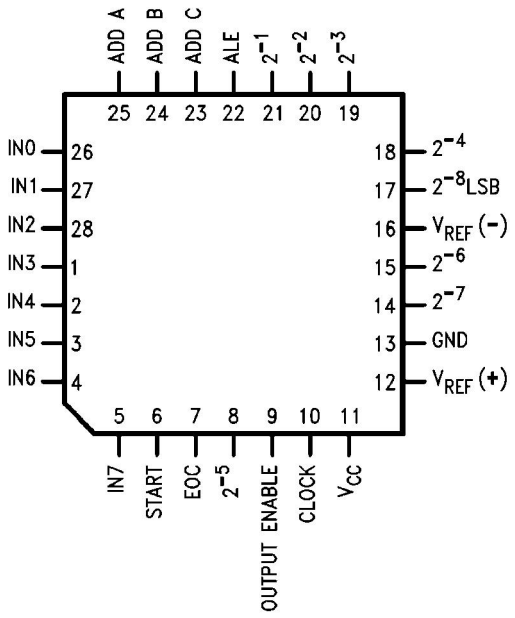

567212

Order Number ADC0808CCV or ADC0809CCV
See NS Package V28A

Ordering Information

Temperature Range		−40°C to +85°C		
Package Outline		NA28E Molded DIP	V28A Molded Chip Carrier	V28A Molded Chip Carrier (Tape and Reel)
Error	±½ LSB Unadjusted	ADC0808CCN	ADC0808CCV	ADC0808CCVX
	±1 LSB Unadjusted	ADC0809CCN	ADC0809CCV	ADC0809CCVX

Absolute Maximum Ratings

(Notes 2, 1)

If Military/Aerospace specified devices are required, please contact the National Semiconductor Sales Office/ Distributors for availability and specifications.

Supply Voltage (V_{CC}) (Note 3)	6.5V
Voltage at Any Pin	−0.3V to (V_{CC} +0.3V)
Except Control Inputs	
Voltage at Control Inputs	−0.3V to +15V
(START, OE, CLOCK, ALE, ADD A, ADD B, ADD C)	
Storage Temperature Range	−65°C to +150°C
Package Dissipation at T_A=25°C	875 mW
Lead Temp. (Soldering, 10 seconds)	
Dual-In-Line Package (plastic)	260°C
Molded Chip Carrier Package	
Vapor Phase (60 seconds)	215°C
Infrared (15 seconds)	220°C
ESD Susceptibility (Note 8)	400V

Operating Conditions

(Notes 1, 2)

Temperature Range	$T_{MIN} \le T_A \le T_{MAX}$
	$-40°C \le T_A \le +85°C$
Range of V_{CC}	4.5 V_{DC} to 6.0 V_{DC}

Electrical Characteristics – Converter Specifications

Converter Specifications: V_{CC}=5 V_{DC}=V_{REF+}, $V_{REF(-)}$=GND, $T_{MIN} \le T_A \le T_{MAX}$ and f_{CLK}=640 kHz unless otherwise stated.

Symbol	Parameter	Conditions	Min	Typ	Max	Units
	ADC0808					
	Total Unadjusted Error	25°C			±½	LSB
	(Note 5)	T_{MIN} to T_{MAX}			±¾	LSB
	ADC0809					
	Total Unadjusted Error	0°C to 70°C			±1	LSB
	(Note 5)	T_{MIN} to T_{MAX}			±1¼	LSB
	Input Resistance	From Ref(+) to Ref(−)	1.0	2.5		kΩ
	Analog Input Voltage Range	(Note 4) V(+) or V(−)	GND − 0.1		V_{CC} + 0.1	V_{DC}
$V_{REF(+)}$	Voltage, Top of Ladder	Measured at Ref(+)		V_{CC}	V_{CC} + 0.1	V
$\frac{V_{REF(+)}+V_{REF(-)}}{2}$	Voltage, Center of Ladder		(V_{CC}/2) − 0.1	V_{CC}/2	(V_{CC}/2) + 0.1	V
$V_{REF(-)}$	Voltage, Bottom of Ladder	Measured at Ref(−)	−0.1	0		V
I_{IN}	Comparator Input Current	f_c=640 kHz, (Note 6)	−2	±0.5	2	µA

Electrical Characteristics – Digital Levels and DC Specifications

Digital Levels and DC Specifications: ADC0808CCN, ADC0808CCV, ADC0809CCN and ADC0809CCV, $4.75 \le V_{CC} \le 5.25V$, $-40°C \le T_A \le +85°C$ unless otherwise noted

Symbol	Parameter	Conditions	Min	Typ	Max	Units
ANALOG MULTIPLEXER						
$I_{OFF(+)}$	OFF Channel Leakage Current	V_{CC}=5V, V_{IN}=5V,				
		T_A=25°C		10	200	nA
		T_{MIN} to T_{MAX}			1.0	µA
$I_{OFF(-)}$	OFF Channel Leakage Current	V_{CC}=5V, V_{IN}=0,				
		T_A=25°C	−200	−10		nA
		T_{MIN} to T_{MAX}	−1.0			µA
CONTROL INPUTS						
$V_{IN(1)}$	Logical "1" Input Voltage		(V_{CC} − 1.5)			V
$V_{IN(0)}$	Logical "0" Input Voltage				1.5	V

Symbol	Parameter	Conditions	Min	Typ	Max	Units
$I_{IN(1)}$	Logical "1" Input Current (The Control Inputs)	V_{IN}=15V			1.0	µA
$I_{IN(0)}$	Logical "0" Input Current (The Control Inputs)	V_{IN}=0	−1.0			µA
I_{CC}	Supply Current	f_{CLK}=640 kHz		0.3	3.0	mA
DATA OUTPUTS AND EOC (INTERRUPT)						
$V_{OUT(1)}$	Logical "1" Output Voltage	V_{CC} = 4.75V I_{OUT} = −360µA I_{OUT} = −10µA	 **2.4** **4.5**			 V V
$V_{OUT(0)}$	Logical "0" Output Voltage	I_O=1.6 mA			0.45	V
$V_{OUT(0)}$	Logical "0" Output Voltage EOC	I_O=1.2 mA			0.45	V
I_{OUT}	TRI-STATE Output Current	V_O=5V V_O=0	 −3		3	µA µA

Electrical Characteristics – Timing Specifications

Timing Specifications V_{CC}=$V_{REF(+)}$=5V, $V_{REF(-)}$=GND, t_r=t_f=20 ns and T_A=25°C unless otherwise noted.

Symbol	Parameter	Conditions	Mln	Typ	Max	Units
t_{STCLK}	Start Time Delay from Clock	(*Figure 5*)	300		900	ns
t_{WS}	Minimum Start Pulse Width	(*Figure 5*)		100	200	ns
t_{WALE}	Minimum ALE Pulse Width	(*Figure 5*)		100	200	ns
t_s	Minimum Address Set-Up Time	(*Figure 5*)		25	50	ns
t_H	Minimum Address Hold Time	(*Figure 5*)		25	50	ns
t_D	Analog MUX Delay Time From ALE	R_S=0Ω (*Figure 5*)		1	2.5	µs
t_{H1}, t_{H0}	OE Control to Q Logic State	C_L=50 pF, R_L=10k (*Figure 8*)		125	250	ns
t_{1H}, t_{0H}	OE Control to Hi-Z	C_L=10 pF, R_L=10k (*Figure 8*)		125	250	ns
t_c	Conversion Time	f_c=640 kHz, (*Figure 5*) (Note 7)	90	100	116	µs
f_c	Clock Frequency		10	640	1280	kHz
t_{EOC}	EOC Delay Time	(*Figure 5*)	0		8 + 2 µS	Clock Periods
C_{IN}	Input Capacitance	At Control Inputs		10	15	pF
C_{OUT}	TRI-STATE Output Capacitance	At TRI-STATE Outputs		10	15	pF

Note 1: Absolute Maximum Ratings indicate limits beyond which damage to the device may occur. DC and AC electrical specifications do not apply when operating the device beyond its specified operating conditions.

Note 2: All voltages are measured with respect to GND, unless otherwise specified.

Note 3: A Zener diode exists, internally, from V_{CC} to GND and has a typical breakdown voltage of 7 V_{DC}.

Note 4: Two on-chip diodes are tied to each analog input which will forward conduct for analog input voltages one diode drop below ground or one diode drop greater than the V_{CC}n supply. The spec allows 100 mV forward bias of either diode. This means that as long as the analog V_{IN} does not exceed the supply voltage by more than 100 mV, the output code will be correct. To achieve an absolute 0V_{DC} to 5V_{DC} input voltage range will therefore require a minimum supply voltage of 4.900 V_{DC} over temperature variations, initial tolerance and loading.

Note 5: Total unadjusted error includes offset, full-scale, linearity, and multiplexer errors. See *Figure 3*. None of these A/Ds requires a zero or full-scale adjust. However, if an all zero code is desired for an analog input other than 0.0V, or if a narrow full-scale span exists (for example: 0.5V to 4.5V full-scale) the reference voltages can be adjusted to achieve this. See *Figure 13*.

Note 6: Comparator input current is a bias current into or out of the chopper stabilized comparator. The bias current varies directly with clock frequency and has little temperature dependence (*Figure 6*). See paragraph 4.0.

Note 7: The outputs of the data register are updated one clock cycle before the rising edge of EOC.

Note 8: Human body model, 100 pF discharged through a 1.5 kΩ resistor.

Functional Description

MULTIPLEXER

The device contains an 8-channel single-ended analog signal multiplexer. A particular input channel is selected by using the address decoder. *Table 1* shows the input states for the address lines to select any channel. The address is latched into the decoder on the low-to-high transition of the address latch enable signal.

TABLE 1. Analog Channel Selection

SELECTED ANALOG CHANNEL	ADDRESS LINE		
	C	B	A
IN0	L	L	L
IN1	L	L	H
IN2	L	H	L
IN3	L	H	H
IN4	H	L	L
IN5	H	L	H
IN6	H	H	L
IN7	H	H	H

CONVERTER CHARACTERISTICS

The Converter

The heart of this single chip data acquisition system is its 8-bit analog-to-digital converter. The converter is designed to give fast, accurate, and repeatable conversions over a wide range of temperatures. The converter is partitioned into 3 major sections: the 256R ladder network, the successive approximation register, and the comparator. The converter's digital outputs are positive true.

The 256R ladder network approach (*Figure 1*) was chosen over the conventional R/2R ladder because of its inherent monotonicity, which guarantees no missing digital codes. Monotonicity is particularly important in closed loop feedback control systems. A non-monotonic relationship can cause oscillations that will be catastrophic for the system. Additionally, the 256R network does not cause load variations on the reference voltage.

The bottom resistor and the top resistor of the ladder network in *Figure 1* are not the same value as the remainder of the network. The difference in these resistors causes the output characteristic to be symmetrical with the zero and full-scale points of the transfer curve. The first output transition occurs when the analog signal has reached +½ LSB and succeeding output transitions occur every 1 LSB later up to full-scale.

The successive approximation register (SAR) performs 8 iterations to approximate the input voltage. For any SAR type converter, n-iterations are required for an n-bit converter. *Figure 2* shows a typical example of a 3-bit converter. In the ADC0808, ADC0809, the approximation technique is extended to 8 bits using the 256R network.

The A/D converter's successive approximation register (SAR) is reset on the positive edge of the start conversion start pulse. The conversion is begun on the falling edge of the start conversion pulse. A conversion in process will be interrupted by receipt of a new start conversion pulse. Continuous conversion may be accomplished by tying the end-of-conversion (EOC) output to the SC input. If used in this mode, an external start conversion pulse should be applied after power up. End-of-conversion will go low between 0 and 8 clock pulses after the rising edge of start conversion.

The most important section of the A/D converter is the comparator. It is this section which is responsible for the ultimate accuracy of the entire converter. It is also the comparator drift which has the greatest influence on the repeatability of the device. A chopper-stabilized comparator provides the most effective method of satisfying all the converter requirements.

The chopper-stabilized comparator converts the DC input signal into an AC signal. This signal is then fed through a high gain AC amplifier and has the DC level restored. This technique limits the drift component of the amplifier since the drift is a DC component which is not passed by the AC amplifier. This makes the entire A/D converter extremely insensitive to temperature, long term drift and input offset errors.

Figure 4 shows a typical error curve for the ADC0808 as measured using the procedures outlined in AN-179.

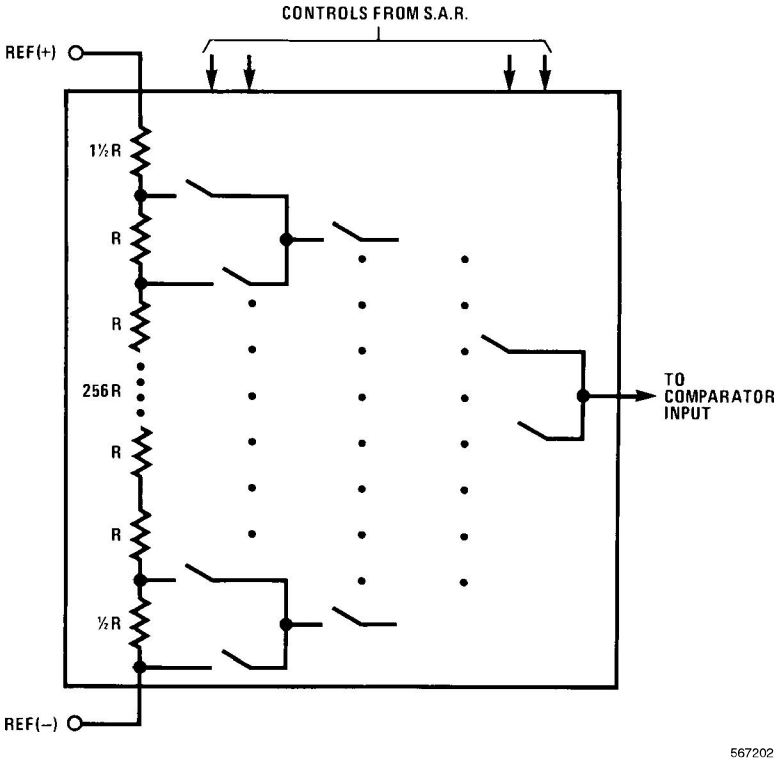

FIGURE 1. Resistor Ladder and Switch Tree

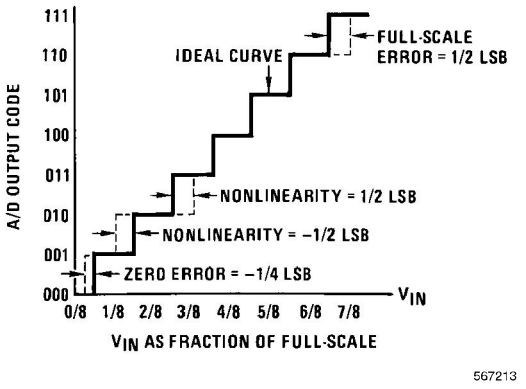

FIGURE 2. 3-Bit A/D Transfer Curve

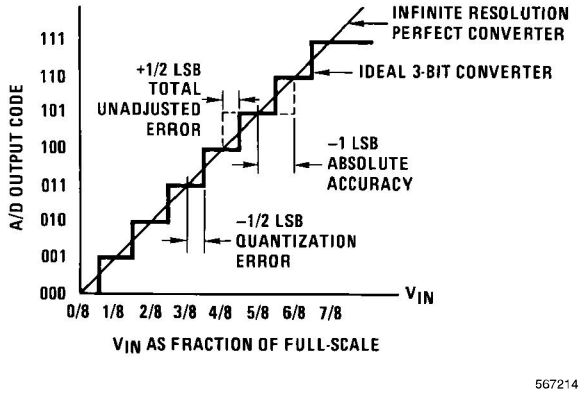

FIGURE 3. 3-Bit A/D Absolute Accuracy Curve

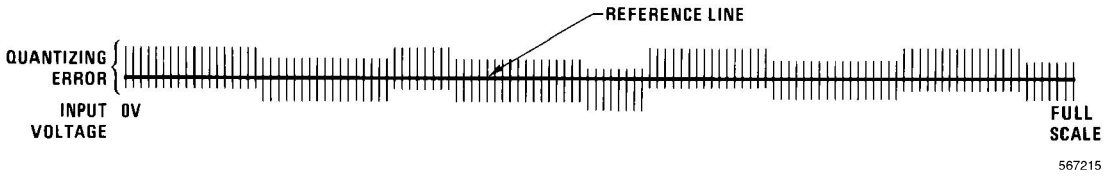

FIGURE 4. Typical Error Curve